Microbial Natural Product Discovery through Nutritional and Epigenetic Manipulation

by

Mohammed Aldholmi

University of East Anglia

Norwich Research Park, Norwich NR4 7TJ

Supervisor: Prof. A. Ganesan

Second Supervisor: Prof. Barrie Wilkinson

Thesis for the degree of Doctor of Philosophy

2020

This copy of the thesis has been supplied on condition that anyone who consults it is understood to recognise that its copyright rests with the author and that use of any information derived therefrom must be in accordance with current UK Copyright Law. In addition, any quotation or extract must include full attribution.

Abstract

Microbial natural products represent a significant portion of small-molecule drugs approved for clinical use, especially as anti-infective and anticancer agents. Nevertheless, most clinically used anti-infective and anticancer agents suffer from resistance and other drawbacks such as adverse effects, drug interactions and poor pharmacokinetic properties. Some of the main challenges in the natural product discovery field are the high rediscovery rates and low yield of natural products. One of the factors contributing to this problem is the fact that the genes responsible for the production of a great number of natural products are transcriptionally inactive (silent) or poorly expressed under laboratory conditions, resulting in undetectable concentrations of the corresponding products. Therefore, this project aimed at activating natural product genes in *Euglena* microalgae, *Aspergillus* fungi and actinomycete bacteria through nutritional and epigenetic manipulation.

Nutritional manipulation of *Euglena* resulted in the discovery of five novel natural products from *E. gracilis*, named euglenatides A-E, with moderate antifungal activity and potent antiproliferative activity. The investigation of other *Euglena* species revealed that euglenatide-related metabolites are produced by *E. mutabilis* and *E. sanguinea*. In *Aspergillus* fungi, nutritional manipulation led to significant changes in metabolite profiles leading to a substantial increase in the antimicrobial activity. Similarly, epigenetic manipulation led to a significant increase in the titre levels of phenylahistin in *A. calidoustus* and penicillic acid in *A. westerdijkiae*. Finally, nutritional manipulation in actinomycete bacteria led to higher yields of heronamides in *Streptomyces* sp. CMB-0406 while epigenetic manipulation did not display noticeable effects on the metabolite profile.

Access Condition and Agreement

Each deposit in UEA Digital Repository is protected by copyright and other intellectual property rights, and duplication or sale of all or part of any of the Data Collections is not permitted, except that material may be duplicated by you for your research use or for educational purposes in electronic or print form. You must obtain permission from the copyright holder, usually the author, for any other use. Exceptions only apply where a deposit may be explicitly provided under a stated licence, such as a Creative Commons licence or Open Government licence.

Electronic or print copies may not be offered, whether for sale or otherwise to anyone, unless explicitly stated under a Creative Commons or Open Government license. Unauthorised reproduction, editing or reformatting for resale purposes is explicitly prohibited (except where approved by the copyright holder themselves) and UEA reserves the right to take immediate ‘take down’ action on behalf of the copyright and/or rights holder if this Access condition of the UEA Digital Repository is breached. Any material in this database has been supplied on the understanding that it is copyright material and that no quotation from the material may be published without proper acknowledgement.

Table of Contents

Table of Figures

List of Tables

List of Abbreviations and Symbols

°C	Degree Celsius
µM	Micromolar
^{13}C	Carbon NMR
1D	One dimensional
^{1}H	Proton NMR
2D	Two dimensional
5-AC	5-azacytidine
A-549	Human lung adenocarcinoma epithelial cells
ADP	Adenosine diphosphate ribose
Ala	Alanine
antiSMASH	antibiotics and Secondary Metabolite Analysis Shell
Asn	Asparagine
Asp	Aspartate
BGCs	Biosynthetic gene clusters
br dd	Broad doublet of doublets
brd	Broad doublet
brs	Broad singlet
CCAP	Culture collection of algae and protozoa
CFU	Colony-forming units
COSY	Correlation spectroscopy
d	Doublet
d	Deuterated
Da	Dalton
dd	Doublet of doublets
DMSO	Dimethyl sulfoxide
DNA	Deoxyribonucleic acid
DNMTIs	Inhibitors of DNMTs
DNMTs	DNA methyltransferases
DNP	Dictionary of natural products
dt	Doublet of triplets
EG:JM	1:1, euglena gracilis medium:Jaworski's medium
EGCG	Epigallocatechin gallate
EtOAc	Ethyl acetate
FDA	Food and drug administration
FDAA	1-fluoro-2,4-dinitrophenyl-5-l-alanine amide

FDVA	1-fluoro-2,4-dinitrophenyl-5-l-valine amide
g	Gram
Glc	Glucose
Gln	Glutamine
Glu	Glutamate
Gly	Glycine
GNPS	Global natural product social molecular networking
GPY medium	Glucose peptone yeast extract medium
h	Hour
H_2O	Water
HATs	Histone acetyltransferases
HCl	Hydrochloric acid
HDACIs	Inhibitors of HDACs
HDACs	Histone deacetylases
HMBC	Heteronuclear multiple bond coherence
HPLC	High-performance liquid chromatography
HRMS	High-resolution mass spectrometry
HSQC	Heteronuclear single quantum coherence
Hz	Hertz
IC_{50}	Half maximal inhibitory concentration
IR	Infrared radiation
J	Spin-spin coupling constant (Hz)
L	Litre
LB	Luria-Bertani broth
LBA	Luria-Bertani agar
LC	Liquid chromatography
m	Multiplet
m/z	Mass-to-charge ratio
m^{-2}	Per square meter
MCF-7	Breast adenocarcinoma cells
MeOH	Methanol
mg	Milligram
MHz	Megahertz
min	Minute
mL	Millilitre
mM	Millimolar
MPDB	Malt peptone dextrose broth

MRSA	Methicillin-resistant *Staphylococcus aureus*
MS	Mass spectrometry
MS/MS	Coupled mass spectrometers
MSSA	Methicilin susceptible *Staphylococcus aureus*
MTS	3-(4,5-dimethylthiazol-2-yl)-5-(3-carboxymethoxyphenyl)-2-(4-sulfophenyl)2h-tetrazolium
mult.	Multiplicity
N	Natural products
NaCl	Sodium chloride
NAD	Nicotinamide adenine dinucleotide
$NaHCO_3$	Sodium bicarbonate
NaOH	Sodium hydroxide
ND	Semisynthetic derivatives
nm	Nanometre
nM	Nanomolar
NM	Mimics of natural products
NMR	Nuclear magnetic resonance
NOESY	Nuclear overhauser effect spectroscopy
NP Atlas	Natural products atlas
NPBPs	Natural product biosynthetic pathways
NRPs	Non-ribosomal peptides
NRPSs	Non-ribosomal peptide synthetases
OSMAC	One strain, many compounds
PDA detector	Photodiode array
PDA medium	Potato dextrose agar medium
PDB	Potato dextrose broth
PDBA	PDB medium supplemented with agar
PDYB	Potato dextrose yeast broth
pH	Potential of hydrogen
PKs	Polyketides
PKSs	Polyketide synthases
Pro	Proline
psi	Pounds per square inch
q	Quartet
RiPPs	Ribosomally synthesised and post-translationally modified peptides
rpm	Revolutions per minute
RT	Retention time
S	Totally synthetic

s	Singlet
S*	Synthetic drugs with natural product pharmacophore
s^{-1}	Per second
SB	Sodium butyrate
SBHA	Suberohydroxamic acid
SDA	Sabouraud dextrose agar
Ser	Serine
SMURF	Secondary metabolite unknown regions finder
t	Triplet
T_0	Zero time
TAC	Total absorbance chromatogram
T_f	Final time
THP-1	Acute monocytic leukaemia
TSA	Trichostatin a
U	Unit
UPLC	Ultra-performance liquid chromatography
UV	Ultraviolet
UV/Vis	Ultraviolet/visible
VPA	Valproic acid
x g	Units of times gravity
µg	Microgram
µL	Microliter
µM	Micromolar

(Dedication) إهداء

بِسۡمِ ٱللَّهِ ٱلرَّحۡمَٰنِ ٱلرَّحِيمِ

بعد حمد الله وشكره أهدي هذا العمل إلى:

والدَيَّ العزيزين اللذَين دعماني وَأخفيا عني أوجاعهما وهمومهما لِكَيلَا يُشتتا انتباهي عن دراستي.

زوجتي الغالية التي أعانتني أثناء غُربتي.

ابنتي الحبيبة التي كثيراً ما انتظرَت عودتي من المعمل قبل أن يغلبها النعاس.

أخي الذي رحَلَ إلى ربه وما زلتُ طفلاً وأختي التي رحَلَت إلى ربها وما زالت طفلة.

إخواني وأخواتي الذين كانوا داعمين لي وفخورين بي.

والدَيْ وإخوان زوجتي الذين دعموني طوال فترة دراستي.

أقاربي وأصدقائي الباقين منهم والرّاحلين إلى ربّهم.

أساتذتي المخلصين.

In the Name of Allah, the Most Gracious, the Most Merciful

After praising and thanking Allah, I dedicate this work to:

My dear parents who supported me and hid their diseases and concerns from me so that they do not distract me from my studies.

My beloved wife who assisted me through my expatriate experience.

My beloved daughter who had often been waiting for my return from the lab before falling asleep.

My late brother who passed away when I was still a child and my late sister who passed away when she was still a child.

My brothers and sisters who have been supportive and proud of me.

My parents and brothers-in-law who supported me throughout my studies.

My relatives and friends who are still alive and those who have passed away.

My sincere instructors.

Acknowledgements

I would like to express my profound appreciation to my supervisor Prof. A. Ganesan for the encouragement, advice, patience, motivation and intellectual support throughout my doctoral journey. I am extremely thankful to Prof. Ganesan for providing me with the opportunities to grow up as a researcher and build an excellent network with natural product scientists around the world through conferences, meetings and a short-term scientific mission. I would also like to thank my second supervisor Prof. Barrie Wilkinson, for his supportive suggestions and guidance during my PhD. I greatly appreciate the supervision and guidance provided by Prof. Rob Field during my work in his lab. I would also like to extend my sincere thanks to the students and researchers in my supervisors' labs for being supportive and great friends.

I am grateful to professors, researchers, technicians and students at the University of East Anglia and John Innes Centre for their collaboration, training and support. I express my sincere gratitude to Prof. Maria O'Connell for the excellent training and guidance regarding cytotoxic assays. I also thank Dr Alexei Maklakov and Hanne Carlsson (School of Biological Sciences, UEA) for performing the antinematodal experiments. Special thanks to Philip Schuler for being a supportive labmate and friend, as well as an amazing mycologist and pharmacologist. My thanks extend to Dr Mahmoud Abdelhamid, Dr Marco Cominetti, Dr Antony Hinchliffe, Lionel Hill, Paul Brett, Dr Gerhard Saalbach and Julia Mundy for their technical support and training. I am also thankful to the undergraduate students (Elizabeth Everingham and James Murphy) who contributed to the *Aspergillus* chapter of this thesis.

I am grateful to our collaborators outside the Norwich Research Park for their collaboration and assistance. Thanks to Dr Ellis O'Neill, for the help regarding the

molecular network and for supplying the *Euglena* strains. I also want to express my appreciation to Dr Olga Genilloud and her group at Fundación Medina, Granada, Spain, for hosting the short-term scientific mission. Special thanks to Dr Fernando Reyes, Dr Ignacio Pérez-Victoria, Dr Ruben Tormo, Dr Mercedes de la Cruz, Dr Caridad Díaz, Dr Jesús Martín and Daniel Carretero for their support and guidance during my mission. I am incredibly grateful to Prof. Thierry Gefflaut (Université Clermont Auvergne, France) and Dr Armin Bauer (Sanofi, UK) for supplying the standard amino acids that were vital for the stereochemistry assignment of euglenatides.

I owe a great debt of gratitude to my dear parents, Jaber Aldholmi and Jameelah Alfaifi, and to my wife and daughter, Abrar Alfaifi and Reetal Aldholmi, respectively, for their endless support, love, encouragement and prayers. I want to extend my sincere gratitude to my brothers, sisters, relatives and friends who have constantly encouraged me and supported me throughout my studies.

Finally, I appreciate the generous financial support provided by Imam Abdulrahman Bin Faisal University, Saudi Arabia. Equally appreciated is the financial funding of the short-term scientific mission in Spain provided by the COST action Epichembio. *Aspergillus* strains were kindly supplied by the US Agricultural Research Service (USDA-ARS).

Conferences and Publications

1. The results obtained with *Aspergillus calidoustus and Aspergillus westerdijkiae* have been published in the Journal of Antibiotics. M. Aldholmi, B. Wilkinson, A. Ganesan, J. Antibiot. (Tokyo). 2020, 73, 410–413.
2. A review of antifungal natural products has been published in Pharmaceuticals. M. Aldholmi, P. Marchand, I. Ourliac-Garnier, P. Le Pape, A. Ganesan, Pharmaceuticals 2019, 12, 182.
3. Poster presentation, 27th Annual GP2A Medicinal Chemistry Conference, 21st – 23rd August 2019 in Nottingham, UK.
4. Poster presentation, RSC Chemical Biology and Bio-organic Group Postgraduate Symposium, 26th April 2019 in Southampton, UK.
5. Oral presentation, COST CM1406 Epigenetic Chemical Biology, 18th – 20th February 2019 in Faro, Portugal.
6. Poster presentation, 30th International Symposium on the Chemistry of Natural Products and the 10th International Congress on Biodiversity (ISCNP30 & ICOB10), 25th – 29th November 2018 in Athens, Greece.

Chapter One

1. Overview of bioactive microbial natural products and manipulation of biosynthetic pathways

1.1. Overview of bioactive microbial natural products

Natural products are defined differently from one field to another with the broadest definition applying the term natural products to all substances from nature, including crude materials, extracts and isolated compounds.[1] Within the field of organic chemistry, the definition is confined to single chemical compounds produced by living organisms and commonly known as primary and secondary metabolites.[2] The definition within the medicinal chemistry field is restricted further to use the term natural products as a synonym for low-molecular-weight secondary metabolites.[3] Unlike secondary metabolites, primary metabolites are present in abundant amount in many organisms and are essential for their survivability.[2] In contrast, secondary metabolites are not directly involved in the growth of the producing organisms but are produced in small amounts for specific purposes such as competitive functions and communication between organisms.[4] Many secondary metabolites have biological activity against specific targets in prokaryotes, eukaryotes or both of them as they have been optimized through evolution for use against competing organisms.[5] Natural products can also involve compounds that are derived from natural products by partial synthesis (semi-synthesis) or prepared by chemical synthesis (total synthesis) if the resultant product is chemically equivalent to the original natural product.[6]

There are different ways for classifying natural products, but they are commonly classified by their biosynthetic origin. The main classes of natural products include

peptides, polyketides and fatty acid-derived substances, alkaloids, terpenoids and steroids, specialised carbohydrates and shikimic-acid-derived natural products.[1,2] Some natural products are hybrid products arising from more than one biosynthetic pathway or undergoing further modifications after the main biosynthetic reactions. Most microbial natural products are derived from polyketides (PKs), non-ribosomal peptides (NRPs) and ribosomally synthesised and post-translationally modified peptides (RiPPs).[7,8] PKs and NRPs are biosynthesised through chemical reactions catalysed by domains of mega-enzymes known as polyketide synthases (PKSs) and non-ribosomal peptide synthetases (NRPSs), respectively.[9]

Natural products, their derivatives and their synthetic analogues have been significant contributors in the medical field as medicines themselves or as leads for other medicines, especially as anti-infective and anticancer agents.[10] Analysis of all small-molecule drugs approved by the FDA between January 1981 and September 2019 indicated that approximately 31.6% are natural products (N) or semisynthetic derivatives (ND) and 35.1% are mimics of natural products or synthetic drugs with natural product pharmacophore (NM and S*) while only 33.3% are totally synthetic (S) drugs (Figure 1.1).[11] The analysis also revealed that only 15.7% of small-molecule anticancer drugs approved by the FDA between January 1981 and September 2019 are totally synthetic drugs, while the remaining owe their origin to natural products (Figure 1.2). Of all small-molecule anti-infective drugs approved by the FDA between January 1981 and September 2019, around 66% belong to the natural products categories (N, ND, NM and S*, Figure 1.3).[11]

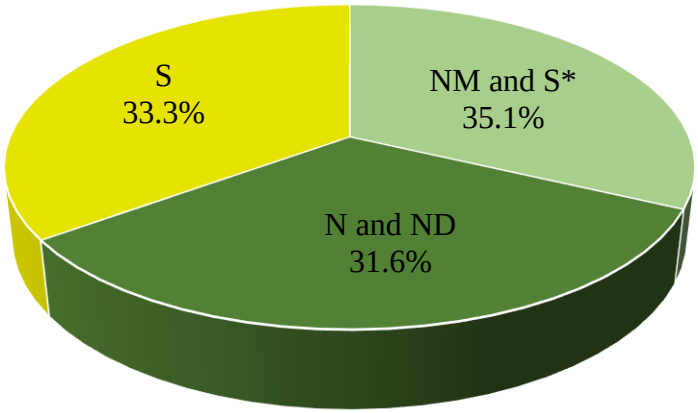

Figure 1.1 Small-molecule drugs approved by the FDA between January 1981 and September 2019, based on data reported by Newman and Cragg.[11]

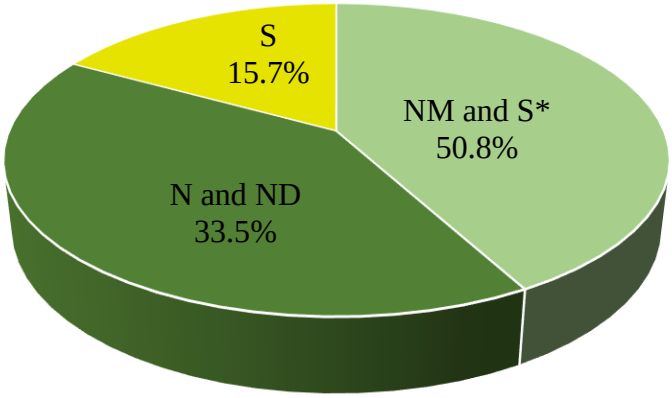

Figure 1.2 Small-molecule anticancer drugs approved by the FDA between January 1981 and September 2019, based on data reported by Newman and Cragg.[11]

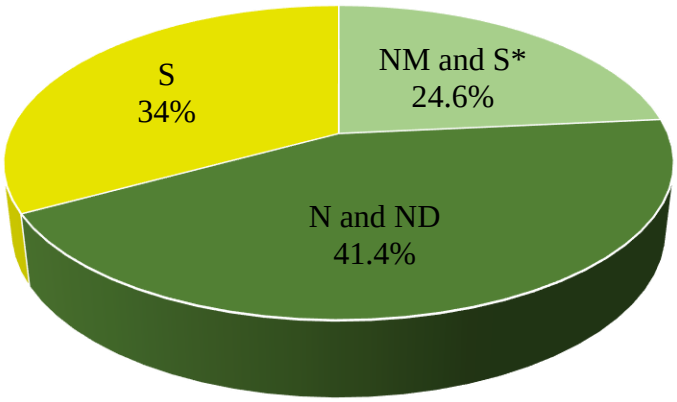

Figure 1.3 Small-molecule anti-infective drugs approved by the FDA between January 1981 and September 2019, based on data reported by Newman and Cragg.[11]

Microbial natural products represent a significant portion of approved drugs, particularly antimicrobial and anticancer drugs. It is estimated that 97% of all antibacterial natural products approved by the FDA between 1930 and 2013 were isolated or derived from microorganisms.[12] The main classes of antibacterial agents originated from actinomycete bacteria (Figure 1.4) and ascomycetous fungi (Figure 1.5).

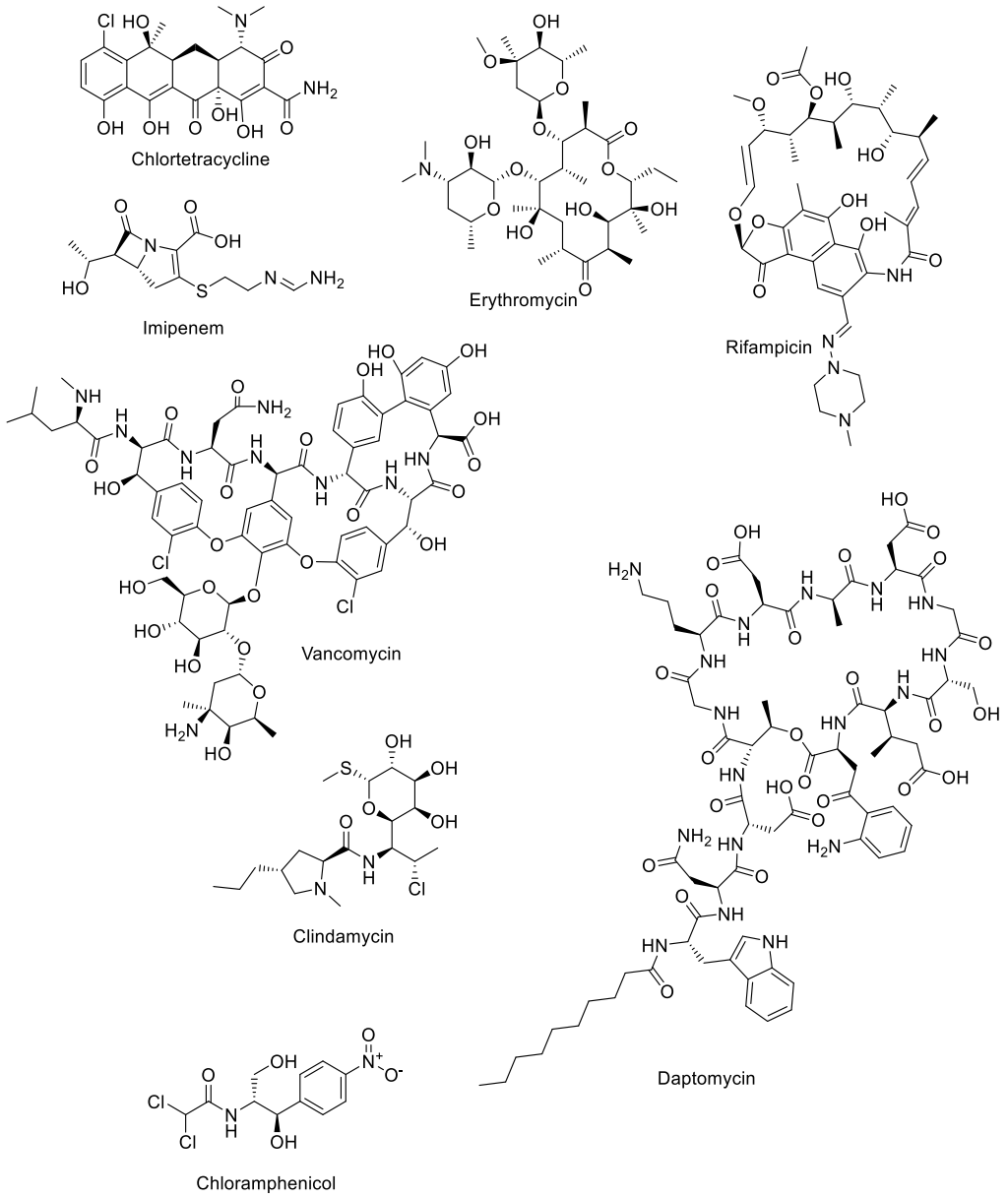

Figure 1.4 Approved antibacterial agents originating from actinomycete bacteria.

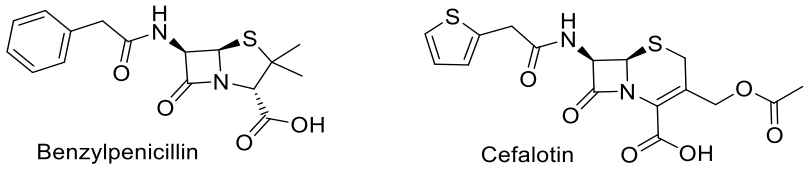

Figure 1.5 Approved antibacterial agents originating from ascomycetous fungi.

The first antibacterial natural product approved by the FDA was the aminoglycoside streptomycin, isolated from the actinomycete *Streptomyces griseus*.[13] Other examples for approved antibacterial agents originating from actinomycetes include tetracyclines (e.g. chlortetracycline), macrolides (e.g. erythromycin), ansamycins (e.g. rifampicin), carbapenems (e.g. imipenem), amphenicols (e.g. chloramphenicol), lincosamides (e.g. clindamycin), glycopeptides (e.g. vancomycin) and cyclic lipopeptides (e.g. daptomycin).[13–18] The antibacterial agents isolated from ascomycetous fungi involve penicillins (e.g. benzylpenicillin) and cephalosporines (e.g. cefalotin).[19,20]

All approved antifungals of natural product origin arise from actinomycete bacteria (Figure 1.6) and ascomycetous fungi (Figure 1.7). Actinomycete bacteria are the producers of approved antifungal polyenes such as amphotericin B, nystatin and natamycin[21], while ascomycetous fungi are the origin of the antifungal lipopeptides (echinocandins) and polyketide griseofulvin.[22,23] Since the echinocandin natural products are not optimal in terms of pharmacokinetics, semisynthetic derivatives were optimised and approved for clinical use, including anidulafungin prepared from echinocandin B, caspofungin prepared from pneumocandin B_o, and micafungin prepared from FR901379.[22] In our recent review of antifungal leads from natural products discovered between 2010 and 2019, microbial natural products represent 65% of the discovered compounds with unique scaffolds and an MIC < 10 μg/mL or IC_{50} < 10 μM against human pathogenic fungi (Figure 1.8).[24]

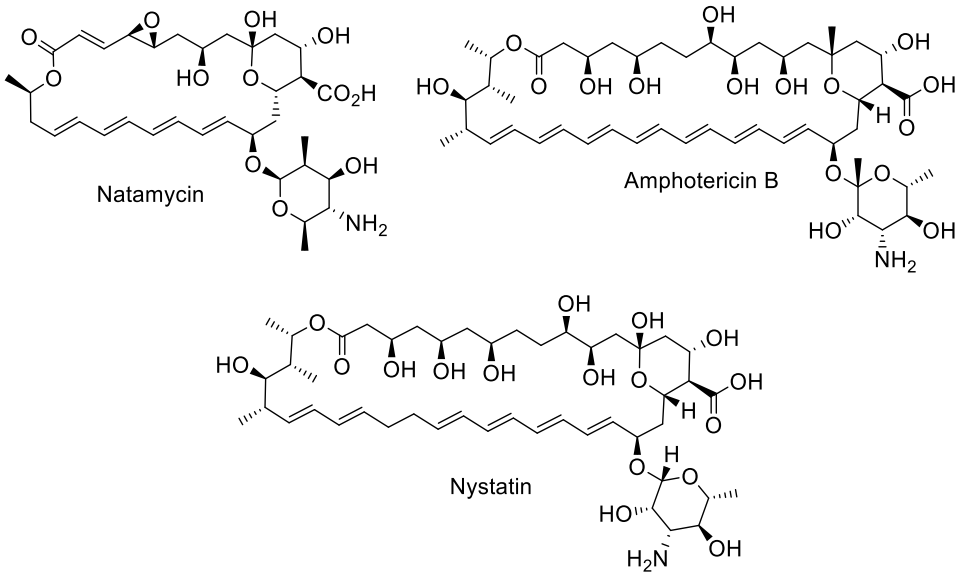

Figure 1.6 Approved antifungal agents isolated from actinomycete bacteria.

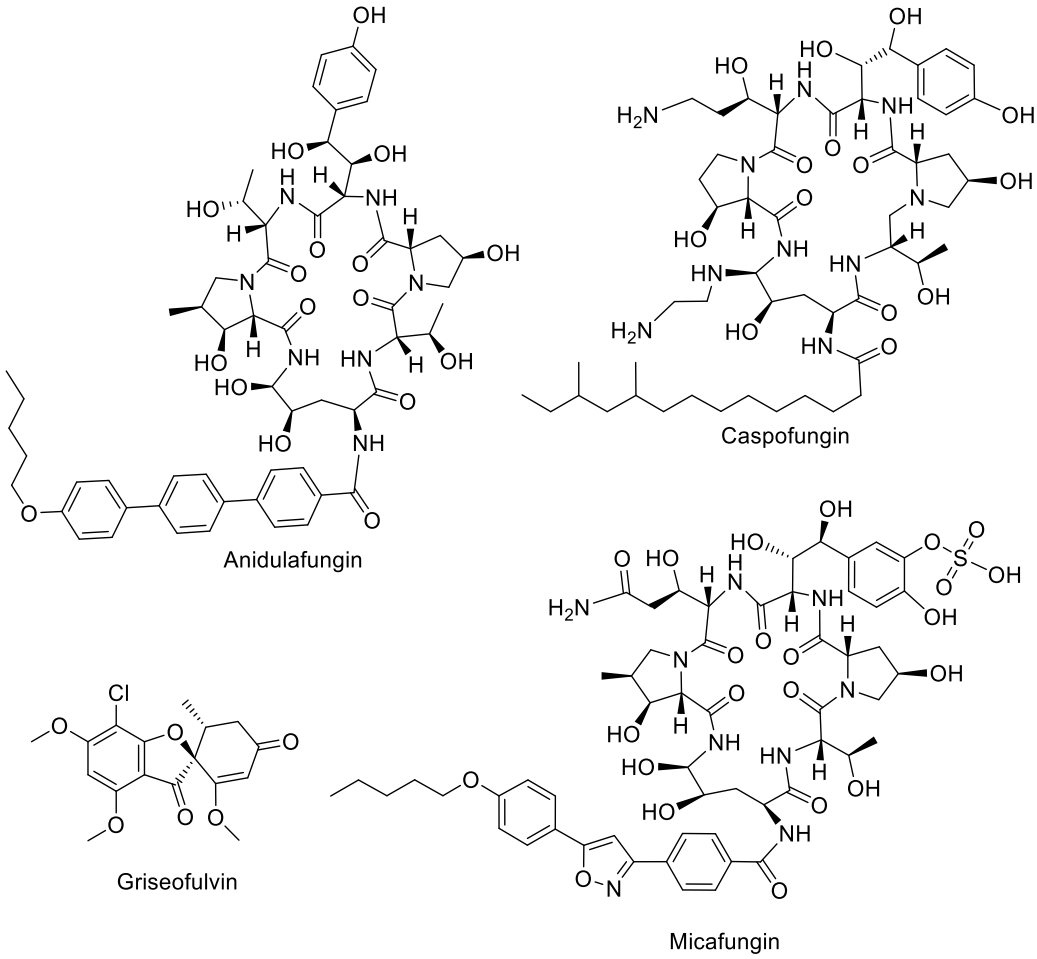

Figure 1.7 Approved antifungal agents originating from ascomycetous fungi.

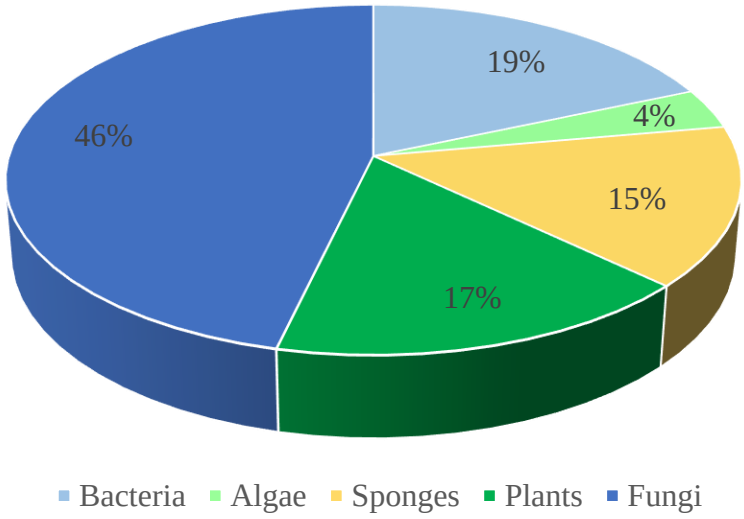

Figure 1.8 Source of antifungal leads from natural products discovered between 2010 and 2019 with unique scaffolds and an MIC < 10 µg/mL or IC_{50} < 10 µM against human pathogenic fungi, this figure is adapted from Aldholmi et.al.[24]

Microbial natural products such as actinomycin D, anthracyclines, bleomycins, mitosanes and anthracenones are among the most important approved anticancer agents.[25] Actinomycin D and plicamycin (anthracenone) were the first microbial anticancer agents approved by the FDA between 1960 and 1970 (Figure 1.9).[26,27] In 1973, a mixture of two closely related glycopeptides, bleomycin A_2 (55-70%) and bleomycin B_2 (25-32%), was approved by the FDA for cancer treatment (Figure 1.10).[28] After this approval, two new classes of microbial anticancer agents, mitosanes (i.e. mitomycin) and anthracyclines (i.e. doxorubicin, daunorubicin and idarubicin), were approved between 1974 and 1990 (Figure 1.11).[29,30] All approved drugs mentioned above are microbial natural products isolated from *Streptomyces* species, except idarubicin which is a semi-synthetic analogue of daunorubicin.[30]

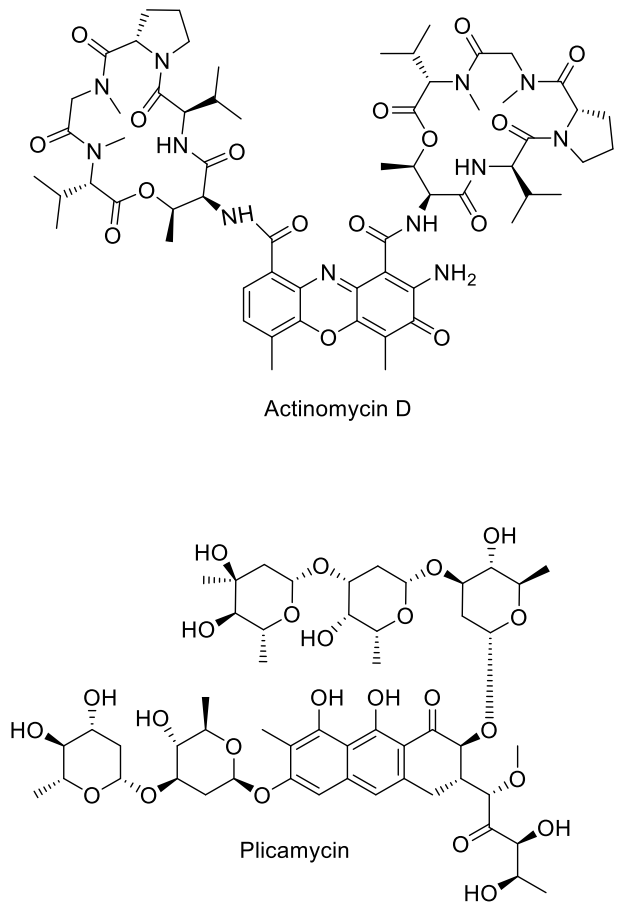

Figure 1.9 Chemical structures of actinomycin D and plicamycin.

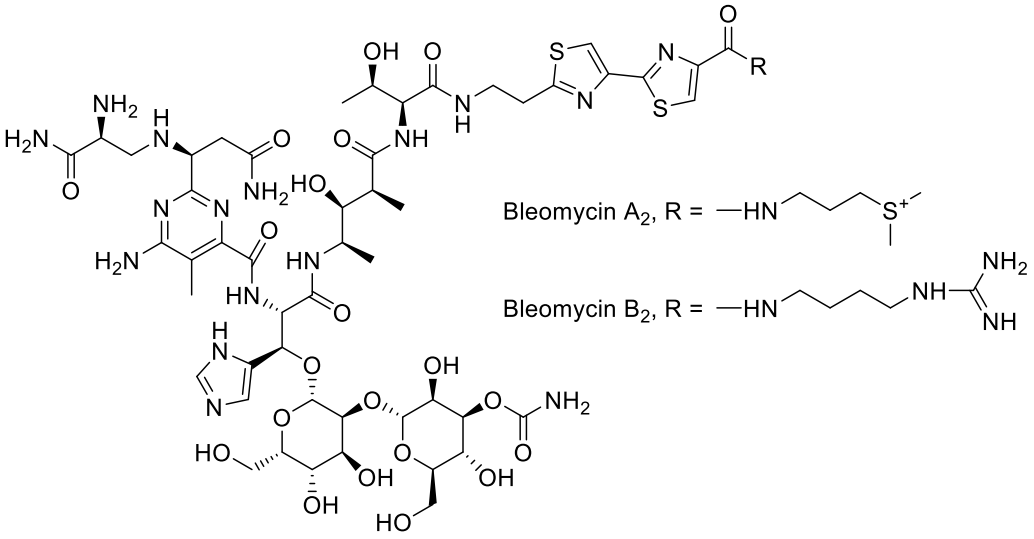

Figure 1.10 Chemical structures of bleomycins A_2 and B_2.

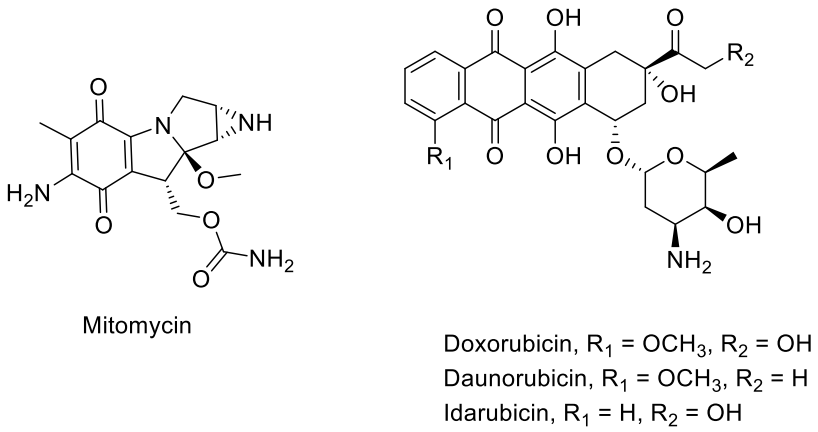

Figure 1.11 Chemical structures of approved mitomycin and anthracyclines.

The soil myxobacterium *Sorangium cellulosum* is the source of microbial secondary metabolites known as epothilones with significant anti-neoplastic activity.[31] In 2007, ixabepilone, a semi-synthetic analogue of epothilone B, was approved by the FDA for the treatment of aggressive metastatic and locally advanced breast cancer no longer responding to currently available therapies.[31] Ixabepilone has a similar mechanism to paclitaxel, interfering with tubulin, but it has a simpler structure than paclitaxel (Figure 1.12).[32] Paclitaxel was first isolated from the plant *Taxus brevifolia* but has also been reported from endophytic fungi such as *Taxomyces andeanae* and *Fusarium redolens*.[33,34]

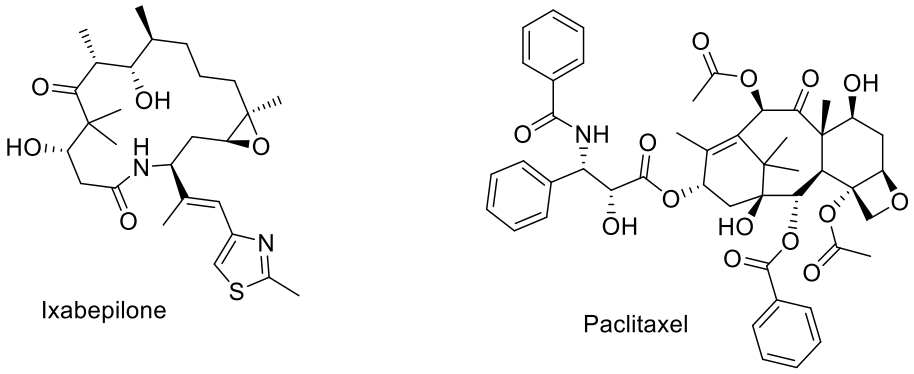

Figure 1.12 Chemical structures of ixabepilone and paclitaxel.

1.2. Challenges and opportunities in natural product discovery

Although a long list of anti-infective and anticancer drugs has been approved by regulatory authorities, most clinically used drugs suffer from resistance and other drawbacks such as adverse effects, drug interactions and poor pharmacokinetic properties.[24,35,36] Moreover, most large pharmaceutical companies have reduced or even terminated their natural product discovery programs despite the inspiring history of microbial natural products. Some of the main factors that contributed to this situation are the high rediscovery rates and low yield of natural products being insufficient for isolation, structure elucidation and pharmacological evaluation.[37,38]

To overcome the above-mentioned challenges, unusual environments such as caves, hydrothermal vents and Antarctic waters have been explored to increase the opportunity for discovering novel natural products.[39] This approach has been effective in terms of discovering novel metabolites, but it has some challenges, including the accessibility of the unique environments, experience requirement for taxonomical identification and costs of field trips for sample collection.[37,40] An alternative approach is the manipulation of natural product biosynthetic pathways (NPBPs) using several strategies, including OSMAC (one strain, many compounds), co-cultivation of organisms, genetic engineering and epigenetic manipulation.[41] OSMAC approach states that a single strain produces different metabolites with the variation of medium composition (nutritional manipulation) and other cultivation conditions such as pH, temperature, oxygen concentration, salinity and cultivation status.[42,43] Nutritional and epigenetic manipulation are the two strategies employed

in this PhD project to induce the production of novel natural products and increase the yield of other metabolites.

The sequencing of microbial genomes has demonstrated that genes involved in the biosynthesis of microbial secondary metabolites typically exist in clusters known as biosynthetic gene clusters (BGCs, Figure 1.13).[44] Analysis of BGCs revealed that even well-studied organisms such as *Streptomyces* bacteria and *Aspergillus* fungi are capable of producing a significantly larger number of secondary metabolites than has been previously identified from those organisms.[45] This is probably because the genes responsible for the production of a great number of secondary metabolites are transcriptionally inactive (silent) or poorly expressed under laboratory conditions, resulting in undetectable concentrations of the corresponding products.[46] Such biosynthetic genes are referred to as "cryptic". For example, *Streptomyces coelicolor* A3 (2) that has served as a model organism for bioactive-metabolite producers for more than five decades had been known to produce five secondary metabolites before genome sequencing.[47] Upon the release of the genome sequence, initial bioinformatic analysis unveiled 24 potential BGCs that were extended later to 31 BGCs with the development of bioinformatics tools for BGCs analysis.[45,47]

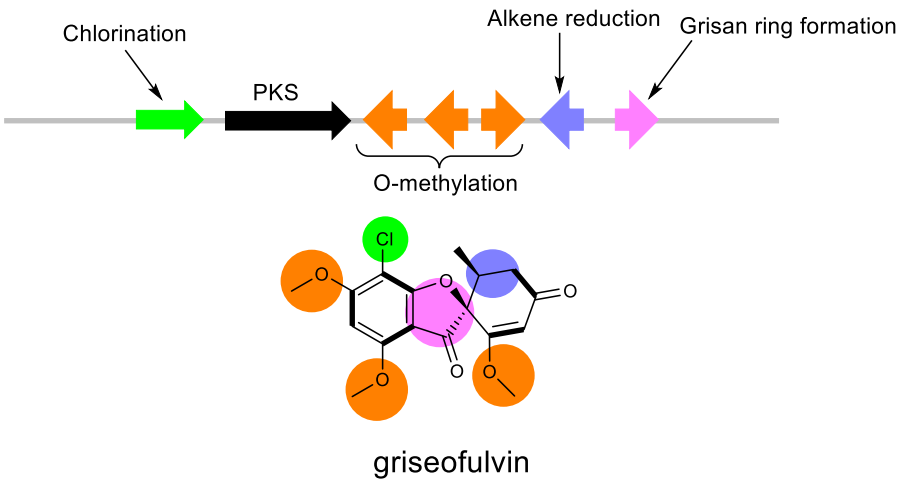

Figure 1.13 BGC of griseofulvin showing the genes involved in griseofulvin biosynthesis clustered together, this figure is adapted from Cacho et.al.[48]

Remarkably, genomic and transcriptomic analysis has also shown that many microorganisms previously considered incompetent candidates for natural product discovery harbour considerable numbers of BGCs.[49,50] For instance, genomic analysis of several strains of *Clostridium* proposed that this group can be a promising source of novel natural products.[51] Moreover, genomic and transcriptomic analysis of several microalgal species revealed the presence of a great number of NRPSs and PKSs.[52,53] Two of those species are *Coccomyxa subellipsoidea* and *Euglena gracilis*, which are well known as green algae model organisms but were not believed to be rich sources of secondary metabolites before genome and transcriptome release. Therefore, genome mining (the recognition of previously uncharacterised natural product BGCs) can be exploited for identification and manipulation of cryptic BGCs to enable the production of novel natural products and increase the yield of minor metabolites. For instance, genome mining of *S. coelicolor* sequence and other microbial sequences prompted the induction and identification of new natural products.[54–58] Noteworthy, most organisms with sequenced genomes or transcriptomes can be effortlessly obtained from private or public culture collections.

1.3. Mining and manipulation of NPBPs for natural product discovery

This project is guided by genomic and transcriptomic information, beginning with genome or transcriptome mining and finishing with molecular networking of related metabolites (Figure 1.14). The first step in the genome or transcriptome-based natural product discovery is to select the candidate microorganism for mining. The selection is based on several factors, including the accessibility of the genome or transcriptome data and availability of the strain from culture collections or

collaborating laboratories. In addition, the candidates should be easy to cultivate within the available facilities and have a reasonable growth rate. Furthermore, literature is searched to ensure that the candidate organism is suitable for the employed manipulation strategy.

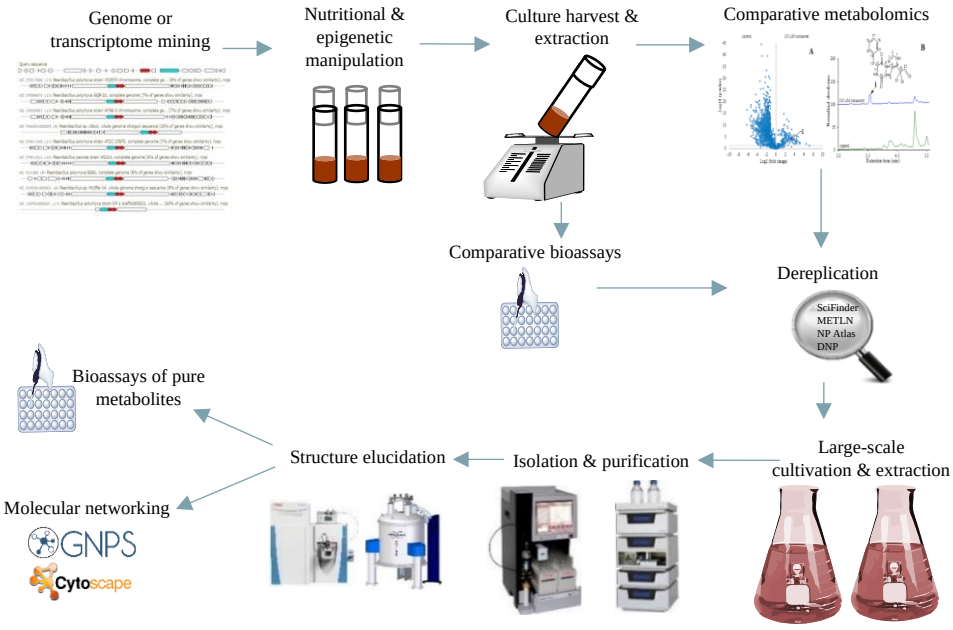

Figure 1.14 Workflow for microbial natural product discovery through nutritional and epigenetic manipulation.

Genome or transcriptome mining is the identification of previously uncharacterised natural product BGCs within genome or transcriptome sequences based on homology with portions of known BGCs.[59] The genome contains all genes of an organism while the transcriptome only represents the expressed genes that were transcribed from the genome under specific conditions.[60] Although the transcriptome only covers transcriptionally active genes, it is valuable when the genome is not available as it shows the BGCs that are poorly expressed or their respective secondary metabolites are not detected for other reasons. The genome and transcriptome sequences are obtained from public databases (e.g. GenBank) and analysed for the presence of BGCs using bioinformatics tools such as antibiotics and Secondary Metabolite Analysis Shell (antiSMASH)[44,61] and Secondary Metabolite Unknown

Regions Finder (SMURF).[62] These tools can identify genes encoding most of the common microbial biosynthetic enzymes such as NRPSs and PKSs. If the natural product BGCs analysis has been previously published, the first step is skipped, and the published data is used for guided-natural product discovery.

The next step is the manipulation of cryptic BGCs through the cultivation of microorganisms with different nutrients or chemical epigenetic modifiers. The cultures are then extracted with organic solvents and the extracts from different conditions are compared using one of two different methods: comparative metabolomics or comparative bioassays. Comparative metabolomics is the comparison of the metabolic profiles of an organism, at a specific point in time and under specific conditions.[63] This is a crucial step for determination and prioritisation of conditions that produce high quantities of metabolites of interest. Targeted metabolic profiling aims at analysing defined groups of metabolites, while untargeted metabolomics is a comprehensive analysis of all the measurable metabolites in the analysed sample.[64] The latter is utilized in this project.

One of the main techniques employed to obtain chemical profiles is the high-performance liquid chromatography (HPLC) connected to ultraviolet (UV) or photodiode array (PDA) detectors. The absorbance intensity of the peaks on chromatograms is proportional to the concentration of the respective metabolites enabling the comparison of the production in different conditions. A chromatogram can contain spectral information at a single wavelength or within a specified range (total absorbance chromatogram, TAC), depending on the type of detector. The limitations in this technique are the coelution of different metabolites and the absence of UV chromophores leading to a set of metabolites being undetectable. Nuclear magnetic resonance (NMR) is an alternative method that is not biased towards

molecular class but the major limitation in this technique is its inherently low sensitivity.[65] In contrast, the mass spectrometry (MS) is an extraordinarily sensitive analytical method that is usually combined with ultra-performance liquid chromatography (UPLC) or HPLC. The ion intensity of metabolites is typically proportional to the concentration of the respective metabolites which enables relative quantification of a broad range of metabolites, but this technique is limited by the bias in ionisation efficiency.[63] However, none of the analytical methods are perfect but the high sensitivity of UV and MS detectors coupled to HPLC or UPLC provides a general overview of the relative amounts of metabolites present in samples.

The obtained metabolomics datasets can be compared and visualised using different methods. In this project, comparative overlaid chromatograms and volcano plots are employed for the visualisation of the results. Volcano plots are commonly used with statistical results of omics data such as genomics, transcriptomics, proteomics and recently metabolomics.[66,67] In metabolomics, they are used to identify changes in metabolite quantities produced under different conditions. They represent the statistical significance from a t-test (as -log10 of the p-value) versus the log2 of fold change on the y and x-axes, respectively.[68] Consequently, metabolites that are present in nearly equivalent amounts in two samples appear near the centre of the volcano plot and those with large fold changes appear farther left or right from the centre. The reproducible components with high statistical significance (low p values) appear toward the top of the plot.

Another method to compare extracts obtained from microbial cultivation under different conditions is by evaluation of their biological activity. If a bioactive compound is induced, the biological activity should be proportional to the induced amount when an appropriate bioassay is employed. Biological assays can be performed

on crude extracts or their fractions to evaluate relevant biological activities for drug discovery. However, this strategy is limited by the types of bioassays that can be performed and it suffers from overlooking low abundance compounds in complex mixtures.[69] Additionally, the observed biological activity might be due to the presence of previously known molecules. Moreover, some natural product chemistry labs do not have access to the required bioassay screening facilities. Collaboration with bioassay screening labs is an option, but it usually takes time to get the results from collaborators, leading to delay in the process of natural product discovery. If the comparative bioassays approach is used, isolation and purification of bioactive metabolites can be guided by bioassays (bioassay-guided isolation).[70]

Large-scale cultivation is normally required for the isolation and structure elucidation of the desired metabolites. Isolation and structure elucidation of natural products require time, finance and considerable skills, especially with low-yield natural products. Therefore, it is vital to ensure that the target metabolites are novel via searching informative databases such as METLIN, Natural Products Atlas (NP Atlas), Dictionary of Natural Products (DNP) and SciFinder, a process known as "dereplication".[71] Literature searching of the organisms under investigation is a crucial step to avoid isolating previously identified metabolites from the same organism. Some metabolites are produced by unrelated organisms; therefore, different characteristics should be used for literature searching. High-resolution mass spectrometry (HRMS) is one of the critical techniques used for dereplication through searching databases with accurate mass. Fragmentation data from coupled mass spectrometers (MS/MS) can be used to search spectral libraries such as Global Natural Product Social Molecular Networking (GNPS), METLIN and MassBank. Mass spectrometry-based molecular networking is a new method used for dereplication and

identification of structurally similar molecules through MS/MS fragmentation pattern.[72] Moreover, UV/Vis spectra can assist in dereplication when used with MS and MS/MS data for literature searching. Accordingly, MS, MS/MS and UV/Vis detectors combined to liquid chromatography can be used for the analysis of crude extracts and dereplication before conducting the next expensive and time-consuming stages of natural product discovery.

Initial separation of metabolites can be obtained by partitioning and flash chromatography. Some pure natural products can be obtained with initial separation methods, but most require method development and purification on HPLC instruments. This is more likely when metabolites are produced in small amounts or belong to the same chemical class with minor structural differences. After purification, several methods are utilised for structural analysis such as MS, MS/MS, infrared radiation (IR), NMR, UV, polarimeter, X-ray crystallography and chemical derivatisation. While low-abundance metabolites can be satisfactorily analysed by sensitive mass spectrometry, NMR analysis is more challenging with scarce samples. Nevertheless, the recent evolution of high-field NMR spectrometers equipped with microcryoprobes has increased the NMR sensitivity enabling structural characterisation by one dimensional (1D) and two dimensional (2D) NMR with a few micrograms.[73]

X-ray structural analysis is the most powerful method for the assignment of the three-dimensional structure of natural products. However, this technique requires a single crystal with suitable quality for the X-ray diffraction. The stereochemistry of peptide natural products can be assigned by chromatographic comparison of the amino acid residues with standard amino acids. The direct separation without chemical derivatisation of a pair of enantiomers normally requires a specific type of stationary

phases known as a chiral phase. This chromatography system is more expensive and complicated than the normal and reversed-phase chromatography.[74] Moreover, most amino acids have poor UV absorption requiring expensive types of detectors such as mass spectrometry. However, chromatographic separation of enantiomeric amino acids can be achieved on achiral stationary phases after chemical derivatisation, indirect approach. This approach is often simpler, less expensive and offers greater resolution and choices of chromatographic conditions over most direct methods.[75]

Chemical derivatisation is normally performed by reacting the enantiomers with an optically pure chiral reagent to form diastereomers prior to chromatographic analysis.[75] Marfey's reagent, 1-fluoro-2,4-dinitrophenyl-5-L-alanine amide (FDAA), is commonly used as a chiral reagent for chemical derivatisation and separation of enantiomeric amino acids.[76] Moreover, structural variants of Marfey's reagent have been prepared by the replacement of the alanine moiety with other amino acids such as phenylalanine and valine.[77] The structural variant 1-fluoro-2,4-dinitrophenyl-5-L-valine amide (FDVA) has been shown to offer the largest difference in retention times of diastereomers compared to reagents containing alanine or phenylalanine moieties.[78] All of these reagents normally react within an hour under mild alkaline conditions at 40 °C and allow detection at sub-nanomolar range due to the presence of the dinitrophenyl chromophore that strongly absorbs at 340 nm.[77,78]

The pure metabolite is evaluated for its biological activity once it is confirmed to be a novel natural product. Moreover, a molecular network can be constructed from structurally related compounds produced by other organisms. This step paves the way toward the discovery of related molecules that might have some advantages over the original natural product such as higher yield, higher potency, superior selectivity or better physicochemical properties. A molecular network is a visual representation of

structurally related compounds that share similar MS/MS fragmentation patterns.[79] GNPS is the most common molecular networking tool that aligns the MS/MS spectra and generates molecular networks.[80] Network visualisation can be performed online on the GNPS web platform or preferably with specialised visualisation software such as Cytoscape.[81]

1.3.1. Nutritional manipulation

Nutrients are organic and inorganic ingredients required for microbial growth and metabolism. The main nutrients in cultivation media function as sources of carbon, nitrogen, sulphur, phosphorus, potassium, magnesium, calcium, iron and trace elements. Organic carbon represents the source of energy for all heterotrophs, in contrast to autotrophs which acquire their energy from light (photosynthesis) or inorganic compounds (chemosynthesis).[82] Nitrogen is required for the synthesis of nitrogen-containing cellular substances such as proteins and nucleic acids.[83] In addition to their use for energy and biomass building, carbon and nitrogen sources provide carbon and nitrogen units for the production of secondary metabolites. The type and concentration of carbon and nitrogen sources employed for microbial cultivation have been shown to have a remarkable effect on microbial secondary metabolism.[42] Nutritional manipulation is the alteration of nutrients in the media employed for microbial cultivation. Although this is probably one of the simplest strategies for the induction of cryptic BGCs, the mechanisms behind the influence on secondary metabolism are much more complex and vary significantly between microorganisms.[84,85] Nevertheless, this strategy has led to the discovery of a variety of novel natural products.[86,87]

Martin et al.[85] reported global regulatory effects on primary and secondary metabolism in *Streptomyces coelicolor* when cultivated with different sources and concentrations of carbon, nitrogen and phosphorous. Nutritional manipulation in actinomycete bacteria led to the isolation of a variety of new natural products such as a spectinabilin derivative (**1**) from *Streptomyces* sp. 1H-GS5,[88] three new streptazolin derivatives (**2**-**4**) and streptenol E (**5**) from *Streptomyces* sp. A1,[89] and a new eudesmane sesquiterpenoid (**6**) and one new analogue of virginiae butanolide E (**7**) from *Lentzea violacea* AS08[90] (Figure 1.15). The production of the polyketide antibiotic SBR-22 by *Streptomyces psammoticus* BT-408 varied significantly between different carbon and nitrogen sources, with the highest yield observed with the carbon and nitrogen sources glucose and ammonium nitrate, respectively.[91] Although SBR-22 displayed antibacterial activity against MRSA (methicillin-resistant *Staphylococcus aureus*), the complete structure of this antibiotic is still unknown.

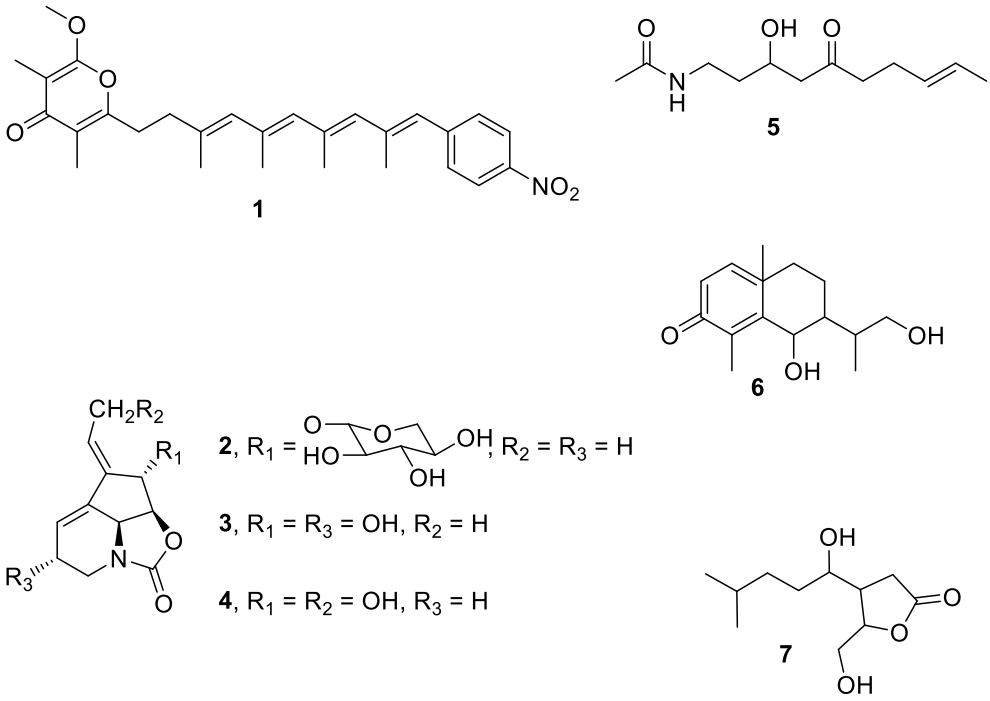

Figure 1.15 Chemical structures of natural products **1**-**7**.

Genome mining and nutritional manipulation in *Streptomyces* sp. CS led to the isolation of several natural products, including three new ansamycin antibiotics (Figure 1.16, **8**-**10**).[92] Similarly, the cultivation of *Streptomyces* strain C34 in two different media containing glucose or glycerol as carbon sources resulted in the isolation of four new ansamycin polyketides (Figure 1.17, **11**-**14**).[93] Remarkably, compounds **11** and **12** were produced in the glucose-containing medium while compounds **11**, **13**, and **14** were found in the glycerol-containing medium.

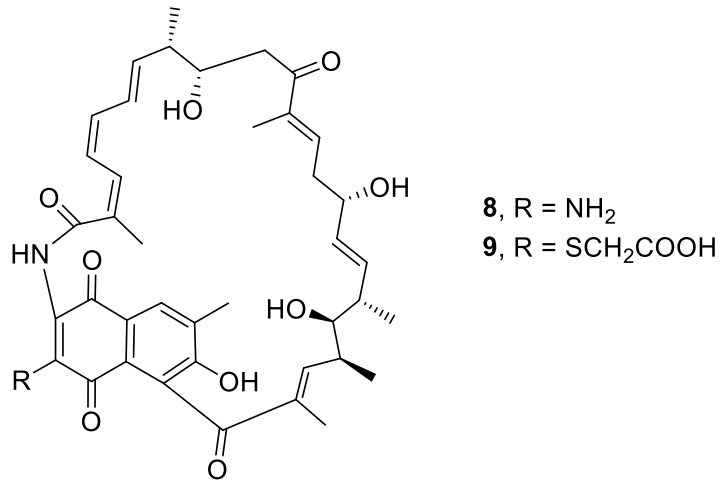

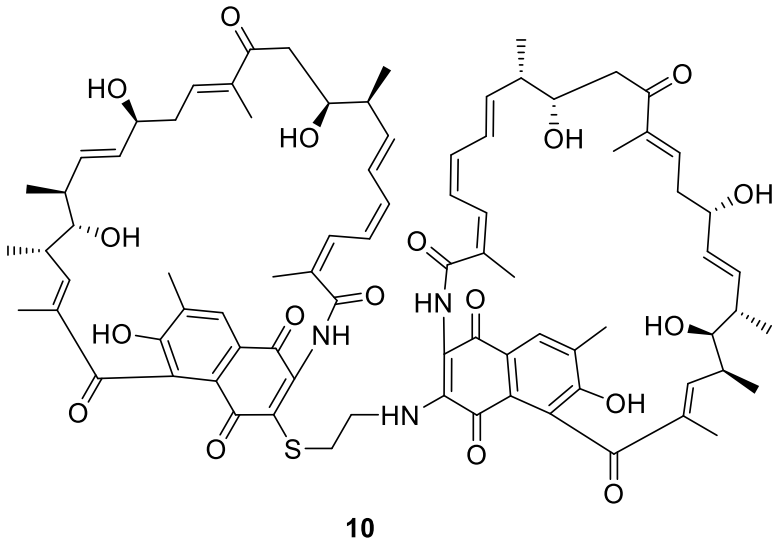

10

Figure 1.16 Chemical structures of natural products **8**-**10**.

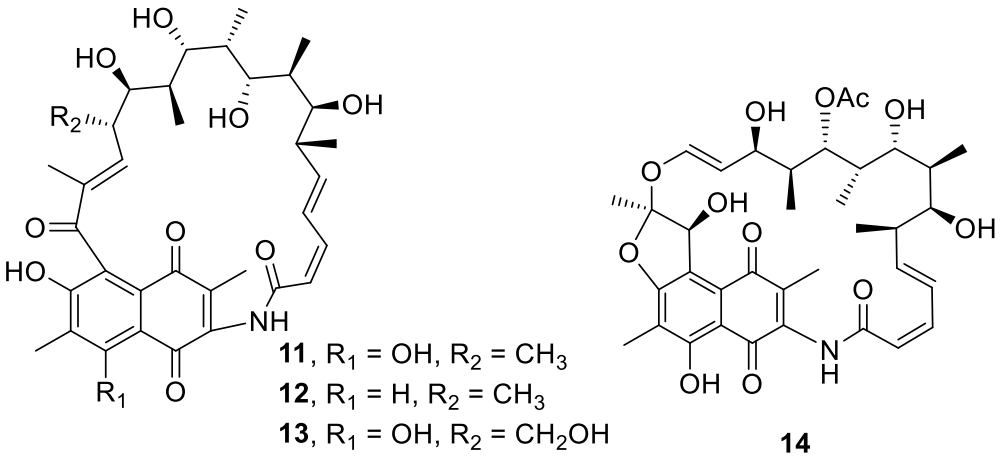

Figure 1.17 Chemical structures of natural products **11**-**14**.

This strategy has also resulted in higher yields of important antibiotics produced by non-actinomycete species (Figure 1.18). Genomic analysis of two *Vibrionaceae* strains, *Vibrio coralliiltycus* S2052 and *Photobacterium galatheae* S2753, revealed a capability for the biosynthesis of secondary metabolites and utilisation of chitin as a carbon source.[94] When the strains were cultured on chitin-containing media, several secondary metabolite BGCs were significantly up-regulated compared to culturing on glucose-containing media. The up-regulation was more significant during the stationary phase than the exponential phase for the majority of the BGCs. The production of two antibiotics andrimid (**15**) and holomycin (**16**) biosynthesised by *V. coralliiltycus* S2052 and *P. galatheae* S2753, respectively, was stimulated in media containing chitin as the sole carbon source compared to glucose-cultivated cells. In the aquaculture probiotic strain *Pseudomonas* sp. MCCB 103, comparison of different nutrients revealed that mannitol and urea were the carbon and nitrogen sources, respectively, that allowed the highest production of both the biomass and the phenazine antibiotic pyocyanin (**17**).[95] Furthermore, the combination of mannitol and urea, as well as the supplementation with mineral salts, were necessary for the maximum biomass and pyocyanin production.

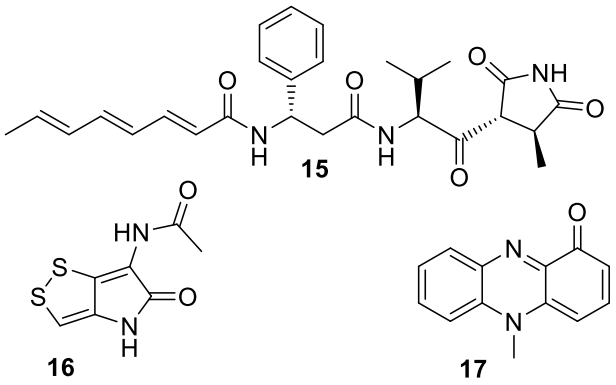

Figure 1.18 Chemical structures of natural products **15**-**17**.

The type and concentration of nutrients have been widely reported as inducers or inhibitors of fungal growth and metabolism. Nutritional manipulation has led to the isolation of novel natural products from the fungal genus *Aspergillus* (Figure 1.19). The cultivation of the sediment-derived *Aspergillus niger BRF-074* in different media led to the isolation of a novel furan ester derivative (**18**) with cytotoxic activity against HCT-116 cell line.[96] This compound was only produced in MPDB (malt peptone dextrose broth) medium and absent in others such as PDB (potato dextrose broth) and PDYB (potato dextrose yeast broth) media. Similarly, four new rubasperone derivatives (**19**-**22**) were isolated from the mangrove endophytic fungus *Aspergillus tubingensis* GX1-5E upon replacing the PDB medium with rice medium.[97] In *in vitro* cytotoxicity assays, compound **19** displayed mild activity against tumour cell lines. Genome mining and nutritional manipulation of *Aspergillus nidulans* HKI 0410 resulted in the isolation of two novel prenylated quinolin-2-one alkaloids furnished with unprecedented terpenoid side chains (**23**, **24**) from the culture grown on rice medium.[98] In *Aspergillus fumigatus*, the production of fumagillin (**25**) was increased by 15-fold when the nitrogen source sodium nitrate was replaced with L-glutamic acid, while the replacement with L-aspartic acid led to lower production even though the biomass growth was stimulated.[99]

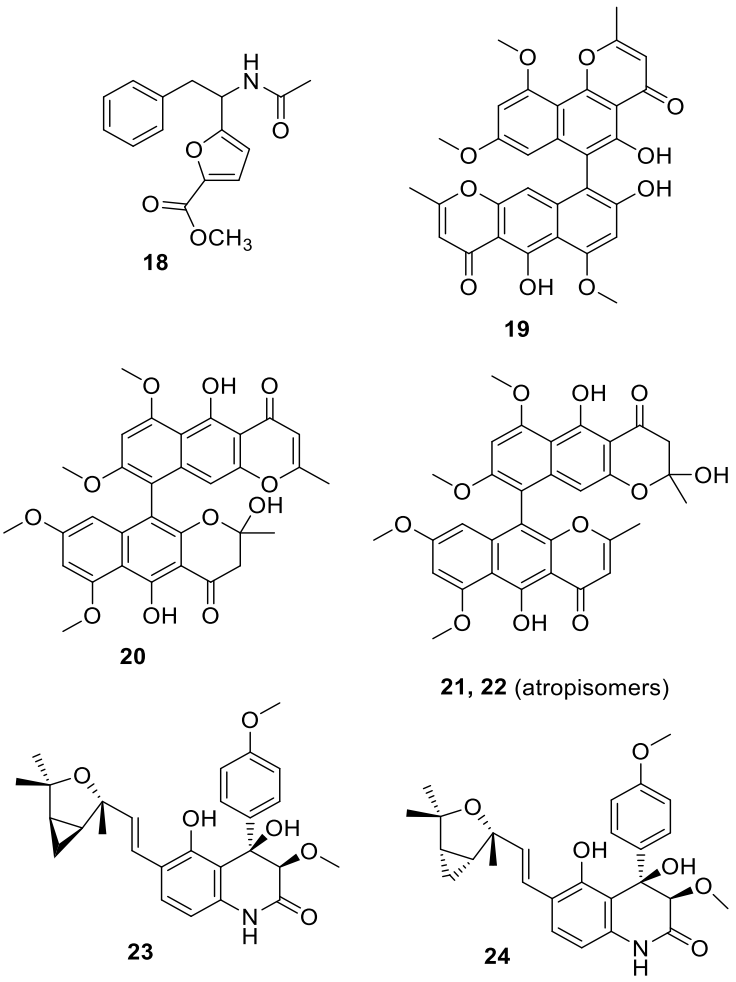

Figure 1.19 Chemical structures of natural products **18**-**24**.

The nutritional effect on the number, type and yield of produced secondary metabolites has also been reported in several *Penicillium* species (Figure 1.20). The effect of the carbon source on the production of fumagillin (**25**) was investigated in *Penicillium scabrosum*, and the maximum yield of fumagillin was reported when employing 1% glucose as a carbon source.[100] Conversely, fumagillin production was repressed by using 3% glucose in the medium, although this concentration allowed the maximum biomass growth. In *Penicillium janthinellum* and *Penicillium duclauxii*, the greatest number of metabolites was observed when the medium contained 10 % sucrose, and the number decreased in direct proportion to the increase in the sucrose concentration.[101] Nutritional manipulation was employed to improve the secondary

metabolite production in *Penicillium oxalicum* and *Penicillium citrinum*.[102] Consequently, two new alkaloids named citrinalins A (**26**) and B (**27**) were isolated and characterised from *P. citrinum*. Interestingly, the highest yield of compound **27** was observed with a nutrient-depleted medium containing only 10% of the nutrients in the original medium.

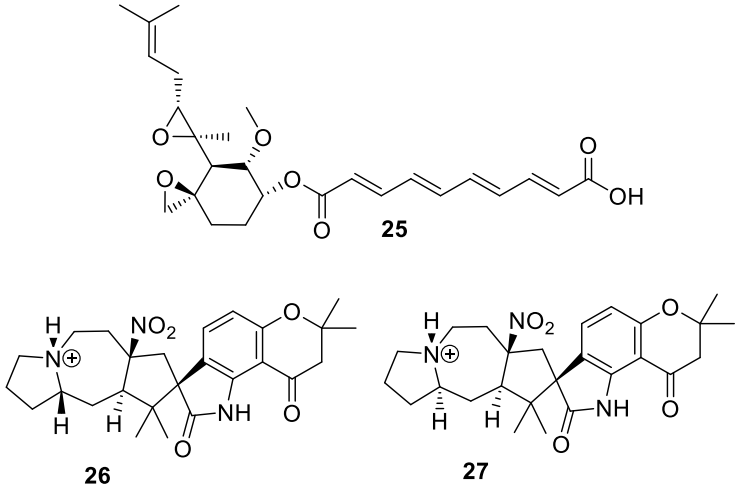

Figure 1.20 Chemical structures of natural products **25-27**.

Nutritional manipulation strategy has also been applied for the discovery of bioactive metabolites from microalgae. Lauritano et al.[103] investigated the bioactivity of crude extracts of 32 microalgal species cultivated in media containing different concentrations of nitrogen and phosphate. Two strains of the diatom *Skeletonema marinoi* (FE60 and FE6) displayed anticancer and antibacterial activities when cultured in nutrient-depleted media while no activity was observed in extracts of nutrient-rich cultures. Interestingly, the nutritional effect can be strain dependent as reported in the two strains of *S. marinoi*. Strain FE60 showed anticancer and antibacterial activities only when cultured in a nitrogen-depleted medium, while strain FE6 had antibacterial properties only when cultivated in a phosphate-depleted medium.[103] On the contrary, extracts of two microalgae, *Skeletonema costatum* and *Chaetoceros pseudocurvisetus*, presented anti-tuberculosis activity only when

cultivated in a nitrogen-rich medium and phosphate-depleted medium, while the nitrogen-depleted cultures had no activity.[104] Furthermore, the influence of the nitrogen concentration on natural product yield has been reported with the microalga *Eustigmatos* cf. *polyphem*.[105] The microalgal growth and the production of the antioxidant pigment violaxanthin (Figure 1.21, **28**) were adversely affected by either excessive or insufficient nitrogen concentrations.[105]

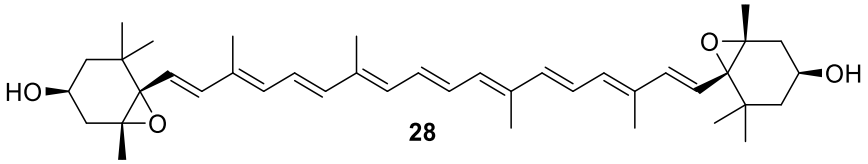

28

Figure 1.21 Chemical structure of natural product **28**.

1.3.2. Epigenetic manipulation

The epigenetic processes refer to the chemical modifications of DNA and its structural proteins without alterations in the DNA nucleotides sequence.[106] In eukaryotes, chromatin is the complex of DNA and histone proteins that are packed within the nucleus of eukaryotic cells. The nucleosome is the fundamental component of chromatin that consists of an octamer of histone proteins (H2A, H2B, H3, and H4), around which 147 base-pairs of DNA are wrapped.[107] In prokaryotes, it is hypothesised that nucleoid structure plays a similar role to eukaryotic chromatin structure being a potential target for epigenetic modifications.[108] The epigenetic processes, including the covalent modifications of DNA and amino acids on histones, are used by organisms to regulate the expression of genes involved in natural product biosynthesis.[109,110] Therefore, manipulation of these epigenetic processes has been used as a strategy for activation of cryptic secondary metabolite BGCs.[110]

Histone proteins undergo several post-translational modifications involving phosphorylation, SUMOylation, ubiquitylation, ADP-ribosylation, biotinylation,

methylation and acetylation.[111] The acetylation of lysine on histones by histone acetyltransferases (HATs) is typically associated with transcriptional activation, whereas histone deacetylases (HDACs) reverse this modification leading to transcriptional inactivation.[112–114] DNA methylation is another major epigenetic process in prokaryotes and eukaryotes, where a cytosine in CpG dinucleotides is methylated by DNA methyltransferases (DNMTs) to generate a 5-methylcytosine.[115] When the DNA is methylated, and histones are deacetylated, chromatin is condensed and inaccessible to transcription factors (heterochromatin), which is repressive regulation of transcription, while the unmethylated DNA and acetylated histones transform the chromatin into a loose transcriptionally active form known as euchromatin (Figure 1.22).[116] The chemical inhibitors of HDACs (HDACIs) and DNMTs (DNMTIs) have an activating effect upon gene transcription, and small molecule inhibitors of these enzymes are approved for clinical use as anticancer agents.[117]

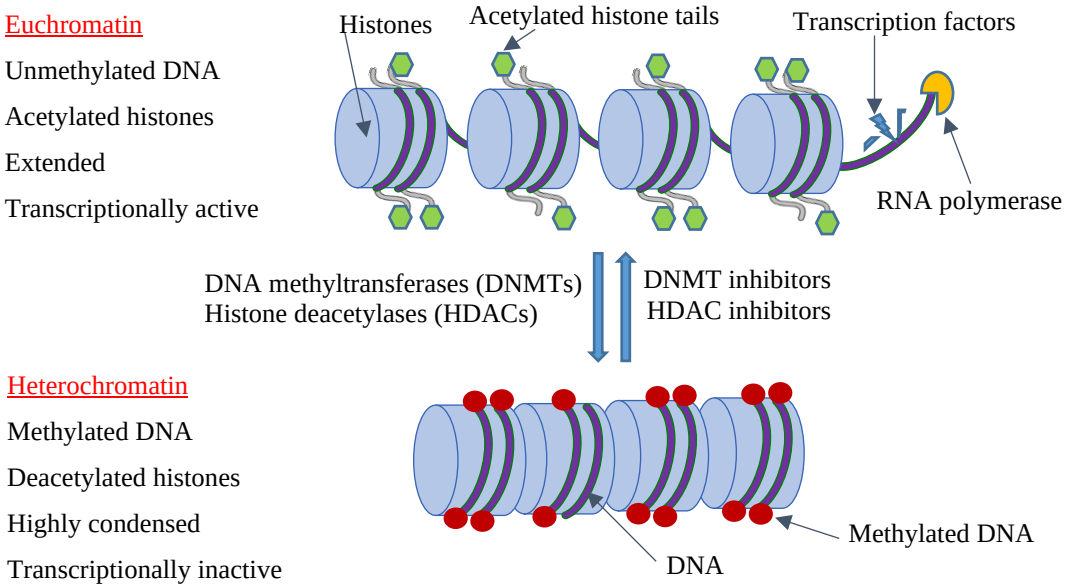

Figure 1.22 An illustrative diagram of heterochromatin and euchromatin.

The deletion of cclA, a component of the COMPASS complex responsible for catalysing histone lysine methylation, induced the expression of secondary metabolite BGCs in *Aspergillus nidulans*.[118] The induced expression of one of the BGCs, named mdp, resulted in the production of several secondary metabolites (Figure 1.23) including emodin (**29**), emodin analogues (**30-35**) and monodictyphenone (**36**). Similarly, the deletion of the hdaA gene (encoding a class II HDAC) in *Aspergillus nidulans* using a molecular genetics approach initiated the transcriptional activation of two gene clusters.[119] The up-regulation of these two gene clusters resulted in increased levels of the corresponding secondary metabolites (Figure 1.24), sterigmatocystin (**37**) and benzylpenicillin (**38**).[119,120] The role of hdaA in secondary metabolite production has also been confirmed in *Aspergillus fumigatus*.[121] However, the removal of those genes is not always possible and has been shown to be lethal to some organisms.[122] Therefore, the molecular genetics approach has been extended by using sublethal doses of chemical epigenetics supplemented to the culture without the necessity for advanced molecular genetics knowledge and equipment. The DNMT and HDAC inhibitors are the major classes of chemical epigenetic modulators utilised in natural product discovery.

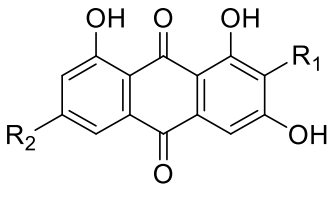

29, R_1=H, R_2 = CH_3
30, R_1 = OH, R_2 = CH_2OH
31, R_1 = NH_2, R_2 = CH_3
32, R_1 = OH, R_2 = CH_3
33, R_1 = H, R_2 = COOH
34, R_1 = H, R_2 = CH_2OH
35, R_1 = NH_2, R_2 = CH_2OH

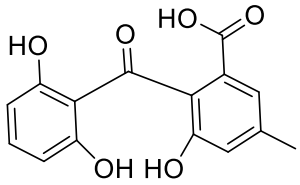

36

Figure 1.23 Chemical structures of natural products **29**-**36**.

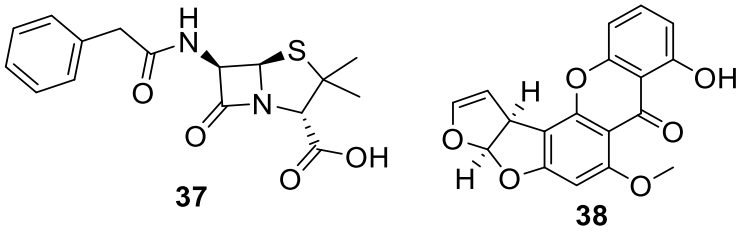

Figure 1.24 Chemical structures of natural products **37** and **38**.

1.3.2.1. HDACIs

Histone deacetylase inhibitors can be classified, based on the classification of HDACs, into zinc-dependent (class I and II) HDAC inhibitors and NAD-dependent HDAC (class III, also known as sirtuins) inhibitors. These inhibitors increase histone acetylation through the inhibition of HDACs, and consequently, increase the expression of secondary metabolite genes.[110] The amino groups of the lysines on histones are usually protonated having electrostatic interaction with the negatively charged phosphate backbone of DNA (Figure 1.25, A).[123] The acetylation of histone lysine eliminates the positive charge and weakens the electrostatic interaction between the acetylated histone and its DNA (Figure 1.25, B). This opens up access to DNA for transcription factors and other enzymes allowing for increased transcription of the previously down-regulated genes.[124]

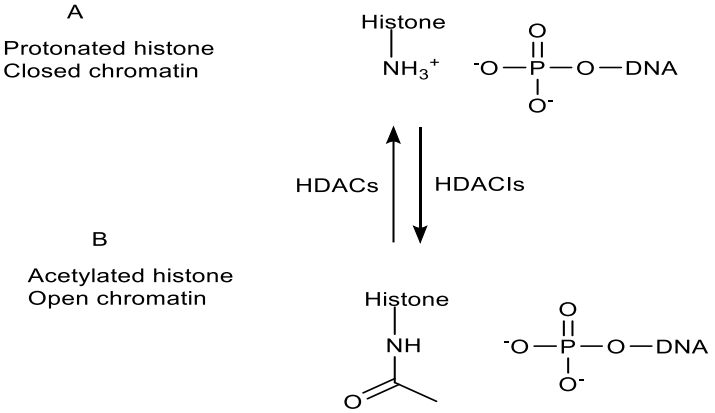

Figure 1.25 Illustration of the interaction between DNA and protonated histones (A), and DNA and acetylated histones (B).

Several zinc-dependent HDACIs including trichostatin A (TSA, **39**), suberoylanilide hydroxamic acid (vorinostat, **40**), suberohydroxamic acid (SBHA, **41**), sodium butyrate (SB, **42**) and valproic acid (VPA, **43**) have been used to induce secondary metabolite production (Figure 1.26). TSA is a natural product produced by *Streptomyces platensis* and one of the most potent zinc-dependent HDAC inhibitors.[125] This modifier demonstrated various transcriptional effects on *Saccharomyces cerevisiae*, including both the down-regulation and up-regulation of genes involved in cell cycle progression, as well as the biosynthesis of amino acids and transport and utilisation of carbohydrates.[126] Interestingly, some of these effects were detectable within 15 min of exposure to TSA.

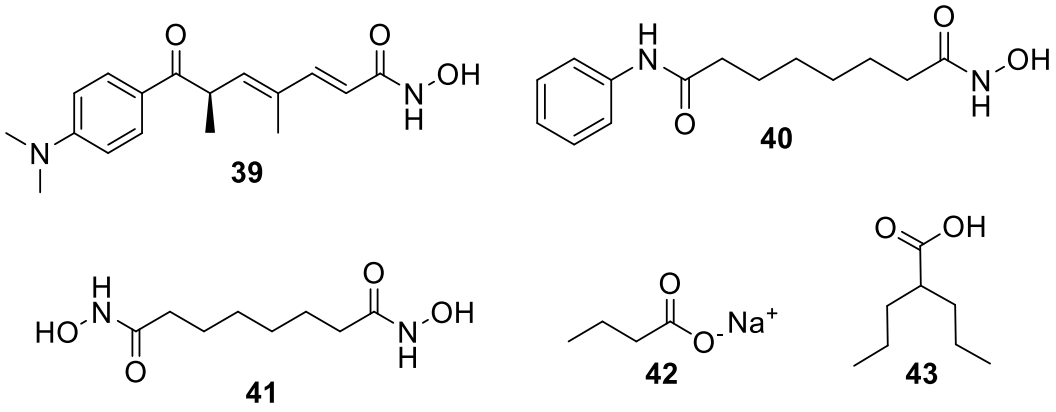

Figure 1.26 Examples of zinc-dependent HDAC inhibitors.

The fermentation of *Aspergillus* species with TSA has been employed for the activation of cryptic BGCs and the discovery of new natural products (Figure 1.27). The treatment of *Aspergillus nidulans* culture with 1 μM TSA led to the reduction of major secondary metabolites while many low-abundance metabolites were significantly increased compared to the untreated culture.[67] The author's explanation for this phenomenon was that the building blocks used in the biosynthesis of previously abundant secondary natural products were consumed by the secondary metabolite BGCs activated with the HDACI. Another explanation might be that some

repressive regulators were activated with the HDACI leading to down-regulation of some secondary metabolite genes. The activated BGCs resulted in the production of lipopeptide aldehydes known as fellutamides: fellutamide B (**44**), antibiotic 1656-G (**45**) and antibiotic 3127 (**46**). It was the first report of **44** and **45** from *Aspergillus nidulans*. However, **46** is known to be produced by *Aspergillus nidulans* but was only biosynthesised by this strain when treated with TSA. In another epigenetic manipulation study, epigenetic modification of *Aspergillus terreus* OUCMDZ-2739 with 10 μM TSA induced the secondary metabolome and led to the characterisation of four new meroterpenoids (**47**-**50**).[127]

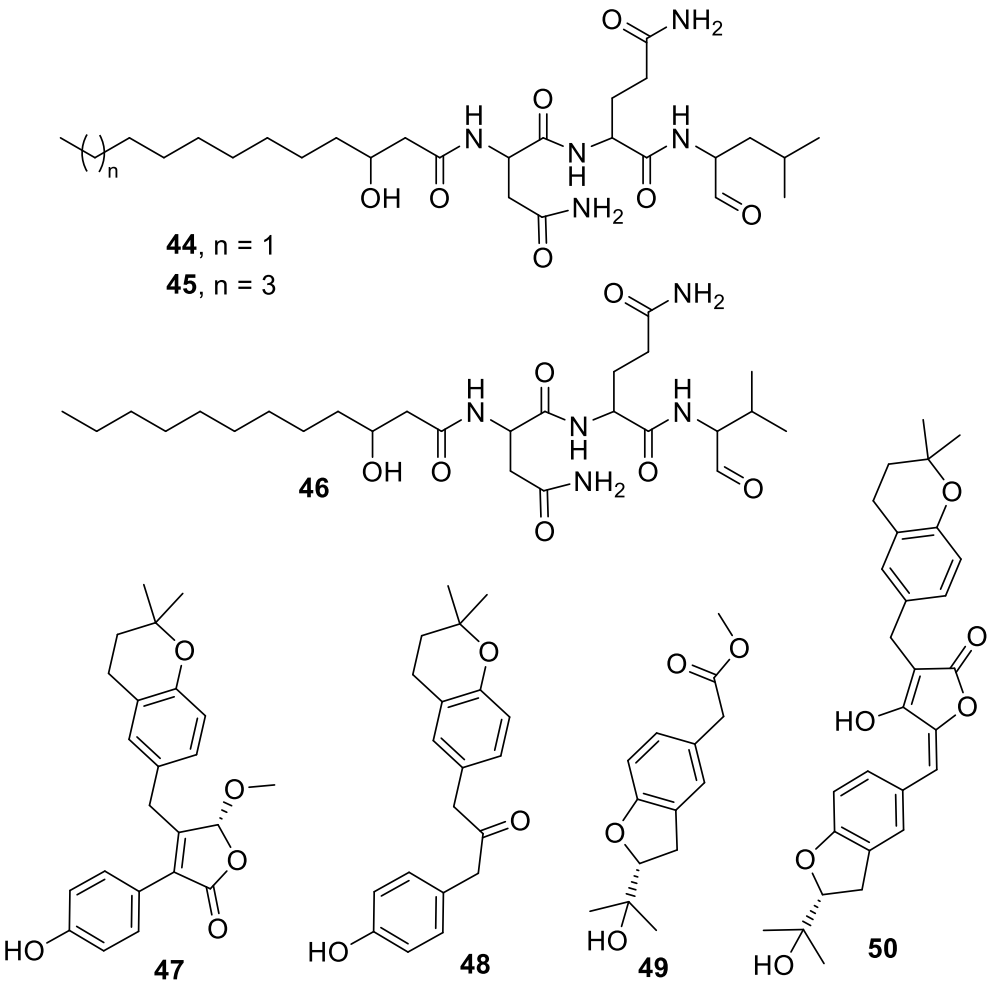

Figure 1.27 Examples of secondary metabolites (**44**-**50**) induced with TSA.

Vorinostat is a potent synthetic zinc-dependent HDACI with a similar molecular structure to TSA. The cultivation of fungal species on media containing 10-100 μM vorinostat led to the discovery of novel natural products (Figure 1.28) such as a new 4-pyridone, named nygerone A (**51**) from *Aspergillus niger*,[128] two new perylenequinones, cladochromes F (**52**) and G (**53**), from *Cladosporium cladosporioides*,[129] a novel cyclodepsipeptide, named EGM-556 (**54**), from the marine *Microascus sp.*,[130] three novel cyclodepsipeptides, desmethylisaridin E (**55**), desmethylisaridin C2 (**56**), and isaridin F (**57**) from *Beauveria feline*,[131] a new chlorinated pentacyclic polyketide, daldinone E (**58**), from *Daldinia sp.*,[132] and three new norditerpenes, aspewentins A-C (**59**-**61**) from *Aspergillus wentii*.[133]

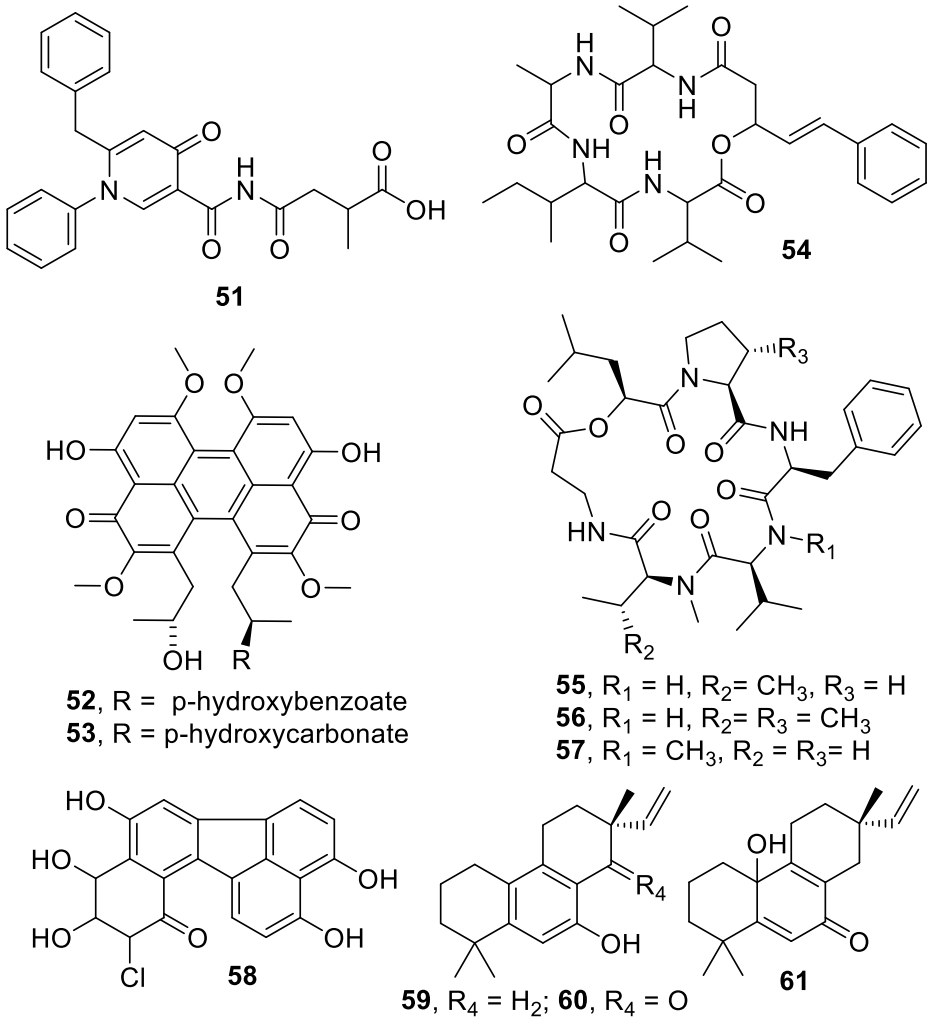

Figure 1.28 Examples of secondary metabolites (**51**-**61**) induced by vorinostat.

Another synthetic analogue of TSA is SBHA, which is an inexpensive alternative to TSA and vorinostat albeit less potent.[123] The treatment of several fungal species with SBHA resulted in substantial changes in the secondary metabolism and induced the production of new secondary metabolites (Figure 1.29) including three new prenylated tryptophan analogues (**62**–**64**) from *Torrubiella luteorostrata*,[134] two new fusaric acid derivatives from *Fusarium oxysporum* (**65**, **66**),[135] and six novel prenylated aromatic polyketides (**67-72)**[136] and two novel spironolactone polyketides (**73**, **74)** from *Chaetomium indicum*.[137]

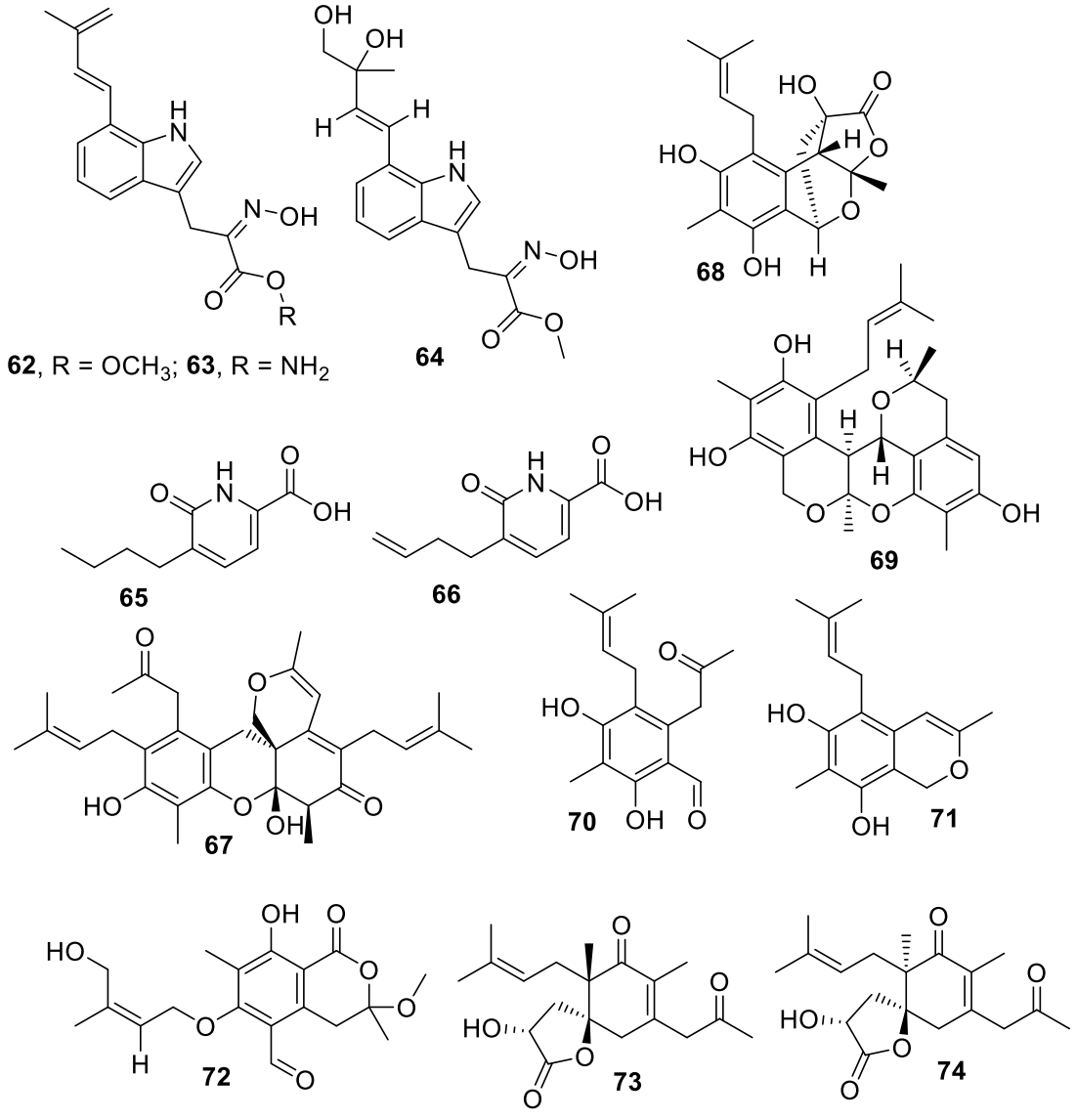

Figure 1.29 Examples of secondary metabolites induced by SBHA.

While the deletion of hdaA (encoding HDAC) in *Calcarisporium arbuscular* triggered the production of new natural products, SBHA failed to induce any changes in the metabolic profile.[138] The concentration of SBHA used in this study was not specified. Therefore, higher doses might be able to induce secondary metabolite production. Alternatively, more potent epigenetic modifiers such as vorinostat might be a better alternative to SBHA. However, it is possible that this fungal species has a defence mechanism against SBHA. This resistance has been already described in the fungal pathogen *Cochliobolus caronum*, which is responsible for the production of the HDAC inhibitor, HC-toxin. This species produces a modified HDAC that is insensitive to HDACIs such as TSA.[139] It is proposed that this modified HDAC protects this fungus from the auto-toxic effect of HC-toxin.

Butyrate is a short-chain fatty acid produced via anaerobic bacterial fermentation, and its salt, SB, has been used as an inducer of secondary metabolite gene expression.[140] For example, the pellet of *Penicillium restrictum* cultivated in the presence of 5 μM SB demonstrated significantly higher antimicrobial activity against MRSA compared to the pellet cultured in the absence of SB.[141] Moreover, the marine fungi *Leucostoma persoonia* and *Cochliobolus lunatus* were cultivated with SB resulting in the activation of cryptic BGCs and enhanced production of new metabolites (Figure 1.30).[142,143] One previously unidentified cytosporone was characterised from the *L. persoonia* culture treated with 100 μM SB and named as cytosporone R (**75**).[143] Furthermore, two new brominated resorcylic acid lactones, 5-bromozeaenol (**76**) and 3,5-dibromozeaenol (**77**), were isolated and identified from the *C. lunatus* culture containing 10 mM SB.[142] Intriguingly, it was discovered that the effect of SB was dose-dependent as the yield of metabolites was lower at concentrations below or above 10 mM. However, the high concentration of this

modifier might cause some effects other than epigenetic such as changing the pH or functioning as a carbon source.

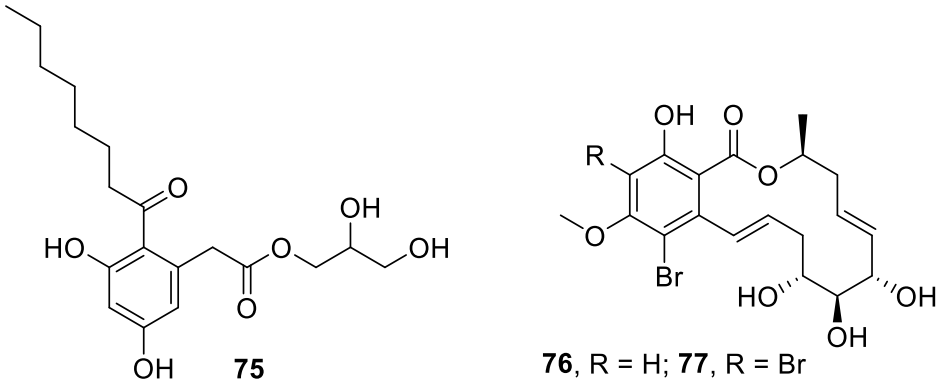

Figure 1.30 Examples of secondary metabolites induced by SB.

VPA is another short-chain fatty acid, which is an antiepileptic drug that has also been reported as an inhibitor of HDACs.[144] The cultivation of *Aspergillus clavatus* with 5 µM VPA induced the production of cytochalasin E (**78**) and pseurotin A (**79**) within 48 h of incubation (Figure 1.31).[145] Additionally, the addition of 5 µM VPA, 5µM TSA or 5 µM SB to the cultures of several fungal species including *Aspergillus clavatus* and *Penicillium alberechii* increased the antimicrobial activity of their supernatants compared to untreated samples.[141] Similarly, *Aspergillus fumigatus* GA-L7 was treated with 500 µM VPA leading to significant overexpression of the BGC involved in the biosynthesis of fumiquinazoline C (Figure 1.31, **80**).[146] This resulted in approximately ten-fold enhancement of fumiquinazoline C yield.

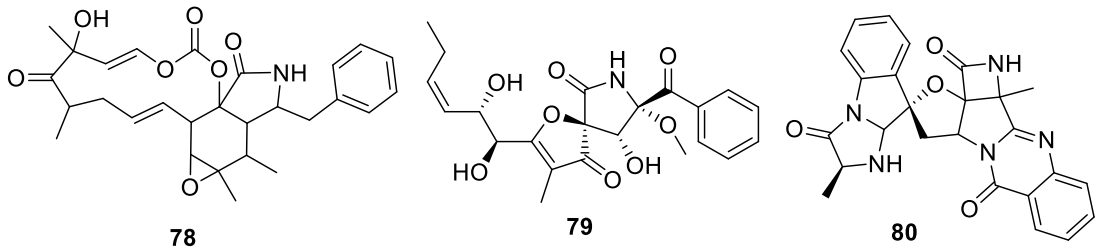

Figure 1.31 Examples of secondary metabolites induced by VPA.

The second class of HDAC inhibitors is NAD-dependent HDAC (class III) inhibitors (Figure 1.32). The best example for this class is nicotinamide (**81**) which is the amide form of vitamin B3 (nicotinic acid) and an important regulator of deacetylation caused by NAD-dependent HDAC.[147] Sirtinol (**82**) and splitomicin (**83**) are also NAD-dependent HDACIs but with poor activity and stability.[148] The treatment of *Chaetomium mollipilium* with the latter two epigenetic modifiers did not produce a detectable enhancement in the metabolic profile. Additionally, the main constituents in the extracts were degradation and hydroxylation products of sirtinol and splitomicin due to their instability.[149]

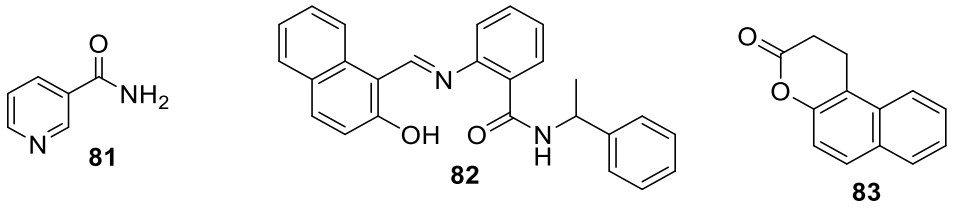

Figure 1.32 Examples of NAD-dependent HDAC inhibitors.

In contrast to modifiers **82** and **83**, epigenetic manipulation with nicotinamide led to the discovery of over ten new secondary metabolites from three fungal species (Figure 1.33). The addition of 100 µM nicotinamide to the *Chaetomium mollipilium* culture induced the secondary metabolism and resulted in the isolation of five new polyketides, mollipilins A-E (**84**-**88**).[149] Similarly, the cultivation of *Graphiopsis chlorocephala*, isolated from the medicinal plant *Paeonia lactiflora*, with 10 µM nicotinamide yielded a remarkable enhancement in secondary metabolite production.[150] This resulted in the isolation of six new benzophenones, cephalanones A-F (**89**-**94**). Moreover, the treatment of *Chaetomium cancroideum* with 50 µM nicotinamide led to the isolation of three new polyketides, chaetophenol G (**95**) and cancrolides A (**96**) and B (**97**).[151]

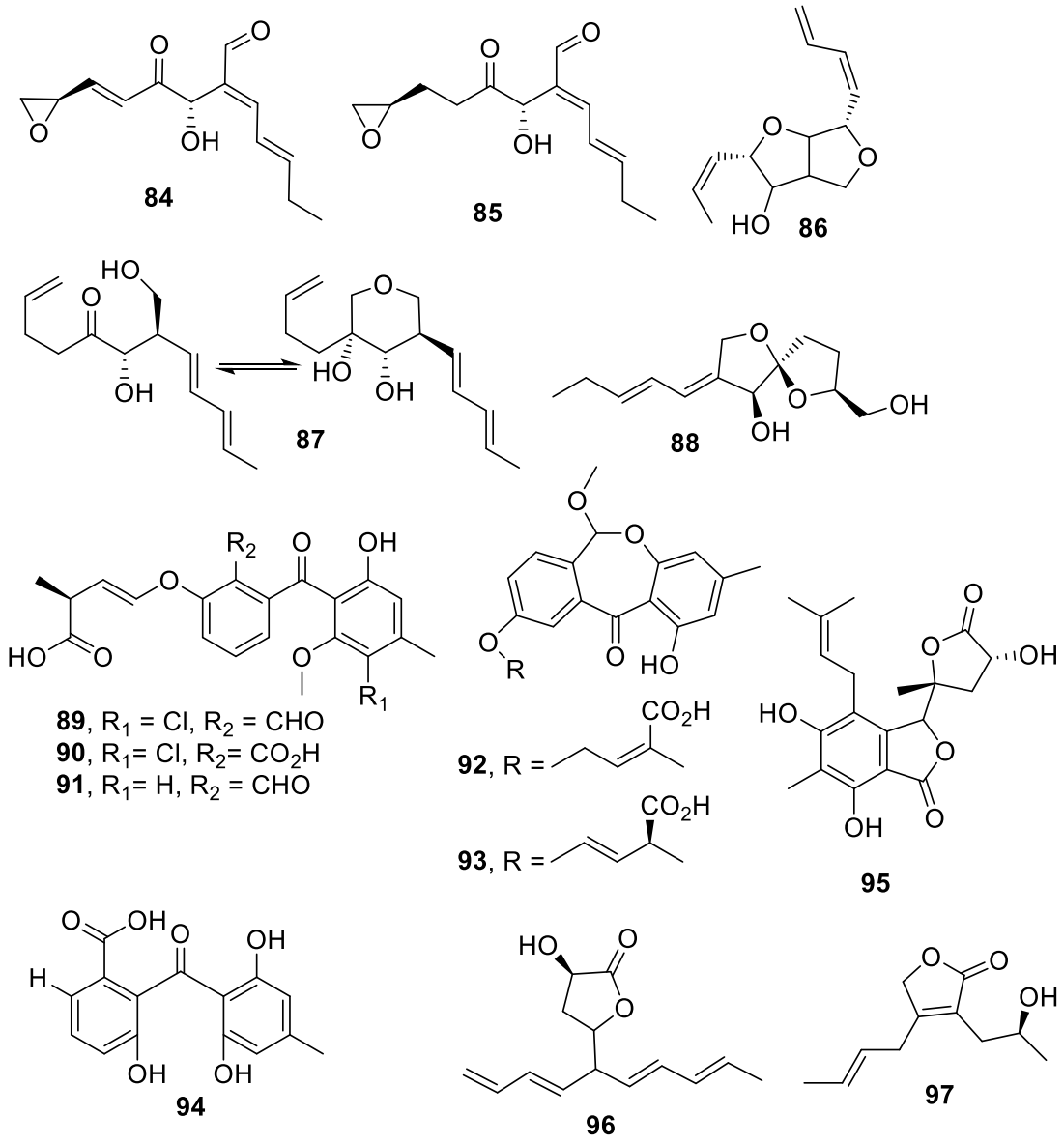

Figure 1.33 Examples of secondary metabolites induced by nicotinamide.

1.3.2.2. DNMTIs

The main classes of DNMTIs are nucleoside and non-nucleoside analogues (Figure 1.34). Nucleoside analogues contain a modified cytosine ring attached to a ribose or deoxyribose moieties, which can incorporate into DNA and cause demethylation. The most well-known examples of the nucleoside analogues are 5-azacytidine (5-AC, **98**) and its analogue decitabine (**99**), but they suffer from instability. Therefore, a better stable alternative is zebularine (**100**), albeit more

expensive.[123] The other class of DNMTIs is the non-nucleoside analogues which bind to the methyltransferase and alter the catalytic action of the enzyme rather than incorporating into DNA.[152] Examples of these inhibitors include the natural product epigallocatechin gallate (EGCG, **101**), antihypertensive hydralazine (**102**) and tryptophan derivative RG108 (**103**).

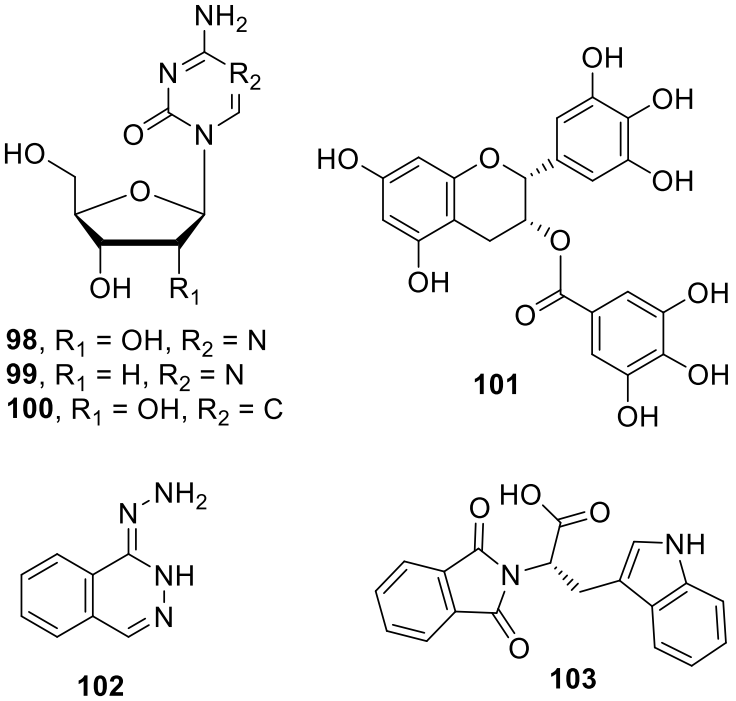

Figure 1.34 Examples of nucleoside and non-nucleoside DNMTIs.

The cultivation of the fungal species, *Neurospora crassa,* on a growth medium containing 30 µM 5-AC increased the carotenoid production by more than 700-fold in comparison to the inhibitor-free control.[153] Nevertheless, 5-AC was toxic to this fungus at doses higher than 30 µM. In another epigenetic experiment, the addition of 50 µM 5-AC to the growth medium resulted in the isolation of two new meroterpenes (**104**, **105**) from *Penicillium citreonigrum*,[154] and a new diethylene glycol phthalate ester monomer (**106**), along with several oligomers of **106**, from *Cochliobolus lunatus*[155] **(**Figure 1.35). Likewise, the treatment of the endophytic fungus, *Muscodor yucatanensis*, with 50 µM 5-AC increased the expression of secondary metabolite

genes including polyketides genes. Interestingly, this effect was even more significant in the next generation when the fungus was transferred to a new medium and studied without any subsequent exposure to 5-AC.[156] Moreover, the effect of 5-AC treatment was more profound than vorinostat on the overexpression of polyketides genes in this fungal species. The presence of 100-500 µM 5-AC in the media led to the discovery of two new polyketides (**107**, **108**) from *Diatrype disciformis*,[129] three new sesquiterpenoids (**109-111**) from *Aspergillus sydowii*,[157] and a new coumarin (**112**) from *Pestalotiopsis* (Figure 1.34).[158]

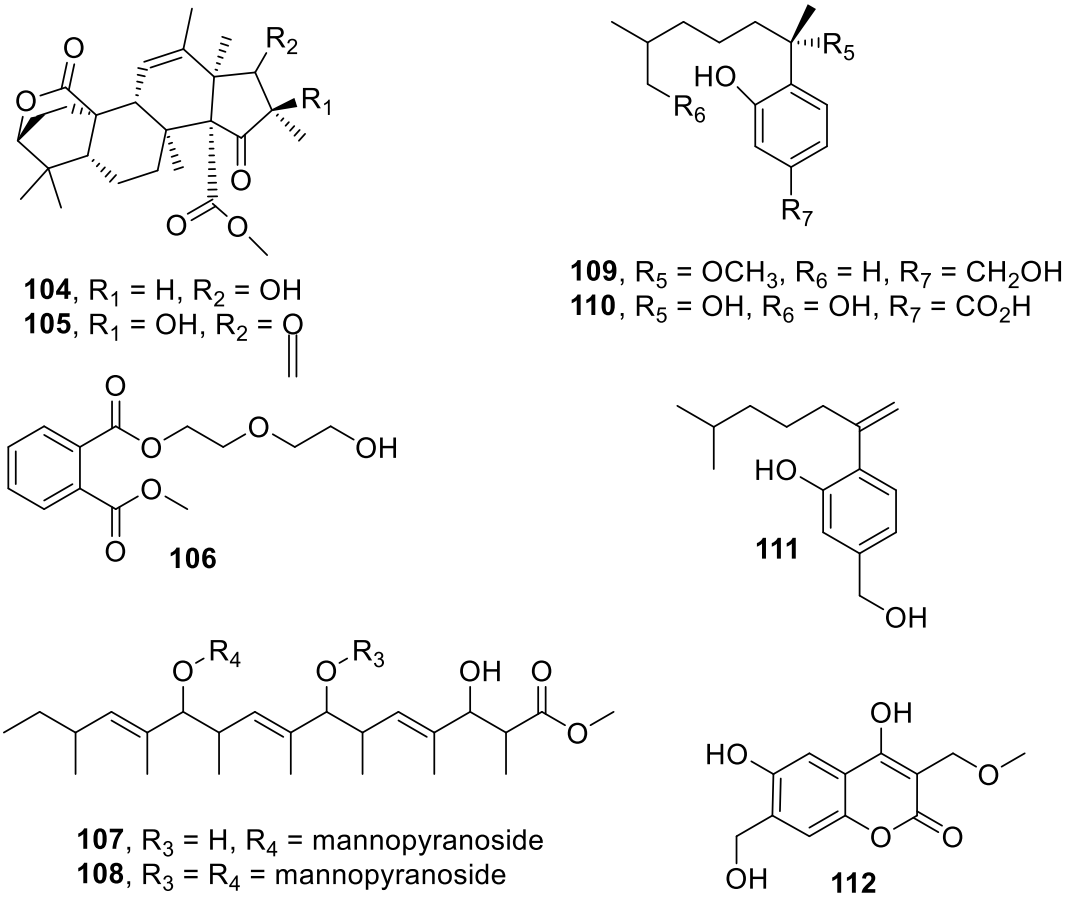

Figure 1.35 Examples of secondary metabolites induced by 5-AC.

The addition of 100 µM hydralazine to the endophytic fungus *Dothiora sp.* CF-285353 increased the production of some secondary metabolites by 32 folds and induced the production of unidentified natural products [159]. One of the induced natural

products was isolated and characterised as cyclo(phenylalanyl-prolyl) (Figure 1.36, **113**). It was demonstrated that the increase in the production of secondary metabolites was slightly higher when the epigenetic modifier was added into both seed and production cultures. Moreover, several biotransformation products of the epigenetic modifier were identified in the hydralazine-treated cultures.

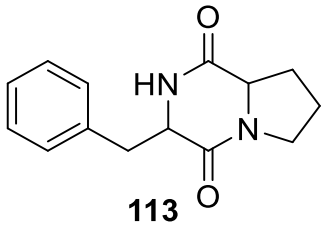

113

Figure 1.36 An example of secondary metabolites induced by hydralazine.

1.3.2.3. Concomitant epigenetic modifiers

The concomitant supplementation of HDACIs and DNMTIs has been demonstrated to have an enhanced effect on the expression of microbial secondary metabolite BGCs. The combined use of 5-AC and SBHA has led to the discovery of several novel natural products (Figure 1.37). For example, the addition of 500 µM 5-AC and 500 µM SBHA induced the secondary metabolism in the plant endophytic fungus *Pestalotiopsis acacia*.[160] This resulted in the production of a novel depside (**114**) and two new methylcoumarins (**115**, **116**). Similarly, the plant pathogen *Ustilago maydis* was shown to produce a novel glycolipid, ustilagic acid C (**117**), when cultivated in the presence of 500 µM 5-AC and 500 µM SBHA.[161] The addition of 1 mM 5-AC and 1 mM SBHA to the growth media led to the isolation of three new eremophilane-type sesquiterpenes (**118-120**) from *Aspergillus* sp. SCSIOW2[162] and a new diphenyl ether-O-glycoside (**121**) from *Aspergillus* sp. SCSIOW3.[163] Compounds **118-120** had moderate nitric oxide inhibitory activities[162] while compound **121** exhibited a protective effect against free radicals.[163]

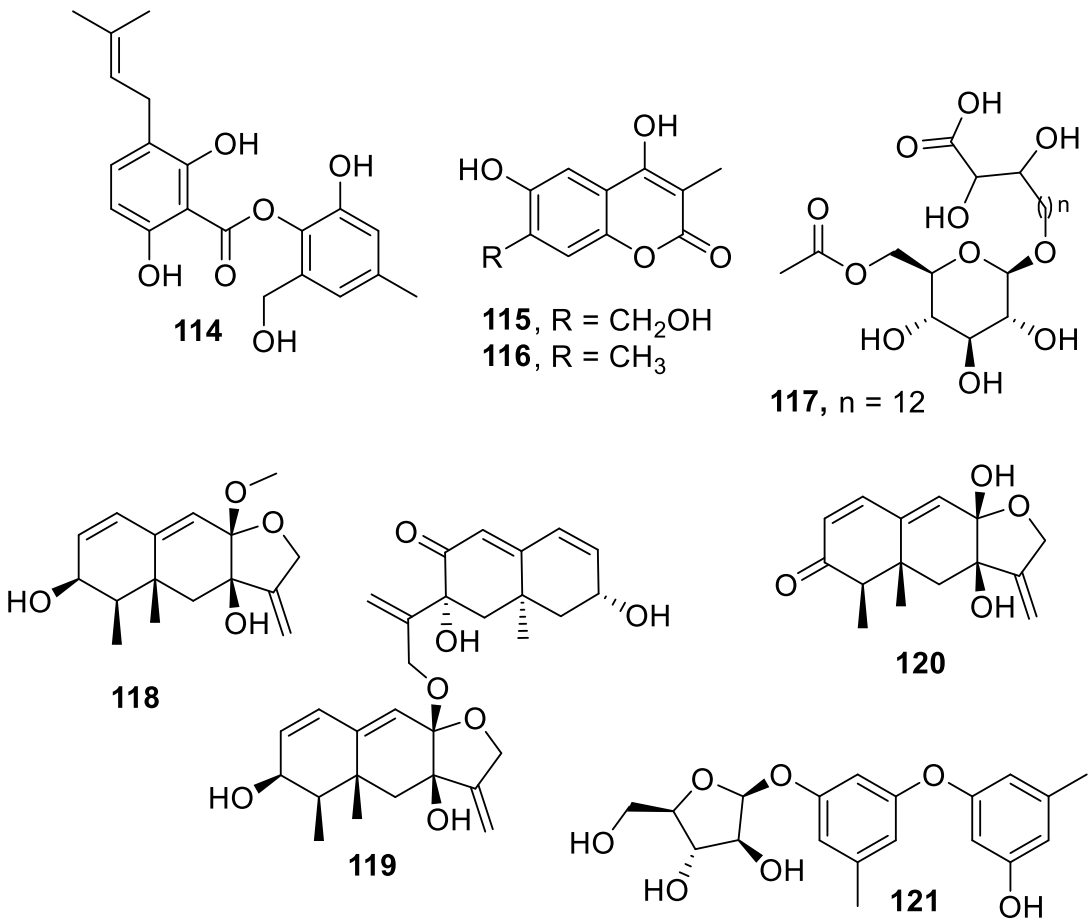

Figure 1.37 Examples of secondary metabolites induced by the concomitant use of 5-AC and SBHA.

A significant enhancement was reported in the production of fungal secondary metabolites with the combination of RG108 and SBHA, leading to the discovery of novel natural products (Figure 1.38). The presence of 100 µM RG108 and 100 µM SBHA in the growth medium resulted in the isolation of a novel polyketide with a unique tetracyclic ring system (**122**), from the entomopathogenic fungus *Isaria tenuipes*.[164] The cultivation of another entomopathogenic fungus, *Gibellula formosana,* with both 1 mM RG108 and 1 mM SBHA, either 1 mM SBHA or 1mM RG108, or modifiers-free control showed that the extract obtained from the cultivation in the presence of both epigenetic modifiers contained numerous induced compounds.[165] This resulted in the isolation of two novel ergosterols (**123**, **124**), and five new isariotin analogues (**125-129**).

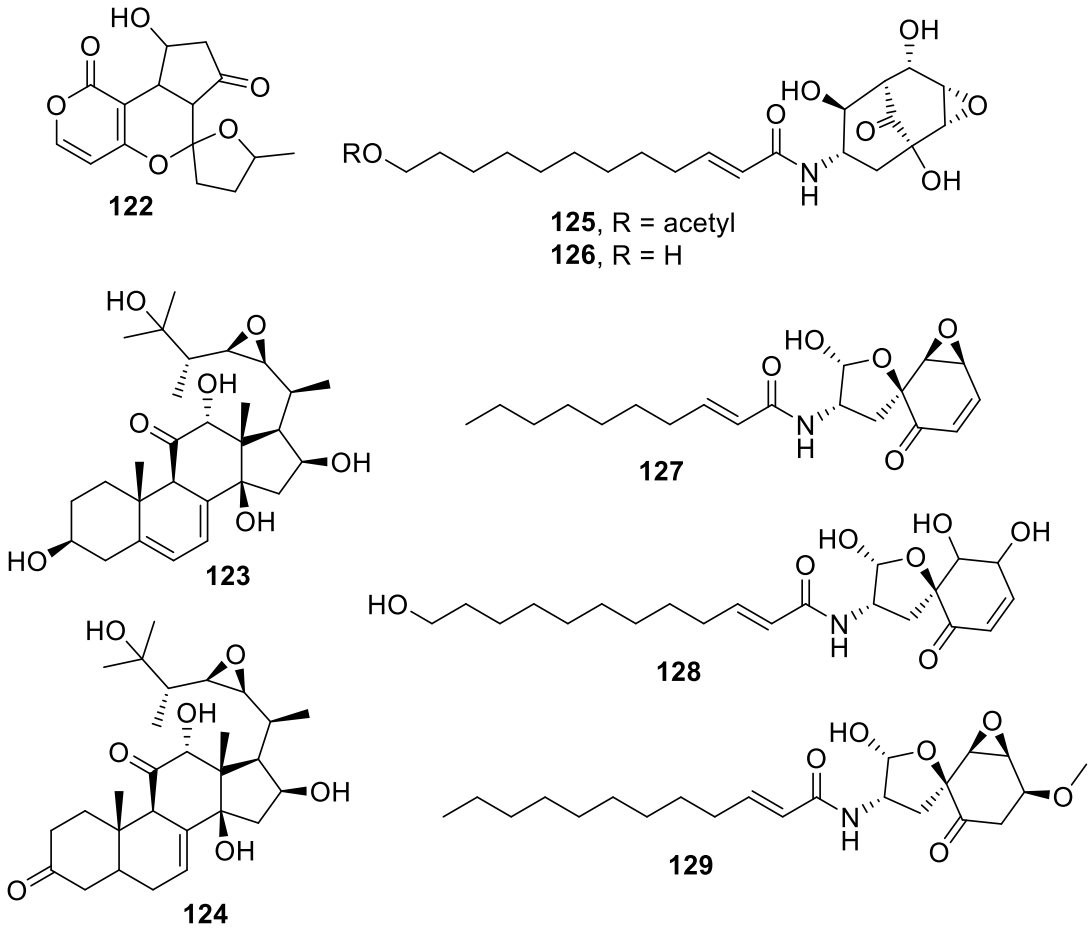

Figure 1.38 Examples of secondary metabolites induced by the concomitant use of RG108 and SBHA.

1.3.2.4. Final remarks

Natural products and their derivatives represent a high percentage of clinically approved medicines with most of the approved anti-infective and anticancer drugs originating from natural products. The sequences of microbial genomes and transcriptomes provide excellent guidance for microbial natural product discovery. Genomic and transcriptomic data of microalgae revealed several BGCs that might encode novel natural products. Transcriptomic analysis indicated that the freshwater microalga *E. gracilis* can be an appropriate candidate for natural product discovery. This microalgal species was selected based on the transcriptomic data and other criteria, as explained in the introduction of chapter 2.

Genome sequencing of several *Aspergillus* species has shown their capability to produce a great number of secondary metabolites. Additionally, nutritional and epigenetic manipulations have been demonstrated as effective strategies for the activation of cryptic BGCs in *Aspergillus*. Five *Aspergillus* species were selected for natural product discovery after genome mining based on the number of cryptic BGCs as well as other criteria, as described in chapter 4.

Finally, although most researchers have been using epigenetic modifiers for natural product discovery from eukaryotes, particularly fungi, some epigenetic modifiers have shown transcriptional effects in bacteria. For example, the treatment of *Streptomyces coelicolor* with HDACIs resulted in the upregulation of certain biosynthetic pathways, including the pigmented polyketides and non-ribosomal peptides.[108] Actinomycete bacteria represent a prolific source of natural products and might be an appropriate candidate for natural product discovery through epigenetic manipulation. Therefore, two actinomycete bacteria were employed for the epigenetic experiments, as described in chapter 5.

1.4. Aims

- Activation of cryptic NRPSs and PKSs in *E. gracilis* through nutritional and epigenetic manipulation.
- Activation of cryptic BGCs in *Aspergillus* through nutritional and epigenetic manipulation.
- Activation of cryptic BGCs in actinomycete bacteria through epigenetic manipulation.
- Isolation and characterisation of induced natural products.
- Investigation of the biological activity of induced natural products.

Chapter Two

2. Nutritional and epigenetic manipulation in *E. gracilis*

2.1. Introduction

Microalgae are microscopic photosynthetic organisms that contain one cell (unicellular) and are commonly found in freshwater and marine systems. Microalgae have conventionally been employed in ecological, biogeochemical, evolutionary, and biological applications.[166] However, the analysis of microalgal genomes and transcriptomes has shown that many microalgae contain genes encoding PKSs and NRPSs that might represent an untapped source of novel natural products (Figure 2.1). The genome and transcriptome data can be used as guidance to select the best microalgal candidate for natural product discovery. For example, *Coccomyxa subellipsoidea* has ten possible PKSs, whereas *Chlorella variabilis* has only two PKSs and a single NRPS.[52] Another microalgal species, *Chlamydomonas reinhardtii*, has been shown to contain a single PKS that is involved in the last condensation step of cell-wall fatty acids identified as mycolic acids.[167,168]

Recently, transcriptome analysis has revealed that *Euglena gracilis* var. *saccharophila* Klebs (strain 1224/7a) has 19 putative NRPSs and 14 PKSs with their corresponding natural products remain to be identified.[169,170] Although *E. gracilis* is the most studied species of *Euglena*; no NRPs or PKs have been isolated from this species.[171] This offers a strong motivation to explore the secondary metabolome of *E. gracilis*. *E. gracilis* is a freshwater microalga that is able to grow in a wide range of conditions: photoautotrophically (using light as an energy source and carbon dioxide as a carbon source), heterotrophically (using an external carbon source), or mixotrophically (combining both modes).[172] The metabolic capability of *E. gracilis*

varies dramatically with alterations of growth conditions, and the gene silencing mechanisms in *E. gracilis* involves epigenetic modifications such as histone methylation, histone deacetylation and DNA methylation.[170] Yuji et al.[173] reported significant effects of nitrogen and carbon sources on *E. gracilis* growth with some amino acids causing complete growth inhibition. Interestingly, the toxic effect of some amino acids was antagonised by the addition of other nitrogen and carbon sources suggesting that different nitrogen and carbon sources at different ratios have significant effects on the metabolism of *E. gracilis*. Therefore, *E. gracilis* appears as an appropriate candidate for natural product discovery through nutritional and epigenetic manipulation.

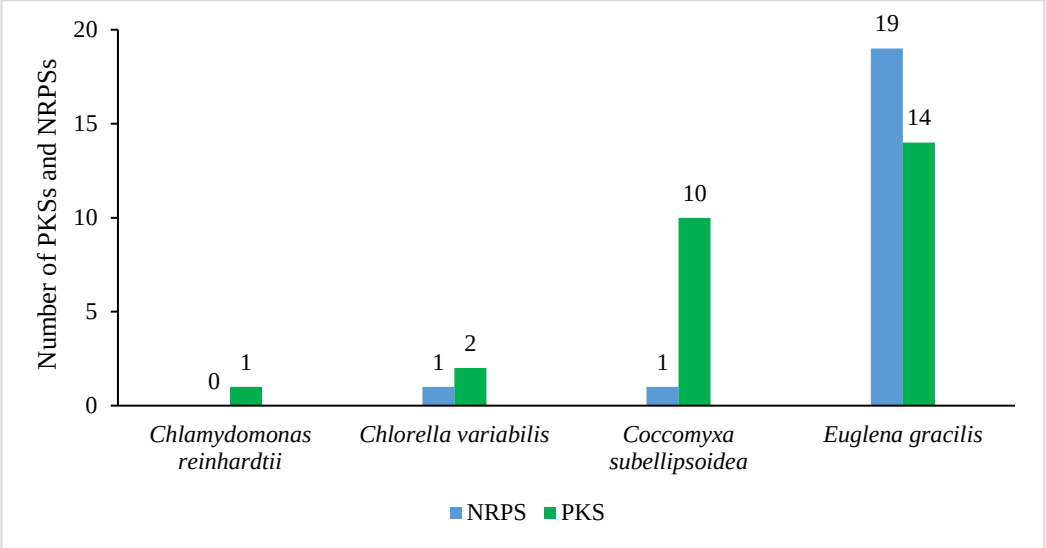

Figure 2.1 Examples of microalgal PKSs and NRPSs.

2.2. Results and discussion

2.2.1. Acidic and basic extracts of *E. gracilis* in EG:JM

The ethyl acetate (EtOAc) extracts of *E. gracilis* cultivated in EG:JM (1:1, *Euglena gracilis* medium:Jaworski's medium) were treated with HCl or NaOH and compared to the medium control (EG:JM). The chromatograms acquired on the LC-

PDA-MS contained a few peaks, which are present in both culture extracts and medium extracts (Figure 2.2). The acid-base extraction was performed to simplify the metabolic profiles and assist the extraction of any acidic and basic minor metabolites. However, based on the LC-PDA-MS results, the extraction protocol used for these samples failed to extract any detectable natural products either from the supernatant or the cells. It is possible that some secondary metabolites are neutral compounds not ionising with acids or bases. Hence, they were not extracted with HCl nor with NaOH.

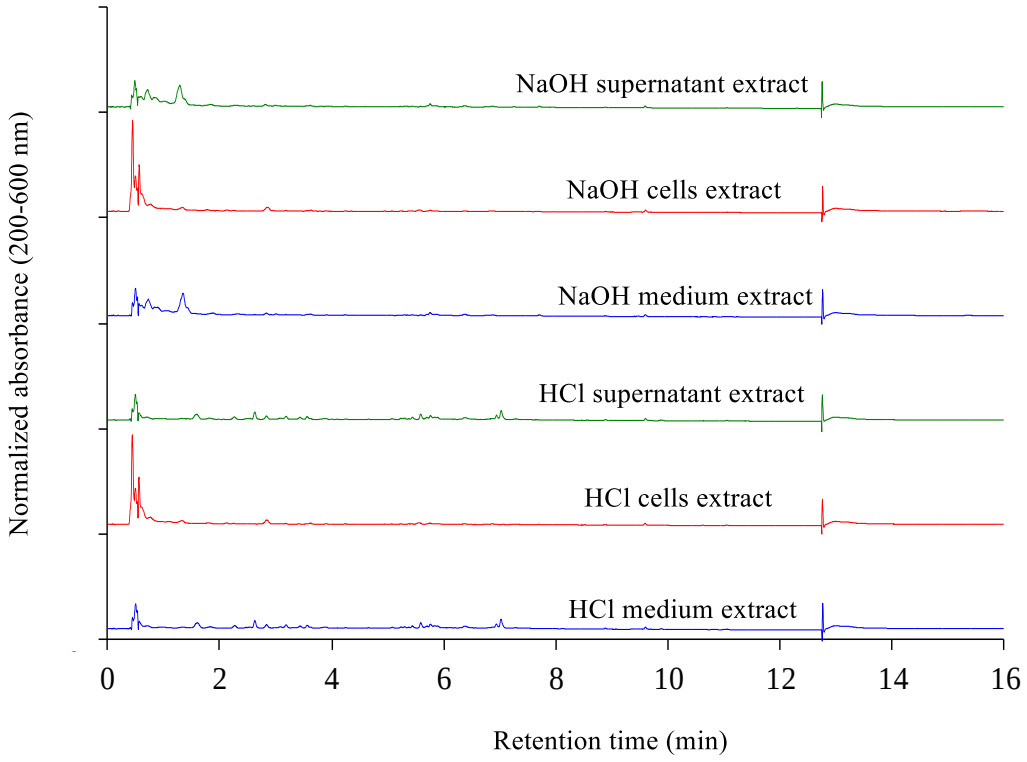

Figure 2.2 TACs (200-600 nm; 100 × 2.1mm, 2.6µm Kinetex C18 column; 0.5 mL/min flow rate; 20-100% acetonitrile over 10 min) of *E. gracilis* extracts cultivated in EG:JM compared to the medium control extracts.

2.2.2. Nutritional and epigenetic manipulation

It is well known that amino acids are essential as nutrients for microbial growth, in addition to their function as precursors for secondary metabolites (e.g. NRPs). Moreover, it has been reported that amino acids can inhibit or induce the biosynthesis

of secondary metabolites. For instance, methionine and norleucine induced the production of cephalosporins by *Cephalosporium* sp.[174] In contrast, lysine inhibited benzylpenicillin biosynthesis in *Penicillium chrysogenum* and was demonstrated to be involved in the regulation of penicillin biosynthesis in low and high-producing strains.[175,176] Moreover, fumagillin production by *Aspergillus fumigatus* was increased by 15-fold with L-glutamic acid compared to sodium nitrate while L-aspartic acid was inferior to sodium nitrate, even though growth was stimulated.[99] Based on the paper published by Yuji et al.[173] about the utilisation and toxicity of exogenous amino acids in *E. gracilis*, it was hypothesised that amino acids might have negative or positive effects on the secondary metabolism of *Euglena*. EG:JM medium might contain amino acids impairing secondary metabolite biosynthesis and others with a positive impact but in small amounts not enough for the production of secondary metabolites. Therefore, individual amino acids were used to replace the nitrogen source in EG:JM medium.

2.2.2.1. L-Glutamate as a nitrogen source

Glutamate (Glu) was selected as a nitrogen source as it had been reported by Yuji et al.[173] as the most effective nutrient among 21 amino acids. Figure 2.3 shows the growth rate of *E. gracilis* in three different media (synthetic medium, complex medium, and synthetic medium + 30 mM Glu) cultivated in the light, and one medium (synthetic medium + 30 mM Glu supplemented with glucose (Glc) as a carbon source) cultivated in the dark. Complex medium, synthetic medium + 30 mM Glu and synthetic medium + 30 mM Glu + Glc were efficient media. The cultures in these three media appeared healthy with a high growth rate and cell density. The culture in the dark had the highest growth rate reaching the stationary phase by the fourth day of

incubation, followed by the complex medium and synthetic medium + 30 mM Glu reaching the stationary phase by the seventh day. The synthetic medium had the slowest growth rate and the lowest cell density even after 13 days of incubation.

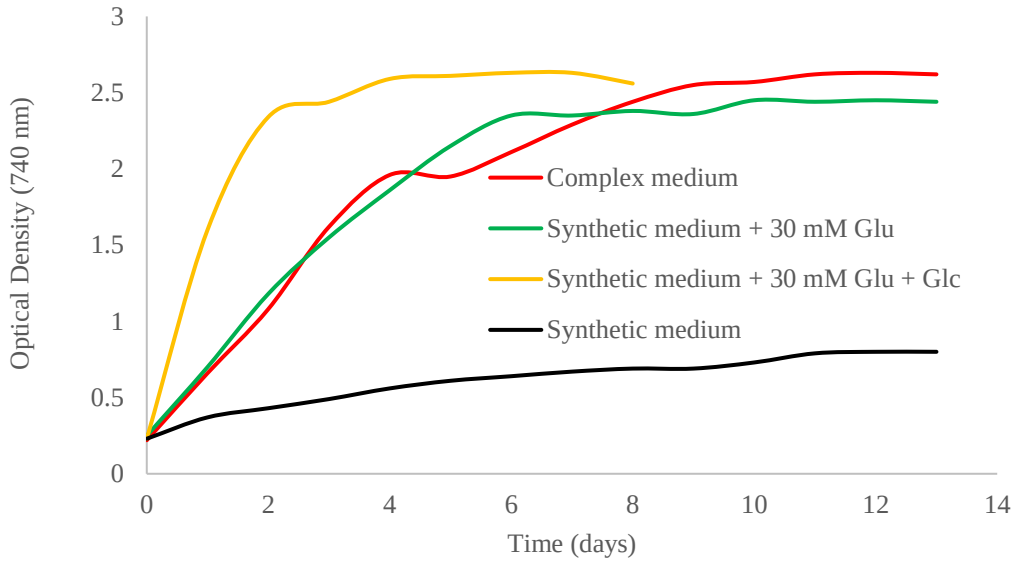

Figure 2.3 Comparison of the growth rate of *E. gracilis* in complex medium, synthetic medium + 30 mM Glu, synthetic medium + 30 mM Glu + Glc and synthetic medium.

2.2.2.2. Metabolic profiles of *E. gracilis* in modified media

E. gracilis was cultivated in the modified media mentioned above, and the growth was monitored using a photobioreactor. Each culture was harvested at the stationary phase, and the cell biomass and supernatant were extracted separately with EtOAc and analysed by HPLC-UV using a 50-100% acetonitrile/water gradient over 22 min. The HPLC traces (at 270 nm) of cell extracts presented a distinct difference between the cultures supplemented with Glu and those without Glu (Figure 2.4). The former showed a major peak at 4.22 min retention time that is hardly detected and completely absent in complex medium and synthetic medium, respectively. Moreover, the intensity of the peak at 4.22 min was at least three times higher in the culture cultivated in the light compared to cultivation in the dark in the presence of Glc as a carbon source, even though the cell density was slightly higher in the latter. Therefore,

in addition to the effect of the nitrogen source on metabolite production, the metabolites are produced in higher amounts in the photoautotrophic culture compared to heterotrophic. The metabolites are likely to be intracellular as they were not detected in the supernatant.

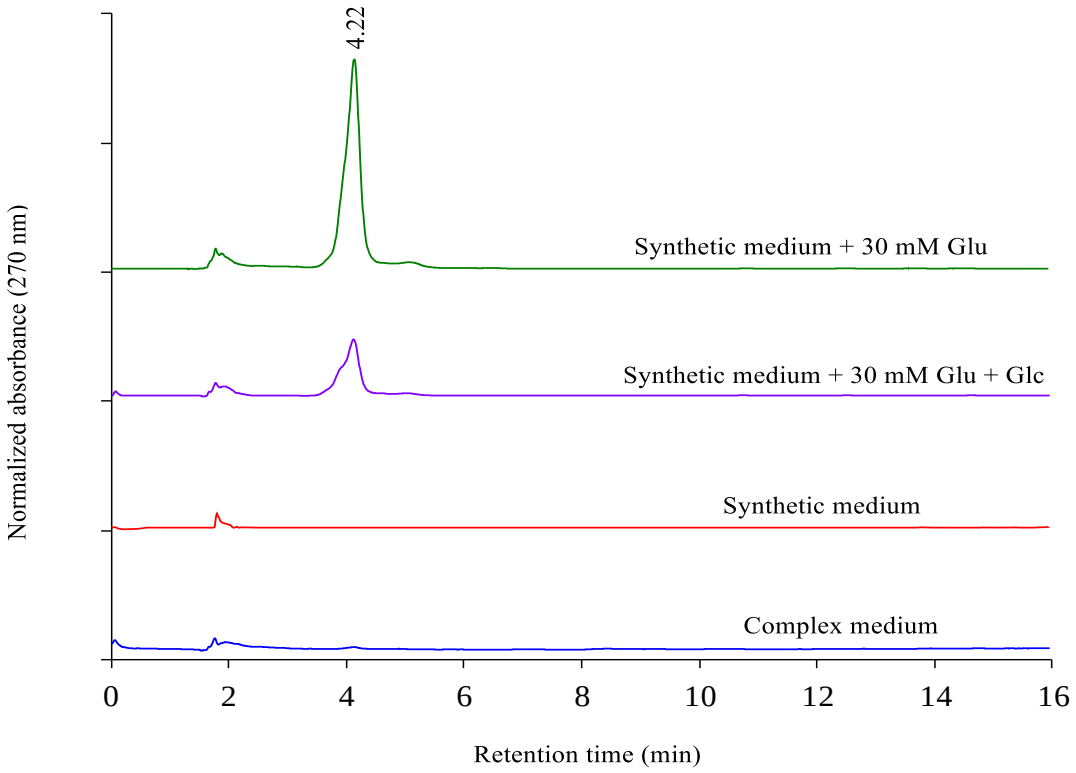

Figure 2.4 HPLC traces (at 270 nm; 150 × 4.6mm, 5µm Agilent C18 column; 1 mL/min flow rate; 50-100% acetonitrile over 22 min) of *E. gracilis* cell extracts cultivated in synthetic medium + 30 mM Glu, synthetic medium + 30 mM Glu + Glc, synthetic medium and complex medium.

LC-PDA-MS analysis of the *E. gracilis* extract (cultivated in synthetic medium + 30 mM Glu) using a 20-100% acetonitrile/water gradient over 10 min exhibited an improved separation (Figure 2.5) indicating that the peak observed on the HPLC trace contains five separated metabolites (**A-E**) along with other mixtures (**M1-M2**). This improved separation might be due to the change of the gradient system, the column, the flow rate, or the LC system. The UV profiles of all metabolites presented maxima of absorbance at 260, 269 and 280 nm, suggesting a conjugated triene substructure (Figure 2.6). The ionisation and fragmentation patterns were also identical for all

metabolites showing $[M + Na]^+$ and two characteristic protonated product ions in the positive ion mode (Figure 2.7) corresponding to a neutral loss of methanol (MeOH, 32 Da) and water (H_2O, 18 Da) and a loss of MeOH (32 Da). In the negative ion mode, $[M - H]^-$ and $[M + Cl]^-$ were detected for all metabolites (Figure 2.8).

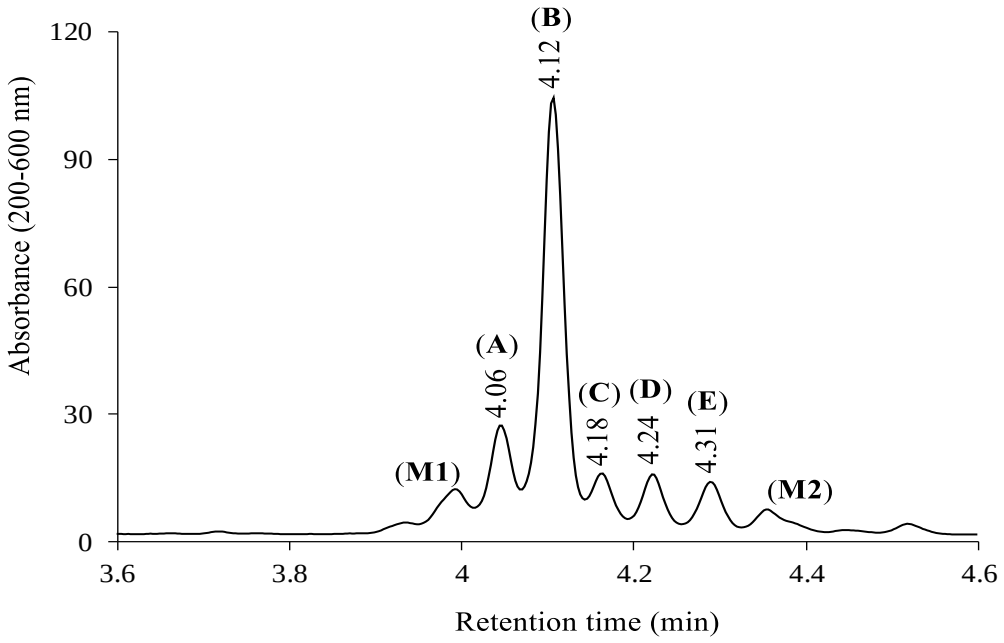

Figure 2.5 Total absorbance chromatogram (200-600 nm; 100 × 2.1mm, 2.6µm Kinetex C18 column; 0.5 mL/min flow rate; 20-100% acetonitrile over 10 min) of *E. gracilis* extract cultivated in synthetic medium + 30 mM Glu.

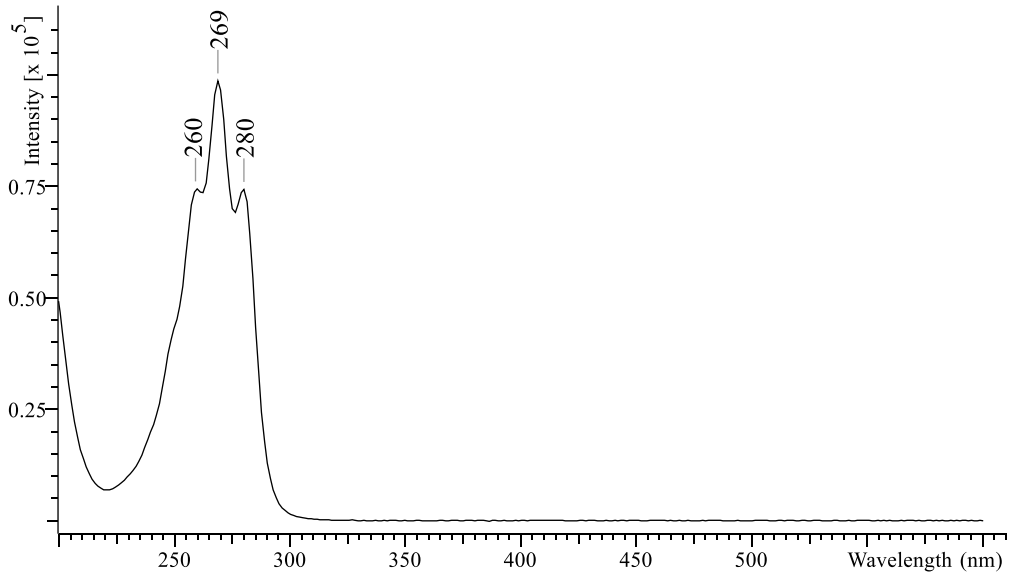

Figure 2.6 UV profile of *E. gracilis* metabolites showing maxima of absorbance at 260, 269 and 280 nm.

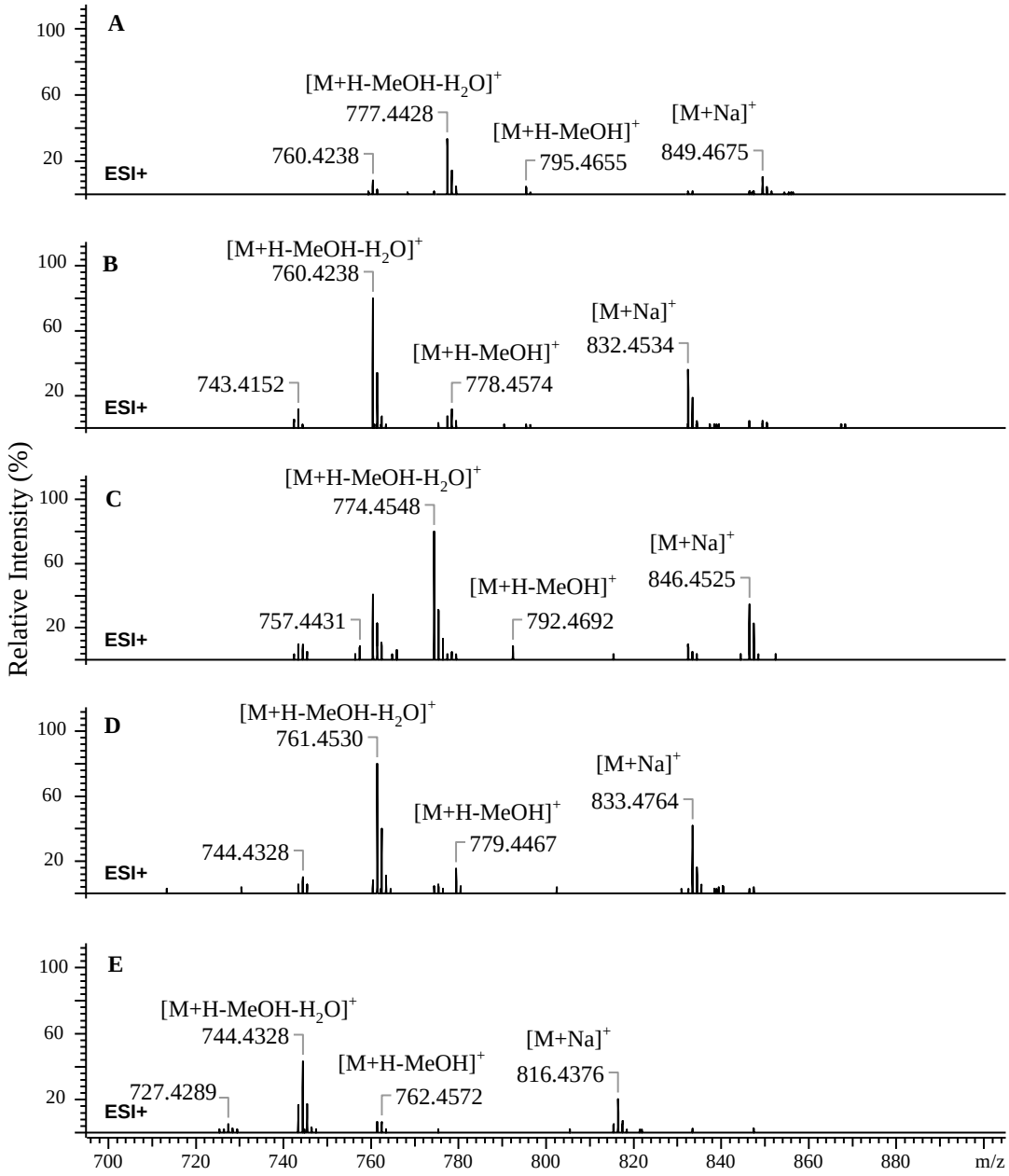

Figure 2.7 Positive ion mode MS spectra of **A**-**E** showing $[M+Na]^+$ and two characteristic protonated product ions corresponding to a neutral loss of 50 Da (loss of H_2O and MeOH) and 32 Da (loss of MeOH).

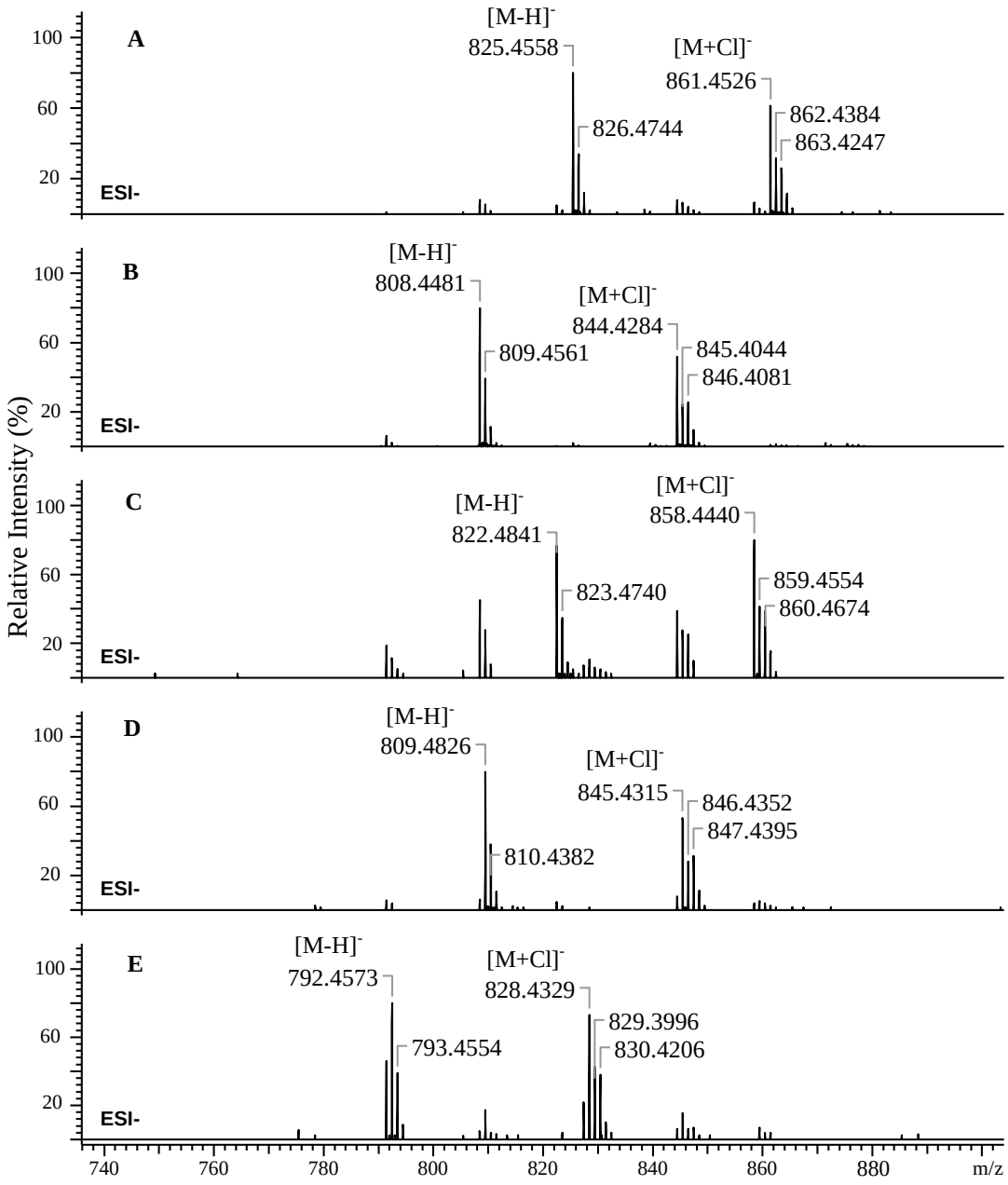

Figure 2.8 Negative ion mode MS spectra of **A-E** showing $[M-H]^-$ and $[M+Cl]^-$.

2.2.2.3. Extraction of *E. gracilis* with methanol versus ethyl acetate

To investigate the best method for cell disruption and extraction, *E. gracilis* cells were harvested by centrifugation from 10 mL cultures and suspended in MeOH or EtOAc. MeOH was effective in cell disruption resulting in the release of the cell contents in the solvent without any additional disruption methods while the cells suspended in EtOAc formed cell clumps retaining their contents inside the cells (Figure 2.9). Therefore, EtOAc requires additional disruption methods to enable cell lysis and release of intracellular components. To compare the extraction with MeOH to EtOAc assisted by a mechanical disruption method, *E. gracilis* cells were harvested from 10 mL cultures and extracted with MeOH or ground in liquid nitrogen and extracted with EtOAc. Both methods appeared effective in cell disruption, releasing the contents of the cells in the employed solvent. After evaporation of the solvents, the residues were dissolved in MeOH and analysed by LC-PDA-MS. Comparing the intensity of the metabolites in MeOH extract to EtOAc extract, it was apparent that MeOH resulted in extraction of a larger amount of the metabolites (Figure 2.10). This could be attributed to the solubility of the metabolites or the cell lysis efficiency of the disruption method.

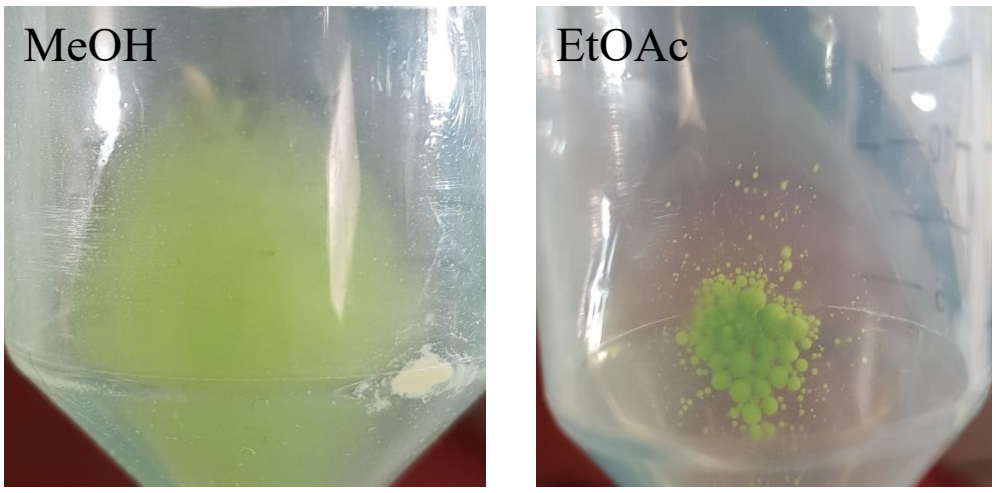

Figure 2.9 *E. gracilis* cells suspended in MeOH or EtOAc.

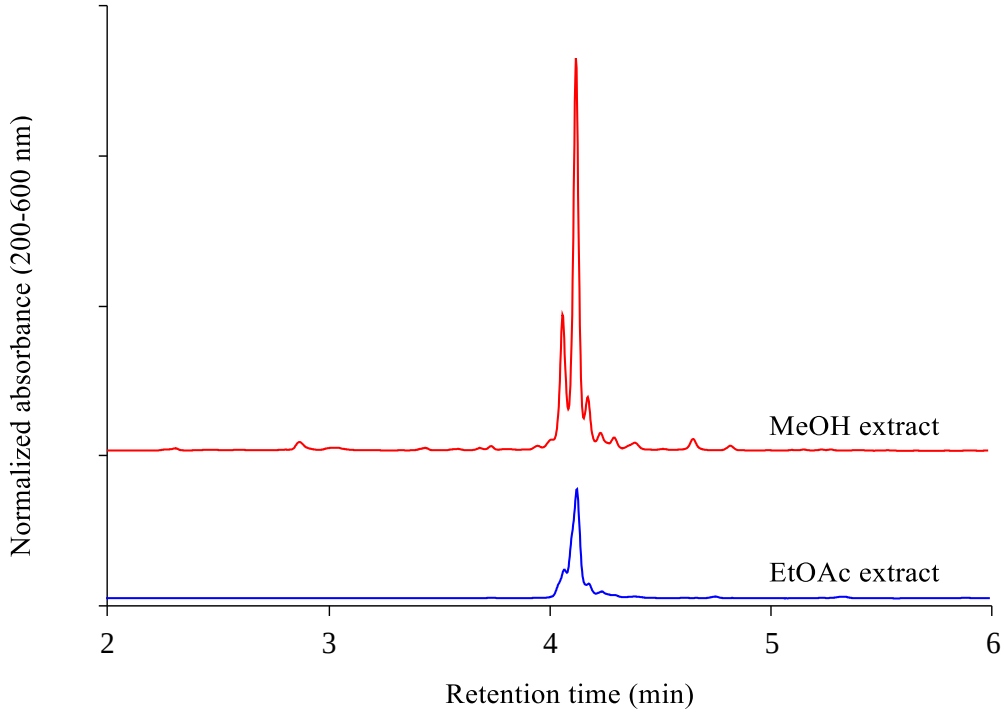

Figure 2.10 Comparative TAC (200-600 nm; 100 × 2.1mm, 2.6µm Kinetex C18 column; 0.5 mL/min flow rate; 20-100% acetonitrile over 10 min) of *E. gracilis* cells extracted with MeOH (MeOH extract) and EtOAc (EtOAc extract).

2.2.2.4. Three-litre culture and method development for separation

E. gracilis cells were harvested from three-litre culture cultivated in synthetic medium + 30 mM Glu and extracted with 90% MeOH.[177] Since *E. gracilis* contains substantial amounts of lipids and pigments, the aqueous MeOH was partitioned with hexane.[177] This transfers most of the lipids and pigments from the aqueous MeOH layer to the hexane layer (Figure 2.11). After partitioning, the aqueous MeOH residue was fractionated on flash chromatography, and the fractions containing the target metabolites were used to develop an HPLC method for separation and purification. The best separation was achieved with a 34% isocratic system of acetonitrile in water without additives and a flow rate of 3 mL/min. However, the purified amount from this culture was insufficient for structure elucidation. In addition to the low yield, a

good amount of the target metabolites was wasted during method development. Moreover, although the extraction protocol is useful for lipids and pigments removal, it might also remove some amount of the target metabolites if they are soluble in hexane.

Figure 2.11 *E. gracilis* cell extract partitioned between 90% MeOH (aqueous MeOH layer) and pure hexane (hexane layer) in a separating funnel.

2.2.2.5. Liquid-liquid extraction

A small-scale experiment was performed to find the best protocol for removal of lipids and pigments without losing the target compounds. *E. gracilis* cells were extracted with 90% MeOH, and the extract was equally distributed in three vials. The aqueous MeOH extract of one of the vials was partitioned with an equal volume of hexane and then dried in a centrifugal evaporator together with the other two vials. The residue from the partitioned extract and one of the remaining residues were each dissolved in 1 mL MeOH. The residue in the third vial was dissolved in 1 mL water,

and all samples were analysed by HPLC using a 20-100% acetonitrile in water gradient. Dissolving the residue in water after evaporation of aqueous MeOH removes lipids and pigments due to their limited solubility in water. However, comparative HPLC traces presented that water is an inappropriate solvent for the target metabolites and has low dissolving capacity compared to aqueous MeOH (Figure 2.12). On the other hand, partitioning of aqueous MeOH extract with hexane did not cause any notable decrease in the metabolite quantity based on comparison of the peak intensity of the partitioned and non-partitioned extracts (Figure 2.12). This makes the extraction with 90% MeOH followed by partitioning with hexane superior to the other methods.

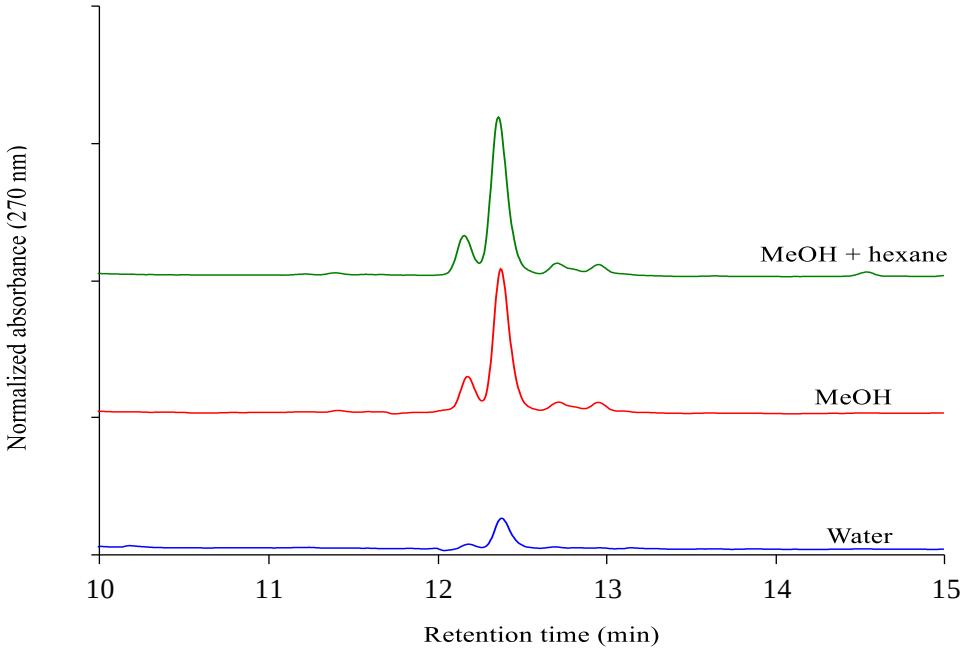

Figure 2.12 Comparative HPLC traces (at 270 nm; 150 × 4.6mm, 5µm Agilent C18 column; 1 mL/min flow rate; 20-100% acetonitrile over 22 min) of *E. gracilis* cell MeOH extract partitioned with hexane (MeOH + hexane), MeOH extract (MeOH) and dried MeOH extract dissolved in water (Water).

2.2.2.6. Epigenetic modifiers for metabolite induction

Epigenetic modifiers were investigated to induce the production of *E. gracilis* metabolites. Vorinostat (HDACI) and 5-AC (DNMTI) were selected as it has been reported that histone deacetylation and DNA methylation are ones of the central

silencing machinery in the *E. gracilis* transcription.[170] The appropriate doses of these modifiers were determined using two-fold serial dilutions performed in a 96-well plate with the highest concentration at 2 mM for vorinostat and 12.5 mM for 5-AC. The growth of *E. gracilis* in the presence of vorinostat at doses equal to or lower than 250 μM did not appear to be negatively affected. However, doses higher than 250 μM of vorinostat were lethal to the strain. Similarly, 5-AC was lethal at doses greater than 781 μM but the growth was completely normal at 781 μM. Nevertheless, the actual lethal dose of 5-AC might be different from the calculated dose as 5-AC suffers from instability, and some of it might have degraded during preparation or directly after addition to the medium.

E. gracilis was cultivated in 50-mL tubes containing 10 mL of synthetic medium + 30 mM Glu and 100 μM vorinostat, 500 μM 5-AC or a combination of the two modifiers (50 μM vorinostat + 250 μM 5-AC). Comparative analysis of MeOH extracts by HPLC (UV detection at 270 nm) did not show noticeable differences between the cultures treated with epigenetic modifiers and control cultures. However, this experiment was limited to UV active metabolites, and it is possible that some metabolites are induced with the epigenetic modifiers but are not UV active or their absorbance is outside the employed UV detection range.

2.2.2.7. Supplementation of complex medium with glutamate

E. gracilis was cultivated in 50-mL tubes containing 10 mL of the complex medium + 30 mM Glu or synthetic medium + 30 mM Glu. The cells were harvested by centrifugation and extracted with 90% MeOH. The extracts were analysed by LC-PDA-MS, and the intensity of the metabolites was compared by overlaying the TACs of the complex medium + 30 mM Glu and synthetic medium + 30 mM Glu extracts

(Figure 2.13). Comparative TACs revealed that the metabolites are produced in significantly higher amounts in synthetic medium + 30 mM Glu. Although the complex medium + 30 mM Glu contained all components of the synthetic medium, the metabolite production was considerably affected by the presence of yeast extract and tryptone. This confirms that the induction observed with 30 mM Glu is not only attributed to the presence of this amino acid but also to the absence of other components that might have a negative effect on the secondary metabolism. Therefore, the use of media with defined composition appears to be crucial for the production of these metabolites.

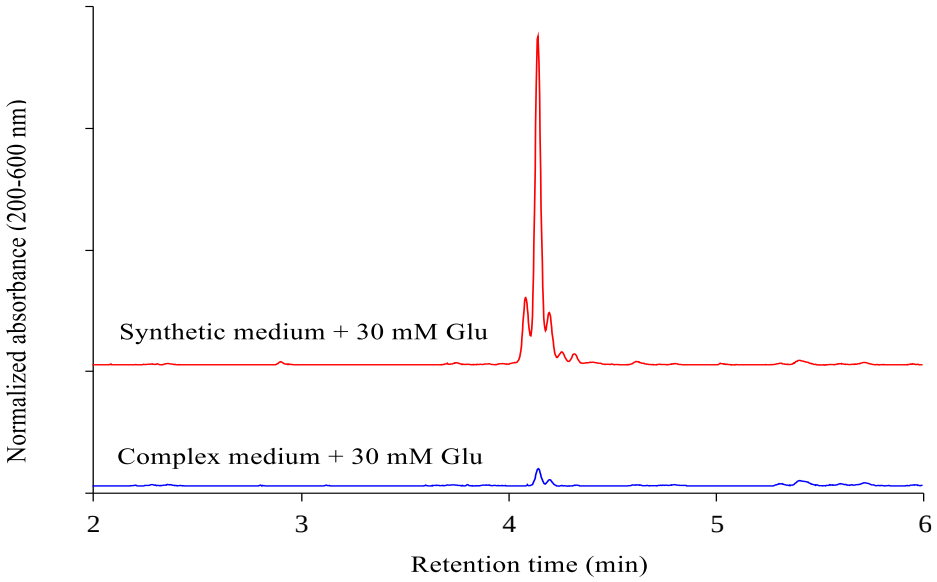

Figure 2.13 Comparative TAC (200-600 nm; 100 × 2.1mm, 2.6µm Kinetex C18 column; 0.5 mL/min flow rate; 20-100% acetonitrile over 10 min) of *E. gracilis* cultivated in the synthetic medium + 30 mM Glu and complex medium + 30 mM Glu.

2.2.2.8. Supplementation of synthetic medium with amino acids

E. gracilis was cultivated in 50-mL tubes containing 10 mL of complex medium (neutral pH and pH 4.8) or synthetic medium supplemented with asparagine (30 mM Asn), 30 mM Glu, serine (30 mM Ser), proline (30 mM Pro), glycine (30 mM Gly), glutamine (30 mM Gln), aspartate (30 mM Asp) or alanine (30 mM Ala). The cells

were harvested and extracted with 90% MeOH. The extracts were analysed by HPLC using a 20-100% acetonitrile in water gradient, and the intensity of the metabolites was compared by overlaying the HPLC traces (Figure 2.14). Asn allowed the highest production of **A-E** and **M2** followed by, in decreasing order, Glu, Gln, Ala, Gly, Asp and Pro. Nevertheless, **M1** appeared to be produced in higher amount in Glu compared to the other amino acids. The metabolites were not detected in the complex medium culture regardless of pH adjustment.

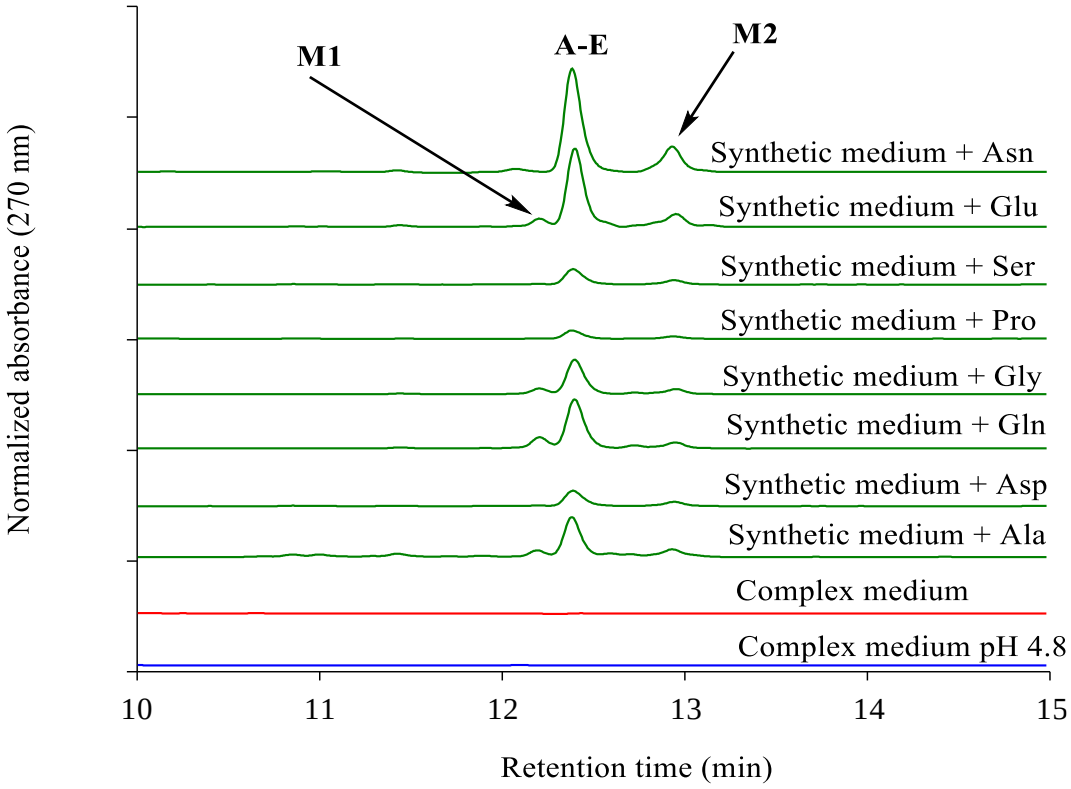

Figure 2.14 Comparative HPLC traces (at 270 nm; 150 × 4.6mm, 5µm Agilent C18 column; 1 mL/min flow rate; 20-100% acetonitrile over 22 min) of *E. gracilis* extracts cultivated in different amino acids and complex medium with neutral pH and adjusted to 4.8.

2.2.2.9. Supplementation of synthetic medium with Asn and Glu

As the highest production of **M1** was observed with 30 mM Glu, and **A-E** and **M2** with 30 mM Asn, it was assumed that combination of the two amino acids might result in high production of all those metabolites. Hence, *E. gracilis* was cultivated in

50-mL tubes containing 10 mL of synthetic medium supplemented with 15 mM Glu, 15 mM Asn or both 15 mM Glu and 15 mM Asn. The cells were harvested and extracted with 90% MeOH. The extracts were analysed by UHPLC, and the intensity of the metabolites was compared by overlaying the UHPLC traces (Figure 2.15).

In synthetic medium + 15 mM Glu + 15 mM Asn, a small amount of **M1** was detected while the intensity of **A-E** was higher in this medium compared to synthetic medium + 15 mM Glu but not significantly different from synthetic medium + 15 mM Asn. Moreover, synthetic medium + 15 mM Glu had the highest intensity of **M1,** although that of **A-E** was lower than the other two media. **M2** was nearly undetectable in any of the three media. To conclude, although the production of **A-E** is higher in 15 and 30 mM Asn, the production of **M1** is higher in 15 and 30 mM Glu. Therefore, synthetic medium + 30 mM Glu is the ideal medium that will enable the production of all separated metabolites and mixtures.

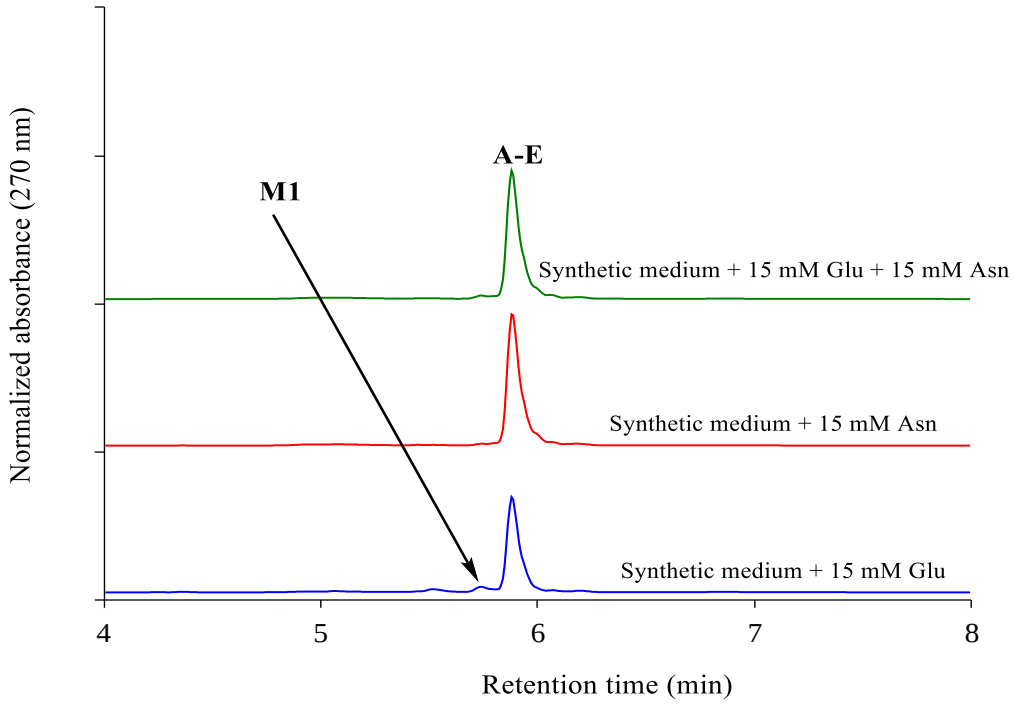

Figure 2.15 Comparative UHPLC traces (at 270 nm; 100 × 2.1mm, 2.6µm Accucore C18 column; 0.5 mL/min flow rate; 20-100% acetonitrile over 10 min) of *E. gracilis* cultivated in synthetic medium + 15 mM Glu, in synthetic medium + 15 mM Asn and in synthetic medium + 15 mM Glu + 15 mM Asn.

2.2.2.10. Determination of the optimum time for extraction

To determine the optimum time for extraction, *E. gracilis* was cultivated in a 1-L flask containing 500 mL of synthetic medium + 30 mM Glu. An aliquot of 10 mL was taken every day for 13 days, starting 24 h after inoculation, and the cells were harvested and extracted with 90% MeOH. The extracts were analysed by UHPLC, and the intensity of the metabolites was compared by overlaying the UHPLC traces (Figure 2.16). The metabolite production had been increasing gradually to reach the highest concentration after ten days of inoculation before it started decreasing for the following three days. This decline in the detected amounts of metabolites might be caused by degradation or conversion of metabolites by *E. gracilis*. Alternatively, it might be a result of cell death and lysis leading to the release of metabolites in the medium as only cell extracts were analysed in this experiment. However, the purpose of this experiment was to determine the optimum time for extraction when the production of metabolites was maximal, which was determined to be the 10th day of inoculation.

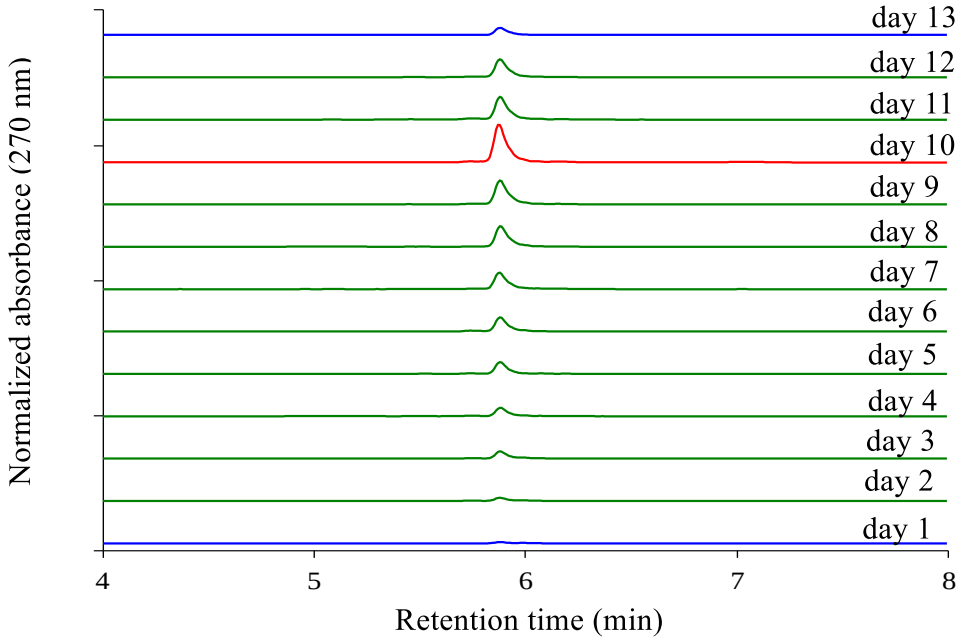

Figure 2.16 Comparative UHPLC traces (at 270 nm; 100 × 2.1mm, 2.6µm Accucore C18 column; 0.5 mL/min flow rate; 20-100% acetonitrile over 10 min) of *E. gracilis* extracts from day 1 to day 13 of inoculation.

2.3. Conclusions and future work

Nutritional manipulation of *E. gracilis* was effective in the induction of secondary metabolites, leading to the production of several metabolites in synthetic medium + 30 mM Glu which are nearly undetectable in the complex medium even when supplemented with Glu. The cultivation of *E. gracilis* in the dark was less efficient for metabolite production than cultivation in the light. MeOH appeared to be superior to EtOAc for cell lysis and extraction. Additionally, partitioning of aqueous MeOH with hexane was an efficient protocol for the removal of lipids and pigments.

The small amounts of the produced metabolites were not enough for structure elucidation on the instruments available at UEA facilities. Therefore, epigenetic modifiers and amino acids supplementation were experimented to increase the yield of secondary metabolites, but both did not improve the yield of all target metabolites. Asn improved the yield of the major metabolites but failed to improve that of the minor metabolites. The optimum time for extraction was found to be ten days after inoculation. Hence, *E gracilis* will be cultured in synthetic medium + 30 mM Glu for ten days to obtain sufficient amounts of these compounds for structure elucidation and biological assays. However, prior to large-scale cultivation, dereplication is an essential step to ensure that the induced metabolites are novel. Finally, other *Euglena* species will be searched for related metabolites using molecular networking.

2.4. Materials and methods

2.4.1. General methods and materials

Unless stated otherwise, all chemicals and solvents were purchased from Sigma-Aldrich, Alfa Aesar or Fisher Scientific. All solvents were of HPLC grade or equivalent. Commercial media and media components were purchased from Sigma-Aldrich, Alfa Aesar, Fisher Scientific or Formedium. Unless stated otherwise, the pH of media was adjusted to 4.8 with 1 N HCl and 1 N KOH prior to autoclaving.

2.4.2. Cultivation of *E. gracilis* in EG:JM

Euglena gracilis var. *saccharophila* Klebs (strain 1224/7A) was obtained from the Culture Collection of Algae and Protozoa (CCAP) (https://www.ccap.ac.uk) and treated with antibiotics to produce axenic cultures using the protocol recommended by CCAP.[178] Cultures were cultivated in EG:JM (*Euglena gracilis* medium (Table 2.1) plus Jaworski's Medium (Table 2.2), replacing ''Lab- Lemco'' with Tryptone)[169] and incubated in a light chamber at 22 ^{o}C on a 14 h light /10 h dark cycle with a light intensity of 100 μmol. photons. m^{-2} s^{-1}. After four days of incubation, *E. gracilis* cells were harvested by centrifugation at 2000 x g and 10 ^{o}C for 5 min and suspended in EG:JM medium. The absorbance at 740 nm was adjusted on a CLARIOstar microplate reader to 0.1 (≈ 4 g of wet cells per litre) using EG:JM medium as a diluent and blank. This suspension was used to inoculate the production media to obtain approximately 0.2 g of wet cells per litre (1:20 dilution). For cultivation in the dark, 2 L of EG:JM, supplemented with 15 g/ L Glc, were inoculated with *E. gracilis* cells, and incubated at 30 ^{o}C and shaken at 200 rpm in the dark for four days.

Table 2.1 EG (*E. gracilis*) medium.

Components	**Per 1000 mL**
Sodium acetate trihydrate	1g
"Lab-Lemco" powder	1g
Tryptone	2g
Yeast extract	2g
Calcium chloride	10 mg
Add constituents above to 1 litre of deionised water and autoclave at 15 psi for 15 minutes.	

Table 2.2 JM (Jaworski's medium).

Stock solutions	**Per 200 mL**
(1) Ca(NO3)2.4H2O	4.0 g
(2) KH2PO4	2.48 g
(3) MgSO4.7H2O	10.0 g
(4) NaHCO3	3.18 g
(5) EDTAFeNa	0.45 g
EDTANa2.2H2O	0.495 g
(6) H3BO3	0.496 g
MnCl2.4H2O	0.278 g
(NH4)6Mo7O24.4H2O	0.20 g
(7) Cyanocobalamin	0.008 g
Thiamine HCl	0.008 g
Biotin	0.008 g
(8) NaNO3	16.0 g
(9) Na2HPO4	7.2 g
Take 1 mL of each stock solution, make up to 1 litre with deionised water and autoclave at 15 psi for 15 minutes.	

2.4.2.1. Acid-base extraction

After four days of cultivation in the dark, the culture was centrifuged at 3130 x g and 4 ^{o}C for 20 min. The pellet and supernatant were separated and extracted with EtOAc followed by acid-base extraction procedure (Figure 2.17). The pellet had been ground in liquid nitrogen using a mortar and pestle before extraction with EtOAc. A medium control was also extracted in the same way to be used for comparison. After solvent evaporation, the residue of each extract was dissolved in an appropriate volume of MeOH to obtain a final concentration of 1 mg/mL and filtered using 0.2 μm PTFE filter (Whatman, Sigma-Aldrich). The extracts from the cells were also passed through SOLA HRP SPE cartridges (Thermo Fisher Scientific) to remove lipids.

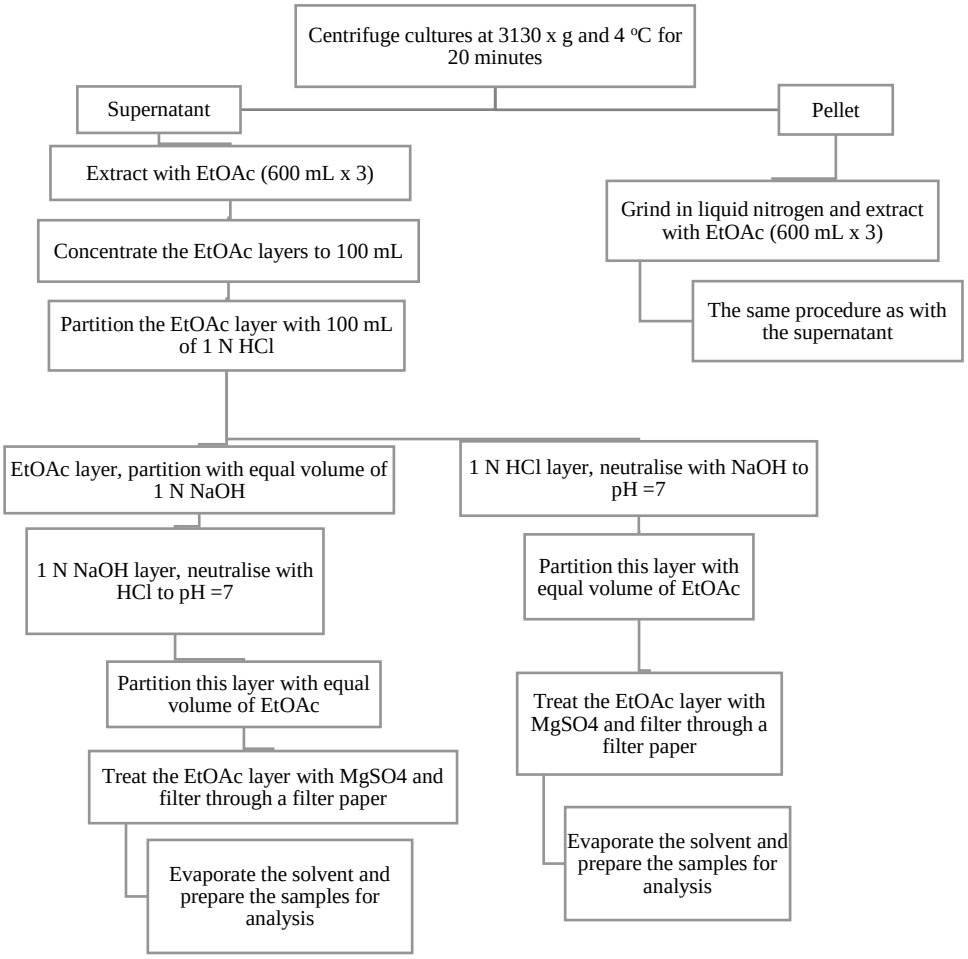

Figure 2.17 Acid-base extraction procedure of *E. gracilis* cultures.

2.4.3. LC-PDA-MS analysis

LC-PDA-MS data were acquired on a Shimadzu Nexera UHPLC attached to a Shimadzu ion-trap-ToF (IT-ToF) mass spectrometer. A 5-µL aliquot of each sample was injected onto a Phenomenex Kinetex EVO-C18 column (100 × 2.1mm, 2.6µm). The following gradient was used (acetonitrile versus 0.1% formic acid in water, at 0.5 mL/min and 40°C): 0 min (20% acetonitrile), 10 min (100% acetonitrile), 12 min (100% acetonitrile), 12.1 (20% acetonitrile), 16.1 min (20% acetonitrile). The instrument collected UV/visible spectra from 200-600 nm and MS spectra from *m/z* 200-2000. MS also collected MS/MS (fragmentation) spectra from the most abundant ions using collision-induced dissociation energy of 50% and a precursor ion width of 3 Da. Spray chamber conditions were 250°C curved desorbation line (CDL), 300°C heat block, 1.5 $L.min^{-1}$ nebuliser gas, and drying gas "on". Sodium trifluoroacetate was used for mass calibration according to the manufacturer's instructions. The LC and MS data were analysed using LabSolutions (Shimadzu), profiling solutions (Shimadzu) and ACD/Spectrus Processor (Advanced Chemistry Development).

2.4.4. Media modification and cultivation

Four different media were prepared: synthetic medium (JM + 1 g L^{-1} sodium acetate trihydrate + 0.1 g L^{-1} calcium chloride), complex medium (synthetic medium + 2 g L^{-1} yeast extract + 3 g L^{-1} tryptone), synthetic medium + 30 mM Glu and synthetic medium + 30 mM Glu + 15 g L^{-1} Glc. The pH was adjusted to 4.8 with 1 N HCl and 1 N KOH [179–181] prior to autoclaving. *E. gracilis* inocula were cultivated in EG:JM medium, and the absorbance at 740 nm was adjusted on a CLARIOstar microplate reader to 0.1 (≈ 4 g of wet cells per litre) using EG:JM medium as a diluent and blank. Cells were harvested by centrifugation at 2000 x g and 10 ^{o}C for 5 min, washed three

times with sterile Milli-Q water to remove any trace components of EG:JM medium, and suspended in the modified medium used for cultivation. This suspension was used to inoculate four 1-L flasks each containing 400 mL of the medium to obtain approximately 0.2 g of wet cells per litre (1:20 dilution). Cultures cultivated in synthetic medium, complex medium and synthetic medium + 30 mM Glu were incubated in a light chamber at 22 ^{o}C on a 14 h light /10 h dark cycle with a light intensity of 100 μmol. photons. m^{-2} s^{-1}. Synthetic medium + 30 mM Glu + Glc culture was incubated in the dark at 30 ^{o}C and shaken at 200 rpm. The growth was measured daily in the flasks using a photobioreactor Algem (Algenuity).

2.4.5. Extraction of modified media cultures

E. gracilis was cultivated in the modified media mentioned above (section 2.4.4), and the growth was monitored using a photobioreactor Algem (Algenuity). Each culture was harvested at the stationary phase by centrifugation at 3130 x g and 4 ^{o}C for 20 min. The cells were ground in liquid nitrogen and extracted with 200 mL EtOAc. The supernatant was freeze-dried and extracted with 200 mL EtOAc. The solvents were evaporated, and the residue of each extract was then re-dissolved in 20 mL MeOH, and 1 mL of each solution was filtered using a 0.2 μm PTFE filter (Whatman, Sigma-Aldrich). The extracts from the cells were also passed through SOLA HRP SPE cartridges (Thermo Fisher Scientific) to remove lipids.

2.4.6. HPLC analysis

HPLC analysis was performed on an Agilent 1200 series system (Agilent Technologies) and an Agilent C18 column (4.6 x 150mm, 5μm). For 50-100% acetonitrile/water gradient, the following gradient was used (acetonitrile versus 0.1% formic acid in water, at 1mL/min and 40°C): 0 min (50% acetonitrile), 22 min (100%

acetonitrile), 24 min (100% acetonitrile), 26 min (50% acetonitrile), 30 min (50% acetonitrile), and the detection was set at 210, 270, 290 and 450 nm. For 20-100% acetonitrile/water gradient, the following gradient was used (acetonitrile versus 0.1% formic acid in water, at 1.3mL/min and 40°C): 0 min (20% acetonitrile), 20 min (100% acetonitrile), 24 min (100% acetonitrile), 25 min (20% acetonitrile), 30 min (20% acetonitrile), and the detection was set at 210, 270, 290 and 450 nm.

2.4.7. Cultivation and extraction of 10-mL cultures in 50-mL tubes

E. gracilis inocula were cultivated in EG:JM medium, and the absorbance at 740 nm was adjusted on a CLARIOstar microplate reader to 0.1 (≈ 4 g of wet cells per litre) using EG:JM medium as a diluent and blank. Cells were harvested by centrifugation at 2000 x g and 10 ^{o}C for 5 min, washed three times with sterile Milli-Q water to remove any trace components of EG:JM medium, and suspended in the modified medium (pH adjusted to 4.8 prior to autoclaving) used for cultivation. This suspension was used to inoculate 50-mL tubes each containing 10 mL of the medium to obtain approximately 0.2 g of wet cells per litre (1:20 dilution). Cultures were cultivated at ambient temperature 22-25 ^{o}C under daylight lamps (2000 lumens). After six days, cultures were centrifuged at 3000 x g and 4 ^{o}C for 20 min, and cells were vortexed in 10 mL 90% MeOH or ground in liquid nitrogen and extracted with 10 mL EtOAc. Cell debris was removed by centrifugation at 3000 x g and 4 ^{o}C for 10 min. After centrifugation, the solvents were evaporated, and the residue of each extract was then dissolved in 1 mL MeOH and passed through SOLA HRP SPE cartridges (Thermo Fisher Scientific) and a 0.2 μm PTFE filter (Whatman, Sigma-Aldrich).

2.4.8. Three-litre culture and method development for separation

E. gracilis inocula were prepared as described above and used to inoculate six 1-L flasks each containing 500 mL of synthetic medium + 30 mM Glu to obtain approximately 0.2 g of wet cells per litre (1:20 dilution). The culture was incubated at ambient temperature 22-25 ^{o}C under daylight lamps (2000 lumens). After six days, the culture was centrifuged at 3130 x g and 4 ^{o}C for 20 min, and the cells were extracted with 1 L 90% MeOH and magnetic stirrer. After an hour, the aqueous MeOH extract was partitioned with an equal volume of hexane to remove lipids and pigments. The aqueous MeOH layer was centrifuged to remove the debris and then evaporated to get the residue (400 mg). This residue was fractionated on a 26 g reversed-phase column attached to an automated flash-chromatography system (CombiFlash Rf, Teledyne Isco) using 30 mL/min flow rate and a linear gradient from 50% to 100% acetonitrile in water (in 6 min) before washing the system with 100% acetonitrile (for 3 min). Fractions containing the target compounds were concentrated to dryness on a centrifugal evaporator to give a residue amount of 43 mg. This amount was dissolved in MeOH, and purification was attempted on an Agilent HPLC system with a semi-preparative C18 column and UV detection at 210 and 270 nm. Method development for purification was performed by changing the following parameters: solvents (acetonitrile, MeOH, water, water + trifluoroacetic acid and water + formic acid); oven temperature; gradient and isocratic systems; flow rate.

2.4.9. UHPLC analysis

UHPLC analysis was performed on a Thermo Scientific Ultimate 3000 UHPLC system and a Thermo Scientific Accucore C18 column (2.1 × 100 mm, 2.6 μm). The following gradient was used (acetonitrile versus 0.1% formic acid in water, at 0.5

mL/min and 40 °C): 0 min (20% acetonitrile), 10 min (100% acetonitrile), 12 min (100% acetonitrile), 12.1 (20% acetonitrile), 16.1 min (20% acetonitrile). The detection was set at 210, 270, 290 and 450 nm.

2.4.10. Liquid-liquid extraction

E. gracilis inocula were prepared as described above and used to inoculate a 100-mL flask containing 50 mL of synthetic medium + 30 mM Glu to obtain approximately 0.2 g of wet cells per litre (1:20 dilution). The culture was incubated at ambient temperature 22-25 ^{o}C under daylight lamps (2000 lumens). After six days, the culture was centrifuged at 3130 x g and 4 ^{o}C for 20 min, and the cells were extracted with 50 mL 90% MeOH. The extract solution was equally distributed in three vials. The aqueous MeOH extract of one of the vials was partitioned with an equal volume of hexane, and then dried in a centrifugal evaporator together with the other two vials. The residue from the partitioned extract and one of the remaining residues were dissolved in 1 mL MeOH. The residue in the third vial was dissolved in 1 mL water, all samples were analysed by HPLC with UV detection at 270 nm.

2.4.11. Cultivation with epigenetic modifiers

The appropriate doses of vorinostat and azacytidine were determined using two-fold serial dilutions in synthetic medium + 30 mM Glu (containing 2% DMSO) with the highest concentration at 2 mM for vorinostat and 12.5 mM for 5-AC. *E. gracilis* cells were harvested from four-day-old culture by centrifugation at 2000 x g and 10 ^{o}C for 5 min and suspended in EG:JM medium. The absorbance at 740 nm was adjusted on a CLARIOstar microplate reader to 0.1 (≈ 4 g of wet cells per litre) using EG:JM medium as a diluent and blank. This cell suspension was used to inoculate a 96-well microtiter plate. Each well contained five µL of the diluted inoculum and 95 µL of

synthetic medium + 30 mM Glu containing the epigenetic modifiers or 2% DMSO (control). The plate was incubated for six days at ambient temperature 22-25 ^{o}C under daylight lamps (2000 lumens) and the growth was measured using a CLARIOstar microplate reader in addition to visual inspection.

Epigenetic experiments were performed in 10-mL flacon tubes containing 9.9 mL of cell suspension and 100 μL of epigenetic stock solutions or DMSO (control). Vorinostat and 5-AC stock solutions were prepared in DMSO and sterilised by filtration under aseptic conditions. The cell suspension was prepared in synthetic medium + 30 mM Glu to obtain approximately 0.2 g of wet cells per litre. The final concentrations of the epigenetic modifiers were 100 μM vorinostat, 500 μM 5-AC or a combination of the two modifiers (50 μM vorinostat + 250 μM 5-AC). Cultures were incubated at ambient temperature 22-25 ^{o}C under daylight lamps (2000 lumens). After six days, the cultures were centrifuged at 3000 x g and 4 ^{o}C for 20 min, and cells were vortexed in 10 mL 90%. MeOH. Cell debris was removed by centrifugation at 3000 x g and 4 ^{o}C for 10 min. After centrifugation, the solvent was evaporated, and the residue of each extract was then dissolved in 1 mL MeOH and passed through SOLA HRP SPE cartridges (Thermo Fisher Scientific) and a 0.2 μm PTFE filter (Whatman, Sigma-Aldrich).

2.4.12. Determination of the optimum time for extraction

E. gracilis inocula were prepared as described above and used to inoculate a 1-L flask containing 500 mL of synthetic medium + 30 mM Glu to obtain approximately 0.2 g of wet cells per litre (1:20 dilution). An aliquot of 10 mL was taken every day for 13 days, starting 24 h after inoculation, and centrifuged at 3000 x g and 4 ^{o}C for 20 min. The cells were harvested and extracted with 90% MeOH. The solvent was

evaporated, and the residue of the extract was stored in a freezer at - 20 ^{o}C until UHPLC analysis. Samples were prepared immediately before analysis by adding 1 mL MeOH and passing the solutions through SOLA HRP SPE cartridges (Thermo Fisher Scientific) and a 0.2 μm PTFE filter (Whatman, Sigma-Aldrich).

Chapter Three

3. Dereplication, isolation, structure elucidation and bioassays of euglenatides A-E

3.1. Introduction

Nutritional manipulation of *E. gracilis* led to the induction of several metabolites. Three-litre culture was insufficient for the isolation and characterisation of the metabolites. However, preliminary literature search suggested that the induced metabolites are novel as their measured masses and UV profiles do not match those of any metabolites previously known from *Euglena*. Besides chlorophyll derivatives, xanthophyll derivatives and fatty acids, there are two metabolites known from *Euglena* genus. These metabolites are euglenapterin from *E. gracilis*[182] and euglenophycin from *E. sanguinea* and other species[183,184] (Figure 3.1). Nevertheless, before implementing large-scale cultivation, extensive dereplication of the induced metabolites is conducted using high-resolution accurate masses, UV profiles and MS/MS spectra. After confirming the novelty of the metabolites, large-scale cultivation is performed to characterise the structure of the metabolites and evaluate their biological activity. Finally, a molecular network is constructed to identify related metabolites produced by other *Euglena* species.

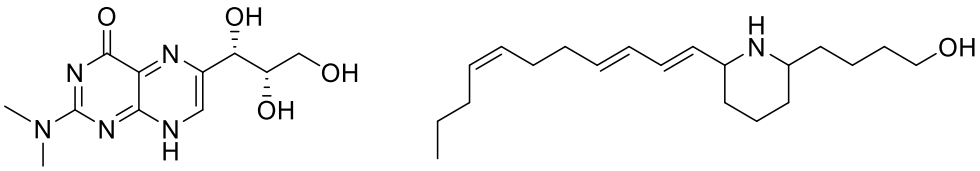

euglenapterin euglenophycin

Figure 3.1 Chemical structures of euglenapterin and euglenophycin.

3.2. Results and discussion

3.2.1. High-resolution MS and dereplication

High-resolution analysis of metabolites **A**-**E** in negative ion mode (Figure 3.2) revealed two signals at *m/z* 825.4612 $[M-H]^-$ (calcd. for $C_{39}H_{65}N_6O_{13}$, 825.4615, Δ= -0.4 ppm) and *m/z* 871.4667 $[M+FA-H]^-$ (calcd. for $C_{40}H_{67}N_6O_{15}$, 871.4670, Δ= -0.3 ppm) indicative of the molecular formula $C_{39}H_{66}N_6O_{13}$ for **A**, two signals at *m/z* 808.4464 $[M-H]^-$ (calcd. for $C_{38}H_{62}N_7O_{12}$, 808.4462, Δ= 0.3 ppm) and *m/z* 854.4519 $[M+FA-H]^-$ (calcd. for $C_{39}H_{64}N_7O_{14}$, 854.4517, Δ= 0.3 ppm) indicative of the molecular formula $C_{38}H_{63}N_7O_{12}$ for **B**, two signals at *m/z* 822.4615 $[M-H]^-$ (calcd. for $C_{39}H_{64}N_7O_{12}$, 822.4618, Δ= -0.4 ppm) and *m/z* 868.4670 $[M+FA-H]^-$ (calcd. for $C_{40}H_{66}N_7O_{14}$, 868.4673, Δ= -0.4 ppm) indicative of the molecular formula $C_{39}H_{65}N_7O_{12}$ for **C**, two signals at *m/z* 809.4659 $[M-H]^-$ (calcd. for $C_{39}H_{65}N_6O_{12}$, 809.4666, Δ= -0.9 ppm) and *m/z* 855.4714 $[M+FA-H]^-$ (calcd. for $C_{40}H_{67}N_6O_{14}$, 855.4721, Δ= -0.8 ppm) indicative of the molecular formula $C_{39}H_{66}N_6O_{12}$ for **D**, and two signals at *m/z* 792.4516 $[M-H]^-$ (calcd. for $C_{38}H_{62}N_7O_{11}$, 792.4513, Δ= 0.4 ppm) and *m/z* 838.4571 $[M+FA-H]^-$ (calcd. for $C_{39}H_{64}N_7O_{13}$, 838.4568, Δ= 0.4 ppm) indicative of the molecular formula $C_{38}H_{63}N_7O_{11}$ for **E**.

Databases (METLIN, NP Atlas, DNP and SciFinder) were searched using the accurate masses and UV profiles, but no known matching natural products were found, suggesting that these are novel metabolites. Likewise, METLIN, GNPS and MassBank were searched with MS/MS spectra. Although some metabolites in databases exhibit some MS/MS spectral similarities to metabolites **A**-**E**, their accurate mass and UV profiles do not match those of **A**-**E**.

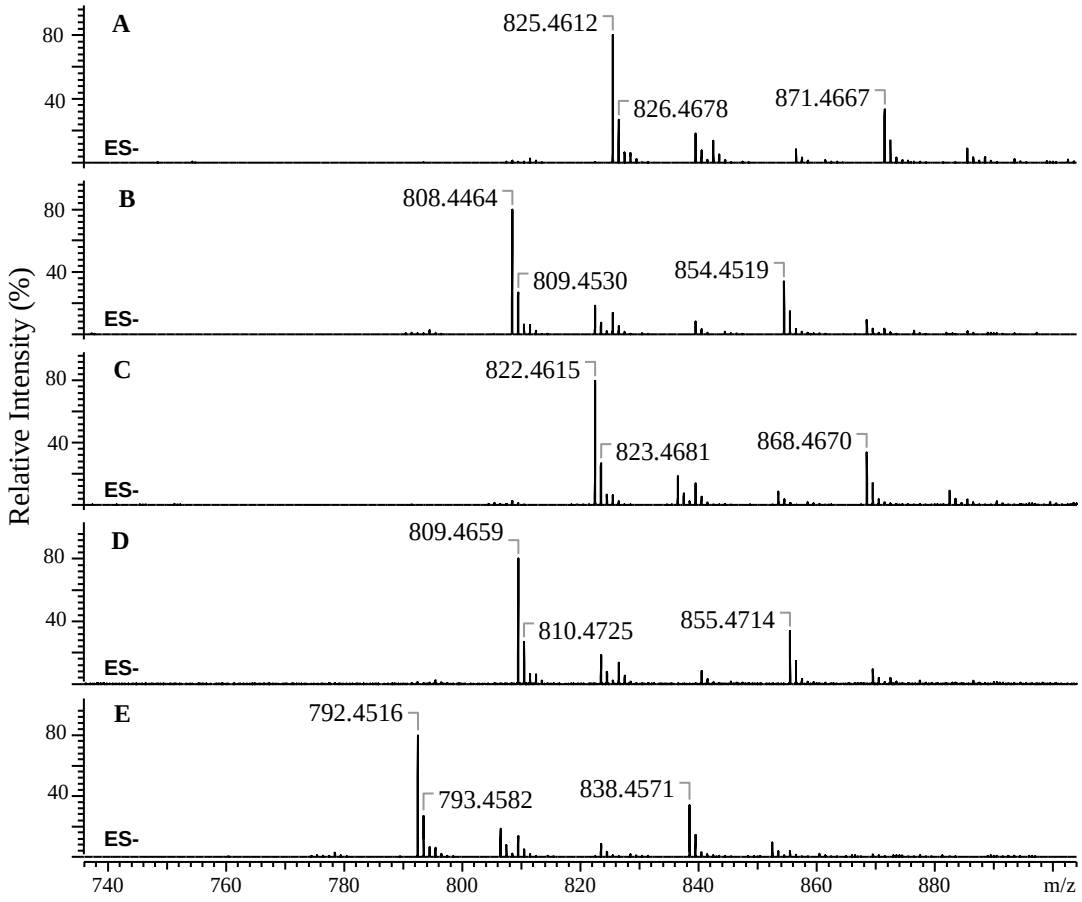

Figure 3.2 Negative ion mode high-resolution MS spectra of **A**-**E**.

3.2.2. Large-scale cultivation, isolation and purification

E. gracilis cells (53 g) were harvested from 18-L culture, extracted with 90% MeOH, partitioned with hexane and the aqueous MeOH was evaporated to obtain a residue of 1.679 g. Initial separation was performed on an automated flash-chromatography system (Figure 3.3) to obtain a mixture of the target metabolites (186.7 mg). This mixture was dissolved in MeOH, and the compounds were purified on a semi-preparative HPLC (Figure 3.4) to afford 2.8 mg of **A**, 5.7 mg of **B**, 2.8 mg of **C**, 2.3 mg of **D** and 2.4 mg of **E**. The purity of compounds **A**-**E** was confirmed by low-resolution LC-UV-MS (Figures 3.5-3.9).

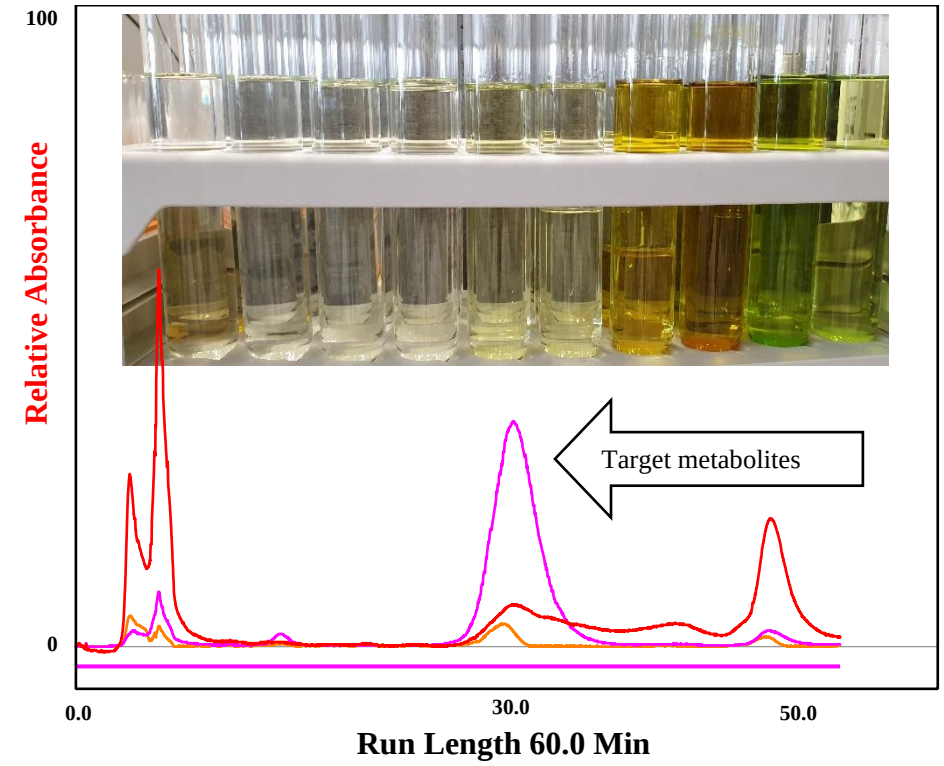

Figure 3.3 Initial separation of *E. gracilis* metabolites (target metabolites) on flash chromatography.

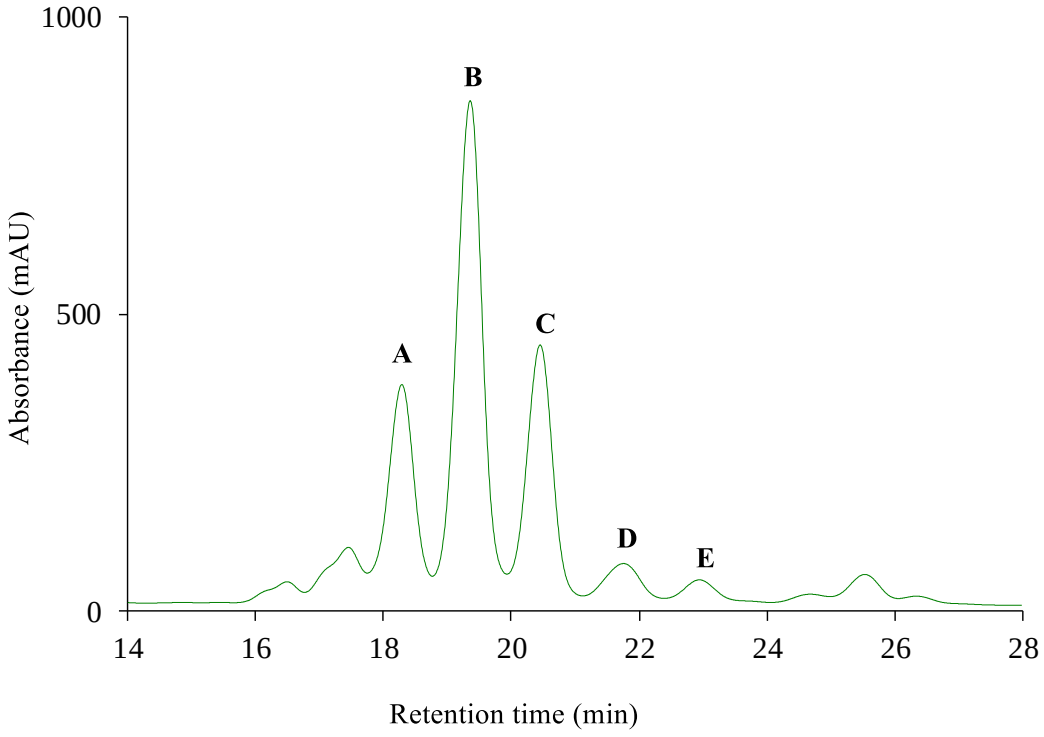

Figure 3.4 Semi-preparative HPLC trace (at 270 nm) of *E. gracilis* metabolites (**A**-**E**).

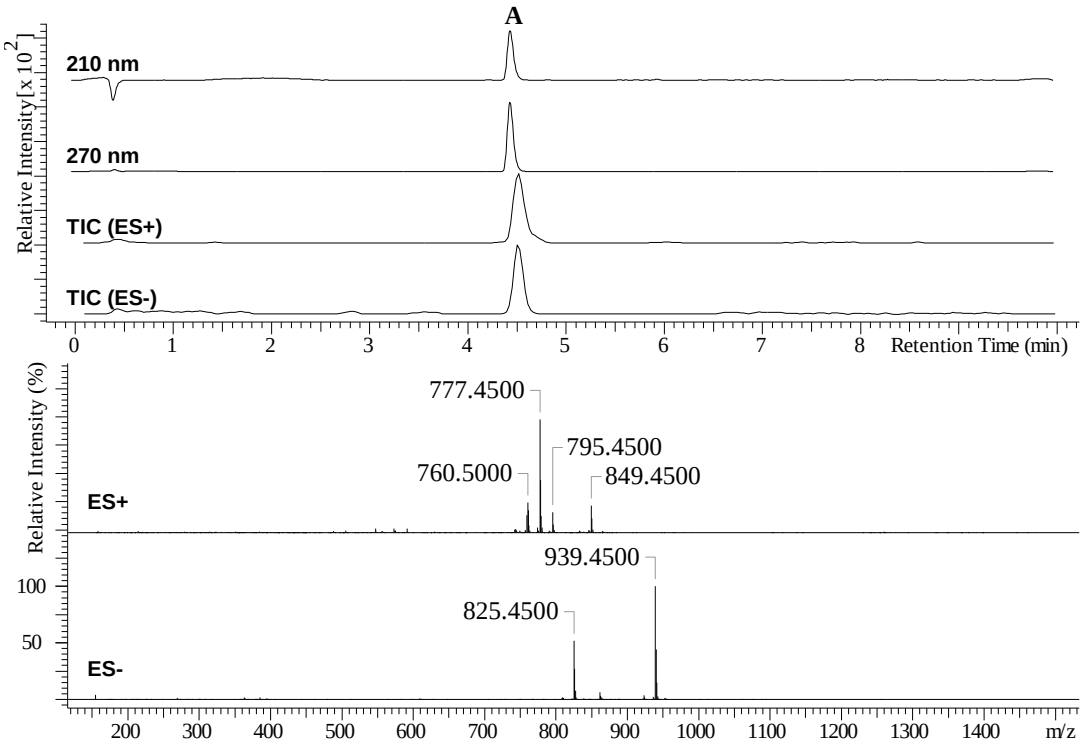

Figure 3.5 LC-UV-MS chromatograms and MS spectra of purified **A**.

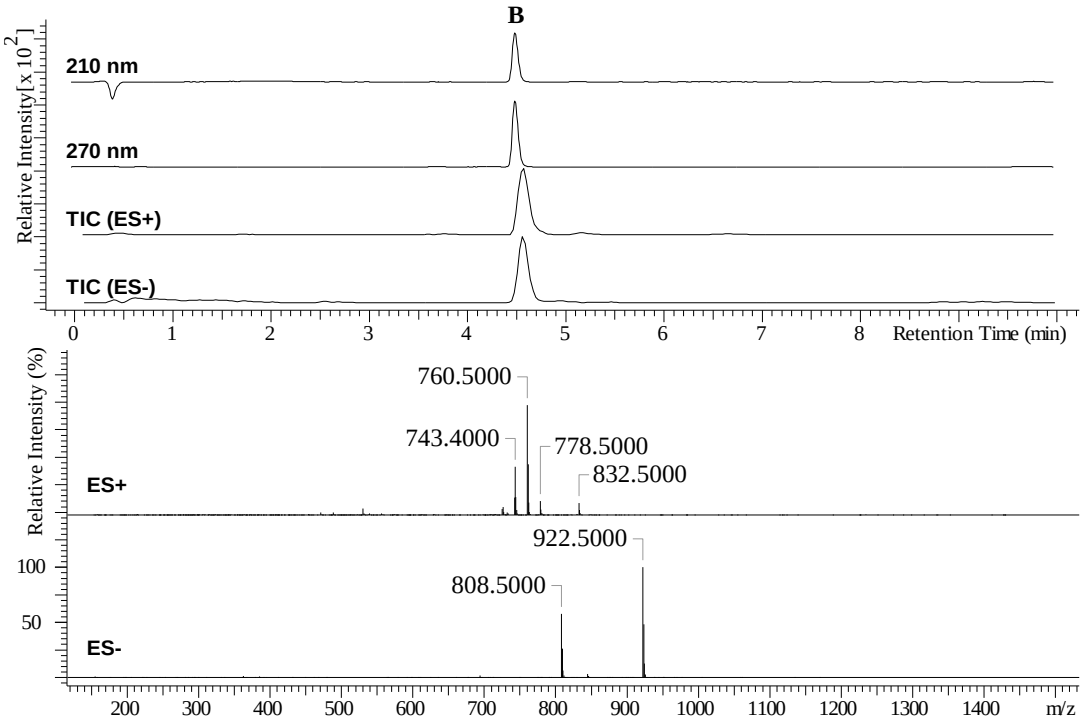

Figure 3.6 LC-UV-MS chromatograms and MS spectra of purified **B**.

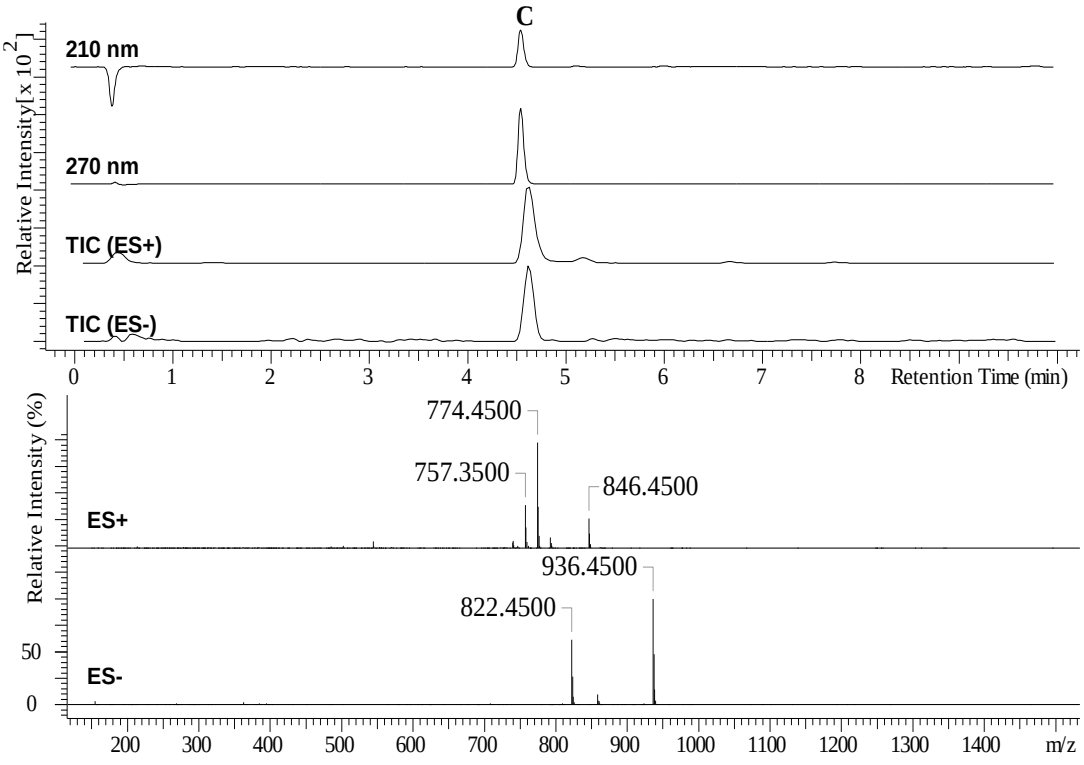

Figure 3.7 LC-UV-MS chromatograms and MS spectra of purified **C**.

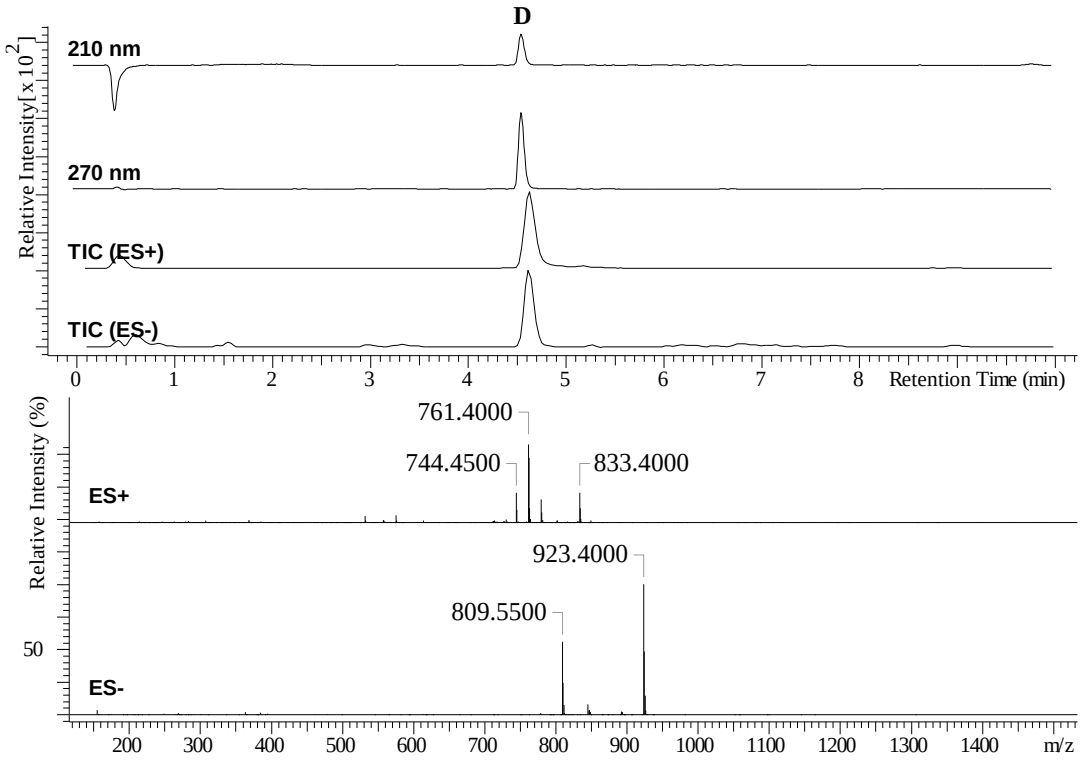

Figure 3.8 LC-UV-MS chromatograms and MS spectra of purified **D**.

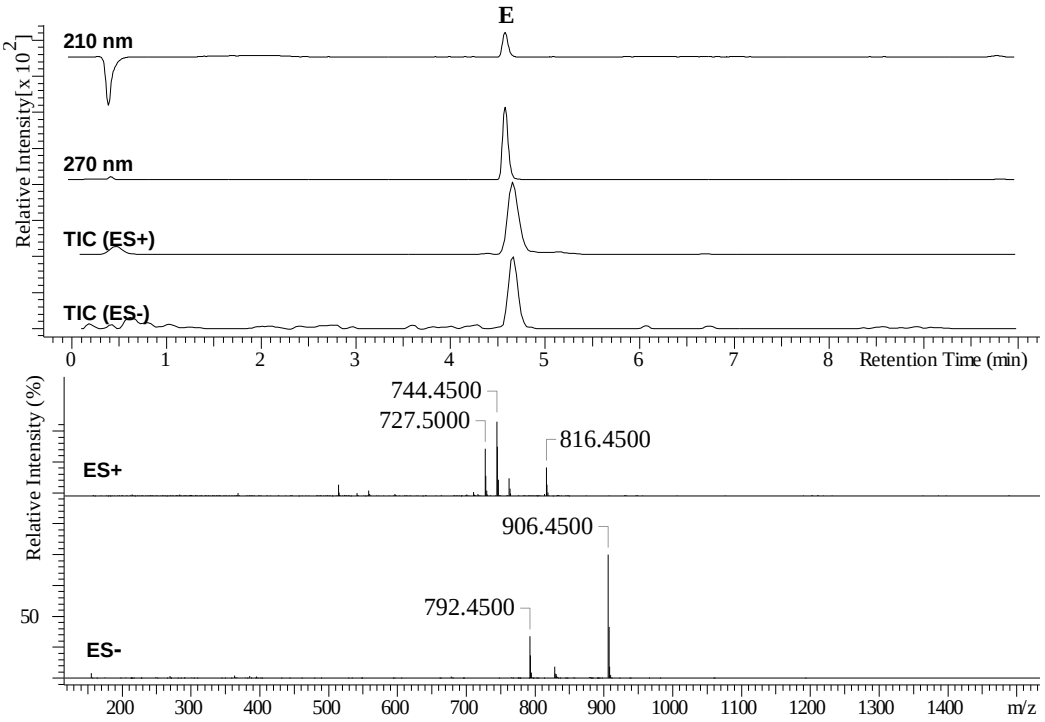

Figure 3.9 LC-UV-MS chromatograms and MS spectra of purified **E**.

3.2.3. Structure elucidation of *E. gracilis* metabolites A-E

The UV profiles of all metabolites presented maxima of absorbance at 260, 269 and 280 nm, suggesting a conjugated triene substructure.[185] IR absorptions at 3347 cm^{-1} (NH) and 1651 cm^{-1} (CO) indicated the presence of amide carbonyl groups while a broad peak at 2873 cm^{-1} indicated the presence of an aliphatic chain (Appendix 8.1). Compound **B** structure was elucidated by NMR during my placement in Fundación Medina in collaboration with Dr Fernando Reyes and Dr Ignacio Pérez-Victoria.

The ^{13}C NMR (Table 3.1) displayed carbonyl carbon signals at δ_C 176.3, 173.4, 172.4, 172.3, 172.1, 171.1 and 169.6. The ^{1}H NMR spectrum (Table 3.1) revealed nine amide protons at δ_H 6.88 (1H, s), 6.90 (1H, d), 7.06 (1H, s), 7.29 (1H, s), 7.36 (1H, s), 7.65 (1H, d), 7.77 (1H, d), 7.78 (1H, s) and 9.02 (1H, d). These data indicated that compound **B** was a peptide. The overlapped signals at δ_H 1.25 in the ^{1}H NMR spectrum and a cluster of methylene carbon signals at δ_C 28.5-31.2 in the HSQC spectrum, in

addition to a methyl group at δ_H 0.85 (3H, t) and δ_C 13.9 indicated that compound **B** is a lipopeptide containing a long alkyl chain. The signals at δ_H 4.31, 4.38, 4.44 and 5.13 were indicative of four hydroxyls while the signals at δ_H 3.13 and δ_C 55.5 indicated the presence of a methoxy group. The presence of a triene was confirmed by the presence of six proton signals at δ_H 5.51 (1H, dd), 5.72 (1H, dt), 6.07 (1H, dd), 6.15 (1H, dd), 6.20 (1H, dd), 6.24 (1H, dd), and six carbon signals at δ_C 135.1, 133.9, 132.8, 131.3, 130.3, 130.0. Analysis of ^{1}H, ^{13}C, and HSQC data (Table 3.1), in addition to the COSY and HMBC correlations (Figure 3.10), revealed the presence of two asparagine residues (Asn I and Asn II), a β-aminoisobutyric acid residue (BAIBA) and a 4,5-Dihydroxynorvaline residue (Dnv I). In addition, there is a unique β-amino-2,5-dihydroxy-7-methoxy-8,10,12-eicosatrienoic acid residue that we have named graciline (Gra) after its origin from *E. gracilis*.

The connectivity of the amino acid residues was established by COSY and HMBC as shown in Figure 3.10. All NH protons correlated to the carbonyls of the amino acid residues in the HMBC spectrum. This with the COSY correlations of the NH protons to the CH_α and CH_β protons in the alpha and beta amino acid residues, respectively, concluded the sequence of the five amino acids of compound **B** as shown in Figure 3.10.

Comparing the NMR spectra of **E** to those of **B** revealed that C-2 on Gra was shielded from 73.0 ppm to 40.9 ppm and the hydroxyl group on this carbon was replaced with an extra hydrogen (Appendix 8.2) as observed on the ^{1}H, ^{13}C, HSQC, COSY and HMBC (Figure 3.11). This confirmed that Gra observed in compound **B** is replaced with a β-amino-5-hydroxy-7-methoxy-8,10,12-eicosatrienoic acid residue (DeoxyGra) in compound **E**.

Table 3.1 ^{1}H and ^{13}C NMR data (500 and 125 MHz, DMSO-d_6) of compound **B**.

Position (No.)	^{13}C ppm	^{1}H ppm mult. (*J* in Hz)	Position (No.)	^{13}C ppm	^{1}H ppm mult. (*J* in Hz)
Dnv I			BAIBA		
C (1)	172.4		C (1)	176.3	
CH (2)	50.3	4.32, m	CH (2)	37.5	2.66, m
NH (2)		7.65, d (7.8)	CH2 (3)	41.7	3.03, brd (13.0), 3.27, m
CH2 (3)	34.3	1.86, m, 1.71, m	NH (3)		7.06, s
CH (4)	67.5	3.43, m	CH3 (4)	16.8	1.04, d (7.1)
OH (4)		4.44, brd (4.7)			
CH2 (5)	66.3	3.32, m, 3.26, m			
OH (5)		4.38, m			
Asn I			Gra		
C (1)	171.1		C (1)	172.3	
CH (2)	49.3	4.45, m	CH (2)	72.9	3.86, dd (9.6, 7.7)
NH (2)		7.77, d (7.9)	OH (2)		5.13, br d (7.7)
CH2 (3)	35.8	2.94, dd (16.8, 5.0) 2.57, dd (16.9, 3.7)	CH (3)	49.1	3.92, m
C (4)	173.4	7.78 s, 7.29 s	NH (3)		6.90 d (9.6)
NH2 (4)			CH2 (4)	40.3	1.69, m, 1.20, m
			CH (5)	63.0	3.47, m
			OH (5)		4.31, m
			CH2 (6)	43.8	1.30, br dd (14.5, 5.1), 1.49, m
Asn II			CH (7)	77.8	3.73, m
C (1)	169.6		CH (8)	133.9	5.51, dd (14.6, 7.6)
CH (2)	51.6	4.06. m	CH (9)	131.3	6.20, dd (14.6, 10.3)
NH (2)		9.02, d (6.5)	CH (10)	130.0	6.15, dd (14.6, 10.3)
CH2 (3)	35.0	2.86, dd (15.7, 4.0) 2.47, dd (15.9, 4.7)	CH (11)	132.8	6.24, dd (14.5, 10.4)
C (4)	172.1		CH (12)	130.3	6.07, dd (15.1, 10.4)
NH2 (4)		7.36, s, 6.88, s	CH (13)	135.1	5.72, dt (15.1, 7.1)
			CH2 (14)	32.1	2.06, q (7.0)
			CH2 (15)	28.7	1.35, m
			CH2 (16)	28.52	1.25, m
			CH2 (17)	28.54	1.25, m
			CH2 (18)	31.2	1.24, m
			CH2 (19)	22.0	1.25, m
			CH3 (20)	13.9	0.85, t (6.8)
			CH3 (21)	55.5	3.13, s

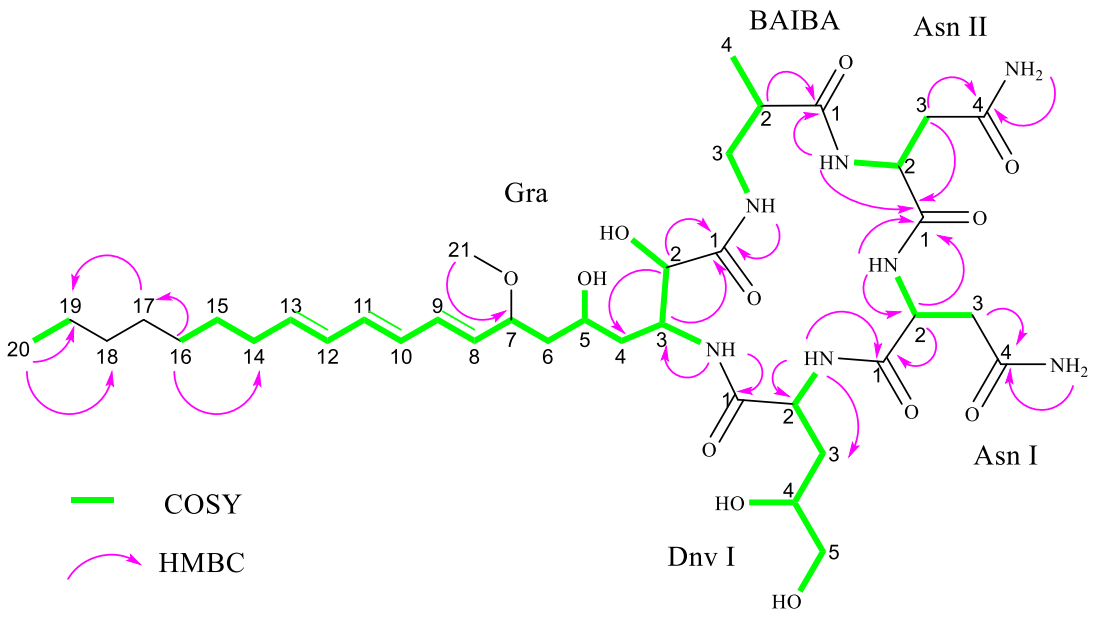

Figure 3.10 Key COSY and HMBC correlations used to establish the molecular connectivity of compound B.

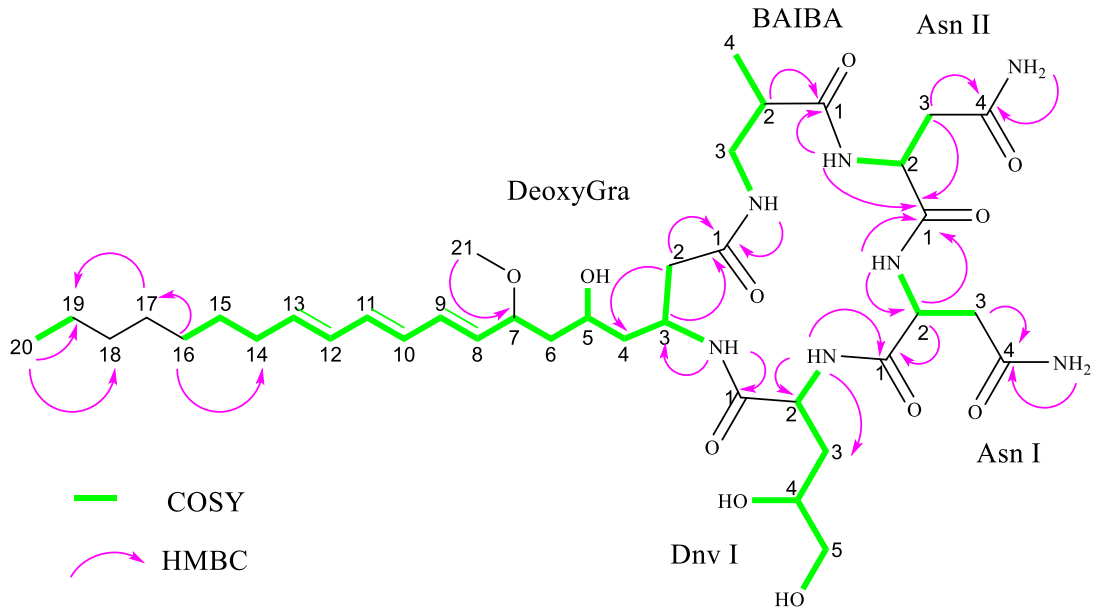

Figure 3.11 Key COSY and HMBC correlations used to establish the molecular connectivity of compound E.

The NMR spectra of **C** were similar to those of **B** except that the former contained an extra methyl group (^{1}H, δ 1.02 ppm; ^{13}C, δ 19.5 ppm) and the chemical shift of C-5 on Dnv I increased from 66.3 ppm to 69.9 ppm (Appendix 8.2). Careful analysis of COSY and HMBC revealed correlations between the new methyl group and C-5 on the Dnv (Figure 3.12). COSY also showed correlations between the hydroxyl groups

and C-4 and C-5 on the Dnv. This unambiguously confirmed that the new methyl group is located at C-5 of the Dnv converting the Dnv to 4,5-Dihydroxynorleucine (Dnl).

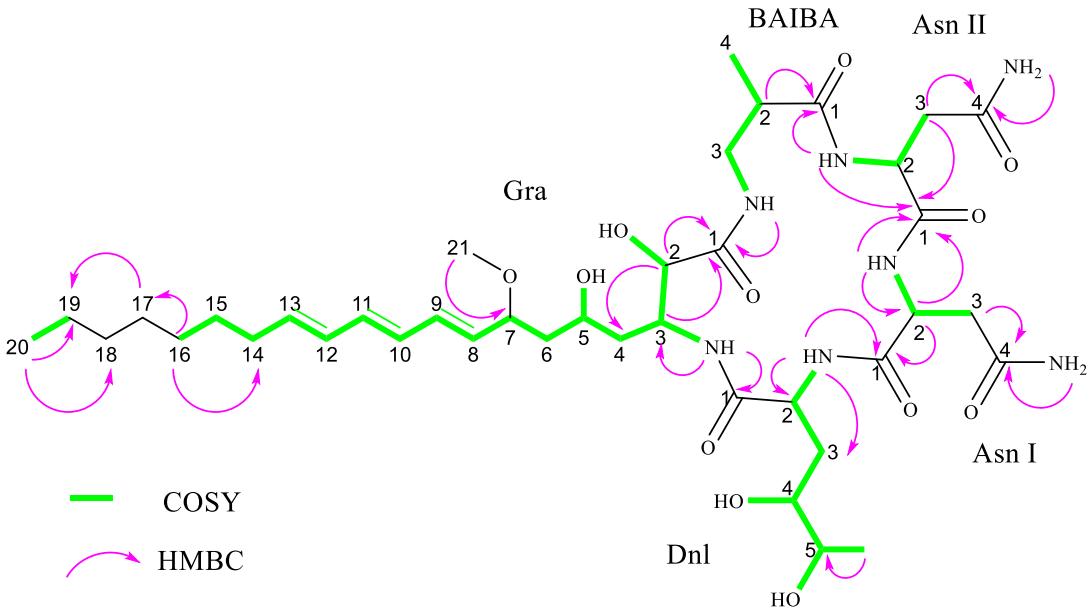

Figure 3.12 Key COSY and HMBC correlations used to establish the molecular connectivity of compound C.

Detailed analysis of NMR data of **A** revealed that it contains the same amino acid residues as **B** except that Asn II residue is replaced with a second Dnv (Dnv II, Table 3.2). The connectivity of the amino acid residues was established by COSY and HMBC as shown in Figure 3.10. The correlation of the NH protons to the carbonyls of the amino acid residues in the HMBC spectrum and the COSY correlations of the NH protons to the CH_{α} and CH_{β} protons in the alpha and beta amino acid residues, respectively, concluded the sequence of the five amino acids of compound **A** as shown in Figure 3.13.. The NMR spectra of **D** resembles those of **A** except that the C-2 on the triene amino acid is shielded from 73.0 ppm to 41.0 ppm because the hydroxyl group on this carbon is replaced with an extra hydrogen (Appendix 8.2) transforming Gra to DeoxyGra as observed on the ^{1}H, ^{13}C, HSQC, COSY and HMBC (Figure 3.14). Compounds **A-E**, that we have named euglenatides A-E, have novel structures and

contain unusual amino acids with some similarities to *Caenorhabditis elegans* metabolites (nemamides A and B, Figure 3.15).[186]

Table 3.2 ^{1}H and ^{13}C NMR data (500 and 125 MHz, DMSO-d_6) of compound **A**.

Position (No.)	**^{13}C ppm**	**^{1}H ppm mult. (*J* in Hz)**	**Position (No.)**	**^{13}C ppm**	**^{1}H ppm mult. (*J* in Hz)**
Dnv I			BAIBA		
C (1)	172.6		C (1)	176.2	
CH (2)	50.6	4.28, m	CH (2)	37.7	2.69, m
NH (2)		7.73, d (7.7)	CH2 (3)	41.8	3.06, brd (12.9), 3.27, m
CH2 (3)	34.5	1.83, m, 1.71, m	NH (3)		7.08, brd (12.7)
CH (4)	67.6	3.42, m	CH3 (4)	17.0	1.07, d (6.9)
OH (4)		4.44, m			
CH2 (5)	66.3	3.22, m, 3.29, m			
OH (5)		4.34, m			
Asn I			Gra		
C (1)	171.2		C (1)	172.3	
CH (2)	49.3	4.45, m	CH (2)	73.0	3.87, d (9.6, 7.5)
NH (2)		7.78, s	OH (2)		5.17, brd (7.5)
CH2 (3)	35.8	2.57, dd (16.5, 3.4), 2.94, dd (16.8, 4.8)	CH (3)	49.2	3.92, m
C (4)	173.6		NH (3)		6.92 d (9.6)
NH2 (4)		7.79 s, 7.29 s	CH2 (4)	40.4	1.69, m, 1.20, m
			CH (5)	63.1	3.47, m
			OH (5)		4.31, m
			CH2 (6)	43.9	1.31, br dd (15.0, 4.8), 1.49, m
Dnv II			CH (7)	77.9	3.73, m
C (1)	170.7		CH (8)	134.0	5.51, dd (14.7, 7.9)
CH (2)	51.6	3.81, m	CH (9)	131.4	6.20, dd (14.6, 10.3)
NH (2)		8.85, d (5.7)	CH (10)	130.1	6.15, dd (14.0, 10.6)
CH2 (3)	32.3	1.89, m	CH (11)	133.0	6.24, dd (14.0, 10.6)
CH (4)	68.1	3.41, m	CH (12)	130.4	6.07, dd (14.0, 10.6)
OH (4)		4.42, m	CH (13)	135.2	5.72, dt (14.1, 7.1)
CH2 (5)	66.3	3.22, m, 3.29, m	CH2 (14)	32.2	2.06, q (7.0)
OH (5)		4.55, m	CH2 (15)	28.8	1.34, m
			CH2 (16)	28.6	1.25, m
			CH2 (17)	28.6	1.25, m
			CH2 (18)	31.3	1.24, m
			CH2 (19)	22.1	1.25, m
			CH3 (20)	14.0	0.85, t (6.9)
			CH3 (21)	55.6	3.13, s

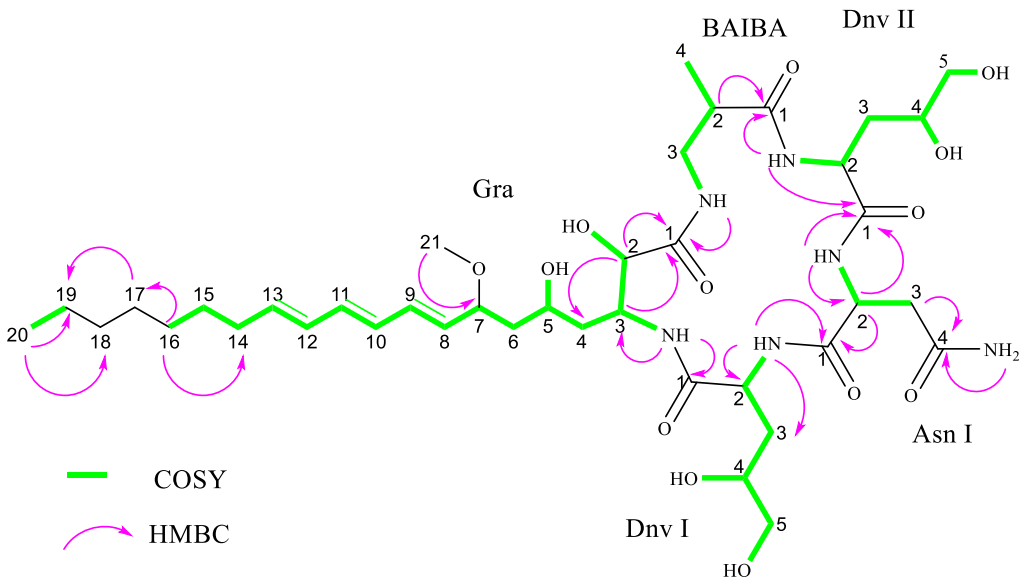

Figure 3.13 Key COSY and HMBC correlations used to establish the molecular connectivity of compound A.

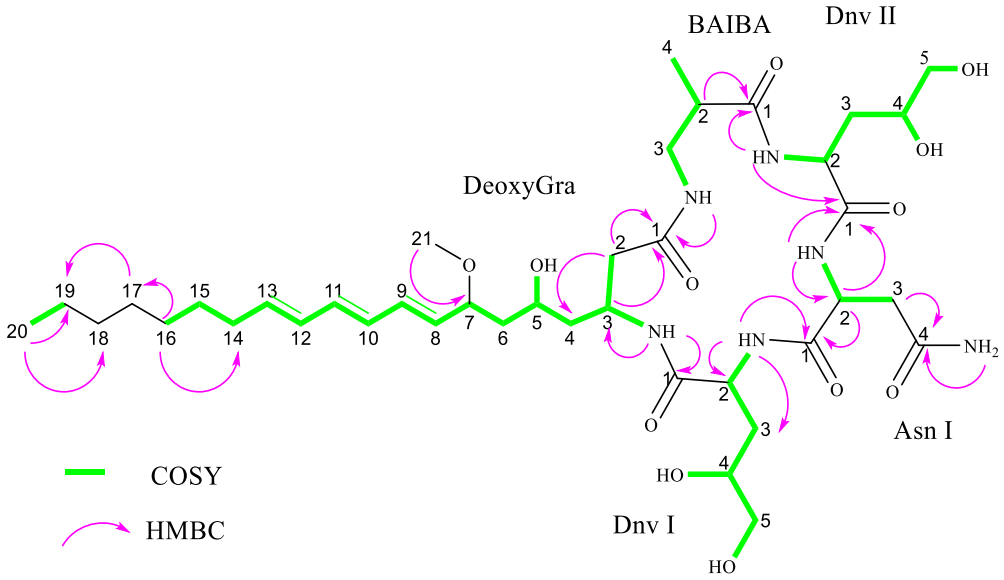

Figure 3.14 Key COSY and HMBC correlations used to establish the molecular connectivity of compound D.

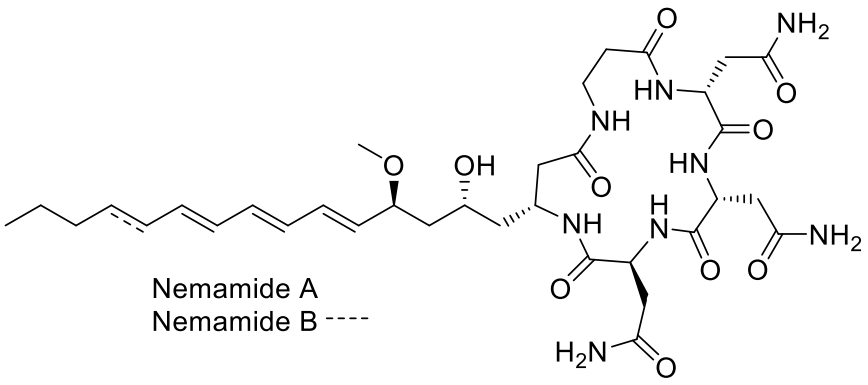

Figure 3.15 Chemical structures of nemamides A and B.

The optical rotations of euglenatides A-E were as follows: euglenatide A: $[\alpha]_D^{25}$ -24.2 (c 0.76, MeOH); euglenatide B: $[\alpha]_D^{25}$ -27.7 (c 0.97, MeOH); euglenatide C: $[\alpha]_D^{25}$ -22.1 (c 0.59, MeOH); euglenatide D: $[\alpha]_D^{25}$ -11.2 (c 0.88, MeOH); euglenatide E: $[\alpha]_D^{25}$ -14.7 (c 0.65, MeOH).

3.2.4. Stereochemistry assignment of euglenatides A-E

3.2.4.1. Crystallisation

Several crystallisation techniques were utilised, including slow solvent evaporation, slow cooling and vapour diffusion.[187] Some transparent glassy materials formed and were sent to Southampton X-ray diffraction unit for structural analysis, but all crystals did not have adequate quality for X-ray diffraction. Euglenatides A and B were tested for crystallization in 96-well crystallization plates against two commercial screens (PACT-premier and JCSG-plus, each with 96 conditions) using sitting-drop vapour diffusion method but this also failed to produce a crystal with a suitable quality.

A sample of pure euglenatide B was sent to crystallisation experts at Crystallise! AG, Switzerland, for crystallisation and X-ray structural analysis. Although some transparent glassy materials formed in the beginning, when exposed to the air, they

turned to a yellowish viscous oil. This suggests that moisture and oxygen might destroy the compound or change its physical consistency. Although one particle provided diffraction, it had low intensities and resolution (3A) being ineffective for structural analysis. Since chemical derivatisation by converting hydroxyl groups to halobenzoic esters or halobenzyl ethers has been shown to facilitate the formation of single crystals for the purpose of X-ray diffraction studies,[188,189] replacement of hydroxyl groups with halobenzyl ethers was trialled with euglenatide B. After 20 h reaction, only a small amount of the original compound was detected by LC-MS along with other molecules smaller than 600 Da which might be degradation products, while the expected derivatised compound was not detected in this sample. After 48 h, neither the original compound nor the expected derivatives were detected.

3.2.4.2. Marfey's analysis

Chemical derivatisation with L-FDVA was used to determine the stereochemistry of the amino acids present in euglenatides A and B.[76,190,191] Asp and BAIBA were commercially available and purchased from Sigma-Aldrich. Dnv authentic standards were not commercially available but were kindly synthesized and provided by Prof. Thierry Gefflaut and Dr Armin Bauer.[192,193] The LC-MS analysis of the hydrolysates indicated that Asn was converted to Asp and reacted with FDVA providing an *m/z* 412.2 in the negative ion mode corresponding to $[FDVA\text{-}Asp\text{-}H]^-$ (Figure 3.16). Comparing the extracted chromatograms of the *m/z* 412.2 in the hydrolysates to the authentic standards revealed the presence of both L-FDVA-L-Asp (RT= 20.66 min) and L-FDVA-D-Asp (RT= 25.52 min) in euglenatide B while euglenatide A contained only L-FDVA-D-Asp (Figure 3.17).

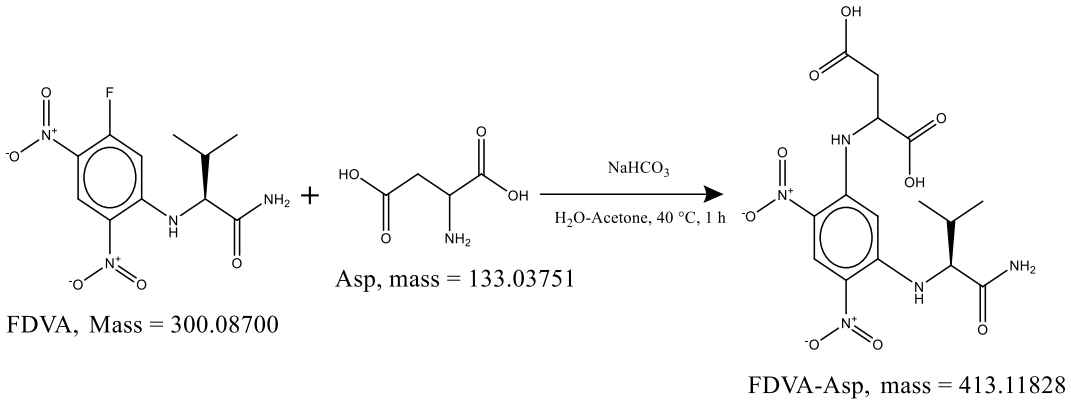

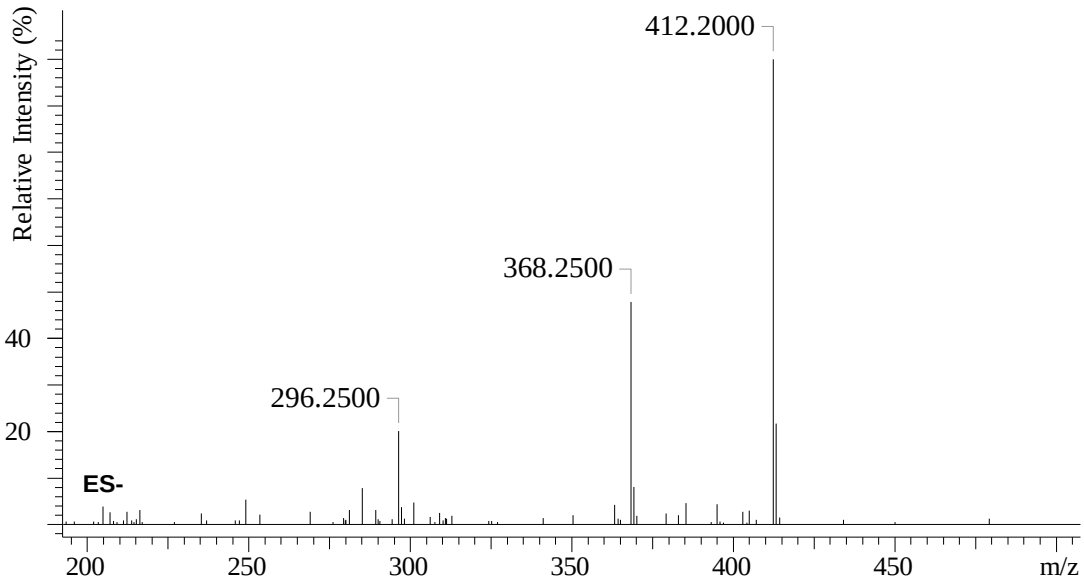

Figure 3.16 Chemical derivatisation and negative ion mode mass spectrum of Asp.

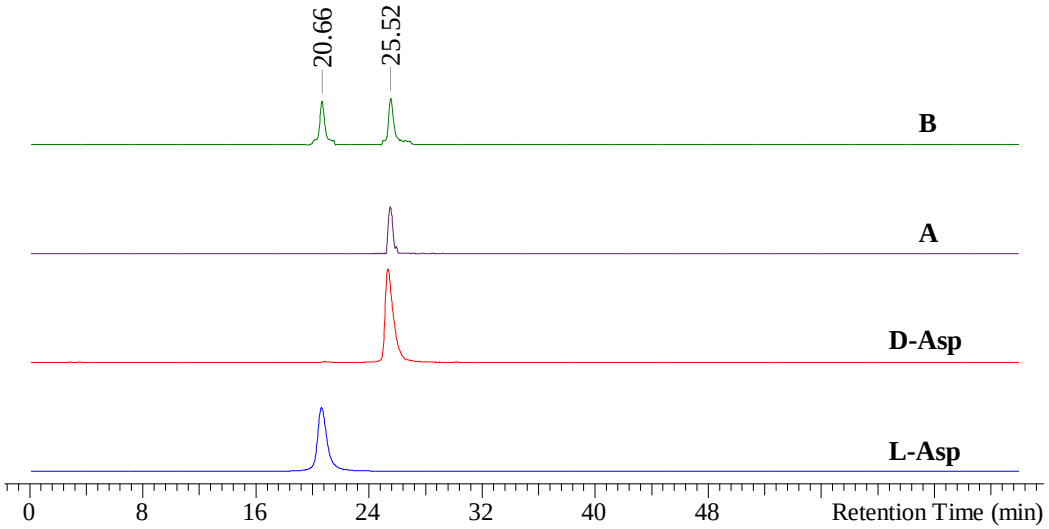

Figure 3.17 Extracted ion chromatograms of the *m/z* 412 in derivatised Asp standards and euglenatides A and B hydrolysates.

Chromatographic separation of BAIBA enantiomers is more challenging as it is difficult to obtain reasonable resolution for derivatised BAIBA diastereomers even when using a relatively long shallow gradient.[194] Nevertheless, with the optimization of chromatographic conditions including mobile phase, stationary phase, temperature, flow rate and isocratic solvent system, it was possible to obtain chromatographic resolution sufficient for assignment of BAIBA configuration. The LC-MS analysis of the hydrolysates and BAIBA enantiomers indicated that the amino acid reacted with L-FDVA to provide an *m/z* 382.0 in the negative ion mode corresponding to [FDVA-BAIBA-H]$^-$ (Figure 3.18). Comparing the extracted chromatograms of the *m/z* 382.0 in the hydrolysates to the authentic standards (L-FDVA-L-BAIBA, RT= 59.47 min; and L-FDVA-D-BAIBA, RT= 56.98 min) revealed the presence of L-FDVA-D-BAIBA in both euglenatides A and B (Figure 3.19).

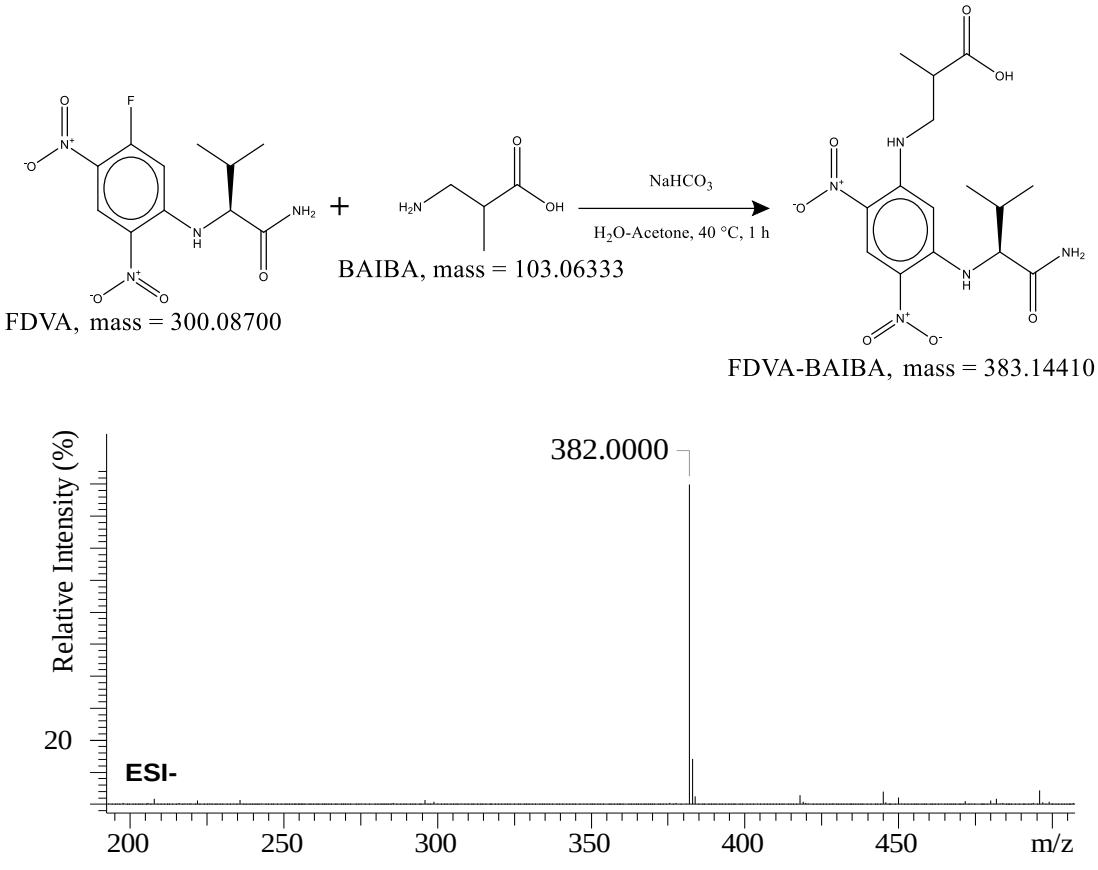

Figure 3.18 Chemical derivatisation and negative ion mode mass spectrum of BAIBA.

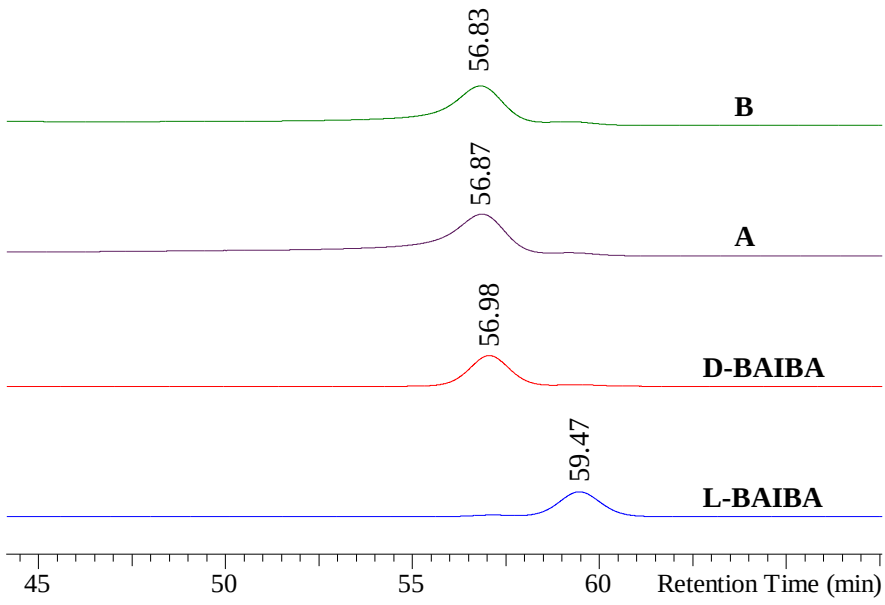

Figure 3.19 Extracted ion chromatograms of the *m/z* 382 in derivatised BAIBA standards and euglenatides A and B hydrolysates.

The Dnv standards provided by Prof. Thierry Gefflaut were not pure but mixtures of L-series: L-Ala (70%) + L-syn-Dnv (26%) + L-anti-Dnv (4%) or D-series: D-Ala (25%) + D-syn-Dnv (9%) + D-anti-Dnv (66%). Nevertheless, the ratio of the isomers was adequate to assign a retention time for each isomer. Moreover, L-anti-norvalinate derivative provided by Dr Armin Bauer was hydrolysed to obtain L-anti-Dnv that was used to confirm the configuration of the Dnv moiety. The LC-MS analysis of the hydrolysates and Dnv diastereomers indicated that the amino acids reacted with L-FDVA to provide an *m/z* 428.1488 in the negative ion mode corresponding to $[FDVA\text{-}Dnv\text{-}H]^-$ (Figure 3.20). Comparing the extracted chromatograms of the *m/z* 428.1488 in the hydrolysates to the authentic standards (L-FDVA-L-anti-Dnv, RT= 17.03 min; L-FDVA-L-syn-Dnv, RT= 32.38 min; L-FDVA-D-anti-Dnv, RT= 24.92 min; L-FDVA-D-syn-Dnv, RT= 29.90 min) revealed the presence of L-FDVA-L-anti-Dnv in both euglenatides A and B (Figure 3.21). Furthermore, the intensity of the Dnv residue in euglenatide A appeared to be

approximately double that in euglenatide B, confirming the presence of two Dnv moieties in euglenatide A with the same configuration.

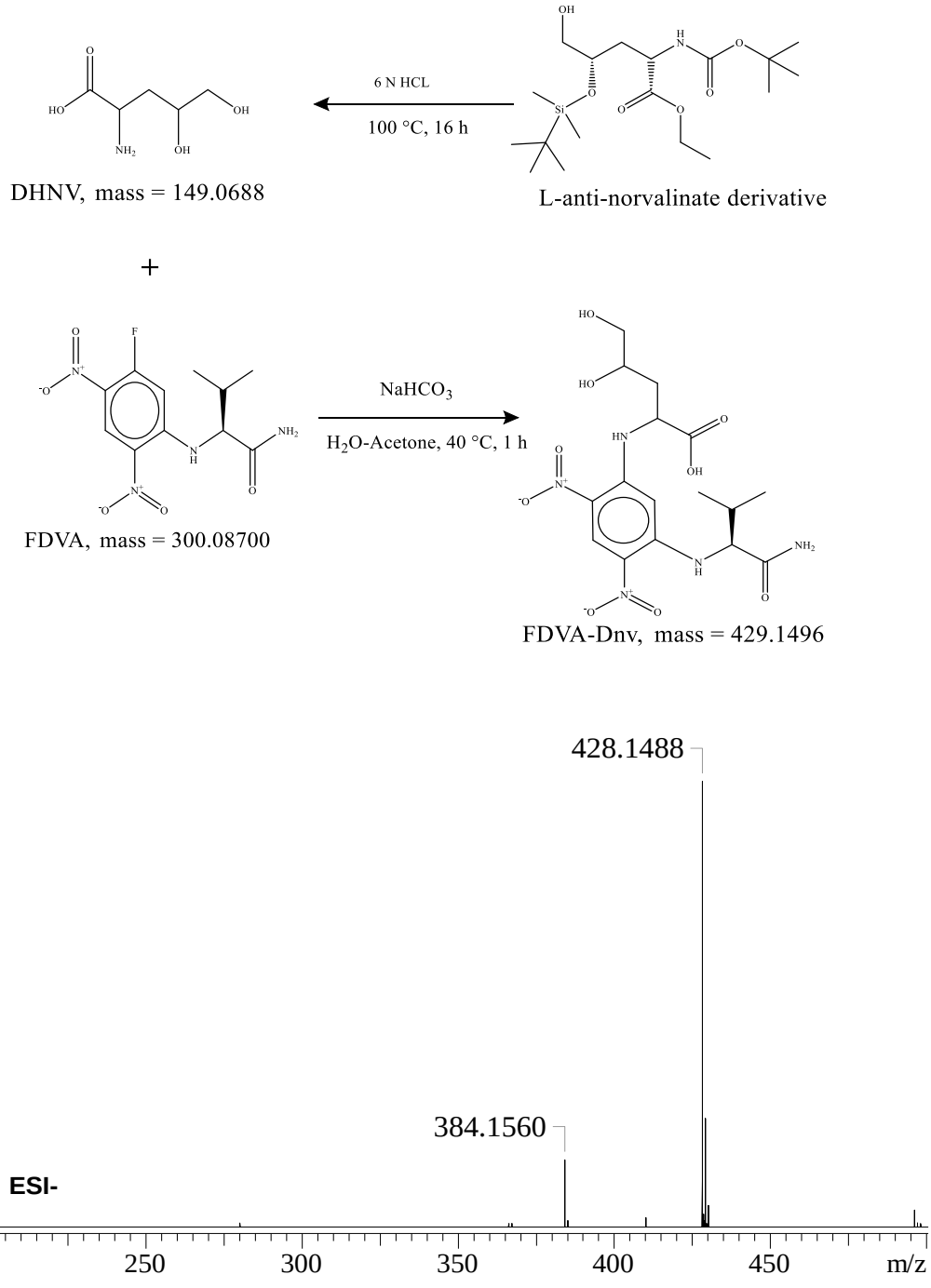

Figure 3.20 Acid hydrolysis of L-anti-norvalinate derivative, and chemical derivatisation and negative ion mode mass spectrum of Dnv.

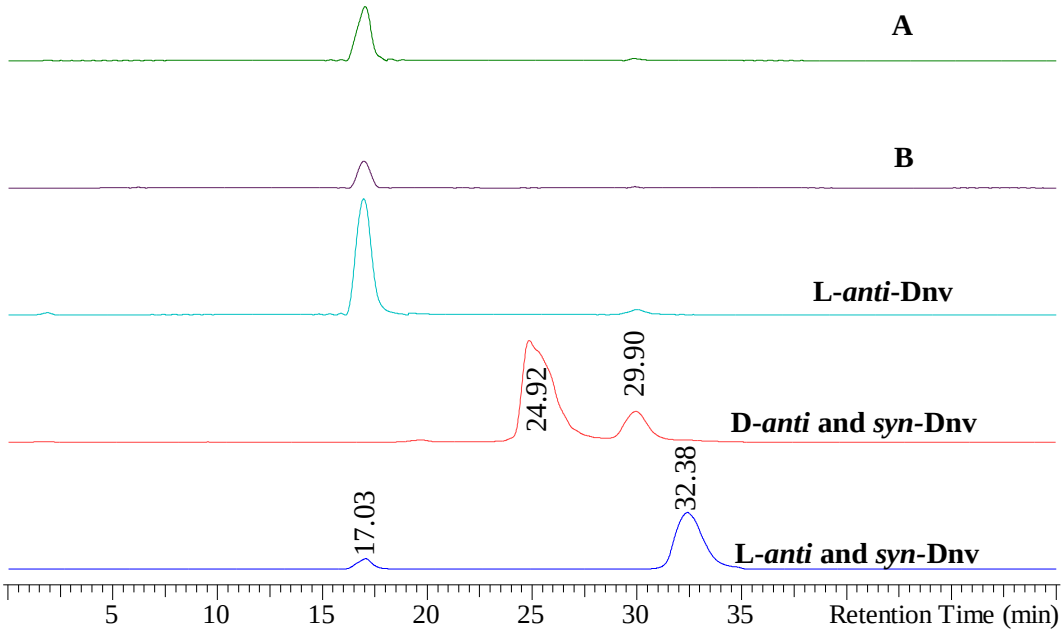

Figure 3.21 Extracted ion chromatograms and spectra of the *m/z* 428 in derivatised Dnv standards and euglenatides A and B hydrolysates.

Finally, the relative configurations of Gra and DeoxyGra were determined by comparison of ^{1}H and ^{13}C NMR chemical shifts, coupling constants, NOESY correlations and CD spectrum to those of nemamide A (Appendices 8.8-8.11). As all data matched those of nemamides, the absolute configurations of euglenatides A-E were proposed as shown in Figures 3.22 and 3.23.

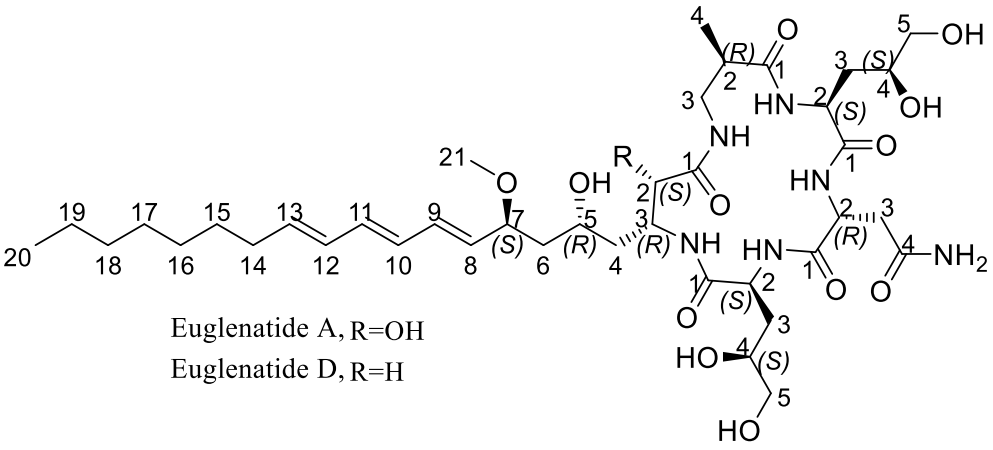

Figure 3.22 Chemical structures and proposed configurations of euglenatides A and D.

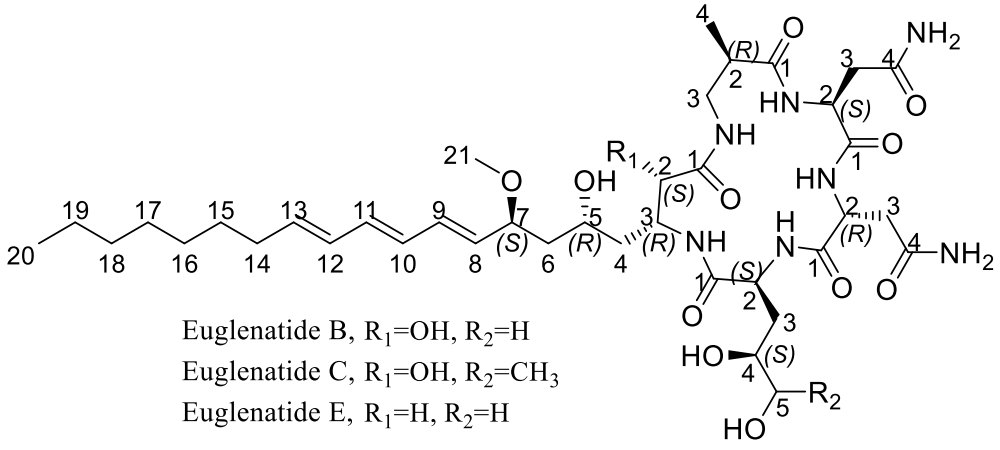

Figure 3.23 Chemical structures and proposed configurations of euglenatides B, C and E.

3.2.5. Antimicrobial activity of euglenatides A-E

Euglenatides A-E were evaluated for their antimicrobial activity against bacteria (methicillin-sensitive *Staphylococcus aureus* (MSSA ATCC 29213), methicillin-resistant *S. aureus* (MRSA MB5393) and *E. coli* ATCC 25922), yeast (*Candida albicans* ATCC 64124), and mould (*Aspergillus fumigatus* ATCC 46645) following previously described methods.[190,195,196] Euglenatides presented antifungal activity, with IC_{50} values ranging from 10.2 to 32.7 µg/mL against *C. albicans* (Figure 3.24) and 3.5 to 6.9 µg/mL against *A. fumigatus* (Figure 3.25). The activity against both yeast (*C. albicans*) and mould (*A. fumigatus*) suggests a broad-spectrum antifungal activity. Remarkably, **A**-**E** did not display any activity against bacteria at the highest tested concentration of 128 µg/mL (Appendix 8.12) suggesting that these compounds have a specific target in eukaryotic cells rather than prokaryotes. Euglenatides A-E were also tested against *C. tropicalis* ATCC 750 and *C. kruseii* ATCC 6258 by Dr Mercedes de la Cruz and Dr Caridad Díaz (Fundación Medina, Spain). The level of activity against these two strains was similar to that against *C. albicans* (Appendix 8.12).

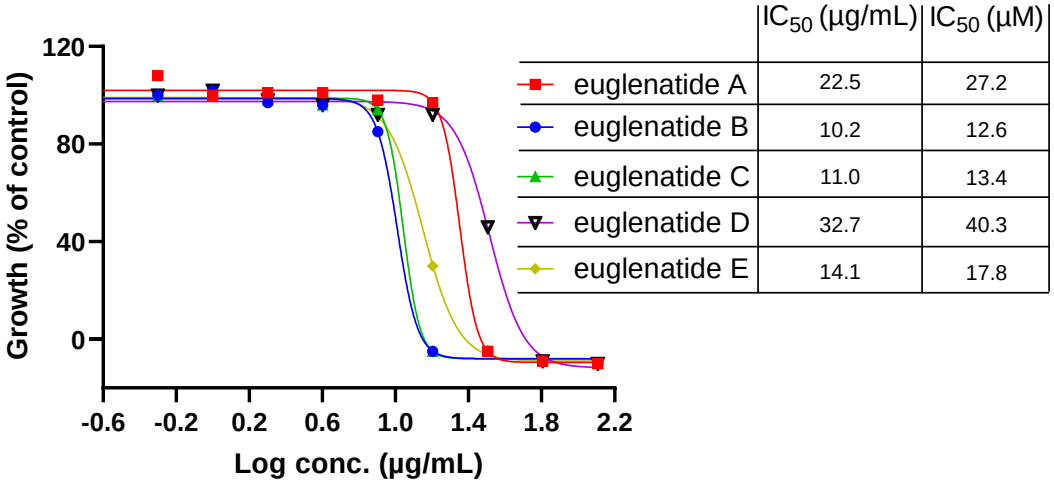

	IC_{50} (µg/mL)	IC_{50} (µM)
euglenatide A	22.5	27.2
euglenatide B	10.2	12.6
euglenatide C	11.0	13.4
euglenatide D	32.7	40.3
euglenatide E	14.1	17.8

Figure 3.24 Dose–response curves and corresponding IC_{50} values of *C. albicans* incubated with euglenatides A, B, C, D and E.

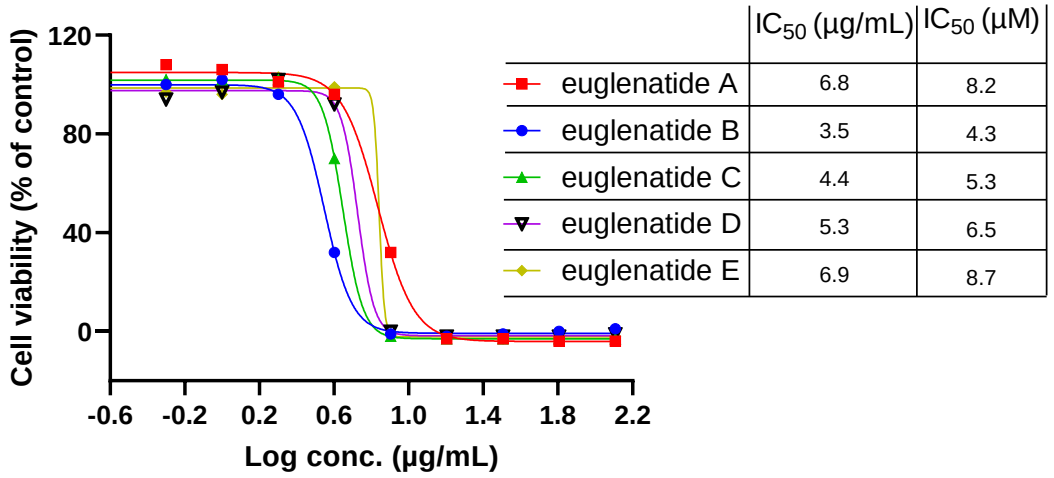

	IC_{50} (µg/mL)	IC_{50} (µM)
euglenatide A	6.8	8.2
euglenatide B	3.5	4.3
euglenatide C	4.4	5.3
euglenatide D	5.3	6.5
euglenatide E	6.9	8.7

Figure 3.25 Dose–response curves and corresponding IC_{50} values of *A. fumigatus* incubated with euglenatides A, B, C, D and E.

3.2.6. Antiproliferative activity of euglenatide B

The IC_{50} of euglenatide B was determined in a panel of human cancer cell lines, including acute monocytic leukaemia (THP-1), breast adenocarcinoma cells (MCF-7) and human lung adenocarcinoma epithelial cells (A-549). Euglenatide B displayed cytotoxic activity at nanomolar levels with IC_{50} values of 533, 773 and 292 nM against THP-1, MCF-7 and A-549, respectively (Figure 3.26). The positive control

(vorinostat) exhibited cytotoxic activity at micromolar levels with IC_{50} values of 2.3, 3.5 and 2.4 µM against THP-1, MCF-7 and A-549, respectively (Figure 3.26).

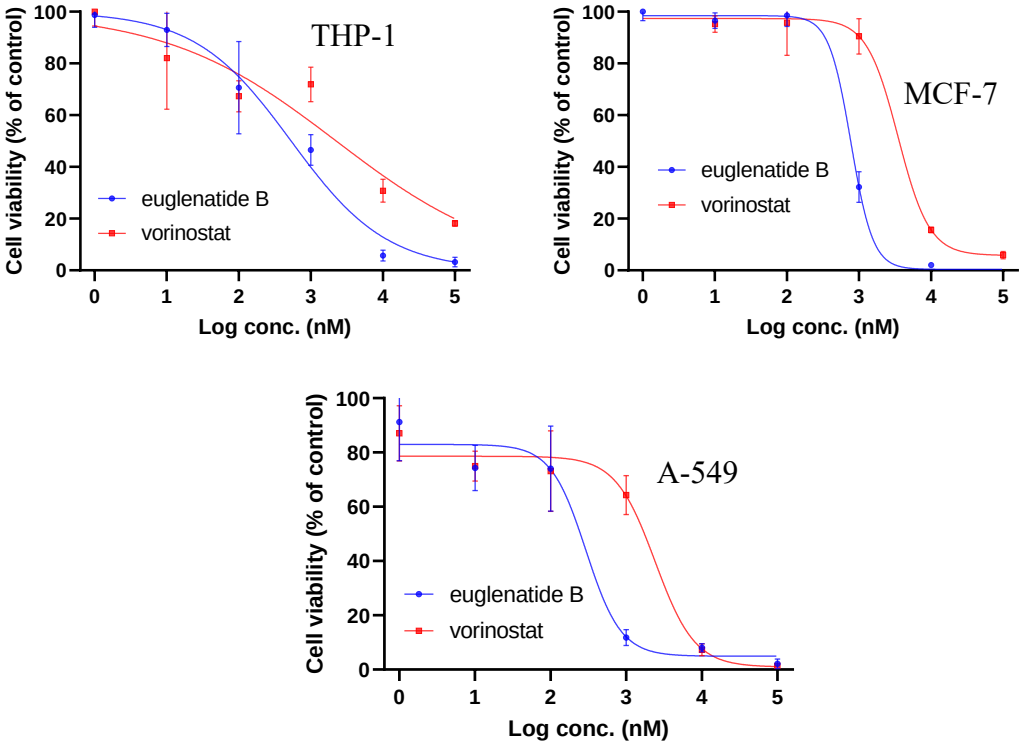

Figure 3.26 Dose–response curves of THP-1, MCF-7 and A-549 cell lines incubated with euglenatide B or vorinostat (positive control). Data points represent the average ± standard error of three replicates.

3.2.7. Antinematodal activity of euglenatide C

Since nemamides A and B were shown to have a positive effect on starvation recovery in *C. elegans*, it was worthy of testing if euglenatides have a similar effect in *C. elegans*. Therefore, three different concentrations of euglenatide C (10 µM, 25 µM and 50 µM) were tested in *C. elegans* by our collaborators in the school of biological sciences, UEA. The conclusion drawn from this experiment was that euglenatide C has a toxic effect at early larval stages of development and does not display an apparent positive effect on starvation recovery.

3.2.8. Algastatic activity of euglenatide B in *E. gracilis*

It is widely believed that a species is capable of avoiding autotoxicity via defensive mechanisms including biosynthesis of toxic compounds in extracellular compartments, excretion of biosynthesised toxic compounds into extracellular compartments, vacuolar sequestration, efflux pumps and modification of the toxic compounds or their target.[197,198] Nevertheless, it has been demonstrated that organisms use toxic metabolites for the regulation of their reproduction and development.[199,200] While low concentrations of toxic metabolites might serve regulatory purposes without negative effects on the producing organism, higher concentrations might result in abnormal processes or even death.[199,200] Moreover, an external application of toxic metabolites might bypass defensive mechanisms, especially when toxic metabolites are biosynthesised or sequestered in extracellular compartments.[200]

To examine the toxicity of euglenatides against the producer, *E. gracilis* was cultivated in EG:JM and treated with different concentrations of euglenatide B, 1 mM vorinostat (positive control) or 1% DMSO (negative control). After four days of treatment, growth was significantly inhibited compared to culture controls (Figure 3.27). However, it appears that the effect is cytostatic rather than cytotoxic as the strain recovered later and achieved a growth level close to the control levels after seven days of treatment (Figure 3.28). This experiment was repeated at 50 μM concentration of euglenatide B in EG:JM and synthetic medium + 30 mM Asn to investigate if the latter medium offers the strain higher tolerance to euglenatides as they are highly produced in this medium. After four days of treatment, there was no significant difference between the inhibition levels in the two media (Figure 3.29). Consequently,

euglenatides might be biosynthesised or stored in isolated compartments to be released and utilised under specific conditions.

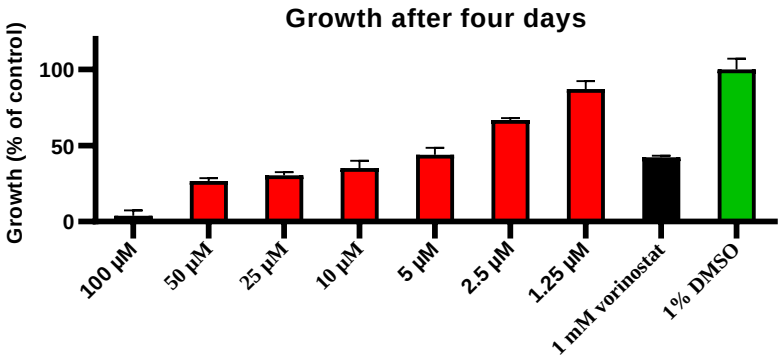

Figure 3.27 Growth of *E. gracilis* in EG:JM after four days of treatment with euglenatide B (1.25 µM to 100 µM), 1mM vorinostat or 1% DMSO (control); data represent the average ± standard error of three replicates.

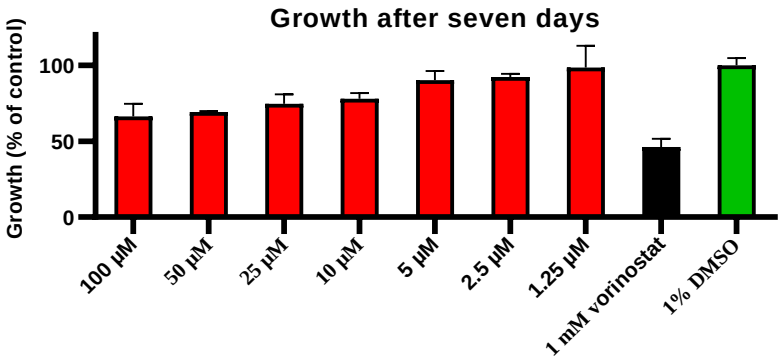

Figure 3.28 Growth of *E. gracilis* in EG:JM after seven days of treatment with euglenatide B (1.25 µM to 100 µM), 1mM vorinostat or 1% DMSO (control); data represent the average ± standard error of three replicates.

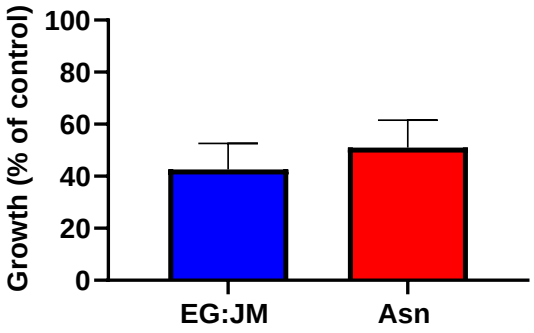

Figure 3.29 Growth of *E. gracilis* in EG:JM (EG:JM) and synthetic medium + 30 mM Asn (Asn) after four days of treatment with 50 µM euglenatide B; data represent the average ± standard error of three replicates.

3.2.9. Related metabolites produced by *E. sanguinea* and *E. mutabilis*

Although *E. gracilis* metabolites displayed potent antifungal and antiproliferative activities, some related metabolites produced by other *Euglena* species might have a higher yield, higher potency, superior selectivity or better physicochemical properties. Therefore, two *Euglena* species, *E. sanguinea* and E. *mutabilis*, were cultivated in complex medium or synthetic medium supplemented with different concentrations of Glu and Asn. *E. sanguinea* displayed limited growth in synthetic medium + 30 mM Glu, synthetic medium + 30 mM Asn and synthetic medium + 60 mM Glu, good growth in synthetic medium + 30 mM Glu + 30 mM Asn, and excellent growth in synthetic medium + 60 mM Asn and complex medium. *E. mutabilis* only had good growth in complex medium.

After ten days of incubation, cultures with good or excellent growth were extracted and analysed by LC-PDA-MS. The TAC of *E. sanguinea* cultivated in synthetic medium + 60 mM Asn contained over 15 peaks while fewer metabolites were detected in the complex medium and even fewer and less abundancy were observed in synthetic medium + 30 mM Glu + 30 mM Asn (Figure 3.30). *E. sanguinea* metabolites showed a UV profile identical to that of *E. gracilis* metabolites. The extract of *E. mutabilis* cultivated in complex medium contained few meltabilities that appeared as intense peaks on the mass spectrometry but were scarcely detected on the TAC (Figure 3.31). This suggests that those metabolites do not contain the conjugated triene system found in *E. gracilis* and *E. sanguinea* metabolites.

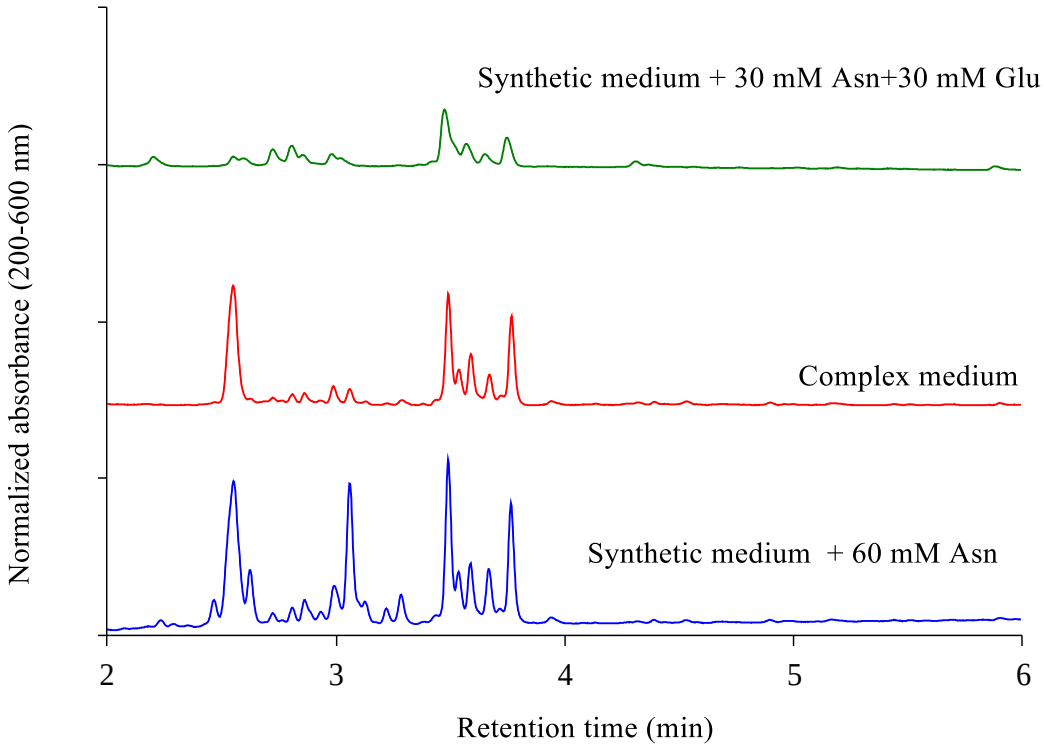

Figure 3.30 Comparative TAC (200-600 nm) of *E sanguinea* cultivated in synthetic medium + 60 mM Asn, complex medium and synthetic medium + 30 mM Asn + 30 mM Glu.

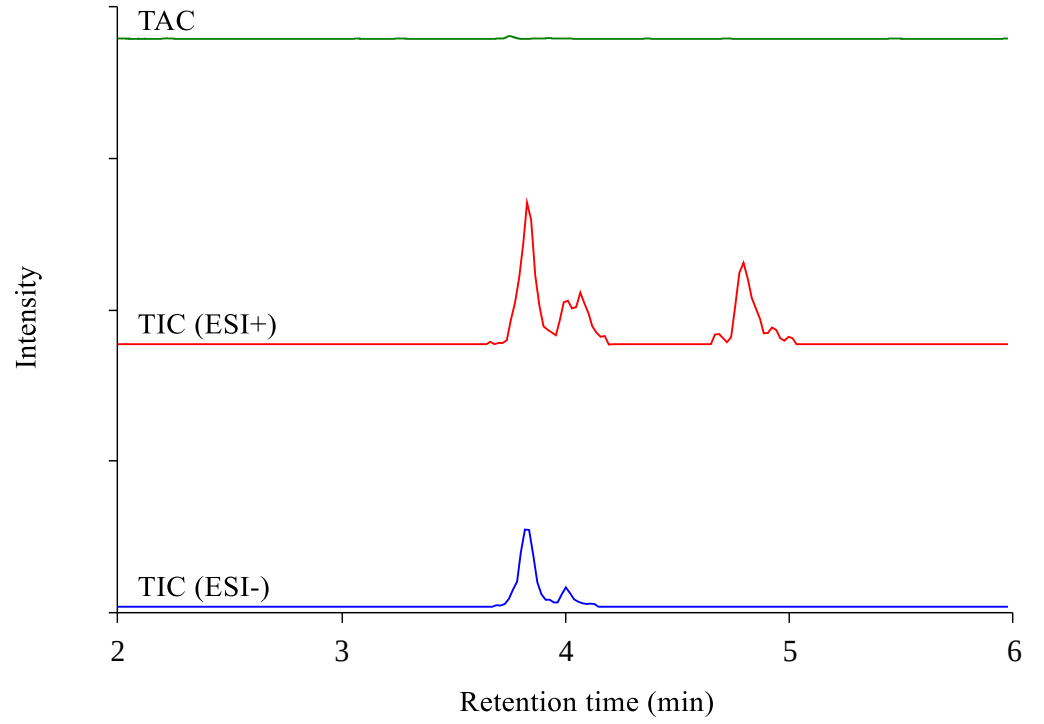

Figure 3.31 Comparative total absorbance (200-600 nm) and total ion chromatograms of *E. mutabilis* cultivated in complex medium.

MS/MS spectra of *E. gracilis, E. sanguinea* and *E. mutabilis* were obtained in negative ion mode and used to construct a molecular network of related metabolites (Figure 3.32). The molecular network is a visual representation of structurally related compounds that share similar MS/MS fragmentation patterns.[79] Each node in the molecular network is labelled with the precursor mass of the molecule deduced from the corresponding MS/MS spectrum. The constructed molecular network contains three groups of three *Euglena* species in different media. Group 1 (pink colour) contains the MS/MS spectra of *E. gracilis* cultivated in the synthetic medium + 30 mM Glu and synthetic medium + 60 mM Asn, group 2 (blue colour) contains the MS/MS spectra of *E. sanguinea* cultivated in the complex medium and synthetic medium + 60 mM Asn, and group 3 (green colour) contains the MS/MS spectra of *E. mutabilis* cultivated in the complex medium.

The structurally similar metabolites are grouped in a cluster, the higher the similarity of compounds, the closer they are in a cluster. For example, precursor masses 808 and 822 represent the MS/MS spectra of euglenatides B and C which are structurally similar with a difference of an extra methyl group in the latter. Precursor masses of euglenatides A and D (825 and 809) appear on the left of the cluster close to each other as they are structurally similar with an additional hydroxyl group in euglenatide A. The colour of the nodes indicates the relative abundance of each metabolite between strains based on the ion intensities of precursors. For instance, metabolite 847 is produced by all three strains while 849 is only produced by *E. mutabilis*. Although all metabolites in the clusters share some fragments, most metabolites are specific to one strain with limited overlapping. Only five metabolites of the euglenatide-related metabolites have been characterized while over 40 metabolites are still unidentified. *E. sanguinea* produces the greatest number of

euglenatide-related metabolites under the investigated conditions, followed by *E. gracilis*. Nevertheless, only the most abundant metabolites are selected for MS/MS fragmentation, and minor metabolites are not included in the molecular network.

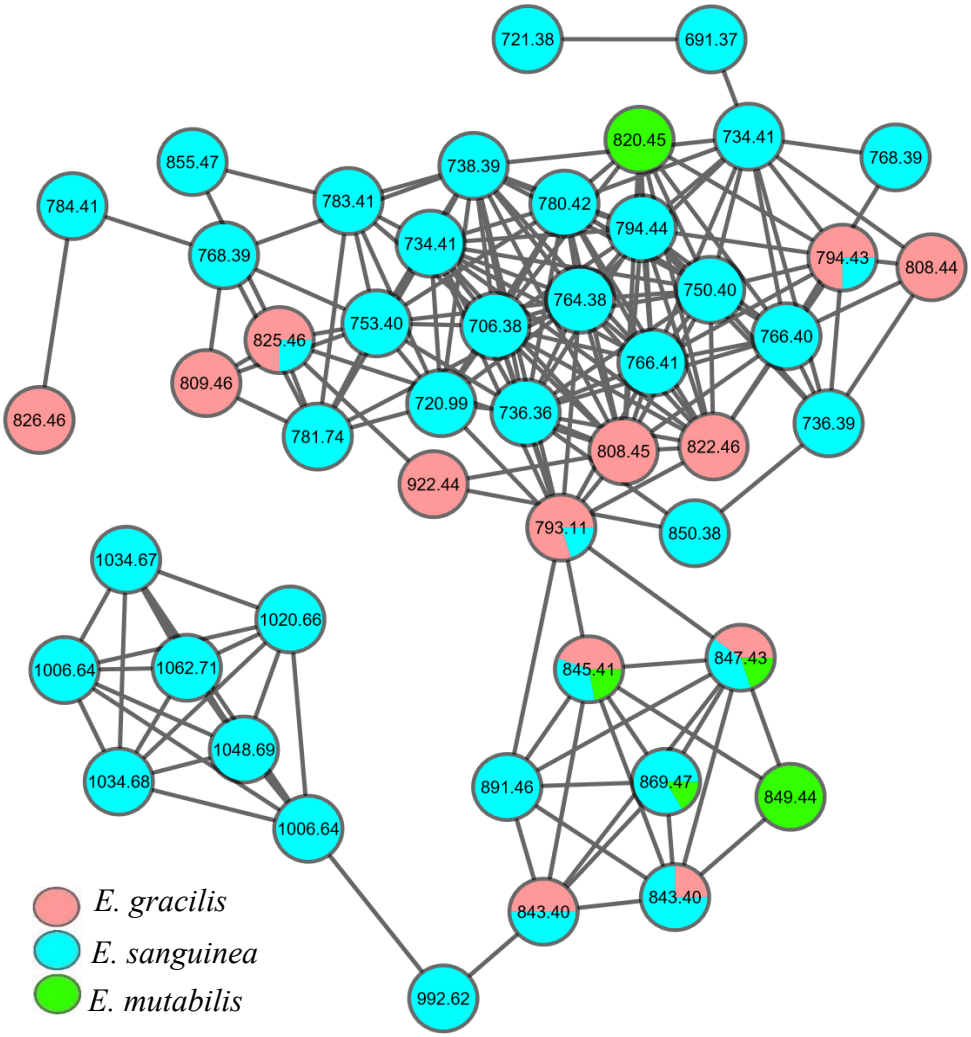

Figure 3.32 A molecular network of the euglenatide-related metabolites produced by *E. gracilis*, *E. sanguinea* and *E. mutabilis* in pink, blue, and green, respectively. Each node represents the precursor mass of a single metabolite, and the colour indicates the relative abundance of each metabolite between strains.

3.2.10. Large-scale cultivation of *E. sanguinea*

E. sanguinea cells (11.8 g) were harvested from a 12-L culture, extracted with 90% MeOH and partitioned with hexane to afford 300 mg of residue. This amount was fractionated on an automated flash-chromatography system to afford 38.3 mg mixture of euglenatide-related metabolites. The residue was dissolved in MeOH, and

purification of the compounds was attempted on a UHPLC system using a semi-preparative C18 column. Several methods were trialled to separate the metabolites, including the method used to purify *E. gracilis* metabolites, with different solvents, temperatures, injection volumes and flow rates. The best separation was achieved with 1 µL injection volume, 20% to 80% acetonitrile in water gradient and 3 mL/min flow rate over 47 min, and all target metabolites were eluted with a retention time between 16 and 25 min (Figure 3.33). However, the separation was not enough to purify individual compounds. Additionally, the increase of the injection volume resulted in poor separation, making it even more difficult to purify enough amount for bioassays and structure elucidation. Therefore, separation and purification of those metabolites require exceptionally long analysis which is time consuming and cost-ineffective. Some options to achieve good separation might be using a normal-phase column or other columns that are designed specifically for peptide isolation.

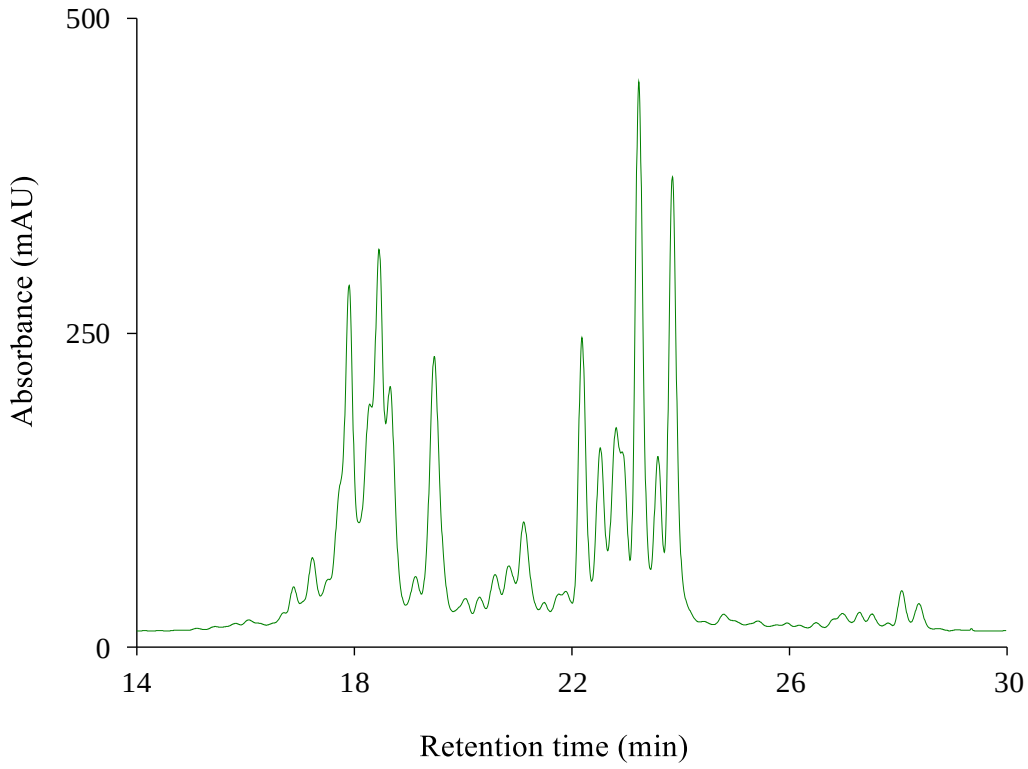

Figure 3.33 Semi-preparative HPLC trace (at 270 nm) of euglenatide-related metabolites produced by *E. sanguinea*.

3.3. Overall discussion and conclusion

Euglenatides contain Asn and unusual amino acids (BAIBA, Gra, DeoxyGra, Dnv and Dnl). All euglenatides isolated from *E. gracilis* cells, cultivated in synthetic medium + 30 mM Glu, contain at least one Asn residue although Asn is absent in the cultivation medium. Moreover, asparagine synthetase, the enzyme that catalyses the last step of asparagine biosynthesis, has not been reported from *Euglena*.[171] BAIBA is an uncommon amino acid in natural products, but it has been reported in a few bacterial and fungal natural products.[201–204] It has also been isolated as a sole amino acid from plants[205,206] and is known as a catabolite of thymine and valine metabolism in human.[207] While the R-form is the enantiomer found in bacteria, plants, fungi and human urine, the S-form has only been reported from human plasma.[201–207] The Gra moiety in euglenatides is similar to the fatty amino acid residue reported from nemamides, but the former has an extra hydroxyl group and two additional methylenes. To the best of our knowledge, the original Dnv and Dnl have not been discovered as a component of natural products although the 5-O-carbamoylated form of Dnv has been found in polyoxin nucleoside peptides[208] and GE81112 tetrapeptides.[209] Moreover, Dnv has been isolated as a sole amino acid from the plant *Lunaria annua*.[210], and is used as an intermediate for the chemical synthesis of clavalanine and echinocandin.[193,211,212]

Euglenatides have a broad spectrum of biological activity against eukaryotic cells with the highest activity against human cell lines and the lowest against the producer *E. gracilis*. Although euglenatides have some structural similarity to nemamides, no biological activity has been reported for the latter metabolites. Moreover, the yield of nemamide A (~ 1.4 µg/L) [186] is considerably lower than that of euglenatide B (~ 316 µg/L). Furthermore, over forty euglenatide-related metabolites

are yet to be characterized and evaluated, which might have higher yields and superior properties in comparison to nemamides and euglenatides A-E.

3.4. Materials and methods

3.4.1. General experiments and materials

Unless stated otherwise, all chemicals and solvents were purchased from Sigma-Aldrich, Alfa Aesar or Fisher Scientific. All solvents were of HPLC grade or equivalent. Commercial media and media components were purchased from Sigma-Aldrich, Alfa Aesar, Fisher Scientific or Formedium. Unless stated otherwise, the pH of media was adjusted to 4.8 with 1 N HCl and 1 N KOH prior to autoclaving.

UV spectra were acquired on an SPD-M20A photodiode array detector attached to a Shimadzu Prominence/Nexera UHPLC. NMR spectra were recorded on a Bruker Avance III spectrometer (500 and 125 MHz for ^{1}H and ^{13}C NMR, respectively) equipped with a 1.7-mm TCI MicroCryoProbe. Chemical shifts were reported in ppm using the signals of the residual solvent as internal reference (δH 2.50 and δC 39.5 ppm for DMSO-d_6). Optical rotations were acquired on a Jasco P-2000 polarimeter (JASCO Corporation, Tokyo, Japan). IR spectra were measured with a JASCO FT/IR-4100 spectrometer (JASCO Corporation) equipped with a PIKE MIRacle™ (JASCO Corporation) single reflection ATR accessory.

3.4.2. High-resolution MS and dereplication

For the accurate mass measurement, high-resolution mass spectra were acquired on a Synapt G2-Si mass spectrometer (Waters) operated in negative ion mode with a scan time of 1.0 second in the mass range of *m/z* 50 to 1200. An aliquot of 7 µL of each sample was injected onto an Acquity UPLC® BEH C18 column, 1.7 µm, 1x100

mm (Waters) maintained at 45 °C and eluted with mobile phases A (water + 0.1% formic acid) and B (acetonitrile + 0.1% formic acid) at a flow rate of 80 µL/min. The following gradient was used: 0-1 min (15% B), 11 min (99% B), 11.1 min (15 % B), 15 min (15 % B). The following parameters were used: capillary voltage = 2.5 kV; cone voltage = 40 V; source temperature = 130 °C; desolvation temperature = 350 °C; source offset 80 V. Leu-enkephalin peptide was used as a lock mass (*m/z* = 554.2620) measured every 30 seconds during the run.

MS/MS spectra *E. gracilis* metabolites were acquired using the LC-PDA-MS analysis method, as described in chapter 2 (section 2.4.3). The spectra were converted to a compatible format using LabSolutions software (Shimadzu) and used to search Global Natural Products Social Molecular Networking.[80] For METLIN and MassBank searching, spectra of metabolites were extracted using ACD/Spectrus Processor and exported as lists of peaks. The peaks lists were used to search METLIN and MassBank for structurally similar molecules.

3.4.3. Large-scale cultivation, isolation and purification

E. gracilis inocula were prepared as described in chapter 2 (section 2.4.4) and used to inoculate 18 L of synthetic medium + 30 mM Glu to obtain approximately 0.2 g of wet cells per litre (1:20 dilution). The culture was cultivated at ambient temperature 22-25 ^{o}C under daylight lamps (2000 lumens). After ten days, the culture was centrifuged at 3130 x g and 4 ^{o}C for 20 min, and the pellet (53 g) was extracted with 1 L 90% MeOH on a magnetic stirrer. After an hour, the aqueous MeOH extract was partitioned with an equal volume of hexane to remove lipids and pigments. The aqueous MeOH layer was centrifuged to remove the debris and then evaporated to get the residue (1.679 g). This amount was dissolved in 50 mL MeOH along with 15 g of

C18 powder, and the solvent was evaporated. The resulting powder was halved into two columns packed with 65 g reversed-phase resin, previously equilibrated with 20% acetonitrile before a frit was added on the top. The extract loaded on the column was fractionated on an automated flash-chromatography system (CombiFlash Rf, Teledyne Isco) using 18 mL/min flow rate and a linear gradient from 20% to 70% acetonitrile in water (in 40 min) followed by a ramp to 100% acetonitrile in 4 min before washing the column for 16 min.

Fractions containing the target compounds were concentrated to dryness on a centrifugal evaporator to give a residue amount of 186.7 mg. This amount was dissolved in MeOH, and the compounds were purified on a semi-preparative C18 column attached to Gilson HPLC system with UV detection at 210 and 270 nm, using 34% isocratic acetonitrile in water and 3 mL/min flow rate. The purity of the isolated compounds was confirmed by injecting an aliquot in an Agilent 1100 LC-DAD-MS system using a Zorbax SB-C8 column (2.1 × 30 mm, 5 μm, flow rate 0.3 mL/min, 40 °C) with a linear gradient from 10% B to 100% B in 6 min followed by 2 min hold at 100% B before returning to10% B and equilibrating the system for 2 min. Solvent A was 10% acetonitrile in water, and solvent B was 90% acetonitrile in water, both supplemented with 1.3 mM trifluoroacetic acid and ammonium formate.

3.4.4. Crystallisation and chemical derivatisation

Slow solvent evaporation and slow cooling of euglenatides A, B and C were performed using different percentages of MeOH in water, acetone, EtOAc or toluene, and vapour diffusion using MeOH in the inner vial and diethyl ether in the outer vial.[187] For the sitting-drop vapour diffusion method, two commercial screens (PACT-premier and JCSG-plus, each with 96 conditions) were used for crystallisation

in 96-well crystallisation plates.[213] Euglenatides A and B were prepared in Milli-Q water to obtain a concentration of 1.8 mg/mL and centrifuged at 13000 rpm to remove insoluble materials. Each well contained 0.4 µL of euglenatides A or B and 0.4 µL of precipitant, and a reservoir containing 50 µL of precipitant. Plates were incubated at 20 °C in the dark and monitored daily under a microscope for three months. This experiment was repeated with a higher concentration of euglenatide B (10 mg/mL).

Chemical derivatisation to facilitate the formation of single crystals for the purpose of X-ray diffraction studies was performed as described by Kuroda *et al*.[188] Briefly, triethylamine (5.5 µL, 75 mM), and 4-bromobenzyl chloride (7.7 mg, 75 mM) were successively added to a solution of euglenatide B (3 mg, 7.5 mM) in N,N-dimethylformamide (0.5 mL) at 0 °C. The reaction mixture was stirred at room temperature for 20 h, then an aliquot (20 µL) of the reaction mixture was diluted with 200 µL MeOH and analysed by LC-PDA-MS. After 48 h, brine (2 mL) was added, and the resulting mixture was extracted with EtOAc (10 mL x 3). The organic phase was combined and concentrated on a Rotavapor. The residue was dissolved in 1 mL MeOH and analysed by LC-PDA-MS.

3.4.5. Marfey's analysis

To determine the configurations of the two asparagine amino acids, euglenatides A and B were hydrolysed in sealed vials with 6 N HCl (0.5 mg/mL) at 110 °C for 16 h. The hydrolysates were evaporated to dryness in a centrifugal evaporator, and the residues were dissolved in 50 µL of Milli-Q water. Stock solutions of the amino acid standards (50 mM, L-Asp and D-Asp, Sigma-Aldrich) were prepared in Milli-Q water. The hydrolysates and standard amino acids (50 µL) were treated with 20 µL of 1 M $NaHCO_3$ and 150 µL of 1-fluoro-2,4-dinitrophenyl-5-L-valine-amide (L-FDVA,

Marfey's reagent; 1% w/v in acetone) and heated at 40 °C for 1 h. Reactions were quenched with 20 µL of 1 N HCl, and an aliquot (10 µL) was diluted with acetonitrile (40 µL) and analysed by an Agilent 1100 LC-DAD-MS system (UV detection at 340 nm and ESI-MS detection in positive and negative modes). The following gradient was used (solvent A versus solvent B) on a Waters X-Bridge C18 column (4.6 × 150 mm, 5 µm) maintained at 40 °C, 0.0 min (10% B), 50.0 min (27% B), 54.0 min (100% B), 60.0 min (100% B), 61.0 min (10% B), 70.0 min (10% B), at a flow of 1 mL/min. Solvent A was 10% acetonitrile in water, and solvent B was 90% acetonitrile in water, both supplemented with 1.3 mM trifluoroacetic acid and ammonium formate.

L-BAIBA and D-BAIBA were purchased from Sigma-Aldrich and prepared similarly to Asp standards. The LC-PDA-MS analysis was performed on a Shimadzu 2020 single quadrupole LC-PDA-MS system (UV/visible detection range from 200 to 600 nm and ESI-MS detection in positive and negative modes) using an Accucore C18 column (2.1 × 100 mm, 2.6 µm) maintained at 50 °C. An isocratic solvent system of MeOH/water (25/75) with 0.1% formic acid was used at a flow of 0.350 mL/min over 70 min. L-syn-Dnv, L-anti-Dnv, D-syn-Dnv, D-anti-Dnv and L-anti-norvalinate derivative were kindly provided by Prof. Thierry Gefflaut and Dr Armin Bauer.[192,193] The L-anti-norvalinate derivative was hydrolysed in a sealed vial with 6 N HCl (1 mg/mL) at 110 °C for 16 h, and the hydrolysate was evaporated to dryness in a centrifugal evaporator. The hydrolysates and reference standards were prepared as described for the Asp standards. The LC-PDA-MS analysis was performed on a Shimadzu Prominence/Nexera IT-ToF LC-PDA-MS system (UV/visible detection range from 200 to 600 nm and ESI-MS detection in positive and negative modes) using an Accucore C18 column (2.1 × 100 mm, 2.6 µm) maintained at 30 °C. The following elution system was used (MeOH versus 0.1% formic acid in water, at 0.200 mL/min):

0.0-34.0 min (30% MeOH), 35.0 min (100% MeOH), 40.0 min (100% MeOH), 42.0 (30% MeOH), 50.0 min (30% MeOH).

3.4.6. Antimicrobial assays

Euglenatides A-E were evaluated for their antimicrobial activity against bacteria (methicillin-sensitive *S. aureus* (MSSA ATCC 29213), methicillin-resistant *S. aureus* (MRSA MB5393) and *E. coli* ATCC 25922), yeast (*C. albicans* ATCC 64124), and mould (*A. fumigatus* ATCC46645) following previously described methods.[190,195,196] Each peptide was serially diluted in DMSO with a dilution factor of 2 to provide ten concentrations for all assays, and the final concentrations of each peptide were ranging from 128 to 0.25 µg/mL. Results were analysed using Microsoft Excel and GraphPad Prism 8.0 software.

To assess the antibacterial activity, thawed stock inocula suspensions from cryovials of each microorganism (MSSA ATCC 29213, MRSA MB5393 and *E. coli* ATCC 25922) were streaked onto LBA (Luria-Bertani agar plates, 40 g/L) and incubated overnight at 37 °C. Isolated colonies of each microorganism were inoculated into Luria-Bertani broth medium (LB, 25 g/L) and incubated overnight (MSSA and MRSA) or for two hours (*E.coli*) at 37 °C with shaking at 220 rpm. After incubation for the specified periods, cultures were diluted in Miller Hinton II medium to attain assay inocula of approximately 5-6 × 10^5 CFU/mL (MSSA and *E. coli*) and 1.1 × 10^6 CFU/mL (MRSA). In 96-well microplates, 90 µL/well of the diluted inoculum were mixed with 1.6 µL/well of each concentration of each compound and 8.4 µL/well of Miller Hinton II medium. Aztreonam 20-0.078125 µg/mL was used as a positive control with *E. coli* and vancomycin 32-0.25 µg/mL with MSSA and MRSA. Absorbance was measured at 612 nm with a multimode plate reader (EnVision Perkin

Elmer) at T_0 (zero time) immediately before incubation at 37 °C for 20 h. After this period, the assay plates were agitated using a DPC Micromix-5 and the absorbance was measured at T_f (final time). The following equation was used to calculate growth inhibition: Growth (% control) = 100 × {[(T_f Absorbance of treated culture - T_0 Absorbance of treated culture) - (T_f Absorbance of broth medium - T_0 Absorbance of broth medium)]/ [(T_f Absorbance of untreated culture - T_0 Absorbance of untreated culture) - (T_f Absorbance of broth medium - T_0 Absorbance of broth medium)]}.

To evaluate the activity against yeast, Sabouraud Dextrose Agar (SDA) plates were inoculated with frozen stocks of *C. albicans* ATCC 64124 and incubated at 35 °C. After 24 h, a few colonies were harvested from the plates and suspended in RPMI liquid medium prepared from RPMI-1640 medium (20.8 g of RPMI powder in 1.8 L) supplemented with 13.4 g of yeast nitrogen base, 72 mL of 50% glucose and 80 mL of 1 M HEPES. The liquid medium was filtered after adjusting the volume to 2 L with Milli-Q water. The optical density of C. *albicans* suspension was adjusted to 0.25 at 660 nm using the liquid medium as a diluent and blank. This inoculum was diluted 1:10 and reserved on ice until used for inoculation. In 96-well microplates, 90 µL/well of the diluted inoculum was mixed with 1.6 µL/well of each concentration of each compound and 8.4 µL/well of the liquid medium. Amphotericin B was used as a positive control. Absorbance was measured at 612 nm with a multimode plate reader (EnVision Perkin Elmer) at T_0 (zero time) immediately before incubation at 37 °C for 20 h. After this period, the assay plates were agitated using a DPC Micromix-5, and the absorbance was measured at T_f (final time). Growth inhibition was calculated using the equation mentioned above.

To test the antifungal activity against *A. fumigatus*, PDA plates were flooded with Tween saline (0.025% v/v of Tween 80 and 8 g/L NaCl), and colonies were

harvested in RPMI liquid medium by gently scraping the surface of the agar with a sterile spatula to prepare a conidial suspension. This suspension was filtered through sterile chiffon, and the concentration was determined by counting the conidia in a Neubauer chamber. The inoculum was approximately 2.5×10^4 CFU/mL. Resazurin stock solution of 0.02 g in 100 mL was prepared from resazurin sodium salt (R7017, Sigma Aldrich) in Milli-Q water, sterilised by filtration and used as an indicator of eukaryotic cell viability (0.002% final concentration). Resazurin is a blue oxidation-reduction dye that is itself weakly fluorescent until it is irreversibly reduced to the pink-coloured and highly red-fluorescent resorufin.[195] In 96-well microplates, 90 µL/well of the inoculum were mixed with 1.6 µL/well of each concentration of each compound and 8.4 µL/well of the liquid medium. Amphotericin B and Rifampicin were used as positive and negative controls, respectively. The plates were incubated at 37 °C for 25-30 h without agitation. After incubation, fluorescence was recorded on a multimode plate reader (EnVision Perkin Elmer) using wavelength settings for resorufin (excitation 570 nm, emission 600 nm). Growth inhibition was calculated using the equation mentioned above but using the fluorescence instead of absorbance. Wells with 0.002% resazurin in broth medium were used as blanks.

3.4.7. Antiproliferative assay

Three cancer cell lines (from ECACC) were cultured in RPMI 1640 medium (A549 and THP-1 cell lines) or DMEM (MCF-7 cell line) medium supplemented with 10% fetal calf serum, 2 mM L-glutamine, 100 U/mL penicillin and 100 µg/mL streptomycin (Invitrogen). Cells (3×10^4 /100 µL for THP-1 and 6×10^3 /100 µL for A549 and MCF-7) were seeded in 96-well plates and treated immediately (THP-1) or after 22 h (A549 and MCF-7) with 1 µL of DMSO (vehicle control) or 1 µL of the

compound in DMSO at different concentrations in triplicate, and plates were incubated at 37 °C and 5% CO_2. Cell viability was assessed by CellTiter 96 Aqueous One Solution Cell Proliferation Assay (Promega) following the manufacturer's instructions. The assay contains MTS (3-(4,5-dimethylthiazol-2-yl)-5-(3-carboxymethoxyphenyl)-2-(4-sulfophenyl)-2H-tetrazolium) reagent, which is a colourimetric method that measures mitochondrial metabolic activity. After 72 h of incubation, MTS assay reagent (10 µL) was added to the cells, and plates were incubated further for 1.5 h for A549 and MCF-7 and 4 h for THP-1. Following this, absorbance was measured at 490 nm using a Polarstar Optima microplate reader (BMG Labtech). Wells with only culture medium and MTS solution were used to determine the background, and cells treated with 1% DMSO were used as the negative controls. Cell viability of treated cells was calculated relative to the negative controls after background correction of all wells. IC_{50} values were calculated using GraphPad Prism 8.0 software.

3.4.8. Antinematodal and algastatic activity

Antinematodal activity experiments were conducted by our collaborators in the School of Biological Sciences, UEA.

For algastatic activity, *E. gracilis* cells were harvested from four-day-old culture by centrifugation at 2000 x g and 10 ^{o}C for 5 min and suspended in EG:JM or synthetic medium + 30 mM Asn. The absorbance at 740 nm was adjusted on a CLARIOstar microplate reader to 0.1 (≈ 4 g of wet cells per litre) using EG:JM or synthetic medium + 30 mM Asn as a diluent and blank. This inoculum was diluted 1:20 (≈ 0.2 g of wet cells per litre) and used to inoculate a 96-well microtiter plate. Each well contained 99 µL of the diluted inoculum and 1 µL of DMSO (vehicle control) or 1 µL of the

compound in DMSO at two-fold serial dilutions with the highest concentration at 100 μM and the lowest at 1.25 μM. The plate was incubated at ambient temperature 22-25 ^{o}C under daylight lamps (2000 lumens), and the absorbance was measured at 740 nm after four and seven days of incubation. Wells with only growth medium were used for background correction, cells treated with 1% DMSO were used as negative controls, and cells treated with 1 mM of vorinostat were used as positive controls. Three replicates per condition were performed, and the percentage of growth inhibition was calculated relative to the negative controls after background correction of all wells. Results were analysed using Microsoft Excel and GraphPad Prism 8.0 software.

3.4.9. Euglenatide-related metabolites and molecular networking

E. sanguinea and *E. mutabilis* were provided by Dr Ellis O'Neill (Nottingham University, UK). *E. gracilis, E. sanguinea* and *E. mutabilis* were cultivated in the following media: synthetic medium + 30 mM Glu; synthetic medium + 30 mM Asn; synthetic medium + 60 mM Asn; synthetic medium + 60 mM Glu; synthetic medium + 30 mM Glu + 30 mM Asn; complex medium. Inocula preparation, cultivation and extraction were performed as described in chapter 2 (section 2.4.7). Extracts were analysed by a Shimadzu LC-PDA-MS as described in chapter 2 (section 2.4.3). The LC and MS data were processed using ACD/Spectrus, and the MS/MS spectra were converted to an mzXML file format using LabSolutions software (Shimadzu). GNPS spectral library[80] was searched for similar molecules using the converted files of MS/MS spectra (GNPS; https://gnps.ucsd.edu) and used to construct a molecular network of euglenatide-related metabolites. The following GNPS parameters were used:[214] Parent Mass Tolerance = 1 Da, Min Pairs Cos = 0.6, Min Matched Peaks = 3, Network TopK = 15, MSCluster = ON, Minimum Peak Intensity = 25, Filter

Precursor Window = OFF, Filter Library = OFF, and Filter peaks in 50 Da Window = OFF. The molecular network was exported from GNPS and analysed using the visualisation software Cytoscape.[81]

3.4.10. Large-scale cultivation of *E. sanguinea*

E. sanguinea inocula were prepared as described for *E. gracilis* in chapter 2 (section 2.4.7) and used to inoculate 12 L of the complex medium. The culture was cultivated at ambient temperature 22-25 ^{o}C under daylight lamps (2000 lumens). After ten days, the culture was centrifuged at 5000 x g and 4 ^{o}C for 10 min, and the pellet (11.8 g) was extracted with 1 L 90% MeOH in water and a magnetic stirrer. After an hour, the aqueous MeOH extract was partitioned with an equal volume of hexane to remove lipids and pigments, and the aqueous MeOH layer was centrifuged to remove the debris and then evaporated to get the residue (300 mg).

The extract was loaded on a 43 g C18 column, previously equilibrated with 10% MeOH, and fractionated on an automated flash-chromatography system (CombiFlash Rf, Teledyne Isco) using 40 mL/min flow rate and a linear gradient from 10% to 100% MeOH in water (in 22 min) before washing the column with 100% MeOH (for 10 min). Fractions containing the target compounds were combined and concentrated to dryness to give a residue amount of 38.3 mg. The residue was dissolved in 3 mL MeOH, and purification of the compounds was attempted using a semi-preparative C18 column on an Agilent 1290 Infinity UHPLC system equipped with a diode array detector with detection at 210 and 270 nm. Several methods were attempted to separate the metabolites including the method used to purify the *E. gracilis* metabolites, using different elution modes, solvent systems, injection volumes, temperatures and flow rates.

Chapter Four

4. Nutritional and epigenetic manipulation in *Aspergillus*

4.1. Introduction

Filamentous ascomycete fungi are the source of some of the major antibacterial and antifungal classes approved by the FDA, as demonstrated in chapter one. *Aspergillus* and *Penicillium* are the well-known natural product producers from this fungal class. Both *Aspergillus* and *Penicillium* are easy to cultivate under a wide range of conditions and have a fast growth rate. However, the large number of available genome sequences and accessibility of strains from culture collections are the main advantages to *Aspergillus*. Moreover, nutritional and epigenetic manipulation strategies have been successfully used with a great number of *Aspergillus* species, as explained in chapter one.

Genome mining of *Aspergillus nidulans* revealed 56 putative secondary metabolite core genes including 29 PKS and PKS-like genes, 26 NRPS and NRPS-like genes, and one hybrid NRPS-PKS gene.[215] Fewer than 50% of those secondary metabolite biosynthetic genes could have been linked to known metabolites.[216] Similarly, it was reported that the soil fungus, *Aspergillus niger*, harbour 31 PKS, 15 NRPS, and 9 hybrid NRPS-PKS BGCs and that fewer than 30% of these BGCs were transcribed under various culture conditions.[217] Although several metabolites remain to be identified from *A. nidulans* and *A. niger*, both nutritional and epigenetic strategies have been employed for the activation of cryptic BGCs in these two species, as described in chapter one. Therefore, over 20 *Aspergillus* genome sequences were searched for BGCs to select the best candidates for natural product discovery.

4.2. Results and discussion

4.2.1. Genome mining

AntiSMASH[44] was used to search the genomes of over twenty *Aspergillus* species for natural product BGCs. The genomes of five *Aspergillus* species contained a large number of putative BGCs (>50): *A. calidoustus* NRRL 281, *A. westerdijkiae* NRRL 3174, *A. bombycis* NRRL 26010, *A. carbonarius* NRRL 369 and *A. fischeri* NRRL 181. Importantly, only a few of the predicted BGCs could be linked to known metabolites (Figure 4.1). Additionally, these five species are available in the US Agricultural Research Service (USDA-ARS) culture collection and have distinct coloured colonies that are helpful to differentiate them and avoid cross-contamination (Figure 4.1). Therefore, these *Aspergillus* species appeared to be appropriate candidates for natural product discovery.

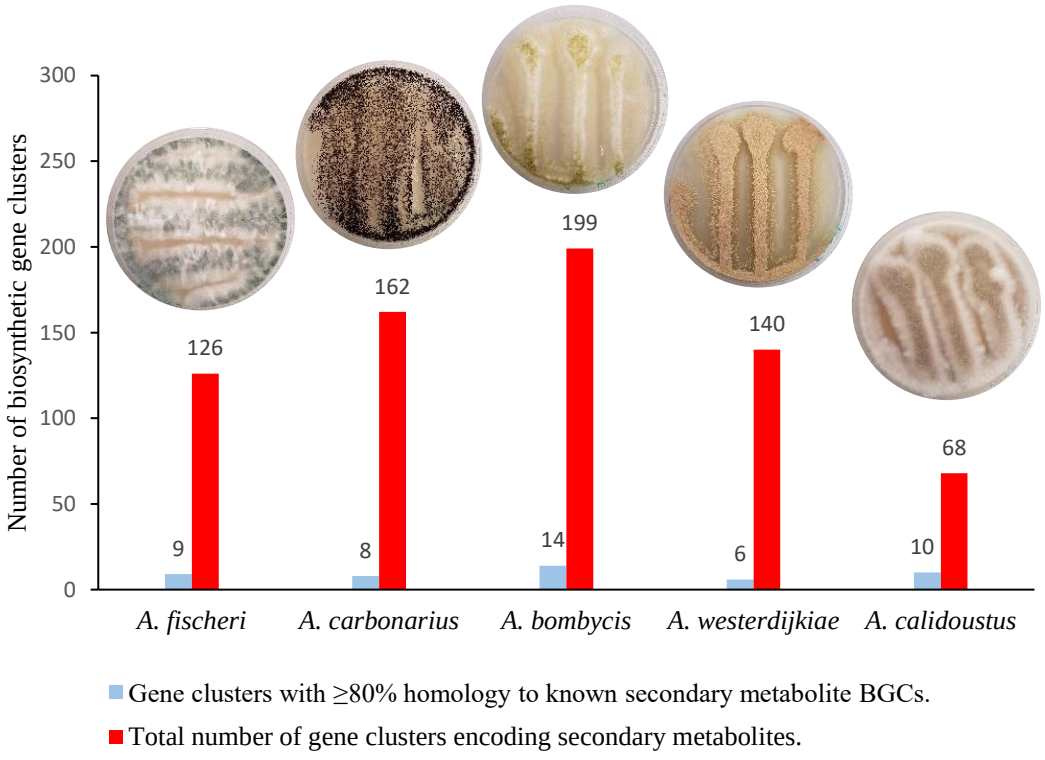

Figure 4.1 BGCs detected by antiSMASH in the genomes of *A. calidoustus*, *A. westerdijkiae*, *A. bombycis*, *A. carbonarius* and *A. fischeri*, and their corresponding growth on PDA plates.

4.2.2. Epigenetic manipulation of *A. carbonarius* in PDB

A. carbonarius had the fastest growth rate on the PDA plates among the other species showing full growth after four days of inoculation. Therefore, agar plugs from the *A. carbonarius* plate were used to inoculate 10 mL of PDB containing 200 µM of the DNMT inhibitor 5-AC, 100 µM of the HDAC inhibitor vorinostat or a combination of 100 µM 5-AC and 50 µM vorinostat. The concentrations of epigenetic modifiers were selected based on the previous studies mentioned in chapter one, and higher concentrations of 5-AC were used due to its instability. After seven-day incubation, the effect of the epigenetic modifiers was apparent in the colour of the treated cultures compared to the control (Figure 4.2). Comparative chromatograms of EtOAc extracts displayed induced set of metabolites in the cultures treated with 5-AC or 5-AC and vorinostat combination, eluting between 7.70 and 7.90 min (Figure 4.3). The epigenetic effect observed in the colour of cultures and metabolic profiles is more significant with the concomitant addition of 5-AC and vorinostat compared to the cultures treated with only one modifier.

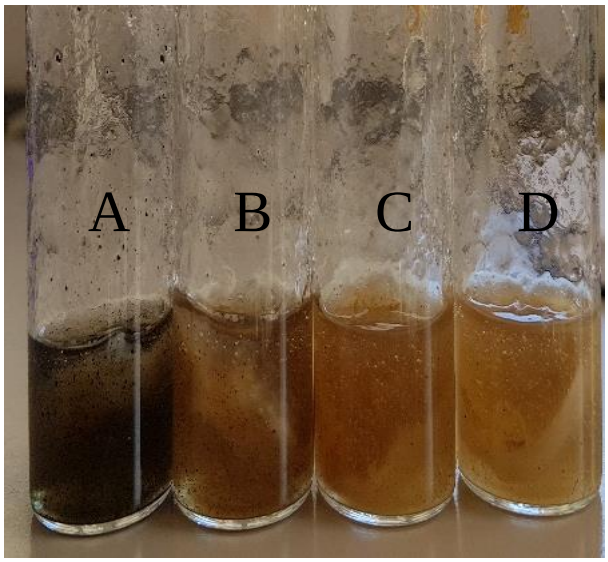

Figure 4.2 *A. carbonarius* cultures treated with 100 µM vorinostat (B), 200 µM 5-AC (C), or a combination of 50 µM vorinostat and 100 µM 5-AC (D) compared to the epigenetic-free control (A).

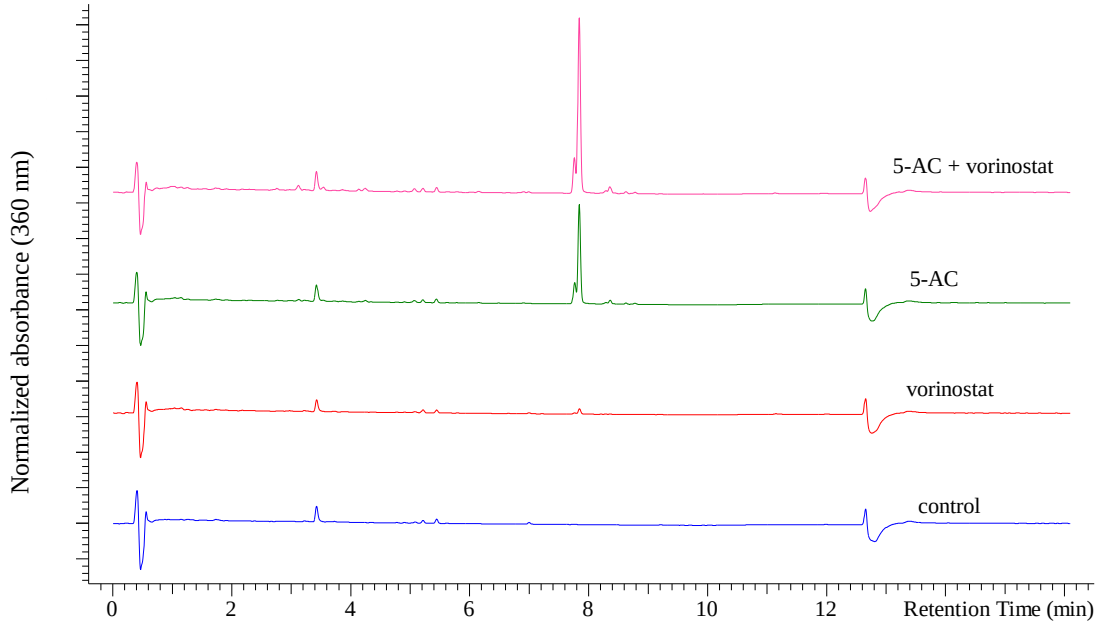

Figure 4.3 HPLC-UV chromatograms (360 nm) of *A. carbonarius* (first experiment, seven-day cultivation), control and with 100 μM vorinostat, 200 μM 5-AC or a combination of 50 μM vorinostat and 100 μM 5-AC.

The experiment was repeated with 5-AC or a combination of 5-AC and vorinostat to test the metabolite production after one and two weeks of inoculation. Although the amount was still increased with the epigenetic modifiers, the induced metabolite was also detected in the control after one-week cultivation (Figure 4.4). In addition, a new peak, which was not detected in the previous experiment, appeared with the epigenetic modifiers at 4.46 min, and there was no difference between the colours of treated cultures and control. After two weeks, there was barely any difference between the treated cultures and the control (Figure 4.5). Nevertheless, it was apparent that the longer cultivation led to higher production of many metabolites that were produced at small or undetected amounts after one-week cultivation. The inconsistency in the results might be caused by the nonhomogeneous conidia employed for inoculation, which might cause some growth and metabolism variations depending on the age and density of conidia on each agar plug. Therefore, the next

experiments are performed with homogenised inocula and a minimum of six replicates, when practicable, and efforts are focused on the reproducible induced-metabolites.

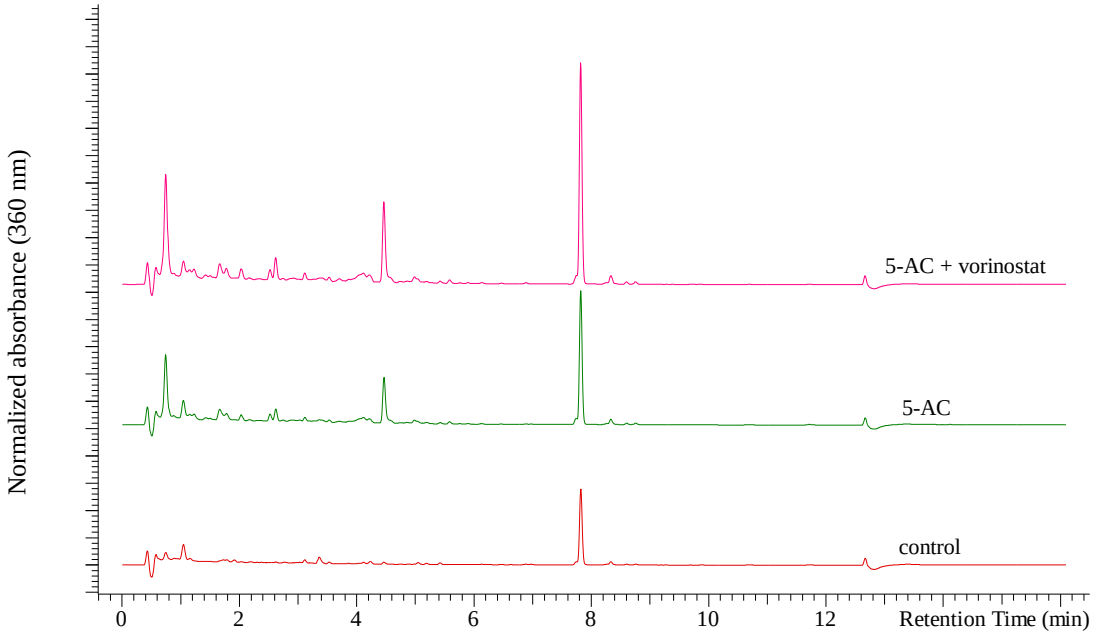

Figure 4.4 HPLC-UV chromatograms (360 nm) of *A. carbonarius* (second experiment, one-week cultivation), control and with 200 µM 5-AC or a combination of 50 µM vorinostat and 100 µM 5-AC.

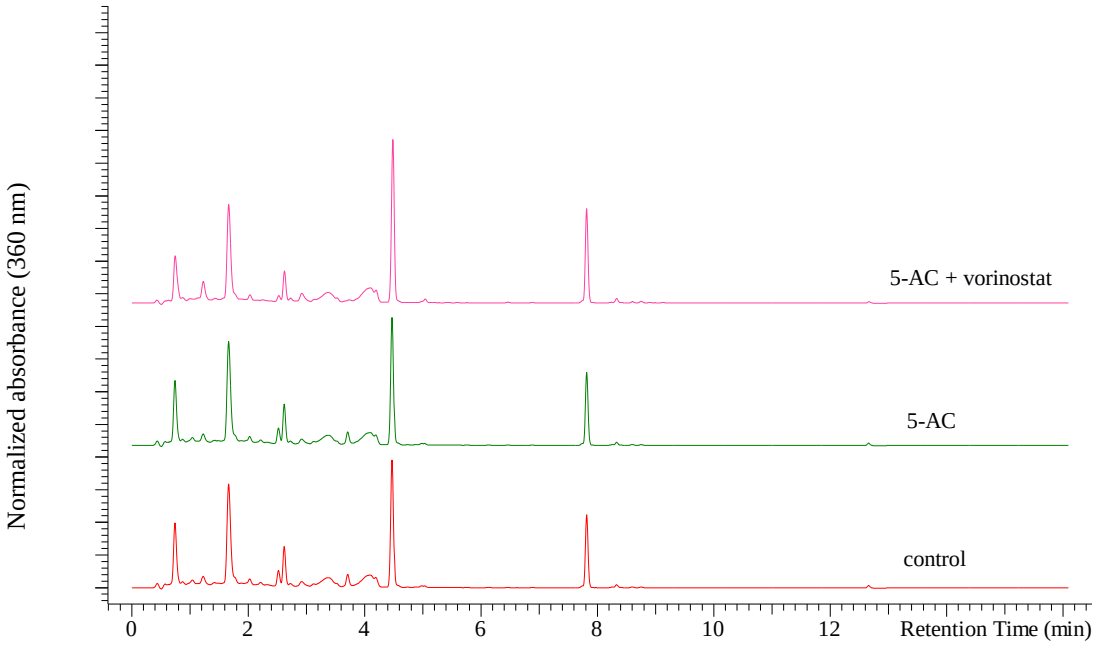

Figure 4.5 HPLC-UV chromatograms (360 nm) of *A. carbonarius* (second experiment, two-week cultivation), control and 200 µM 5-AC or a combination of 50 µM vorinostat and 100 µM 5-AC.

4.2.3. Epigenetic and nutritional manipulation of *A. bombycis*

Two types of *A. bombycis* inocula were compared; PDA plugs and semi-solid SMYA medium (neopeptone 1%, maltose 4%, yeast extract 1% and agar 0.4%). Eight replicates of PDB (10 mL) were inoculated with agar plugs or homogenised SMYA inocula and cultivated for seven days. Cultures were extracted with an equal volume of acetone, and the samples were analysed by LC-MS. Volcano plots of the MS data (Figure 4.6) displayed significant differences between the cultures inoculated with agar plugs and those with SMYA inocula. Although some metabolites appeared to be produced in higher quantities with the agar inocula, SMYA inocula led to higher production of most metabolites.

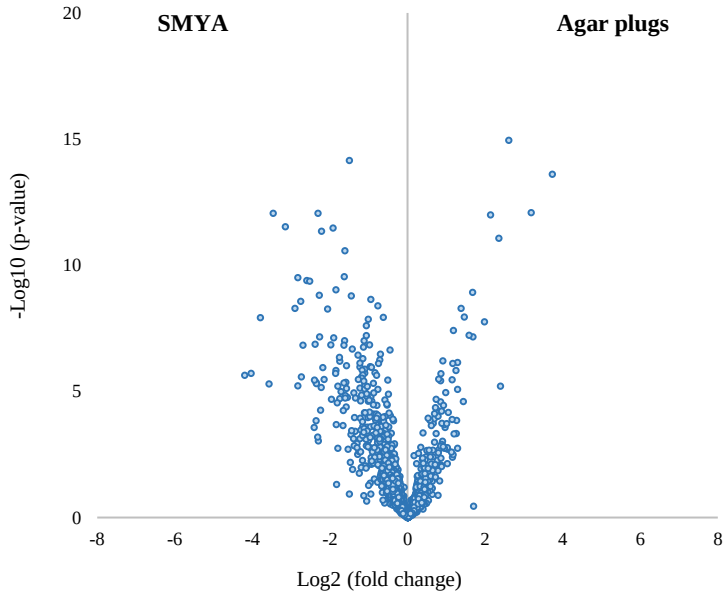

Figure 4.6 Volcano plot representation of variation in *A. bombycis* metabolite profiles with two different inocula, SMYA and agar plugs, (n = 8) (-log10 of t-test statistical p-value on y-axis vs. log2 of ion intensity ratio on x-axes; the horizontal dashed line shows where p-value = 0.05).

The effect of the epigenetic modifiers, vorinostat, VPA, 5-AC and hydralazine, was investigated in cultures inoculated with SMYA or agar plugs, eight replicates per condition. Volcano plots analysis of vorinostat-treated cultures demonstrated several metabolites significantly induced by vorinostat with both types of inocula (Figures 4.7

and 4.8). The antibacterial activity of the treated cultures against MRSA was compared to the extracts of *A. bombycis* cultivated in eleven different media along with PDB controls. The treated cultures did not show higher antibacterial activity compared to the controls. Interestingly, the extract of one of the employed media (GSY) exhibited complete inhibition of MRSA that was not observed with other extracts (Figure 4.9, A). Similarly, the treated cultures did not have higher antifungal activity against *A. fumigatus* compared to the controls, while the cultures in MMK2 medium caused the strongest inhibition of *A. fumigatus* (Figure 4.9, B). Therefore, nutritional manipulation with different media appears to induce the production of some bioactive metabolites which are not produced with epigenetic modifiers. Since the employed media were trialled during my placement in Spain and the media were taken from Medina proprietary database, the following experiments including dereplication, isolation and structure elucidation are continued by our collaborators in Fundación Medina.

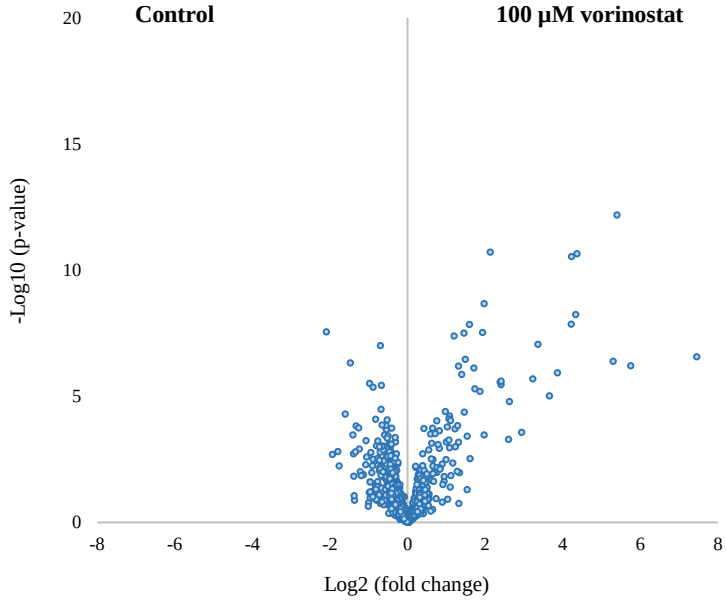

Figure 4.7 Volcano plot representation of variation in *A. bombycis* metabolite profiles in the presence of vorinostat using SMYA inoculum, (n = 8) (-log10 of t-test statistical p-value on y-axis vs. log2 of ion intensity ratio on x-axes; the horizontal dashed line shows where p-value = 0.05).

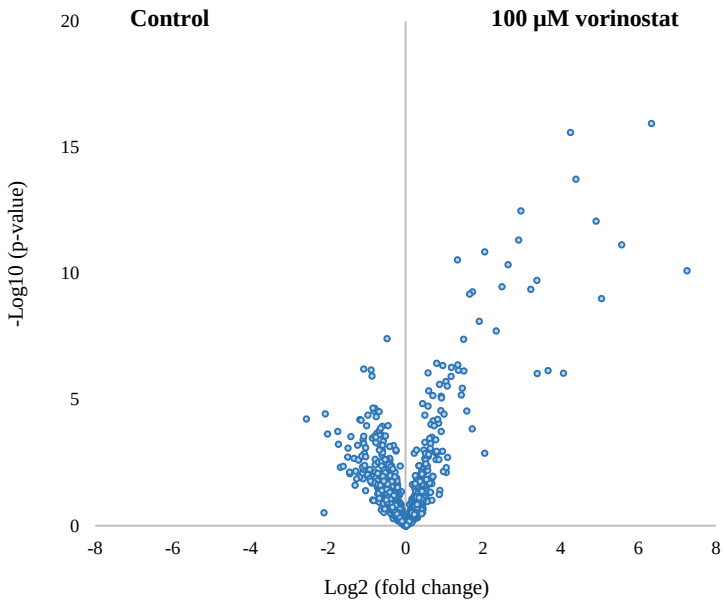

Figure 4.8 Volcano plot representation of variation in *A. bombycis* metabolite profiles in the presence of vorinostat using agar plugs inoculum, (n = 8) (-log10 of t-test statistical p-value on y-axis vs. log2 of ion intensity ratio on x-axes; the horizontal dashed line shows where p-value = 0.05).

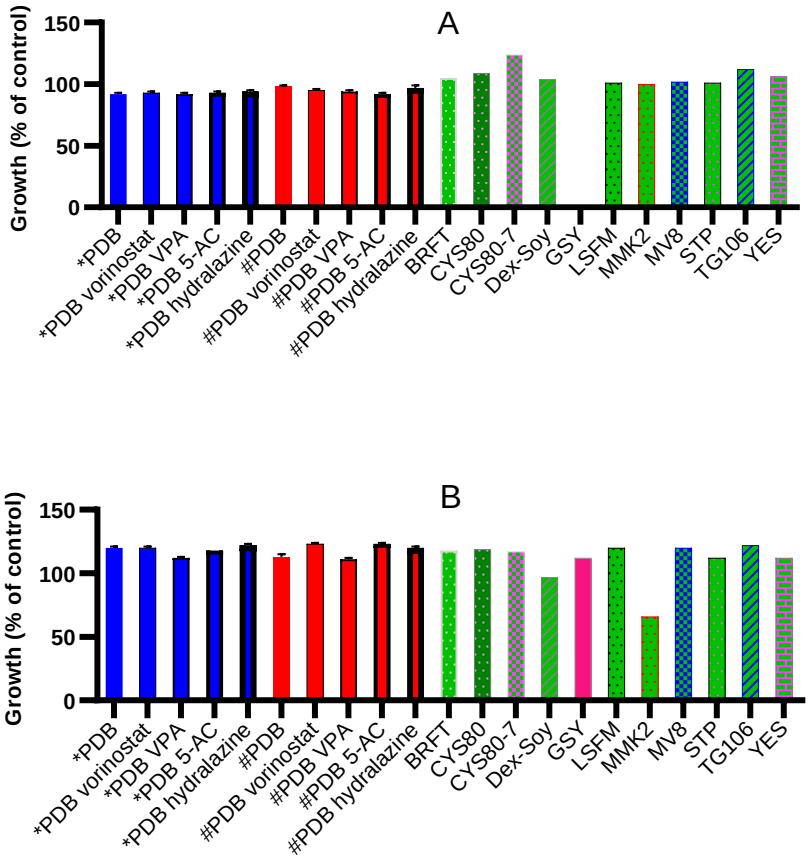

Figure 4.9 Growth inhibition of MRSA (A) and *A. fumigatus* (B) in the presence of *A. bombycis* extracts obtained from cultures grown in PDB with and without epigenetic modifiers using two types of inocula, SMYA inoculum (*) or agar plugs (#), along with extracts from cultures grown in elven different media inoculated with SMYA culture. Data points represent the average ± standard error of eight replicates.

4.2.4. Epigenetic experiments in *Aspergillus* complete medium (*this section is adapted from our publication in the Journal of Antibiotics*[218])

Homogenised PDBA (PDB medium supplemented with 2.5 g/L agar) cultures of the five *Aspergillus* species were used to inoculate *Aspergillus* complete medium (glucose 2.5% and yeast extract 0.5%) containing 200 µM 5-AC or 100 µM vorinostat. After seven-day incubation, the metabolite profiles of EtOAc extracts from *A. calidoustus* and *A. westerdijkiae* revealed significant differences in the presence of vorinostat compared to the control fermentations. Therefore, a detailed analysis of the secondary metabolite profiles in these two species was performed. Six replicates of small-scale (10 mL) fermentations were carried out in *Aspergillus* complete medium in the presence or absence of 100 µM vorinostat. The extracts from each fermentation were characterised by LC-MS with UV detection at a single wavelength of 254 nm and electrospray ionisation mass spectrometry. Data analysis through volcano plots (Figure 4.10) revealed significant global effects of vorinostat on metabolite production, with many metabolites either increased or reduced in their levels compared to control fermentations.

Subsequently, lists were compiled for natural products predicted from these species by antiSMASH and natural products previously reported from these or closely related species on the *Aspergillus* website (https://www.aspergillus.org.uk/) and DNP (Appendix 8.13). As a result, a total of five metabolites could be tentatively identified: emericellamide A, emericellamide B and phenylahistin from *A. calidoustus*, and ochratoxin A and penicillic acid from *A. westerdijkiae* (Figure 4.11). These results powerfully illustrate the OSMAC concept.[42] Thus, the majority of metabolites observed under the employed specific fermentation conditions could not be readily identified. Conversely, metabolites associated with these species in the literature were

undetectable under these conditions. Nevertheless, the high sensitivity of mass spectrometry and the ability to detect metabolites at low abundance enables preliminary conclusions on metabolite diversity and identity to be drawn without the need to isolate pure compounds from the extract.

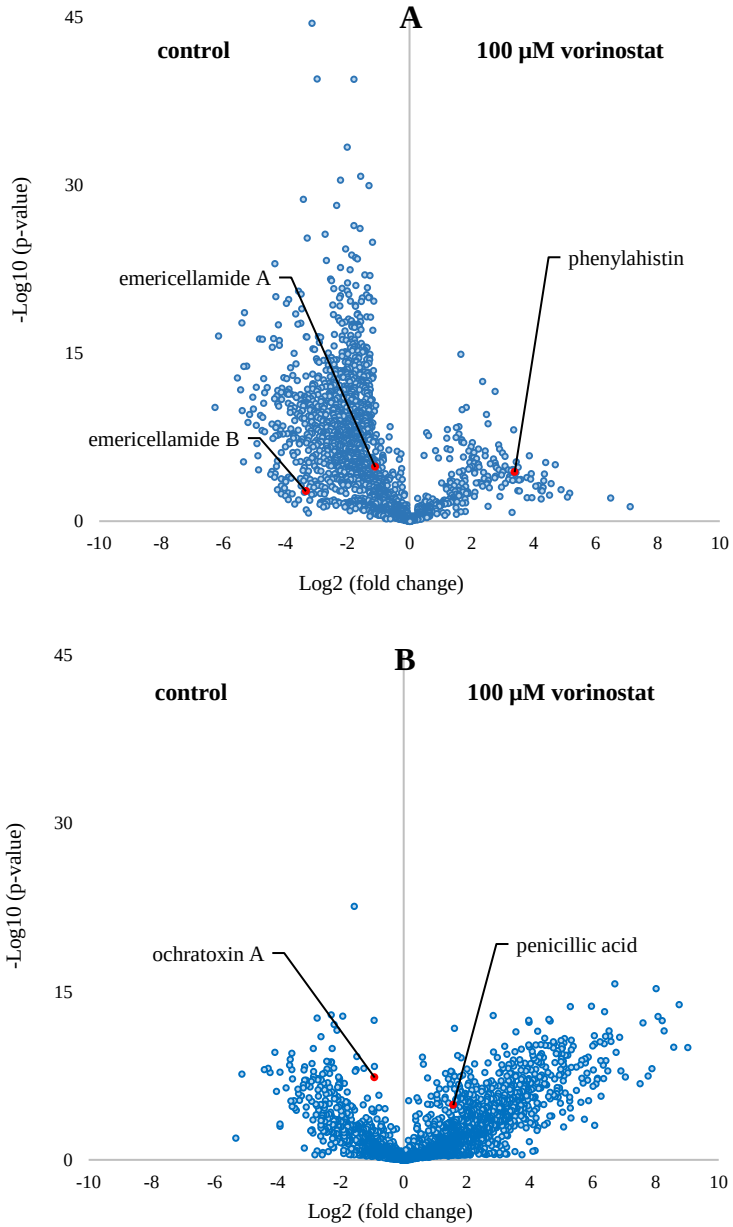

Figure 4.10 (A) Volcano plot representation of variation in metabolite profiles of *A. calidoustus* extracts (n = 6), (-log10 of t-test statistical p-value on y-axis vs. log2 of ion intensity ratio on x-axes; the horizontal dashed line shows where p-value = 0.05). Three metabolites were identified: emericellamides A and B were reduced in production levels by vorinostat whereas phenylahistin was increased. (B) Volcano plot representation of variation in metabolic profiles of *A. westerdijkiae* extracts (n = 6). Two metabolites were identified: ochratoxin A was reduced in production levels by vorinostat whereas penicillic acid was increased.

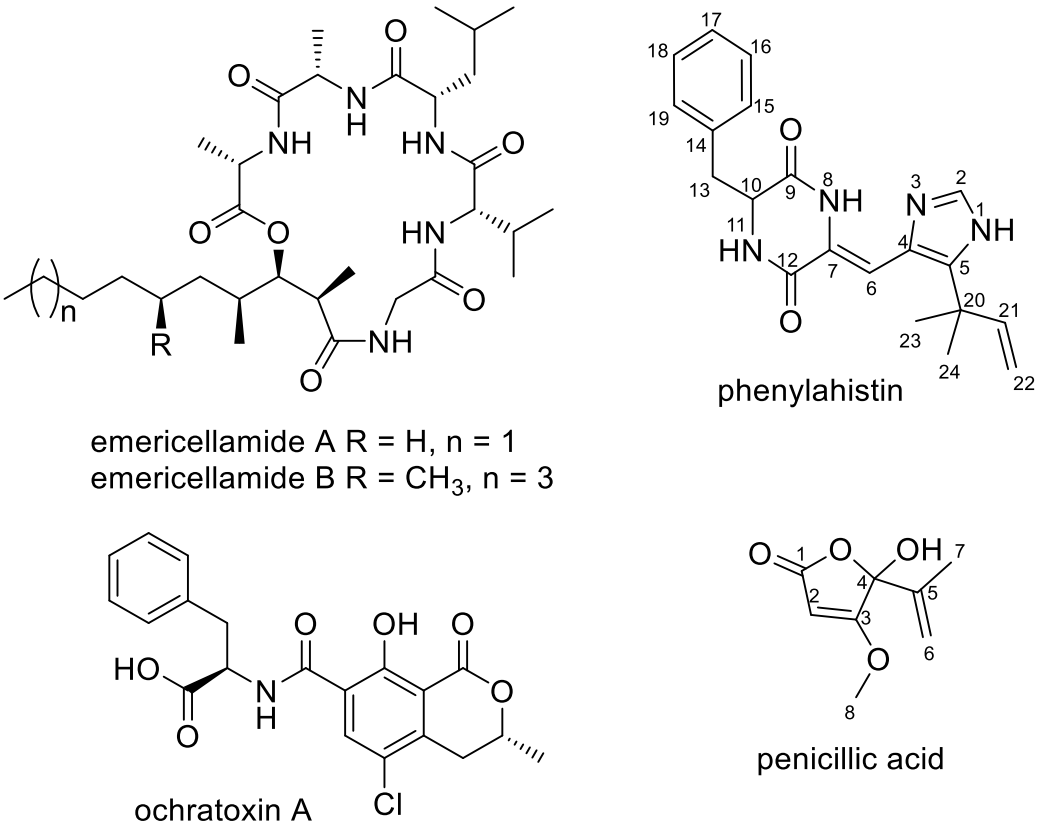

Figure 4.11 Chemical structures of emericellamide A, emericellamide B and phenylahistin from *A. calidoustus*, and ochratoxin A and penicillic acid from *A. westerdijkiae*.

A more detailed LC-PDA-MS analysis was carried out, generating UV-visible spectra, MS and MS/MS fragmentation data (Appendix 8.14) for the extracts. The additional data confirmed the identity of emericellamide A, emericellamide B and ochratoxin A although the actual amounts in the small-scale fermentation were insufficient for isolation. Furthermore, antiSMASH identified putative BGCs in *A. calidoustus* and *A. westerdijkiae* (Appendix 8.15) with 80% homology to the reported emericellamide and ochratoxin BGCs in other species.[219,220] Meanwhile, the HPLC chromatograms indicated one main metabolite each in *A. calidoustus* and *A. westerdijkiae* whose production levels were increased by the action of vorinostat (Figure 4.12). While the MS molecular ions and UV spectra suggested they were phenylahistin and penicillic acid, this could not be unambiguously affirmed by MS/MS

fragmentation patterns. In order to elucidate the structures of these two compounds, large scale fermentation was performed.

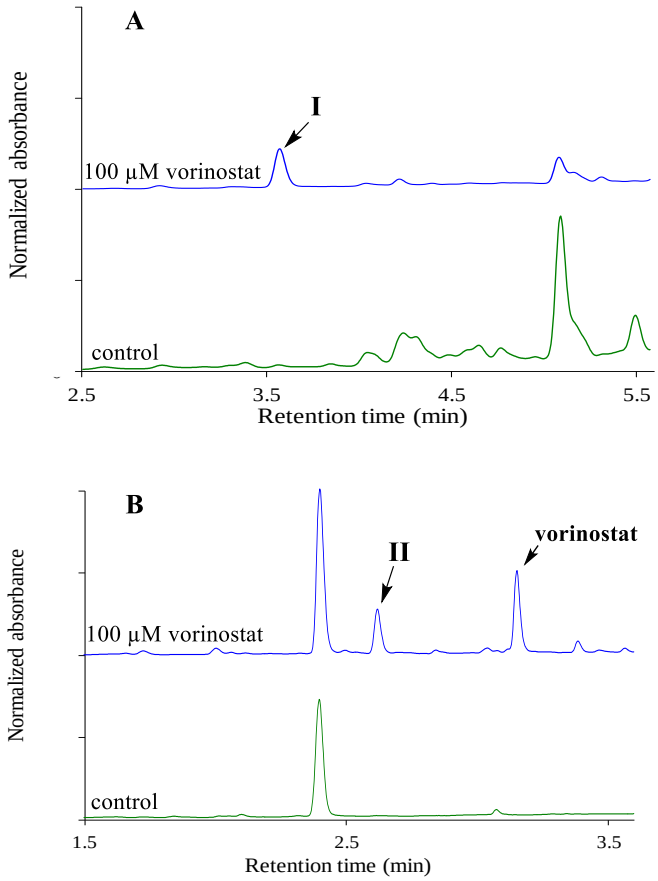

Figure 4.12 (A) HPLC-UV chromatograms (254 nm) of *A. calidoustus* fermentations, control and with 100 µM vorinostat. The metabolite **I** induced by vorinostat is indicated. (B) HPLC-UV chromatograms (254 nm) of *A. westerdijkiae* fermentations, control and with 100 µM vorinostat. The metabolite **II** induced by vorinostat is indicated, as well as the drug itself.

The metabolite profiles of large-scale fermentations of *A. calidoustus* (4 L) and *A. westerdijkiae* (4.5 L) treated with 100 µM vorinostat were similar to the smaller scale experiments. With *A. calidoustus*, 0.7 mg of the pure induced compound was isolated and analysed by HRMS to reveal an accurate mass *m/z* 351.18164 $[M + H]^+$, suggesting a molecular formula of $C_{20}H_{22}N_4O_2$ (calcd. for $C_{20}H_{23}N_4O_2$, 351.18155, Δ= 0.3 ppm). The molecular formula, together with the UV spectrum (λ_{max} 202, 233, 320 nm) and 1D/2D NMR spectra (Appendix 8.14) all matched with the reported data[221] for the diketopiperazine alkaloid phenylahistin (**I**). Alkaloid **I** is an inhibitor

of tubulin polymerisation which displays in vivo antitumor activity,[221,222] and the synthetic analogue plinabulin (Figure 4.13) is currently in phase III clinical development for the treatment of advanced non-small cell lung cancer.[223] Phylogenetically, the species *A. calidoustus* under investigation is closer to the drimane sesquiterpenoid producers *A. pseudodeflectus*, *A. insuetus* and *A. keveii* rather than *A. ustus*,[224] the previously reported source of **I**. In *A. ustus*, **I** was isolated as a scalemic mixture from a culture in solid agar medium and its production associated with conidia formation, whereas in this experiment **I** is isolated as a scalemic mixture from the liquid culture of *A. calidoustus*. In the *A. calidoustus* 4 L-scale fermentation, the isolation of sufficient phenylahistin for structure elucidation would be impossible without the significant induction (ten-fold in the volcano plot, Figure 4.10) by vorinostat. Although the genomes of *A. ustus* and *A. calidoustus* were compared by antiSMASH, it was not possible to clearly identify a common BGC that might be responsible for phenylahistin biosynthesis.

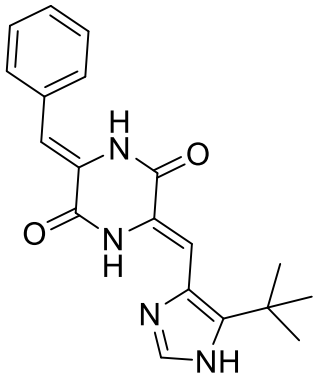

plinabulin

Figure 4.13 Chemical structure of the phenylahistin synthetic analogue, plinabulin.

From the large-scale fermentation of *A. westerdijkiae*, 162 mg of the major metabolite induced by vorinostat were purified and analysed by HRMS to reveal a molecular formula of $C_8H_{10}O_4$ predicted from the observed MS *m/z* 171.06520 [M +

H]$^+$ (calcd. for $C_8H_{11}O_4$, 171.06519, Δ= 0.1 ppm). Together with the UV absorption at 224 nm and NMR spectra (Appendix 8.14), the data confirmed the identity of the natural product as the polyketide penicillic acid (**II**), first isolated from *Penicillium puberulum* in 1913 and later from other *Penicillium* and *Aspergillus* species.[225,226] A broad spectrum of biological activity including antibacterial, antifungal, antiviral, antitumor and herbicidal activity has been reported for **II**. It is produced in substantial amounts by *Aspergillus* species grown on sucrose-based media, but normally in limited or undetectable amounts in the glucose-based media employed in this experiment.[227] Only about 1 mg of penicillic acid could be isolated from a large scale (1.5 L) control fermentation without vorinostat. Thus, the induction of penicillic acid levels by vorinostat in the large-scale fermentation was more than fifty-fold and much higher than the three-fold effect observed in the small-scale fermentation. While penicillic acid production was previously induced in an *Aspergillus* species grown in glucose peptone yeast-extract medium (GPY) by the addition of anthracenone,[228] the mechanism is unknown whereas in this study the induction could be attributed to the epigenetic effect of HDAC inhibition by vorinostat.

4.2.5. Concomitant use of epigenetic modifiers in *Aspergillus* complete medium at different stages (*the experiments in this section were performed by undergraduate students under my supervision*)

The experiments in this section were primarily performed to investigate the concomitant use of epigenetic modifiers on metabolite profiles. The second purpose of these experiments was to test the effect of the presence of epigenetic modifiers in the seed cultures as it has been reported that the epigenetic influence on secondary metabolism can be enhanced by the addition of epigenetic modifiers in the seed

cultures as well as the production stage.[159] Additionally, it has been demonstrated that the epigenetic effect can be inherited by the next fungal generations without exposing them again to epigenetic modifiers.[156] Based on these precedents, seed cultures of the five *Aspergillus* species were prepared in 10 mL PDBA in the presence of 200 µM 5-AC, 100 µM vorinostat or a combination of 100 µM 5-AC and 50 µM vorinostat. Seed cultures with DMSO were also cultivated under the same conditions to be employed as controls. After seven days, these cultures were used to inoculate 10 mL of *Aspergillus* complete medium in the presence or absence of the epigenetic modifiers, and the production cultures were cultivated for seven days before extraction.

Based on the HPLC analysis (UV detection at 210, 254, 280 and 360 nm), the metabolite profiles of EtOAc extracts from all species did not show any enhanced effect when the modifiers were added in both seed and production cultures compared to addition only in production cultures. In the modifier-free production cultures, there was no apparent influence of the addition of epigenetic modifiers in seed cultures compared to the controls. Furthermore, the combination of epigenetic modifiers did not display a significant effect on the metabolite profiles compared to the presence of a sole modifier. Nevertheless, the results from these experiments were inconclusive due to the presence of inconsistencies between the replicates. Due to finance and time limitations, it was only possible to produce two replicates per condition which were insufficient for statistical analysis.

4.3. Overall discussion and conclusion

The cultivation of *A. carbonarius* led to higher yields of some metabolites; however, a more significant effect on metabolite profiles was observed with longer cultivation times of this species in PDB. In *A .bombycis,* although the metabolic profile

was significantly affected by epigenetic manipulation, nutritional manipulation resulted in the production of bioactive metabolites that were only detected in GSY and MMK2 media. The bioactive metabolites are under investigation by our collaborators in Fundación Medina. *A. calidoustus* and *A. westerdijkiae* experienced significant changes in secondary metabolite production upon laboratory fermentation with the HDAC inhibitor vorinostat. Both metabolite induction and repression were observed. Through analysis of putative BGCs, the likely BGCs responsible for the production of emericellamides in *A. calidoustus* and ochratoxin in *A. westerdijkiae* could be identified. The titre levels of phenylahistin (**I**) in *A. calidoustus* and penicillic acid (**II**) in *A. westerdijkiae* were substantially increased by vorinostat, illustrating the potential of epigenetic manipulation for improving the fermentation efficiency and yield of biologically active natural products.

4.4. Materials and methods

4.4.1. General experimental procedures

Unless stated otherwise, all chemicals and solvents were purchased from Sigma-Aldrich, Alfa Aesar or Fisher Scientific. All solvents were of HPLC grade or equivalent. Commercial media and media components were purchased from Sigma-Aldrich, Alfa Aesar, Fisher Scientific or Formedium. UV spectra were acquired on an SPD-M20A photodiode array detector attached to a Shimadzu Prominence/Nexera UHPLC. NMR spectra of phenylahistin were recorded on a Bruker Avance Neo spectrometer equipped with a helium-cooled cryoprobe (600 and 150 MHz for ^{1}H and ^{13}C NMR, respectively). Chemical shifts were reported in ppm using the signals of the residual solvent as internal reference (δH 7.26 and δC 77.1 ppm for $CDCl_3$). NMR spectra of penicillic acid were recorded on a Bruker Avance (500 and 125 MHz for ^{1}H

and ^{13}C NMR, respectively). Chemical shifts were reported in ppm using the signals of the residual solvent as internal reference (δH 2.50 and δC 39.5 ppm for DMSO-d_6). NMR solvents were purchased from VWR. The specific rotation of phenylahistin was recorded on a Perkin Elmer 341 polarimeter. IR spectrum of penicillic acid was recorded on a PerkinElmer Fourier transform infrared spectrometer.

4.4.2. Fungal strains and inocula preparation

A. calidoustus NRRL 281, *A. westerdijkiae* NRRL 3174, *A. bombycis* NRRL 26010, *A. carbonarius* NRRL 369 and *A. fischeri* NRRL 181 were obtained from the US Agricultural Research Service (USDA-ARS). The spores were initially rehydrated by suspension in sterile MQ water for five hours, and a few drops of the spores suspension were used to inoculate a commercial potato dextrose agar solid medium (PDA0102, Formedium). The plates were incubated at 25 °C for 24 hours before sealing them with parafilm and incubating them until sporulation. Subsequently, conidia were harvested, and stocks were prepared and preserved as frozen conidia and mycelia in 10% glycerol at -80 °C.

Solid inocula (agar plugs) were prepared by plating a sample of cryopreserved stocks on PDA, and 5-mm diameter agar plugs were cut from each plate with a sterile Transfer Tube (Spectrum Laboratories) and used to inoculate liquid media (two plugs /10 mL). Semi-solid inocula were prepared in SMYA (neopeptone 1%, maltose 4%, yeast extract 1% and agar 0.4%) or PDBA (a commercial PDB medium supplemented with 2.5 g/L agar, Formedium, UK) as described by Bills et al.[229] Briefly, agar plugs obtained from the strains cultivated on PDA at 25 °C for seven days were used to inoculate tubes containing 10 mL of SMYA or PDBA medium and two sterile coverslips (22 x 22 mm). The cultures were incubated at 25 °C and 200 rpm, where

shaking with the coverslips continually sheared agar plugs and *Aspergillus* hyphae.[229] After seven days, the tubes were vortexed to produce homogenous hyphal inocula that were used to inoculate liquid media (300 µL /10 mL).

4.4.3. Epigenetic manipulation of *A. carbonarius* in PDB

A. carbonarius was cultivated in 10 mL of PDB containing 200 µM 5-AC (a DNMT inhibitor), 100 µM vorinostat (an HDAC inhibitor) or a combination of 100 µM 5-AC and 50 µM vorinostat at 25 ˚C and shaking at 150 rpm for seven days. The control cultures contained 10 mL PDB, the inoculum and the same percentage of DMSO used in modifier-treated cultures. After seven-day incubation, ten µL of each vial were transferred to PDA plates to test morphological changes and contamination. The remaining cultures were extracted by adding an equal volume of EtOAc and two coverslips and shaking the tubes for five minutes to accelerate extraction. After centrifugation, the EtOAc layer was transferred to glass vials and the solvent removed in a centrifugal evaporator, and the residues were resuspended by shaking with 3 mL of UHPLC-grade MeOH for 5 minutes.

A 1 mL aliquot of the MeOH solution was passed through a Thermo Scientific™ SOLA™ HRP SPE cartridge and analysed by an Agilent 1290 Infinity UHPLC system equipped with a diode array detector with UV detection at 210, 254 270 and 360 nm. A 5 µL sample from each sample was injected onto a 100×2.1mm 2.6µm Thermo Scientific™ Accucore™ C18 column and chromatographed using the following gradient (acetonitrile versus 0.1% formic acid in water, at 0.5 mL/min and 40 °C): 0.01 min (20% acetonitrile), 10 min (100% acetonitrile), 12 min (100% acetonitrile), 12.1 (20% acetonitrile), 16.1 min (20% acetonitrile). Results were analysed and processed using ACD/Spectrus software.

4.4.4. Epigenetic and nutritional manipulation of *A. bombycis*

Media used for cultivation were taken from Medina proprietary database although some have been published.[230,231] After seven days of incubation, ten μL of each vial were transferred to PDA plates to test morphological changes and contamination, and the remaining were extracted with an equal volume of acetone and shaking at 220 rpm for 1 h.[230] The resultant extracts were centrifuged, and 11 mL of supernatant from each vial were mixed with 600 μL DMSO in glass tubes. These mixtures were concentrated under nitrogen to a final volume of 3 mL and filtered through 96-well filter plates. The antimicrobial activities of the filtrates were evaluated against MRSA and *A. fumigatus* as described in chapter 3 (section 3.4.6) but using 90 μL/well of the inoculum and 10 μL/well of each filtrate. Results were analysed using Microsoft Excel and GraphPad Prism 8.0 software.

MS data of cultures treated with vorinostat and their corresponding controls were generated by injecting an aliquot (2 μL) of the filtrate in an Agilent 1100 LC-MSD system using a Zorbax SB-C8 column (2.1 × 30 mm, 5 μm, flow rate 0.3 mL/min, 40 °C) with a linear gradient from 10% B to 100% B in 6 min followed by 2 min hold at 100% B before returning to10% B and equilibrating the system for 2 min. Solvent A was 10% acetonitrile in water, and solvent B was 90% acetonitrile in water, both supplemented with 1.3 mM trifluoroacetic acid and ammonium formate. The instrument collected MS spectra from *m/z* 150-1500 in both positive and negative modes. Mass ions and their corresponding intensities were extracted using MASS Studio software.[232] The t-test statistical *p*-value of ion intensities and volcano plots were performed using Microsoft Excel. The unpaired equal variance and two-tailed distribution options were used for the t-test. The x-axis of volcano plots represents log 2 of ion intensity ratio, and the y-axis represents −log 10 of t-test statistical *p*-value.

4.4.5. Epigenetic experiments in *Aspergillus* complete medium

4.4.5.1. Small-scale cultivation, extraction and LC-MS analysis

Six replicates per condition were produced using 300 µL PDBA inoculum in 10 mL of *Aspergillus* complete medium (glucose 2.5% and yeast extract 0.5%) in the presence of 200 µM 5-AC (a DNMT inhibitor) or 100 µM vorinostat (an HDAC inhibitor) at 25 ˚C and shaking at 150 rpm for seven days. The control cultures contained 300 µL inoculum in 10 mL of the *Aspergillus* complete medium and the same percentage of DMSO used in modifier-treated cultures.

After seven-day incubation, ten µL of each vial were transferred to PDA plates to test morphological changes and contamination. The remaining cultures were extracted by adding an equal volume of EtOAc and two coverslips and shaking the tubes for five minutes to accelerate extraction. After centrifugation, the EtOAc layer was transferred to glass vials and the solvent removed in a centrifugal evaporator, and the residues were dissolved in 3 mL of UHPLC-grade MeOH with shaking for 5 minutes. A 1 mL aliquot of the MeOH solution was passed through a Thermo Scientific™ SOLA™ HRP SPE cartridge and analysed by an Agilent LC/MSD TOF system equipped with a single wavelength UV detector. A 5 µL sample from each replicate was injected onto a 100 × 2.1mm 2.6µm Thermo Scientific™ Accucore™ C18 column and chromatographed using the following gradient (acetonitrile versus 0.1% formic acid in water, at 0.5 mL/min and 40 °C): 0.01 min (10% acetonitrile), 10 min (100% acetonitrile), 12 min (100% acetonitrile), 12.1 (10% acetonitrile), 16.1 min (10% acetonitrile). The instrument collected UV data at 254 nm wavelength and MS spectra from *m/z* 150-1500 in both positive and negative modes.

Agilent MassHunter Workstation software was used for the analysis of LC-MS data. The software was set to extract ions with the following parameters: ion RT tolerance 0.1 min and ion intensity threshold 1000 counts. The t-test statistical *p*-value of ion intensities and volcano plots were performed using Microsoft Excel. The unpaired equal variance and two-tailed distribution options were used for the t-test. The x-axis of volcano plots represents log 2 of ion intensity ratio, and the y-axis represents −log 10 of t-test statistical *p*-value. The HPLC-UV overlay traces were produced using ACD/Spectrus software.

MS/MS spectra were collected from the most abundant ions on a Shimadzu ion-trap-ToF (IT-ToF) mass spectrometer attached to a Shimadzu Nexera UHPLC. Collision-induced dissociation energy was 50%, and precursor ion width was 3 Da. Spray chamber conditions were 250 °C curved desorbation line (CDL), 300 °C heat block, 1.5 $L.min^{-1}$ nebuliser gas, and drying gas "on". The instrument was calibrated using sodium trifluoroacetate according to the manufacturer's instructions, immediately before use. The MS and MS/MS data were analysed using LabSolutions (Shimadzu).

4.4.5.2. High-resolution MS

High-resolution MS analysis was performed by direct infusion of 1 μL of the sample dissolved in 70% MeOH into a Waters Synapt G2-Si mass spectrometer operated in positive ion mode with a mass range of *m/z* 50 to 1200. Leu-enkephalin peptide was continuously infused to generate a lock-mass calibration with *m/z* = 556.2766 during the run. MS data were collected with the following parameters: resolution mode, positive ion mode, mass range *m/z* 50-1200 (calibrated with sodium

formate), capillary voltage = 3.0 kV; cone voltage = 40 V; source temperature = 120 °C; desolvation temperature = 350 °C.

4.4.5.3. Large scale fermentation and extraction (*this part was conducted with the help of undergraduate students*)

Large-scale (8 × 500 mL in 1 L Erlenmeyer flasks) *A. calidoustus* and *A. westerdijkiae* (3 × 1500 mL in 3 L Erlenmeyer flasks) fermentations were conducted with *Aspergillus* complete medium containing 100 µM vorinostat and incubated at 25 °C and 150 rpm. After seven days, the culture was extracted twice with an equal volume of ethyl acetate, and the organic layers were combined and dried using a rotary evaporator. The residue was then dissolved in 250 mL of 80% MeOH and partitioned with an equal volume of hexane. After removal of the hexane, the aqueous MeOH layer was dried using a rotary evaporator.

4.4.5.4. Isolation and structure elucidation

The *A. calidoustus* fermentation yielded 1.3 g of material that was initially separated using an automated flash-chromatography system (CombiFlash Rf, Teledyne Isco) with 30 mL/min flow rate and a linear gradient from 30% to 100% MeOH in water (in 30 min) before washing with 100% acetonitrile (for 15 min). Further purification with a semi-preparative C18 column on an Agilent 1290 Infinity UHPLC system equipped with a diode array detector yielded phenylahistin (**I**): 0.69 mg, white powder. $[\alpha]_D^{25}$ +71 (*c* 0.059, MeOH, 63% ee), lit. +123 (*c* 0.13, MeOH) for natural product (75% ee)[221] and +278 for purified (*R*)-enantiomer (98% ee).[222] ^{1}H NMR (600 MHz, $CDCl_3$) δ 8.93 (1H, br s, NH-1), 7.55 (1H, s, H-2), 6.88 (1H, s, H-6), 12.00 (1H, br s, NH-8), 4.33 (1H, m, H-10), 5.68 (1H, br s, NH-11), 2.93 (1H, dd, *J* = 13.62, 10.22 Hz, H-13a), 3.50 (1H, dd, *J* = 13.62, 3.41 Hz, H-13b), 7.25 (2H,

overlap, H-15 and 19), 7.34 (2H, t, *J* = 7.36 Hz, H-16 and 18), 7.27 (1H, overlap, H-17), 6.03 (1H, dd, *J* = 17.44, 10.49 Hz, H-21), 5.16 (1H, d, *J* = 17.44 Hz, H-22a), 5.20 (1H, d, *J* = 10.49 Hz, H-22b), 1.51 (6H, s, H-23 and 24). ^{13}C NMR (150 MHz, $CDCl_3$) δ 132.26 (C2), 132.29 (C4), 136.5 (C5), 105.3 (C6), 123.9 (C7), 164.7 (C9), 57.2 (C10), 159.9 (C12), 41.2 (C13), 135.5 (C14), 129.5 (C15 and 19), 129.1 (C16 and 18), 127.5 (C17), 37.6 (C20), 144.6 (C21), 113.9 (C22), 28 (C23 and 24).

The *A. westerdijkiae* fermentation yielded 3.3 g of material that was separated by an automated flash-chromatography system using 30 mL/min flow rate and a linear gradient from 10% to 100% MeOH in water (in 25 min) before washing with 100% acetonitrile (for 5 min). Further purification by automated flash-chromatography using 30 mL/min flow rate and a linear gradient from 5% to 40% MeOH in water (in 30 min) yielded penicillic acid (**II**): 162 mg, white needles. IR ν_{max} cm^{-1} 3281, 3125, 2852, 1743, 1725, 1633. ^{1}H NMR (DMSO-d_6, 500 MHz) 7.87 (1H, br s, 4-OH), 5.41 (1H, s, H-2), 5.30 (1H, s, H-6a), 5.11 (1H, s, H-6b), 3.85 (3H, s, H-8), 1.65 (3H, s, H-7). ^{13}C NMR (DMSO-d_6, 125 MHz) 179.4 (C1), 170.0 (C3), 140.1 (C5), 115.3 (C6), 102.4 (C4), 89.3 (C2), 59.9 (C8), 17.1 (C7).

Chapter Five

5. Epigenetic and nutritional manipulation in actinomycetes

5.1. Introduction

Actinomycete bacteria are prolific producers of bioactive natural products, including the main classes of the approved antimicrobial and anticancer agents. The approved antibacterial classes including aminoglycosides, tetracyclines, macrolides, ansamycins, carbapenems, amphenicols, lincosamides, glycopeptides and cyclic lipopeptides all originated from actinomycetes.[13–18] Actinomycetes are the producers of the approved antifungal polyenes and anticancer agents such as actinomycins, anthracyclines, bleomycins, mitosanes and anthracenones.[25] Other medically important drugs that originated from actinomycetes include antihyperlipidemic agents such as pravastatin, immunosuppressive drugs such as rapamycin, antiparasitic agents such as avermectins (e.g. ivermectin), and antidiabetic drugs such as acarbose (Figure 5.1).[47]

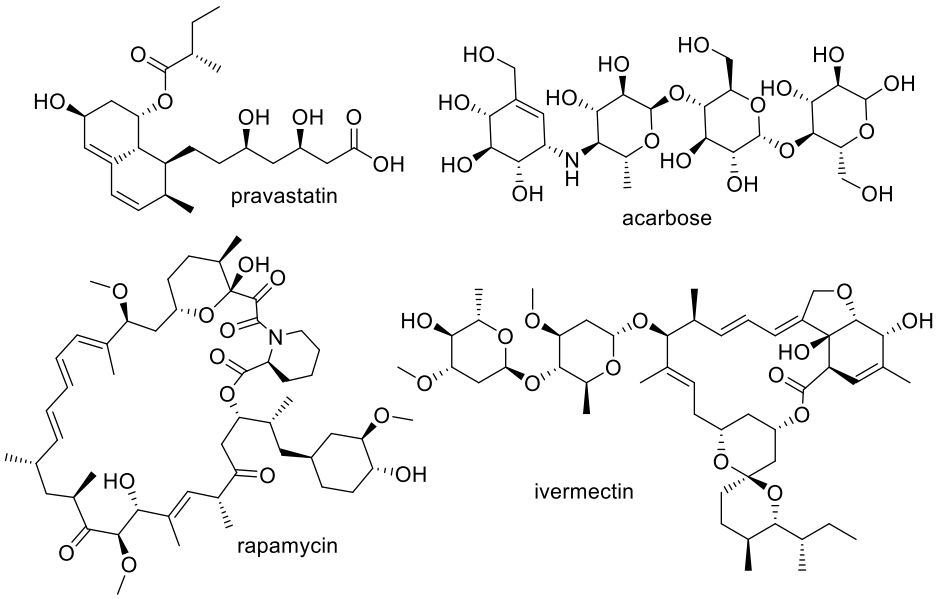

Figure 5.1 Examples of medically important drugs that originated from actinomycete bacteria.

Genome sequences suggest that up to 90% of microbial natural products are only produced under specific conditions.[233] Although actinomycete bacteria have been extensively explored for natural product discovery, genome mining of the well-explored actinomycetes *Streptomyces coelicolor* A3 (2) and *S. avermitilis* unveiled many cryptic BGCs encoding natural products that have not been discovered from these species.[234] Several approaches have been used to activate those BGCs including the chemical epigenetic studies on *Streptomyces coelicolor* A3 (2).[108,235] DNMT genes and HDAC orthologues have been reported from *Streptomyces* and *Saccharopolyspora* genomes.[108,235] Nevertheless, there is a shortage of studies on the use of the epigenetic manipulation strategy for activation of cryptic bacterial BGCs. In Barrie's lab (JIC, UK), genome mining revealed that *Streptomyces* sp. CMB-0406 and *Saccharopolyspora* KY21 each has at least 25 putative BGCs although only a few natural products have been identified from these two species.[236,237] Therefore, the epigenetic manipulation technique was trialled to activate the natural product BGCs in *Streptomyces* sp. CMB-0406 and *Saccharopolyspora* KY21.

5.2. Results and discussion

Streptomyces sp. CMB-0406 and *Saccharopolyspora* KY21 were cultivated in SV2 or SM7 medium in the presence of 0.5% DMSO (control), 10 µM vorinostat, 50 µM vorinostat, 50 µM 5-AC, 100 µM 5-AC or a combination of 10 µM vorinostat and 50 µM 5-AC. The epigenetic modifiers were added after 24 h of inoculation, and the concentrations were determined based on previous studies on *S. coelicolor* A3 (2).[108,235] Since 5-AC suffers from instability, higher concentrations of this modifier were utilized. EtOAc and MeOH solvents were used for extraction of molecules with medium to high polarity. After four-day cultivation of *Streptomyces* sp. CMB-0406 in

SM7, comparative TACs of the EtOAc extracts revealed two new peaks (RT = 1.39 and 1.60 min) in the presence of 10 or 50 µM vorinostat compared to the controls, while 5-AC did not show any effect on the metabolite profile either alone or in combination with vorinostat (Figure 5.2).

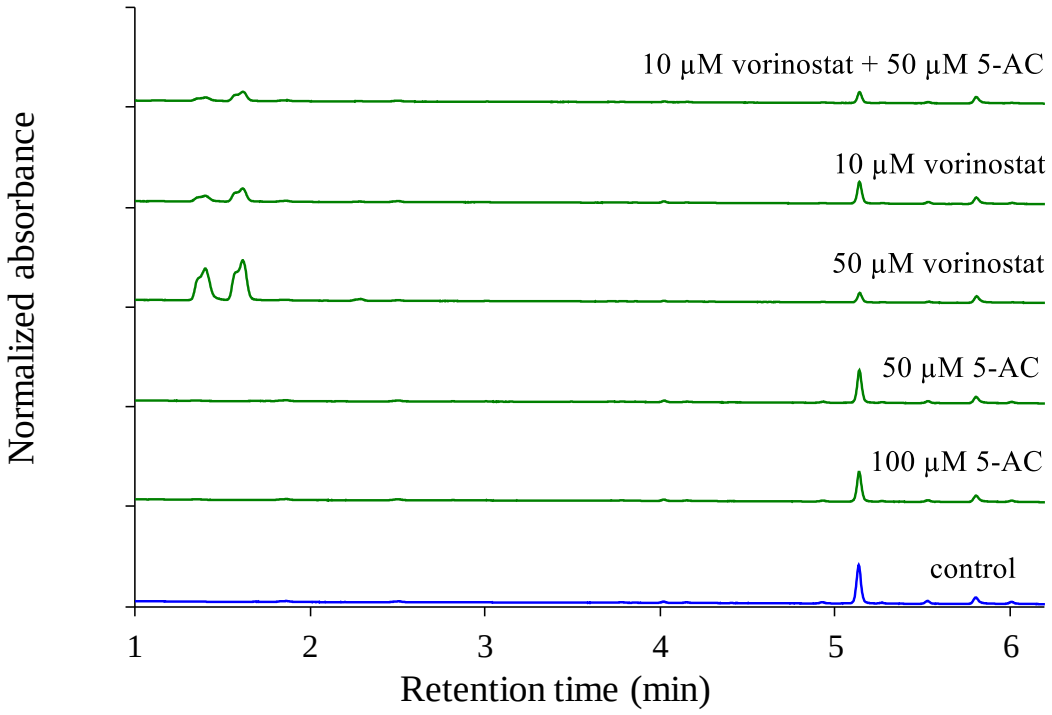

Figure 5.2 Comparative TACs of *Streptomyces* sp. CMB-0406 EtOAc extracts from cultures cultivated in the absence (control) or the presence of epigenetic modifiers.

Comparative TACs of the cultures extracted with MeOH after four days of cultivation demonstrated the same effect of the epigenetic modifiers observed in EtOAc (Figure 5.3). A sample of vorinostat in MeOH was analysed by LC-PDA-MS using the same experimental conditions to determine its retention time and spectra (Figure 5.3). The MS fragmentation patterns and UV spectra of the two new peaks were similar to those of vorinostat (Figure 5.4) but had retention times different from vorinostat (Figure 5.3). This confirmed that neither of these new peaks is an MS fragment of vorinostat as their retention times were different from vorinostat. Moreover, the measured masses do not correspond to any of the known vorinostat

metabolites or degradation products,[238,239] suggesting that they could be bacterial biotransformation products or reactants of vorinostat. Biotransformation products of epigenetic modifiers have been reported from vorinostat and hydralazine in previous studies,[240–242] but the ones detected in this experiment do not match any of the previously reported products. However, the small difference between the masses of the two new peaks and the mass of vorinostat as well as the presence of the main known fragment of vorinostat (*m/z* 232.13)[238,239] in the MS spectra of the new peaks suggest that their structures are not significantly different from that of vorinostat.

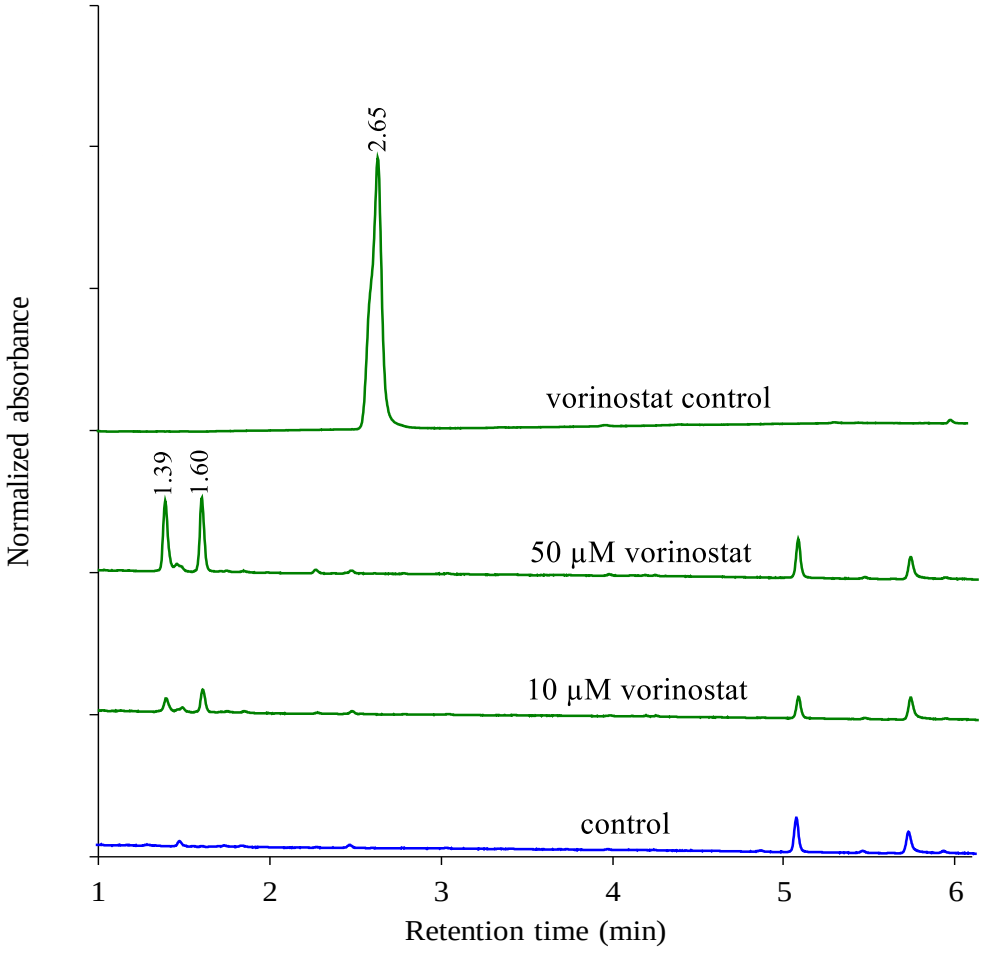

Figure 5.3 Comparative TACs (200-600 nm) of *Streptomyces* sp. CMB-0406 MeOH extracts from cultures cultivated in the absence (control) or the presence of 10 µM or 50 µM vorinostat as well as the vorinostat control (100 µM vorinostat in MeOH) showing a peak of vorinostat at 2.65 min retention time.

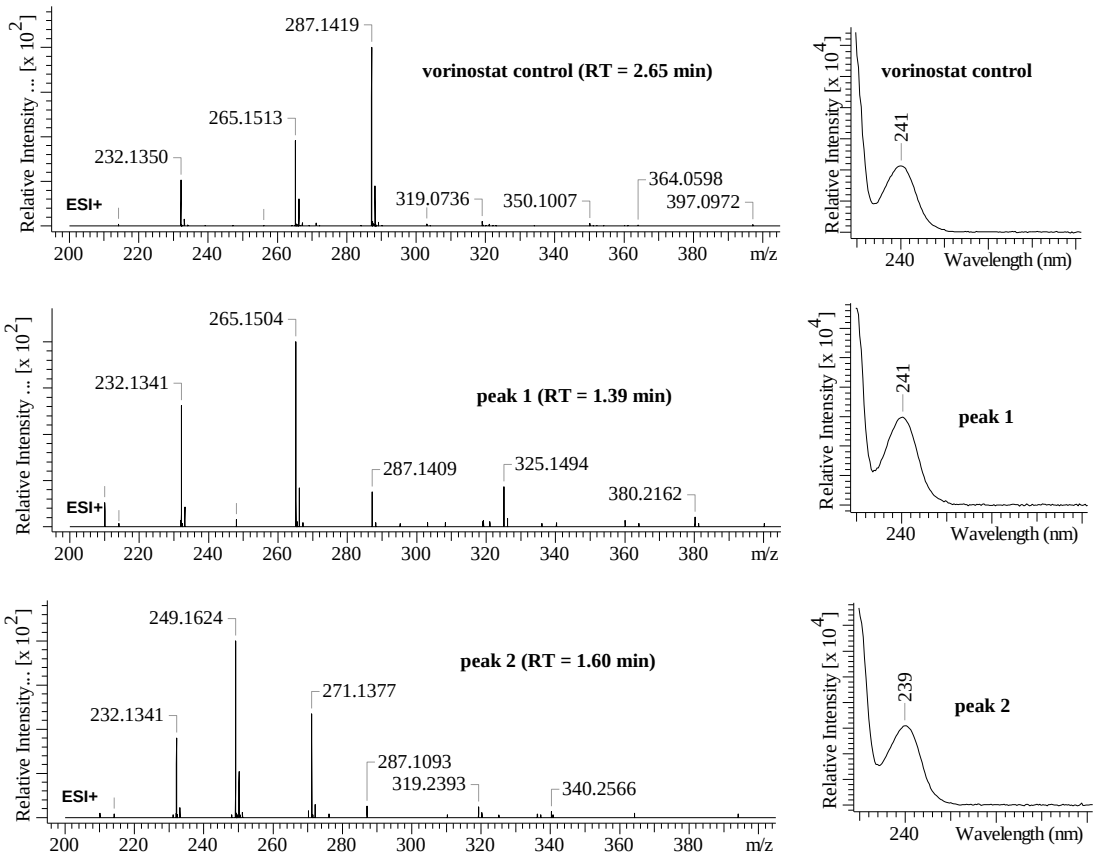

Figure 5.4 MS (positive ion mode) and UV spectra of vorinostat (vorinostat control) and vorinostat-related products (peak 1 and peak 2).

The EtOAc extracts of the SV2 *Streptomyces* sp. CMB-0406 cultures did not show a remarkable difference between the epigenetic-treated cultures and the control cultures. Interestingly, the production of *Streptomyces* metabolites known as heronamides[243] was significantly affected by the medium employed for cultivation (Figure 5.5). The cultures cultivated in SV2 medium contained larger amounts of heronamides and lower or undetectable amounts of vorinostat products in comparison to the SM7 cultures using MS (Table 5.1) and UV traces (Figure 5.6). Moreover, the yield of heroanamides was negatively affected by the presence of vorinostat in SM7 medium. After seven-day cultivation of *Streptomyces* sp. CMB-0406 in SM7 and SV2 media, the metabolic profile fingerprint did not change, but the quantity of heronamides was higher than observed in the four-day extracts.

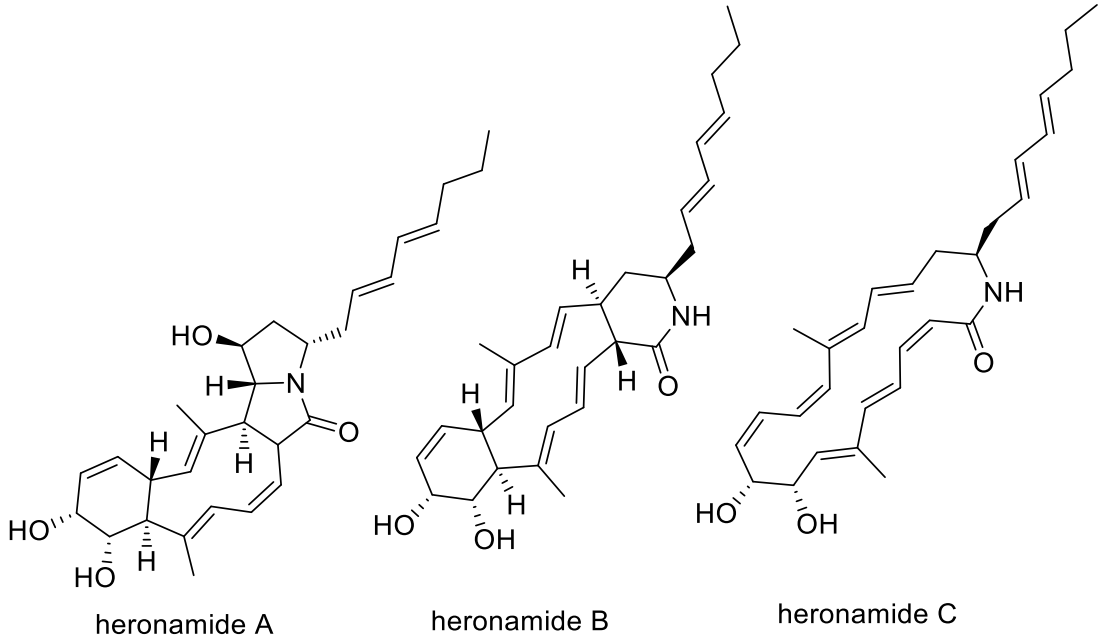

Figure 5.5 Chemical structures of heronamides A-C.

Table 5.1 Comparison of the intensities of the vorinostat products and heronamides in *Streptomyces* sp. CMB-0406 cultures in SM7 and SV2 media with and without 50 µM vorinostat.

Ion *m/z*	**Ion RT**	**Normalised Intensity**				**Compound**
		SM7 control	**SM7 50 µM vorinostat**	**SV2 control**	**SV2 50 µM vorinostat**	
249.1624	1.60	0	4276781	0	2452037	Peak 1
265.1504	1.39	0	4008014	0	0	Peak 2
466.2960	4.22	1256529	779317	3875258	4050196	Heronamide A
450.3023	5.12	5874826	3097358	8738652	9291494	Heronamide B/C

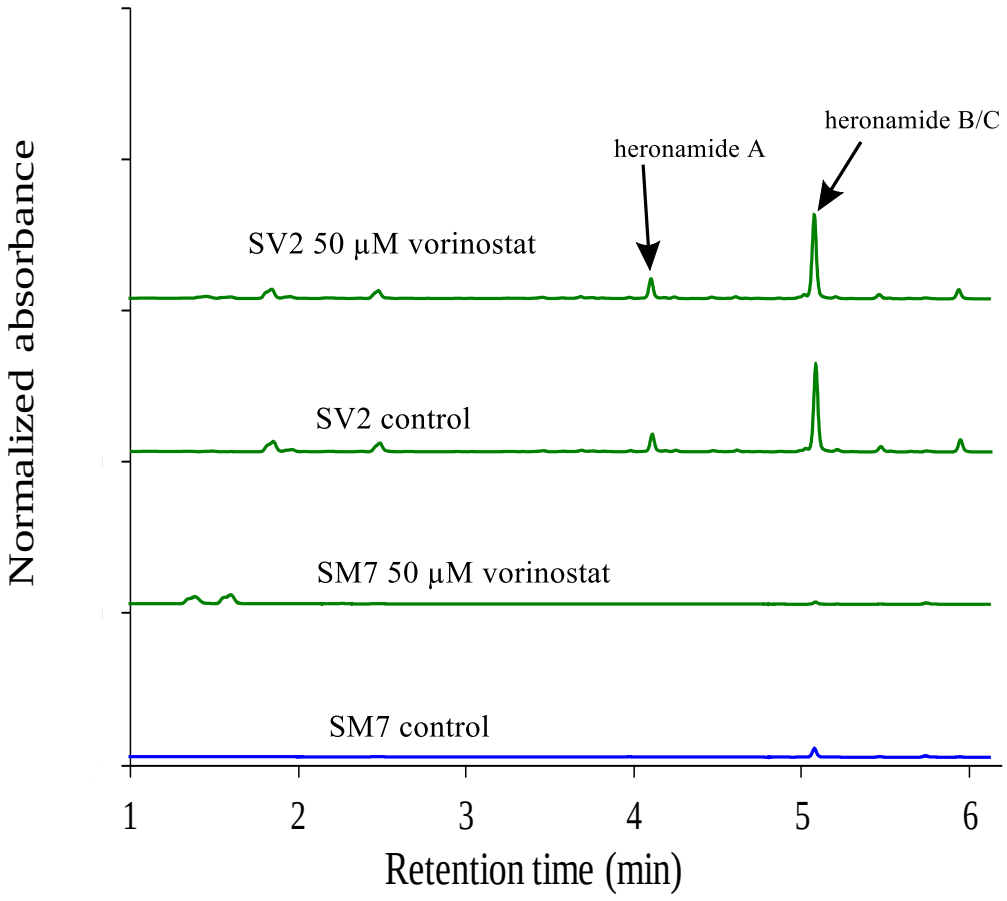

Figure 5.6 Comparative TACs (200-600 nm) of *Streptomyces* sp. CMB-0406 cultivated in SM7 and SV2 medium for four days in the absence (control) and the presence of 50 µM vorinostat.

The cultivation of *Saccharopolyspora* KY21 in SM7 and SV2 medium supplemented with epigenetic modifiers did not change the metabolic profile except for the presence of vorinostat-related products in the cultures supplemented with vorinostat. A new vorinostat-related product was observed in the SM7 *Saccharopolyspora* KY21 culture treated with vorinostat (RT = 2.27) compared to the SM7 *Streptomyces* sp. CMB-0406 vorinostat-treated culture (Figure 5.7). The UV spectrum of the new peak was identical to that of vorinostat, and the MS spectrum contained the main vorinostat fragment (Figure 5.8), indicating that the structural difference between the new vorinostat-related product and vorinostat is insignificant.

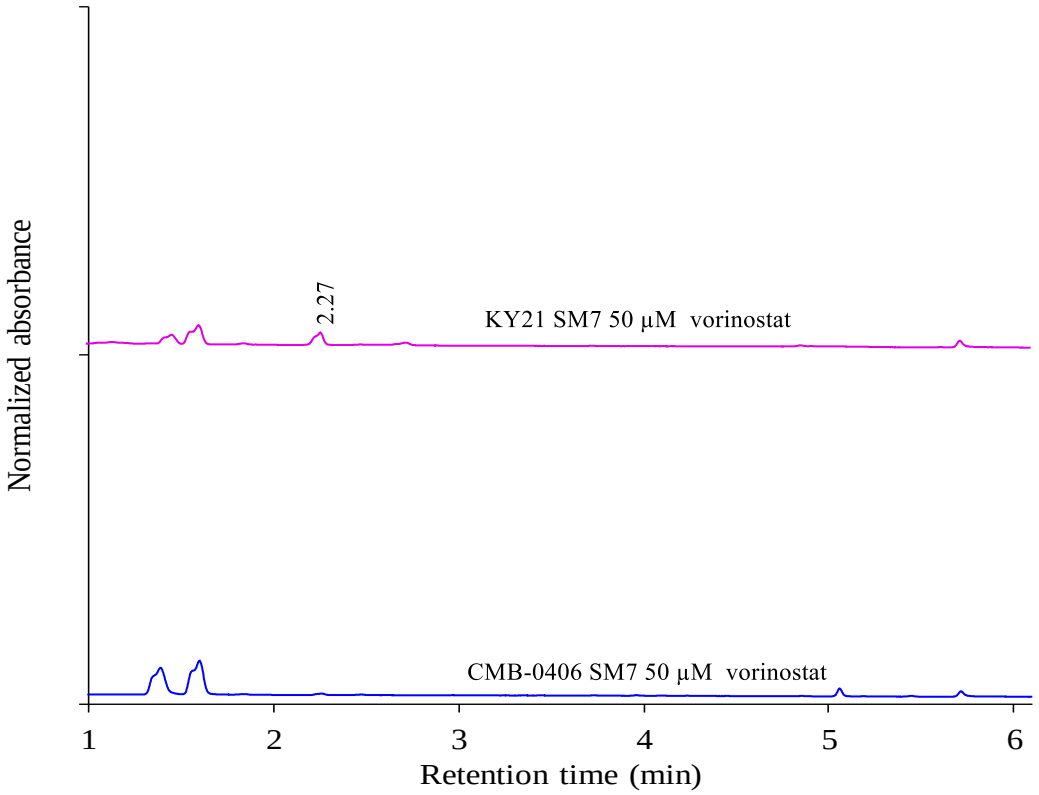

Figure 5.7 Comparative TACs (200-600 nm) of vorinostat-related products observed with *Streptomyces* sp. CMB-0406 and *Saccharopolyspora* KY21 cultivated in SM7 for four days in the presence of 50 µM vorinostat.

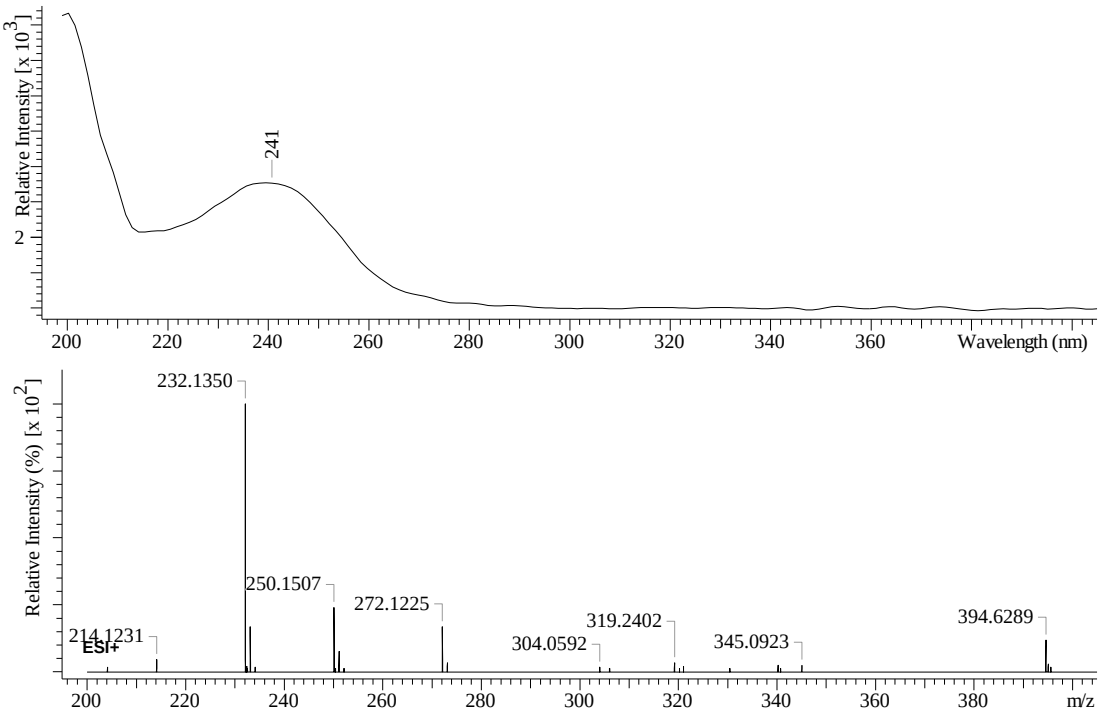

Figure 5.8 UV and MS (positive ion mode) spectra of the new vorinostat-related product observed with *Saccharopolyspora* KY21 in SM7 containing 50 µM vorinostat.

5.3. Overall discussion and conclusion

The epigenetic manipulation of the actinomycete strains did not lead to the production of any new metabolites compared to the control cultures. However, three vorinostat-related products were observed in the extracts of the cultures treated with vorinostat. This might be because these species are efficient in the metabolism of vorinostat converting it to an ineffective form. Although a high concentration of 5-AC was used, the neutral pH of the medium might have accelerated the degradation of this modifier. On the other hand, the cultivation of *Streptomyces* sp. CMB-0406 in SV2 medium resulted in higher yields of heronamides compared to SM7 medium. This indicates that secondary metabolism in this species is affected by the media components and that nutritional manipulation might be an efficient strategy for the discovery of novel metabolites from this species. Nevertheless, this experiment was limited to two media and a more comprehensive range of media should be trialled to investigate the efficiency of nutritional manipulation in this species for natural product discovery.

5.4. Materials and methods

5.4.1. General experimental procedures

Unless stated otherwise, all chemicals and solvents were purchased from Sigma-Aldrich, Alfa Aesar or Fisher Scientific. All solvents were of HPLC grade or equivalent. Commercial media and media components were purchased from Sigma-Aldrich, Alfa Aesar, Fisher Scientific or Formedium.

5.4.2. Epigenetic and nutritional manipulation

Bacterial strains were provided by Prof. Barrie Wilkinson (molecular microbiology department, JIC, UK). *Saccharopolyspora* KY21 was isolated from the Kenyan plant ants, *Tetraponera penzigi*.[244] *Streptomyces* sp. CMB-0406 was isolated from marine sediment collected off the coast of Heron Island, Australia.[243] *Streptomyces* sp. CMB-0406 and *Saccharopolyspora* KY21 were cultured in SV2 medium (1.5 % glucose, 1.5 % glycerol, 1.5 % soya peptone, 0.3 % NaCl, 0.1 % $CaCO_3$; pH 7.0) for three days. These seed cultures were used to inoculate 10 mL of SV2 and SM7 medium (100 µL/10 mL) in the presence of 0.5% DMSO (control), 10 µM vorinostat, 50 µM vorinostat, 50 µM 5-AC, 100 µM 5-AC or a combination of 10 µM vorinostat and 50 µM 5-AC, added after 24 h of inoculation. SM7 medium was composed of (per L): MOPS, 20.9 g; glycerol, 20 mL; sucrose, 2.5 g; NaCl, 0.5 g; L-proline, 15 g; K_2HPO_4, 2.0 g; L-glutamate 1.5 g; 0.2M $MgSO_4$, 10 mL; 0.02M $CaCl_2.2H_2O$, 10 mL; 5 mL of a trace elements solution containing (g/L): $MnCl_2 \cdot 4H_2O$, 0.1; $FeSO_4 \cdot 7H_2O$, 0.1; $ZnCl_2$, 0.05. The medium was adjusted to pH 6.5 before sterilization.

Two replicates of each condition were produced, a sample of 900 µL was taken after four and seven days of inoculation and extracted with an equal volume of MeOH or EtOAc and shaking for 20 min. The mixtures were then centrifuged, and 600 µL of each were transferred to HPLC vials. The MeOH extracts were analysed directly by LC-PDA-MS, while the EtOAc extracts were evaporated in a centrifugal evaporator, dissolved in 600 µL of MeOH and filtered before LC-PDA-MS analysis. LC-PDA-MS analysis was performed on a Shimadzu LC-PDA-MS as described in chapter 2 (section 2.4.3).

Chapter Six

6. Overall conclusion and future work

This project aimed at activating natural product genes in *Euglena* microalgae, *Aspergillus* fungi and actinomycete bacteria through nutritional and epigenetic manipulation. Nutritional manipulation of *Euglena* resulted in the discovery of five novel natural products from *E. gracilis*, named euglenatides A-E, with moderate antifungal activity and potent anticancer activity. Further in-vitro and in-vivo experiments are needed to assess the pharmacodynamic and pharmacokinetic properties of euglenatides as antifungal and anticancer agents. Such experiments will require larger quantities of the natural products. While this is possible by scaling up the algal cultivation, engineered strains or heterologous hosts can be used to improve the yield. However, the genetic engineering and heterologous expression of euglenatides will require the identification of their BGCs. An alternative option involves chemical total synthesis of euglenatides. This strategy can be extended by chemical modification to produce 'unnatural' analogues that might have superior pharmacodynamic or pharmacokinetic properties compared to the original natural products.

The investigation of *E. mutabilis* and *E. sanguinea* revealed that they produce metabolites related to euglenatides discovered from *E. gracilis*. The complexity of the *E. sanguinea* extract did not allow the separation and isolation of the euglenatide-related metabolites to enable structure elucidation and pharmacological evaluation. Therefore, good separation might be achieved by using chromatography columns that are designed specifically for peptide isolation or through other extraction and isolation

protocols. Moreover, the extracts of other *Euglena* species including *E. mutabilis* can be another important source of euglenatide analogues.

In *Aspergillus* fungi, nutritional manipulation of *A. bombycis* resulted in significant changes in metabolite profiles leading to a substantial increase in the antibacterial and antifungal activities. The following experiments including dereplication, isolation and structure elucidation of the bioactive metabolites are continued by our collaborators in Fundación Medina, Spain. The epigenetic manipulation of five *Aspergillus* species led to a significant increase in the titre levels of phenylahistin and penicillic acid in *A. calidoustus* and *A. westerdijkiae*, respectively. Further experiments can involve feeding biosynthetic precursor analogues to the fermentation broth of *A. calidoustus* to produce unnatural phenylahistin analogues. This procedure has been successfully utilised for the production of unnatural beauvericins by the endophytic fungus *Fusarium oxysporum*.[245]

While epigenetic manipulation did not display noticeable effects on the metabolite profiles of the actinomycete strains, nutritional manipulation led to higher yields of heronamides in *Streptomyces* sp. CMB-0406. This indicates that secondary metabolism in this *Streptomyces* species is affected by the media components and that nutritional manipulation might be an efficient strategy for the discovery of novel metabolites from this species. Nevertheless, the nutritional manipulation experiment in the actinomycetes was limited to two media and a more comprehensive range of media should be trialled to investigate the efficiency of nutritional manipulation for natural product discovery.

7. References

[1] M. Heinrich, J. Barnes, J. Prieto-Garcia, S. Gibbons, E. M. Williamson, *Fundamentals of Pharmacognosy and Phytotherapy E-Book*, Elsevier Health Sciences, **2017**.

[2] J. R. Hanson, Ed. , in *Natural Products: The Secondary Metabolites*, The Royal Society Of Chemistry, **2003**, pp. 1–34.

[3] D. A. Williams, W. O. Foye, T. L. Lemke, *Foye's Principles of Medicinal Chemistry*, Lippincott Williams & Wilkins, **2002**.

[4] D. A. Dias, S. Urban, U. Roessner, *Metabolites* **2012**, *2*, 303–336.

[5] P. Hunter, *EMBO Rep.* **2008**, *9*, 838–840.

[6] *Nat. Chem. Biol.* **2007**, *3*, 351.

[7] J. Macheleidt, D. J. Mattern, J. Fischer, T. Netzker, J. Weber, V. Schroeckh, V. Valiante, A. A. Brakhage, *Annu. Rev. Genet.* **2016**, *50*, 371–392.

[8] B. Baral, A. Akhgari, M. Metsä-Ketelä, *Synth. Syst. Biotechnol.* **2018**, *3*, 163–178.

[9] H. Jenke-Kodama, E. Dittmann, *Nat. Prod. Rep.* **2009**, *26*, 874.

[10] A. L. Harvey, *Drug Discov. Today* **2008**, *13*, 894–901.

[11] D. J. Newman, G. M. Cragg, *J. Nat. Prod.* **2020**, *83*, 770–803.

[12] E. Patridge, P. Gareiss, M. S. Kinch, D. Hoyer, *Drug Discov. Today* **2016**, *21*, 204–207.

[13] I. Radecka, C. Martin, D. Hill, in *Novel Antimicrobial Agents and Strategies*, Wiley-VCH Verlag GmbH & Co. KGaA, Weinheim, **2014**, pp. 1–16.

[14] G. Biffi, G. Boretti, A. Di Marco, P. Pennella, *Appl. Microbiol.* **1954**, *2*, 288–293.

[15] R. Lal, S. Lal, *Bioessays News Rev. Mol. Cell. Dev. Biol.* **1994**, *16*, 211–216.

[16] D. P. Levine, *Clin. Infect. Dis.* **2006**, *42*, S5–S12.

[17] J. Birnbaum, F. M. Kahan, H. Kropp, J. S. Macdonald, *Am. J. Med.* **1985**, *78*, 3–21.

[18] H. A. Stevens, *Prim. Care Update Ob. Gyns.* **1997**, *4*, 251–253.

[19] T. J. Dougherty, M. J. Pucci, *Antibiotic Discovery and Development*, Springer Science + Business Media, London, **2012**.

[20] D. Greenwood, in *Antibiotic and Chemotherapy*, Elsevier, **2010**, pp. 170–199.

[21] S. B. Zotchev, *Curr. Med. Chem.* **2003**, *10*, 211–223.

[22] A. Patil, S. Majumdar, *J. Pharm. Pharmacol.* **2017**, *69*, 1635–1660.

[23] R. H. Moseley, in *Drug-Induced Liver Dis.*, Elsevier, **2013**, pp. 463–481.

[24] M. Aldholmi, P. Marchand, I. Ourliac-Garnier, P. Le Pape, A. Ganesan, *Pharmaceuticals* **2019**, *12*, 182.

[25] A. L. Demain, S. Sanchez, *J. Antibiot. (Tokyo).* **2009**, *62*, 5–16.

[26] S. A. Waksman, H. B. Woodruff, *J. Bacteriol.* **1941**, *42*, 231–249.

[27] E. Fernández, U. Weissbach, C. Sánchez Reillo, A. F. Braña, C. Méndez, J. Rohr, J. A. Salas, *J. Bacteriol.* **1998**, *180*, 4929–4937.

[28] H. Umezawa, K. Maeda, T. Takeuchi, Y. Okami, *J. Antibiot. (Tokyo).* **1966**, *19*, 200–209.

[29] J. S. MacDonald, P. V Woolley, T. Smythe, W. Ueno, D. Hoth, P. S. Schein, *Cancer* **1979**, *44*, 42–47.

[30] R. B. Weiss, *Semin. Oncol.* **1992**, *19*, 670–686.

[31] S. Forli, *Curr. Top. Med. Chem.* **2014**, *14*, 2312–2321.

[32] S. Goodin, M. P. Kane, E. H. Rubin, *J. Clin. Oncol.* **2004**, *22*, 2015–2025.

[33] Y. Ji, J. Bi, B. Yan, X. Zhu, *Chin. J. Biotechnol.* **2006**, *22*, 1–6.
[34] S. Garyali, A. Kumar, M. S. Reddy, *J. Microbiol. Biotechnol.* **2013**, *23*, 1372–1380.
[35] G. Housman, S. Byler, S. Heerboth, K. Lapinska, M. Longacre, N. Snyder, S. Sarkar, *Cancers (Basel).* **2014**, *6*, 1769–1792.
[36] C. L. Ventola, *P T* **2015**, *40*, 277–283.
[37] B. David, J.-L. Wolfender, D. A. Dias, *Phytochem. Rev.* **2015**, *14*, 299–315.
[38] D.-X. Kong, M.-Y. Guo, Z.-H. Xiao, L.-L. Chen, H.-Y. Zhang, *Chem. Biodivers.* **2011**, *8*, 1968–1977.
[39] C. R. Pye, M. J. Bertin, R. S. Lokey, W. H. Gerwick, R. G. Linington, *Proc. Natl. Acad. Sci.* **2017**, *114*, 5601–5606.
[40] D. G. I. Kingston, *J. Nat. Prod.* **2011**, *74*, 496–511.
[41] J. A. Takahashi, A. P. C. Teles, A. De Almeida Pinto Bracarense, D. C. Gomes, *Phytochem. Rev.* **2013**, *12*, 773–789.
[42] R. Pan, X. Bai, J. Chen, H. Zhang, H. Wang, *Front. Microbiol.* **2019**, *10*, 294.
[43] H. B. Bode, B. Bethe, R. Höfs, A. Zeeck, *ChemBioChem* **2002**, *3*, 619.
[44] K. Blin, S. Shaw, K. Steinke, R. Villebro, N. Ziemert, S. Y. Lee, M. H. Medema, T. Weber, *Nucleic Acids Res.* **2019**, *47*, W81–W87.
[45] M. Nett, H. Ikeda, B. S. Moore, *Nat. Prod. Rep.* **2009**, *26*, 1362.
[46] C. Corre, G. L. Challis, in *Compr. Nat. Prod. II*, Elsevier, **2010**, pp. 429–453.
[47] G. van Keulen, P. J. Dyson, **2014**, pp. 217–266.
[48] R. A. Cacho, Y. Tang, Y.-H. Chooi, *Front. Microbiol.* **2015**, *5*, 774.
[49] S. Donadio, P. Monciardini, M. Sosio, *Nat. Prod. Rep.* **2007**, *24*, 1073.
[50] S. J. Pidot, S. Coyne, F. Kloss, C. Hertweck, *Int. J. Med. Microbiol.* **2014**, *304*, 14–22.
[51] A.-C. Letzel, S. J. Pidot, C. Hertweck, *Nat. Prod. Rep.* **2013**, *30*, 392–428.
[52] E. Shelest, N. Heimerl, M. Fichtner, S. Sasso, *BMC Genomics* **2015**, *16*, 1015.
[53] T. E. Ebenezer, M. Zoltner, A. Burrell, A. Nenarokova, A. M. G. Novák Vanclová, B. Prasad, P. Soukal, C. Santana-Molina, E. O'Neill, N. N. Nankissoor, et al., *BMC Biol.* **2019**, *17*, 11.
[54] S. Lautru, R. J. Deeth, L. M. Bailey, G. L. Challis, *Nat. Chem. Biol.* **2005**, *1*, 265–269.
[55] B. Silakowski, B. Kunze, G. Nordsiek, H. Blöcker, G. Höfle, R. Müller, *Eur. J. Biochem.* **2000**, *267*, 6476–6485.
[56] J. J. May, T. M. Wendrich, M. A. Marahiel, *J. Biol. Chem.* **2001**, *276*, 7209–7217.
[57] G. L. Challis, *J. Ind. Microbiol. Biotechnol.* **2014**, *41*, 219–232.
[58] Y. Luo, R. E. Cobb, H. Zhao, *Curr. Opin. Biotechnol.* **2014**, *30*, 230–237.
[59] N. Ziemert, M. Alanjary, T. Weber, *Nat. Prod. Rep.* **2016**, *33*, 988–1005.
[60] A. Srivastava, J. George, R. K. M. Karuturi, in *Encycl. Bioinforma. Comput. Biol.*, Elsevier, **2019**, pp. 792–805.
[61] M. H. Medema, K. Blin, P. Cimermancic, V. de Jager, P. Zakrzewski, M. A. Fischbach, T. Weber, E. Takano, R. Breitling, *Nucleic Acids Res.* **2011**, *39*, W339–W346.
[62] N. Khaldi, F. T. Seifuddin, G. Turner, D. Haft, W. C. Nierman, K. H. Wolfe, N. D. Fedorova, *Fungal Genet. Biol.* **2010**, *47*, 736–741.
[63] B. C. Covington, J. A. McLean, B. O. Bachmann, *Nat. Prod. Rep.* **2017**, *34*, 6–24.
[64] L. D. Roberts, A. L. Souza, R. E. Gerszten, C. B. Clish, *Curr. Protoc. Mol. Biol.* **2012**, *98*, 30.2.1-30.2.24.

[65] R. R. Forseth, F. C. Schroeder, *Curr. Opin. Chem. Biol.* **2011**, *15*, 38–47.
[66] W. LI, *J. Bioinform. Comput. Biol.* **2012**, *10*, 1231003.
[67] J. C. Albright, M. T. Henke, A. A. Soukup, R. A. McClure, R. J. Thomson, N. P. Keller, N. L. Kelleher, *ACS Chem. Biol.* **2015**, *10*, 1535–1541.
[68] M. Hur, A. A. Campbell, M. Almeida-de-Macedo, L. Li, N. Ransom, A. Jose, M. Crispin, B. J. Nikolau, E. S. Wurtele, *Nat. Prod. Rep.* **2013**, *30*, 565–583.
[69] J. J. Kellogg, D. A. Todd, J. M. Egan, H. A. Raja, N. H. Oberlies, O. M. Kvalheim, N. B. Cech, *J. Nat. Prod.* **2016**, *79*, 376–386.
[70] A. Sánchez-Medina, K. García-Sosa, F. May-Pat, L. M. Peña-Rodríguez, *Phytomedicine* **2001**, *8*, 144–151.
[71] W. H. Gerwick, B. S. Moore, *Chem. Biol.* **2012**, *19*, 85–98.
[72] J. Y. Yang, L. M. Sanchez, C. M. Rath, X. Liu, P. D. Boudreau, N. Bruns, E. Glukhov, A. Wodtke, R. de Felicio, A. Fenner, et al., *J. Nat. Prod.* **2013**, *76*, 1686–1699.
[73] T. F. Molinski, *Nat. Prod. Rep.* **2010**, *27*, 321.
[74] C. B'Hymer, M. Montes-Bayon, J. A. Caruso, *J. Sep. Sci.* **2003**, *26*, 7–19.
[75] R. Bhushan, H. Bruckner, *Amino Acids* **2004**, *27*, 231–247.
[76] P. Marfey, *Carlsberg Res. Commun.* **1984**, *49*, 591–596.
[77] R. Bhushan, H. Brückner, V. Kumar, D. Gupta, *J. Planar Chromatogr. – Mod. TLC* **2007**, *20*, 165–171.
[78] R. Bhushan, V. Kumar, *Biomed. Chromatogr.* **2008**, *22*, 906–911.
[79] J. Y. Yang, L. M. Sanchez, C. M. Rath, X. Liu, P. D. Boudreau, N. Bruns, E. Glukhov, A. Wodtke, R. de Felicio, A. Fenner, et al., *J. Nat. Prod.* **2013**, *76*, 1686–1699.
[80] M. Wang, J. J. Carver, V. V Phelan, L. M. Sanchez, N. Garg, Y. Peng, D. D. Nguyen, J. Watrous, C. A. Kapono, T. Luzzatto-Knaan, et al., *Nat. Biotechnol.* **2016**, *34*, 828–837.
[81] P. Shannon, *Genome Res.* **2003**, *13*, 2498–2504.
[82] H.-W. Yen, I.-C. Hu, C.-Y. Chen, J.-S. Chang, in *Biofuels from Algae*, Elsevier, **2014**, pp. 23–45.
[83] W. H. Kampen, in *Ferment. Biochem. Eng. Handb.*, Elsevier, **2014**, pp. 37–57.
[84] S. Sánchez, A. Chávez, A. Forero, Y. García-Huante, A. Romero, M. Sánchez, D. Rocha, B. Sánchez, M. Ávalos, S. Guzmán-Trampe, et al., *J. Antibiot. (Tokyo).* **2010**, *63*, 442–459.
[85] J. F. Martín, A. Sola-Landa, F. Santos-Beneit, L. T. Fernández-Martínez, C. Prieto, A. Rodríguez-García, *Microb. Biotechnol.* **2011**, *4*, 165–174.
[86] Z. Shang, X.-M. Li, C.-S. Li, B.-G. Wang, *Chem. Biodivers.* **2012**, *9*, 1338–1348.
[87] O. F. Smetanina, A. N. Yurchenko, E. V Ivanets, A. I. Kalinovsky, Y. V Khudyakova, S. A. Dyshlovoy, G. von Amsberg, E. A. Yurchenko, S. S. Afiyatullov, *J. Antibiot. (Tokyo).* **2017**, *70*, 856–858.
[88] C.-X. Liu, S.-H. Liu, J.-W. Zhao, J. Zhang, X.-J. Wang, J.-S. Li, J.-D. Wang, W.-S. Xiang, *J. Asian Nat. Prod. Res.* **2017**, *19*, 924–929.
[89] C. Puder, S. Loya, A. Hizi, A. Zeeck, *J. Nat. Prod.* **2001**, *64*, 42–45.
[90] A. Hussain, M. A. Rather, M. S. Dar, M. A. Aga, N. Ahmad, A. Manzoor, A. Qayum, A. Shah, S. Mushtaq, Z. Ahmad, et al., *Bioorg. Med. Chem. Lett.* **2017**, *27*, 2579–2582.
[91] P. Sujatha, K. V. V. S. N. Bapi Raju, T. Ramana, *Microbiol. Res.* **2005**, *160*, 119–126.
[92] Y.-H. Yang, X.-L. Fu, L.-Q. Li, Y. Zeng, C.-Y. Li, Y.-N. He, P.-J. Zhao, *J. Nat.*

Prod. **2012**, *75*, 1409–1413.
[93] M. E. Rateb, W. E. Houssen, M. Arnold, M. H. Abdelrahman, H. Deng, W. T. A. Harrison, C. K. Okoro, J. A. Asenjo, B. A. Andrews, G. Ferguson, et al., *J. Nat. Prod.* **2011**, *74*, 1491–1499.
[94] S. Giubergia, C. Phippen, K. F. Nielsen, L. Gram, *mSystems* **2017**, *2*, e00141-16.
[95] R. Preetha, N. S. Jayaprakash, R. Philip, I. S. Bright Singh, *J. Appl. Microbiol.* **2007**, *2*, 1043–1051.
[96] P. K. S. Uchoa, A. T. A. Pimenta, R. Braz-Filho, M. da C. F. de Oliveira, N. N. Saraiva, B. S. F. Rodrigues, L. H. Pfenning, L. M. Abreu, D. V. Wilke, K. G. D. Florêncio, et al., *Nat. Prod. Res.* **2017**, *31*, 2599–2603.
[97] H.-B. Huang, Z.-E. Xiao, X.-J. Feng, C.-H. Huang, X. Zhu, J.-H. Ju, M.-F. Li, Y.-C. Lin, L. Liu, Z.-G. She, *Helv. Chim. Acta* **2011**, *94*, 1732–1740.
[98] K. Scherlach, C. Hertweck, *Org. Biomol. Chem.* **2006**, *4*, 3517–3520.
[99] W. Yang, W.-S. Kim, A. Fang, A. L. Demain, *Curr. Microbiol.* **2003**, *46*, 275–279.
[100] Z. Barboráková, R. Labuda, G. Häubl, D. Tancinová, *J. Microbiol. Biotechnol. Food Sci.* **2012**, *1*, 466.
[101] M. E. Zain, H. H. El-Sheikh, H. G. Soliman, A. M. Khalil, *J. Saudi Chem. Soc.* **2011**, *15*, 239–246.
[102] E. F. Pimenta, A. M. Vita-Marques, A. Tininis, M. H. R. Seleghim, L. D. Sette, K. Veloso, A. G. Ferreira, D. E. Williams, B. O. Patrick, D. S. Dalisay, et al., *J. Nat. Prod.* **2010**, *73*, 1821–1832.
[103] C. Lauritano, J. H. Andersen, E. Hansen, M. Albrigtsen, L. Escalera, F. Esposito, K. Helland, K. Ø. Hanssen, G. Romano, A. Ianora, *Front. Mar. Sci.* **2016**, *3*, 68.
[104] C. Lauritano, J. Martín, M. de la Cruz, F. Reyes, G. Romano, A. Ianora, *Sci. Rep.* **2018**, *8*, 2284.
[105] F. Wang, L. Huang, B. Gao, C. Zhang, *Mar. Drugs* **2018**, *16*, 190.
[106] G. Felsenfeld, *Cold Spring Harb. Perspect. Biol.* **2014**, *6*, a018200.
[107] R. D. Kornberg, Y. Lorch, *Cell* **1999**, *98*, 285–294.
[108] J. M. Moore, E. Bradshaw, R. F. Seipke, M. I. Hutchings, M. McArthur, in *Methods in Enzymology* (Ed.: D.A. Hopwood), Academic Press, Burlington, **2012**, pp. 367–385.
[109] G. Felsenfeld, M. Groudine, *Nature* **2003**, *421*, 448–453.
[110] R. H. Cichewicz, *Nat. Prod. Rep.* **2010**, *27*, 11–22.
[111] B. M. Turner, *Nat. Struct. Mol. Biol.* **2005**, *12*, 110–112.
[112] K. Luger, T. J. Richmond, *Curr. Opin. Genet. Dev.* **1998**, *8*, 140–146.
[113] V. Allfrey, R. Faulkner, A. Mirsky, *Biochemistry* **1964**, *315*, 786–794.
[114] P. Loidl, *Chromosoma* **1994**, *103*, 441–449.
[115] S. J. Clark, J. Harrison, M. Frommer, *Nat. Genet.* **1995**, *10*, 20–27.
[116] Y. Z. Kim, *Brain Tumor Res. Treat.* **2014**, *2*, 7–21.
[117] A. Ganesan, *Philos. Trans. R. Soc. B Biol. Sci.* **2018**, *373*, 20170069.
[118] Y. M. Chiang, E. Szewczyk, A. D. Davidson, R. Entwistle, N. P. Keller, C. C. C. Wang, B. R. Oakley, *Appl. Environ. Microbiol.* **2010**, *76*, 2067–2074.
[119] E. K. Shwab, W. B. Jin, M. Tribus, J. Galehr, S. Graessle, N. P. Keller, *Eukaryot. Cell* **2007**, *6*, 1656–1664.
[120] A. A. Brakhage, *FEMS Microbiol. Lett.* **1997**, *148*, 1–10.
[121] I. Lee, J. H. Oh, E. Keats Shwab, T. R. T. Dagenais, D. Andes, N. P. Keller, *Fungal Genet. Biol.* **2009**, *46*, 782–790.

[122] M. Tribus, I. Bauer, J. Galehr, G. Rieser, P. Trojer, G. Brosch, P. Loidl, H. Haas, S. Graessle, *Mol. Biol. Cell* **2010**, *21*, 345–353.
[123] C. Avendaño, J. C. Menéndez, *Medicinal Chemistry of Anticancer Drugs*, Elsevier, Oxford, UK, **2015**.
[124] M. Grunstein, *Nature* **1997**, *389*, 349–352.
[125] V. Beljanski, in *XPharm: The Comprehensive Pharmacology Reference*, Elsevier, Charleston, **2009**, pp. 1–4.
[126] B. E. Bernstein, J. K. Tong, S. L. Schreiber, *Proc. Natl. Acad. Sci. U. S. A.* **2000**, *97*, 13708–13713.
[127] K. Sun, G. Zhu, J. Hao, Y. Wang, W. Zhu, *Tetrahedron* **2018**, *74*, 83–87.
[128] J. C. Henrikson, A. R. Hoover, P. M. Joyner, R. H. Cichewicz, *Org. Biomol. Chem.* **2009**, *7*, 435–438.
[129] R. B. Williams, J. C. Henrikson, A. R. Hoover, A. E. Lee, R. H. Cichewicz, *Org. Biomol. Chem.* **2008**, *6*, 1895–1897.
[130] H. C. Vervoort, M. Drašković, P. Crews, *Org. Lett.* **2011**, *13*, 410–413.
[131] Y.-M. Chung, M. El-Shazly, D.-W. Chuang, T.-L. Hwang, T. Asai, Y. Oshima, M. L. L. Ashour, Y.-C. Wu, F.-R. Chang, *J. Nat. Prod.* **2013**, *76*, 1260–1266.
[132] L. Du, J. B. King, R. H. Cichewicz, *J. Nat. Prod.* **2014**, *77*, 2454–2458.
[133] F. P. Miao, X. R. Liang, X. H. Liu, N. Y. Ji, *J. Nat. Prod.* **2014**, *77*, 429–432.
[134] T. Asai, T. Yamamoto, Y. Oshima, *Tetrahedron Lett.* **2011**, *52*, 7042–7045.
[135] H.-J. Chen, T. Awakawa, J.-Y. Sun, T. Wakimoto, I. Abe, *Nat. Products Bioprospect.* **2013**, *3*, 20–23.
[136] T. Asai, T. Yamamoto, N. Shirata, T. Taniguchi, K. Monde, I. Fujii, K. Gomi, Y. Oshima, *Org. Lett.* **2013**, *15*, 3346–3349.
[137] T. Asai, T. Taniguchi, T. Yamamoto, K. Monde, Y. Oshima, *Org. Lett.* **2013**, *15*, 4320–4323.
[138] X. M. Mao, W. Xu, D. Li, W. B. Yin, Y. H. Chooi, Y. Q. Li, Y. Tang, Y. Hu, *Angew. Chemie Int. Ed.* **2015**, *54*, 7592–7596.
[139] G. Brosch, M. Dangl, S. Graessle, A. Loidl, P. Trojer, E. Brandtner, K. Mair, J. D. Walton, D. Baidyaroy, P. Loidl, *Biochemistry* **2001**, *40*, 12855–12863.
[140] B. F. Hinnebusch, S. Meng, J. T. Wu, S. Y. Archer, R. A. Hodin, *J. Nutr.* **2002**, *132*, 1012–1017.
[141] C. Zutz, D. Bandian, B. Neumayer, F. Speringer, M. Gorfer, M. Wagner, J. Strauss, K. Rychli, *Biomed Res. Int.* **2014**, *2014*, 540292.
[142] W. Zhang, C. L. Shao, M. Chen, Q. A. Liu, C. Y. Wang, *Tetrahedron Lett.* **2014**, *55*, 4888–4891.
[143] J. Beau, N. Mahid, W. N. Burda, L. Harrington, L. N. Shaw, T. Mutka, D. E. Kyle, B. Barisic, A. Van Olphen, B. J. Baker, *Mar. Drugs* **2012**, *10*, 762–774.
[144] S. Minucci, P. Zhu, O. H. Kra, A. Schimpf, S. Giavara, J. P. Sleeman, F. Lo Coco, C. Nervi, P. G. Pelicci, T. Heinzel, *EMBO J.* **2001**, *20*, 6969–6978.
[145] C. Zutz, A. Gacek, M. Sulyok, M. Wagner, J. Strauss, K. Rychli, *Toxins (Basel).* **2013**, *5*, 1723–1741.
[146] A. Magotra, M. Kumar, M. Kushwaha, P. Awasthi, C. Raina, A. P. Gupta, B. A. Shah, S. G. Gandhi, A. Chaubey, *AMB Express* **2017**, *7*, 43.
[147] F. Berger, M. H. Ramírez-Hernández, M. Ziegler, *Trends Biochem. Sci.* **2004**, *29*, 111–118.
[148] S. S. Mahajan, V. Leko, J. A. Simon, A. Bedalov, *Handb. Exp. Pharmacol.* **2011**, *206*, 241–255.
[149] T. Asai, S. Morita, N. Shirata, T. Taniguchi, K. Monde, H. Sakurai, T. Ozeki, Y. Oshima, *Org. Lett.* **2012**, *14*, 5456–5459.

[150] T. Asai, S. Otsuki, H. Sakurai, K. Yamashita, T. Ozeki, Y. Oshima, *Org. Lett.* **2013**, *15*, 2058–2061.
[151] T. Asai, S. Morita, T. Taniguchi, K. Monde, Y. Oshima, *Org. Biomol. Chem.* **2016**, *14*, 646–651.
[152] J. C. Chuang, *Mol. Cancer Ther.* **2005**, *4*, 1515–1520.
[153] M. S. S. Kritskiĭ, S. I. I. Filippovich, T. P. P. Afanas'eva, G. P. P. Bachurina, V. E. E. Russo, *Prikl. Biokhim. Mikrobiol.* **2001**, *37*, 279–284.
[154] X. Wang, J. G. Sena Filho, A. R. Hoover, J. B. King, T. K. Ellis, D. R. Powell, R. H. Cichewicz, *J. Nat. Prod.* **2010**, *73*, 942–948.
[155] M. Chen, W. Zhang, C. L. Shao, Z. M. Chi, C. Y. Wang, *Mar. Biotechnol.* **2016**, *18*, 409–417.
[156] M. Qadri, Y. Nalli, S. K. Jain, A. Chaubey, A. Ali, G. A. Strobel, R. A. Vishwakarma, S. Riyaz-Ul-Hassan, *Microb. Ecol.* **2016**, 954–965.
[157] Y. M. Chung, C. K. Wei, D. W. Chuang, M. El-Shazly, C. T. Hsieh, T. Asai, Y. Oshima, T. J. Hsieh, T. L. Hwang, Y. C. Wu, et al., *Bioorganic Med. Chem.* **2013**, *21*, 3866–3872.
[158] X.-L. Yang, L. Huang, X.-L. Ruan, *J. Asian Nat. Prod. Res.* **2014**, *16*, 412–417.
[159] V. González-Menéndez, M. Pérez-Bonilla, I. Pérez-Victoria, J. Martín, F. Muñoz, F. Reyes, J. R. Tormo, O. Genilloud, *Molecules* **2016**, *21*, 234.
[160] X. L. Yang, T. Awakawa, T. Wakimoto, I. Abe, *Tetrahedron Lett.* **2013**, *54*, 5814–5817.
[161] X. L. Yang, T. Awakawa, T. Wakimoto, I. Abe, *Tetrahedron Lett.* **2013**, *54*, 3655–3657.
[162] L. Wang, M. Li, J. Tang, X. Li, *Molecules* **2016**, *21*, 473.
[163] X. Li, Z. Xia, J. Tang, J. Wu, J. Tong, M. Li, J. Ju, H. Chen, L. Wang, *Molecules* **2017**, *22*, 1302.
[164] T. Asai, Y. M. Chung, H. Sakurai, T. Ozeki, F. R. Chang, K. Yamashita, Y. Oshima, *Org. Lett.* **2012**, *14*, 513–515.
[165] T. Asai, Y. M. Chung, H. Sakurai, T. Ozeki, F. R. Chang, Y. C. Wu, K. Yamashita, Y. Oshima, *Tetrahedron* **2012**, *68*, 5817–5823.
[166] S. Sasso, G. Pohnert, M. Lohr, M. Mittag, C. Hertweck, *FEMS Microbiol. Rev.* **2012**, *36*, 761–785.
[167] D. Portevin, C. de Sousa-D'Auria, C. Houssin, C. Grimaldi, M. Chami, M. Daffe, C. Guilhot, *Proc. Natl. Acad. Sci.* **2004**, *101*, 314–319.
[168] N. Heimerl, E. Hommel, M. Westermann, D. Meichsner, M. Lohr, C. Hertweck, A. R. Grossman, M. Mittag, S. Sasso, *Plant J.* **2018**, *95*, 268–281.
[169] E. C. O'Neill, M. Trick, L. Hill, M. Rejzek, R. G. Dusi, C. J. Hamilton, P. V. Zimba, B. Henrissat, R. A. Field, *Mol. Biosyst.* **2015**, *11*, 2808–2820.
[170] E. C. O'Neill, M. Trick, B. Henrissat, R. A. Field, E. C. O'Neill, M. Trick, B. Henrissat, R. A. Field, *Perspect. Sci.* **2015**, *6*, 84–93.
[171] S. Inwongwan, N. J. Kruger, R. G. Ratcliffe, E. C. O'Neill, *Metabolites* **2019**, *9*, 115.
[172] A. Gissibl, A. Sun, A. Care, H. Nevalainen, A. Sunna, *Front. Bioeng. Biotechnol.* **2019**, *7*, 108.
[173] Y. Oda, Y. Nakano, S. Kitaoka, *J. Gen. Microbiol.* **1982**, *128*, 853–858.
[174] A. L. Demain, J. F. Newkirk, D. Hendlin, *J. Bacteriol.* **1963**, *85*, 339–344.
[175] J. M. Luengo, G. Revilla, J. R. Villanueva, J. F. Martin, *J. Gen. Microbiol.* **1979**, *115*, 207–211.
[176] J. M. Luengo, G. Revilla, M. J. López, J. R. Villanueva, J. F. Martín, *J. Bacteriol.* **1980**, *144*, 869–876.

[177] R. J. COLE, B. B. JARVIS, M. A. SCHWEIKERT, in *Handb. Second. Fungal Metab.*, Elsevier, **2003**, pp. 17–42.
[178] Scottish Association for Marine Science, "Elimination of bacteria from microalgal culture using antibiotics," can be found under https://www.ccap.ac.uk/documents/Antibiotic_treatment.pdf, **n.d.**
[179] R. a Danilov, N. G. Ekelund, *Folia Microbiol. (Praha).* **2001**, *46*, 549–554.
[180] M. M. Olaveson, C. Nalewajko, *Hydrobiologia* **2000**, *433*, 39–56.
[181] M. T. Croft, A. D. Lawrence, E. Raux-Deery, M. J. Warren, A. G. Smith, *Nature* **2005**, *438*, 90–93.
[182] M. Böhme, W. Pfleiderer, E. F. Elstner, W. J. Richter, *Angew. Chemie Int. Ed. English* **1980**, *19*, 473–474.
[183] P. V. Zimba, P. D. Moeller, K. Beauchesne, H. E. Lane, R. E. Triemer, *Toxicon* **2010**, *55*, 100–104.
[184] P. V. Zimba, I.-S. Huang, D. Gutierrez, W. Shin, M. S. Bennett, R. E. Triemer, *Harmful Algae* **2017**, *63*, 79–84.
[185] K. A. Martínez, C. Lauritano, D. Druka, G. Romano, T. Grohmann, M. Jaspars, J. Martín, C. Díaz, B. Cautain, M. de la Cruz, et al., *Mar. Drugs* **2019**, *17*, 385.
[186] Q. Shou, L. Feng, Y. Long, J. Han, J. K. Nunnery, D. H. Powell, R. A. Butcher, *Nat. Chem. Biol.* **2016**, *12*, 770–772.
[187] B. Spingler, S. Schnidrig, T. Todorova, F. Wild, *CrystEngComm* **2012**, *14*, 751–757.
[188] Y. Kuroda, K. Hasegawa, K. Noguchi, K. Chiba, K. Hasumi, Y. Kitano, *J. Antibiot. (Tokyo).* **2018**, *71*, 584–591.
[189] T. Akita, T. Yamazaki, Y. Uchida, N. Nishiyama, *Polyhedron* **2017**, *136*, 79–86.
[190] J. Martín, T. da S Sousa, G. Crespo, S. Palomo, I. González, J. R. Tormo, M. de la Cruz, M. Anderson, R. T. Hill, F. Vicente, et al., *Mar. Drugs* **2013**, *11*, 387–398.
[191] T. Ohyama, Y. Kurihara, Y. Ono, T. Ishikawa, S. Miyakoshi, K. Hamano, M. Araei, T. Suzuki, H. Igari, Y. Suzuki, et al., *J. Antibiot. (Tokyo).* **2000**, *53*, 1108–1116.
[192] G. Jürjens, S. M. M. Schuler, M. Kurz, S. Petit, C. Couturier, F. Jeannot, F. Nguyen, R. C. Wende, P. E. Hammann, D. N. Wilson, et al., *Angew. Chemie Int. Ed.* **2018**, *57*, 12157–12161.
[193] C. Guérard-Hélaine, E. Heuson, M. Ndiaye, L. Gourbeyre, M. Lemaire, V. Hélaine, F. Charmantray, J.-L. Petit, M. Salanoubat, V. De Berardinis, et al., *Chem. Commun.* **2017**, *53*, 5465–5468.
[194] H. Vemula, Y. Kitase, N. J. Ayon, L. Bonewald, W. G. Gutheil, *Anal. Biochem.* **2017**, *516*, 75–85.
[195] M. C. Monteiro, M. de la Cruz, J. Cantizani, C. Moreno, J. R. Tormo, E. Mellado, J. R. De Lucas, F. Asensio, V. Valiante, A. A. Brakhage, et al., *J. Biomol. Screen.* **2012**, *17*, 542–549.
[196] C. Audoin, D. Bonhomme, J. Ivanisevic, M. Cruz, B. Cautain, M. Monteiro, F. Reyes, L. Rios, T. Perez, O. Thomas, *Mar. Drugs* **2013**, *11*, 1477–1489.
[197] S. Sirikantaramas, M. Yamazaki, K. Saito, *Phytochem. Rev.* **2008**, *7*, 467–477.
[198] S. Sirikantaramas, M. Yamazaki, K. Saito, *Proc. Natl. Acad. Sci.* **2008**, *105*, 6782–6786.
[199] I. T. Baldwin, P. Callahan, *Oecologia* **1993**, *94*, 534–541.
[200] S. Li, P. Wang, W. Yuan, Z. Su, S. H. Bullard, *Sci. Rep.* **2016**, *6*, 29315.
[201] T. Sugawara, A. Tanaka, K. Tanaka, K. Nagai, K. Suzuki, T. Suzuki, *J. Antibiot.*

(Tokyo). **1998**, *51*, 435–438.
[202] Y. Shiono, M. Tsuchinari, K. Shimanuki, T. Miyajima, T. Murayama, T. Koseki, H. Laatsch, T. Funakoshi, K. Takanami, K. Suzuki, *J. Antibiot. (Tokyo)*. **2007**, *60*, 309–316.
[203] Y. Guillou, Y. Robin, *J. Biol. Chem.* **1973**, *248*, 5668–5672.
[204] K. Fuji, E. Fujita, Y. Takaishi, T. Fujita, I. Arita, M. Komatsu, N. Hiratsuka, *Experientia* **1978**, *34*, 237–239.
[205] P. O. Larsen, A. F. Daniel, R. Havanka, T. Briggs, G. A. D. Haslewood, H. Flood, *Acta Chem. Scand.* **1962**, *16*, 1511–1518.
[206] S. ASEN, J. F. THOMPSON, C. J. MORRIS, F. IRREVERRE, *J. Biol. Chem.* **1959**, *234*, 343–346.
[207] J. Stautemas, A. B. P. Van Kuilenburg, L. Stroomer, F. Vaz, L. Blancquaert, F. B. D. Lefevere, I. Everaert, W. Derave, *Front. Physiol.* **2019**, *10*, 1240.
[208] K. Isono, K. Asahi, S. Suzuki, *J. Am. Chem. Soc.* **1969**, *91*, 7490–7505.
[209] L. Brandi, A. Lazzarini, L. Cavaletti, M. Abbondi, E. Corti, I. Ciciliato, L. Gastaldo, A. Marazzi, M. Feroggio, A. Fabbretti, et al., *Biochemistry* **2006**, *45*, 3692–3702.
[210] P. O. Larsen, L. Forsgren, T. A. Bak, P. Holmberg, G. Eriksson, R. Blinc, S. Paušak, L. Ehrenberg, J. Dumanović, *Acta Chem. Scand.* **1967**, *21*, 1592–1604.
[211] J. Ariza, J. Font, R. M. Ortuño, *Tetrahedron Lett.* **1991**, *32*, 1979–1982.
[212] N. Kurokawa, Y. Ohfune, *J. Am. Chem. Soc.* **1986**, *108*, 6041–6043.
[213] C. Dong, H. Deng, M. Dorward, C. Schaffrath, D. O'Hagan, J. H. Naismith, *Acta Crystallogr. Sect. D Biol. Crystallogr.* **2003**, *59*, 2292–2293.
[214] T. H. Eyles, N. M. Vior, A. W. Truman, *ACS Synth. Biol.* **2018**, *7*, 1211–1218.
[215] J. Yaegashi, B. R. Oakley, C. C. C. Wang, *J. Ind. Microbiol. Biotechnol.* **2014**, *41*, 433–442.
[216] J. Romsdahl, C. C. C. Wang, *Medchemcomm* **2019**, *10*, 840–866.
[217] J. C. Henrikson, A. R. Hoover, P. M. Joyner, R. H. Cichewicz, *Org. Biomol. Chem.* **2009**, *7*, 435–438.
[218] M. Aldholmi, B. Wilkinson, A. Ganesan, J. Antibiot. (Tokyo). 2020, 73, 410–413.
[219] Y.-M. Chiang, E. Szewczyk, T. Nayak, A. D. Davidson, J. F. Sanchez, H.-C. Lo, W.-Y. Ho, H. Simityan, E. Kuo, A. Praseuth, et al., *Chem. Biol.* **2008**, *15*, 527–532.
[220] A. Karolewiez, R. Geisen, *Syst. Appl. Microbiol.* **2005**, *28*, 588–595.
[221] K. Kanoh, S. Kohno, T. Asari, T. Harada, J. Katada, M. Muramatsu, H. Kawashima, I. Sekiya, HirokatsuUno, *Bioorg. Med. Chem. Lett.* **1997**, *7*, 2847–2852.
[222] K. Kanoh, S. Kohno, J. Katada, Y. Hayashi, M. Muramatsu, I. Uno, *Biosci. Biotechnol. Biochem.* **1999**, *63*, 1130–1133.
[223] P. Cimino, L. Huang, L. Du, Y. Wu, J. Bishop, J. Dalsing-Hernandez, K. Kotlarczyk, P. Gonzales, J. Carew, S. Nawrocki, et al., *Biomed. Reports* **2019**, *10*, 218–224.
[224] J. Houbraken, M. Due, J. Varga, M. Meijer, J. C. Frisvad, R. A. Samson, *Stud. Mycol.* **2007**, *59*, 107–128.
[225] J. H. Birkinshaw, A. E. Oxford, H. Raistrick, *Biochem. J.* **1936**, *30*, 394–411.
[226] M. Vansteelandt, E. Blanchet, M. Egorov, F. Petit, L. Toupet, A. Bondon, F. Monteau, B. Le Bizec, O. P. Thomas, Y. F. Pouchus, et al., *J. Nat. Prod.* **2013**, *76*, 297–301.
[227] A. Ciegler, *Can. J. Microbiol.* **1972**, *18*, 631–636.

[228] H. Li, Y. Cai, C. Lam, Y. Chen, W. Lan, *Chem. Res. Chinese Univ.* **2010**, *26*, 415–419.
[229] G. F. Bills, G. Platas, A. Fillola, M. R. Jiménez, J. Collado, F. Vicente, J. Martín, A. González, J. Bur-Zimmermann, J. R. Tormo, et al., *J. Appl. Microbiol.* **2008**, *104*, 1644–1658.
[230] V. González-Menéndez, F. Asensio, C. Moreno, N. de Pedro, M. C. Monteiro, M. de la Cruz, F. Vicente, G. F. Bills, F. Reyes, O. Genilloud, et al., *Mycology* **2014**, *5*, 179–191.
[231] F. Vicente, A. Basilio, G. Platas, J. Collado, G. F. Bills, A. González Del Val, J. Martín, J. R. Tormo, G. H. Harris, D. L. Zink, et al., *Mycol. Res.* **2009**, *113*, 754–770.
[232] G. Martínez, V. González-Menéndez, J. Martín, F. Reyes, O. Genilloud, J. R. Tormo, **2017**, pp. 230–244.
[233] J. R. Doroghazi, J. C. Albright, A. W. Goering, K.-S. Ju, R. R. Haines, K. A. Tchalukov, D. P. Labeda, N. L. Kelleher, W. W. Metcalf, *Nat. Chem. Biol.* **2014**, *10*, 963–968.
[234] L. Chen, Y.-M. Lai, Y.-L. Yang, X. Zhao, *Synth. Syst. Biotechnol.* **2016**, *1*, 56–65.
[235] A. Pisciotta, A. Manteca, R. Alduina, *Sci. Rep.* **2018**, *8*, 13686.
[236] E. Vikeli, D. A. Widdick, S. F. Batey, D. Heine, N. A. Holmes, M. J. Bibb, D. J. Martins, N. E. Pierce, M. I. Hutchings, B. Wilkinson, *Appl. Environ. Microbiol.* **2019**, *86*, e01876-19.
[237] T. J. Booth, S. Alt, R. J. Capon, B. Wilkinson, *Chem. Commun.* **2016**, *52*, 6383–6386.
[238] R. A. Parise, J. L. Holleran, J. H. Beumer, S. Ramalingam, M. J. Egorin, *J. Chromatogr. B* **2006**, *840*, 108–115.
[239] L. Liu, J.-C. Detering, T. Milde, W. E. Haefeli, O. Witt, J. Burhenne, *J. Chromatogr. B* **2014**, *964*, 212–221.
[240] M. O. Almeida, A. A. Lopes, P. G. Roberto, B. W. Bertoni, M. T. Pupo, *Phytochem. Lett.* **2018**, *26*, 55–59.
[241] D. A. Adpressa, K. J. Stalheim, P. J. Proteau, S. Loesgen, *ACS Chem. Biol.* **2017**, *12*, 1842–1847.
[242] V. González-Menéndez, M. Pérez-Bonilla, I. Pérez-Victoria, J. Martín, F. Muñoz, F. Reyes, J. R. Tormo, O. Genilloud, *Molecules* **2016**, *21*, 234.
[243] R. Raju, A. M. Piggott, M. M. Conte, R. J. Capon, *Org. Biomol. Chem.* **2010**, *8*, 4682.
[244] R. F. Seipke, J. Barke, D. Heavens, D. W. Yu, M. I. Hutchings, *Microbiologyopen* **2013**, *2*, 276–283.
[245] M. V. Tuiche, A. A. Lopes, D. B. Silva, N. P. Lopes, M. T. Pupo, *Rev. Bras. Farmacogn.* **2014**, *24*, 433–438.

8. Appendices

8.1. IR spectra of euglenatides A-E

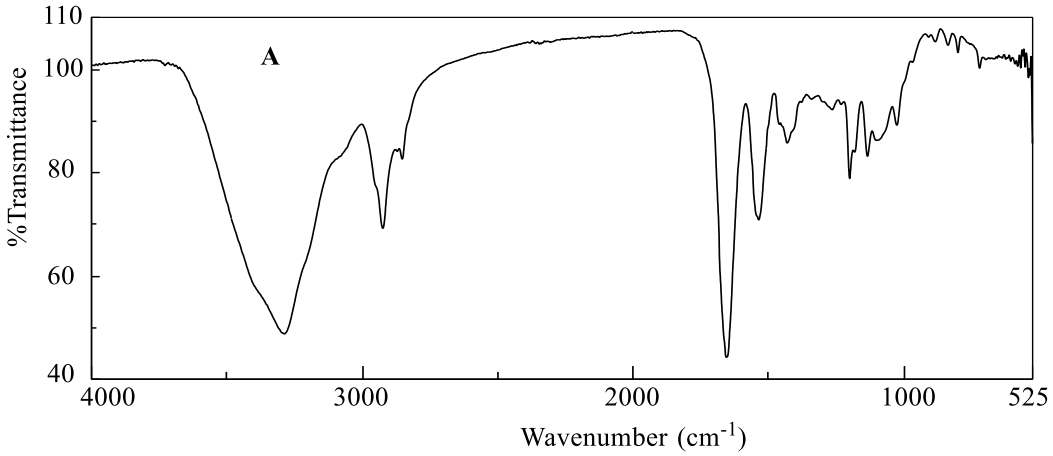

Figure 8.1 IR spectrum of euglenatide A.

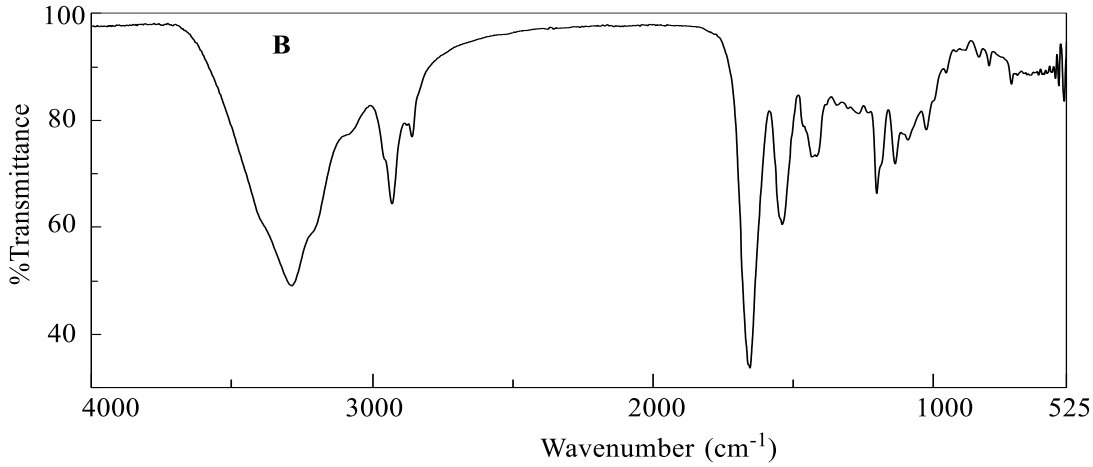

Figure 8.2 IR spectrum of euglenatide B.

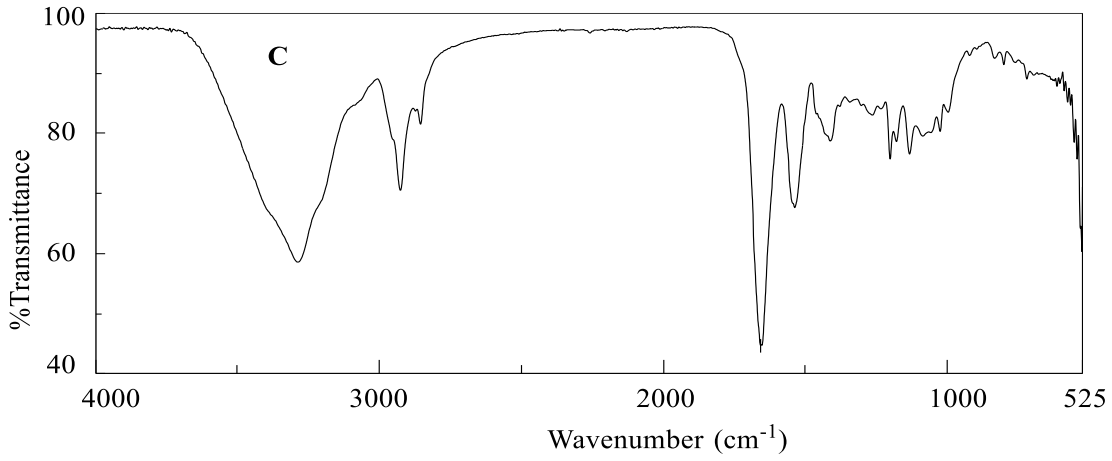

Figure 8.3 IR spectrum of euglenatide C.

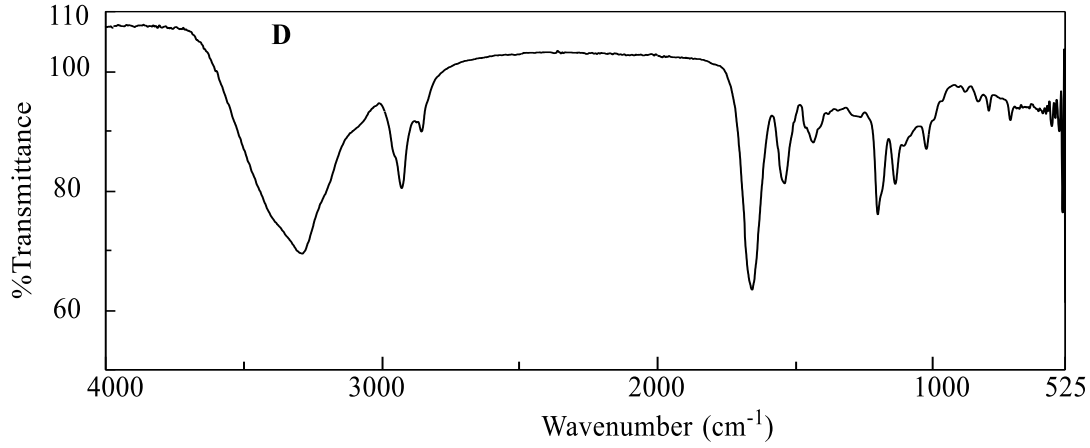

Figure 8.4 IR spectrum of euglenatide D.

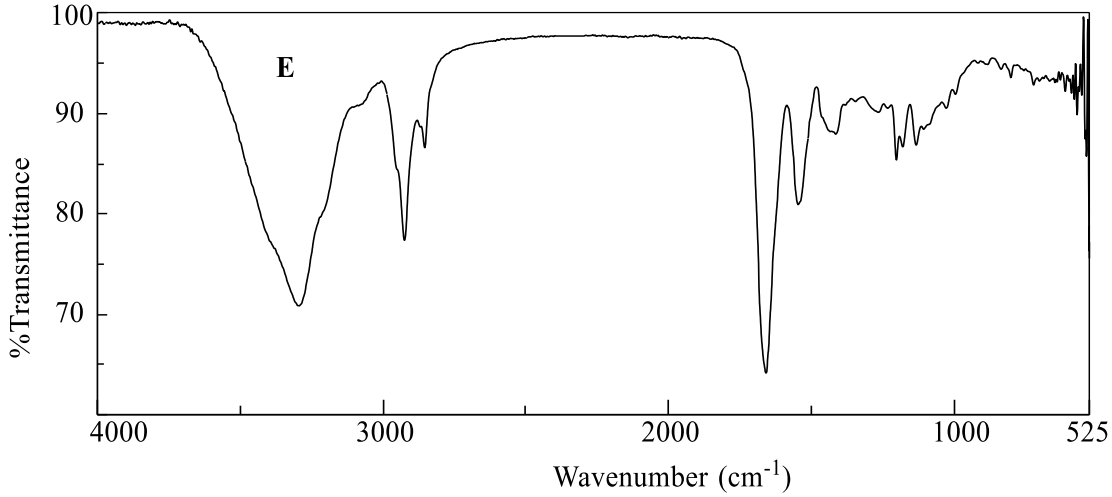

Figure 8.5 IR spectrum of euglenatide E.

8.2. NMR tables of euglenatides C-E.

Table 8.1 ^{1}H and ^{13}C NMR data (500 and 125 MHz, DMSO-d_6) for euglenatide E.

Position (No.)	^{13}C ppm	^{1}H ppm mult. (*J* in Hz)	Position (No.)	^{13}C ppm	^{1}H ppm mult. (*J* in Hz)
Dnv I			BAIBA		
C (1)	172.3		C (1)	176.1	
CH (2)	50.3	4.30, m	CH (2)	38.0	2.64, m
NH (2)		7.64, d (7.8)	CH2 (3)	41.7	2.93, brd (13.0), 3.26, m
CH2 (3)	34.2	1.69, m, 1.87, m	NH (3)		6.94, overlap
CH (4)	67.6	3.43, m	CH3 (4)	17.1	1.02, d (7.1)
OH (4)		4.47, brd (4.7)			
CH2 (5)	66.3	3.24, m, 3.32, m			
OH (5)		4.41, m			
Asn I			DeoxyGra		
C (1)	171.1		C (1)	170.4	
CH (2)	49.4	4.42, m	CH2 (2)	40.9	2.16, dd (13.8, 3.3), 2.47, overlap
NH (2)		7.87, d (7.9)			(9.6)
CH2 (3)	35.6	2.57, dd (16.9, 3.7), 3.01, dd (16.8, 5.0)	CH (3)	45.2	4.08, m (9.6, 6.5, 3.3)
			NH (3)		6.92, overlap
C (4)	173.9		CH2 (4)	44.2	1.32, m
NH2 (4)		7.91 s, 7.39 s	CH (5)	63.3	3.51, m
			OH (5)		4.55, m
			CH2 (6)	43.6	1.30, m, 1.48, m
Asn II			CH (7)	77.8	3.75, m
C (1)	169.7		CH (8)	133.8	5.51, dd (14.6, 7.6)
CH (2)	51.7	4.11. m	CH (9)	131.5	6.19, dd (14.6, 10.2)
NH (2)		8.96, d (6.5)	CH (10)	129.9	6.15, dd (14.5, 10.3)
CH2 (3)	35.0	2.47, dd (15.9, 4.7), 2.87, dd (15.7, 4.0)	CH (11)	133.0	6.24, dd (14.5, 10.3)
			CH (12)	130.3	6.07, dd (15.1, 10.4)
C (4)	172.2		CH (13)	135.3	5.72, dt (15.1, 7.1)
NH2 (4)		7.36, s, 6.88, s	CH2 (14)	32.2	2.06, q (7.0)
			CH2 (15)	28.8	1.35, m
			CH2 (16)	28.5	1.25, m
			CH2 (17)	29.0	1.25, m
			CH2 (18)	31.3	1.25, m
			CH2 (19)	22.1	1.27, m
			CH3 (20)	14.0	0.85, t (6.8)
			CH3 (21)	55.6	3.13, s

Table 8.2 ^{1}H and ^{13}C NMR data (500 and 125 MHz, DMSO-d_6) for euglenatide C.

Position (No.)	^{13}C ppm	^{1}H ppm mult. (*J* in Hz)	Position (No.)	^{13}C ppm	^{1}H ppm mult. (*J* in Hz)
Dnl			BAIBA		
C (1)	172.5		C (1)	176.2	
CH (2)	50.5	4.32, m	CH (2)	37.5	2.66, m
NH (2)		7.65, d (7.8)	CH2 (3)	41.7	3.03, brd (11.2), 3.27, m
CH2 (3)	34.2	1.86, m, 1.71, m	NH (3)		7.06, s
CH (4)	70.6	3.18, m	CH3 (4)	16.9	1.02, t (6.2)
OH (4)		4.27, brd (5.9)			
CH (5)	69.9	3.39, m			
OH (5)		4.18, brd (4.9)			
CH3 (6)	19.5	1.02, t (6.2)			
Asn I			Gra		
C (1)	171.1		C (1)	172.3	
CH (2)	49.3	4.45, m	CH (2)	72.9	3.86, dd (9.6, 7.7)
NH (2)		7.76, d (8.5)	OH (2)		5.13, brd (7.7)
CH2 (3)	35.8	2.57, dd (17.0, 3.6), 2.94, dd (16.9, 5.0)	CH (3)	49.1	3.92, m
C (4)	173.4		NH (3)		6.90 d (9.7)
NH2 (4)		7.79 s, 7.29 s	CH2 (4)	40.3	1.69, m, 1.20, m
			CH (5)	63.0	3.47, m
			OH (5)		4.31, m
			CH2 (6)	43.8	1.30, br dd (14.5, 5.2), 1.49, m
Asn II			CH (7)	77.8	3.73, m
C (1)	169.5		CH (8)	133.9	5.51, dd (14.6, 7.6)
CH (2)	51.6	4.06. m	CH (9)	131.3	6.20, dd (14.6, 10.3)
NH (2)		9.02, d (6.3)	CH (10)	130.0	6.15, dd (14.6, 10.3)
CH2 (3)	35.0	2.86, dd (15.4, 3.9) 2.47, dd (15.5, 4.0)	CH (11)	132.8	6.24, dd (14.5, 10.4)
C (4)	172.1		CH (12)	130.3	6.07, dd (15.1, 10.4)
NH2 (4)		7.36, s, 6.88, s	CH (13)	135.1	5.72, dt (15.1, 7.1)
			CH2 (14)	32.1	2.06, q (7.1)
			CH2 (15)	28.7	1.35, m
			CH2 (16)	28.52	1.25, m
			CH2 (17)	28.54	1.25, m
			CH2 (18)	31.2	1.24, m
			CH2 (19)	22.0	1.25, m
			CH3 (20)	13.9	0.85, t (6.8)
			CH3 (21)	55.5	3.13, s

Table 8.3 ^{1}H and ^{13}C NMR data (500 and 125 MHz, DMSO-d_6) for euglenatide D.

Position (No.)	**^{13}C ppm**	**^{1}H ppm mult. (*J* in Hz)**	**Position (No.)**	**^{13}C ppm**	**^{1}H ppm mult. (*J* in Hz)**
Dnv I			BAIBA		
C (1)	172.3		C (1)	175.9	
CH (2)	50.4	4.26, m	CH (2)	38.2	2.66, m
NH (2)		7.71, d (7.5)	CH2 (3)	41.9	2.92, brd (12.4), 3.24, m
CH2 (3)	34.2	1.85, m, 1.69, m	NH (3)		6.93, overlap
CH (4)	67.7	3.42, m	CH3 (4)	17.4	1.07, br d (7.1)
OH (4)		4.44, m			
CH2 (5)	66.3	3.22, m, 3.29, m			
OH (5)		4.34, m			
Asn I			DeoxyGra		
C (1)	171.2		C (1)	170.4	
CH (2)	49.4	4.42, m	CH2 (2)	41.0	2.16, dd (12.8, 3.1), 2.47, overlap
NH (2)		7.87, d (8.2)			(9.6)
CH2 (3)	35.6	2.58, dd (16.7, 3.2), 2.99, dd (16.9, 4.15)	CH (3)	45.2	4.08, m (9.6, 6.5, 3.3)
C (4)	174.1		NH (3)		6.92, overlap
NH2 (4)		7.93 s, 7.43 s	CH2 (4)	44.2	1.32, m
			CH (5)	63.4	3.51, m
			OH (5)		4.55, m
			CH2 (6)	43.6	1.30, m, 1.49, m,
Dnv II			CH (7)	77.8	3.75, m
C (1)	170.7		CH (8)	133.8	5.51, dd (14.7, 7.7)
CH (2)	51.6	3.85, m	CH (9)	131.5	6.20, dd (14.5, 10.5)
NH (2)		8.85, d (5.3)	CH (10)	130.0	6.15, dd (14.7, 10.6)
CH2 (3)	32.2	1.89, m	CH (11)	133.1	6.24, dd (14.5, 10.5)
CH (4)	68.0	3.41, m	CH (12)	130.4	6.07, dd (15.0, 10.5)
OH (4)		4.42, m	CH (13)	135.3	5.72, dt (15.1, 7.7)
CH2 (5)	66.3	3.22, m, 3.29, m	CH2 (14)	32.2	2.06, q (7.0)
OH (5)		4.57, m	CH2 (15)	28.8	1.35, m
			CH2 (16)	28.6	1.25, m
			CH2 (17)	29.0	1.25, m
			CH2 (18)	31.3	1.23, m
			CH2 (19)	22.1	1.26, m
			CH3 (20)	14.0	0.85, t (6.8)
			CH3 (21)	55.7	3.13, s

8.3. NMR spectra of euglenatide A in DMSO-d_6

8.3.1. ^{1}H NMR spectrum of euglenatide A in DMSO-d_6

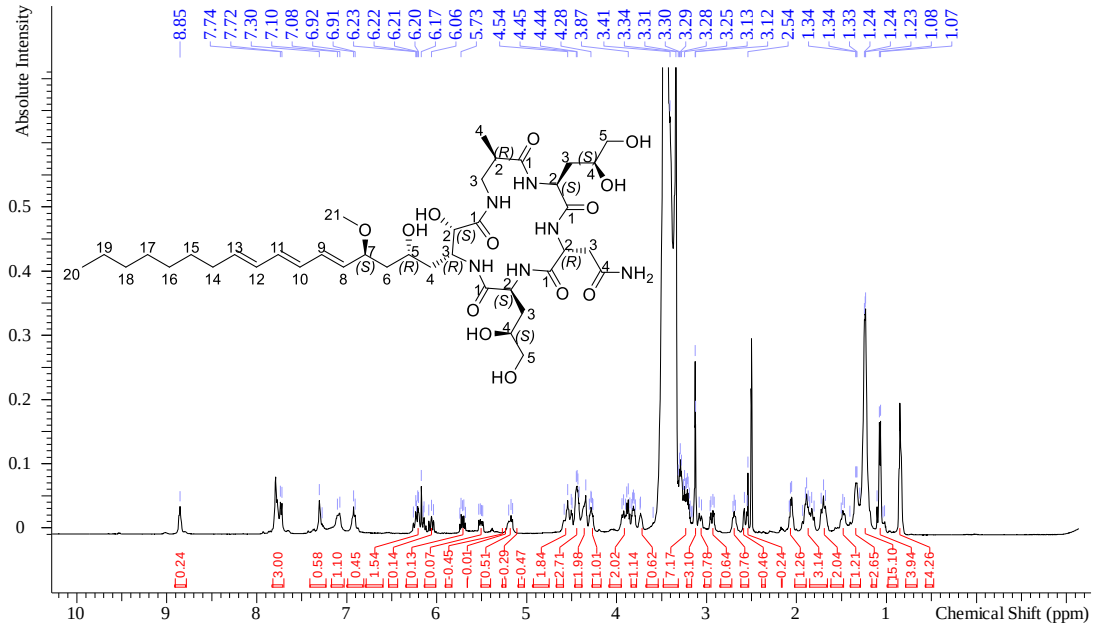

8.3.2. ^{13}C NMR spectrum of euglenatide A in DMSO-d_6

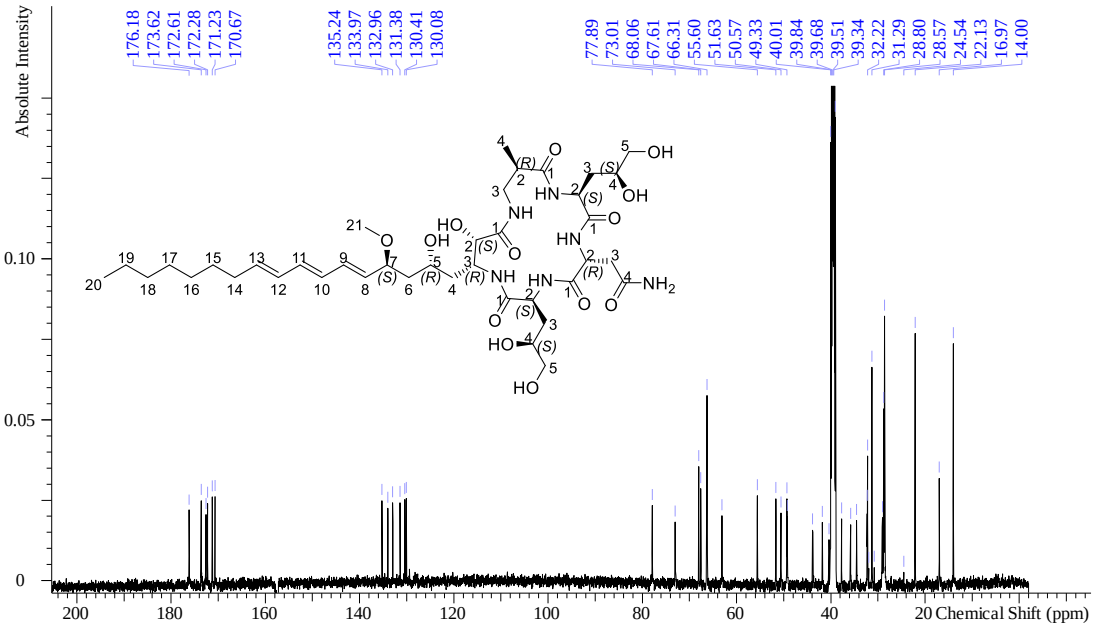

8.3.3. COSY NMR spectrum of euglenatide A in DMSO-d_6

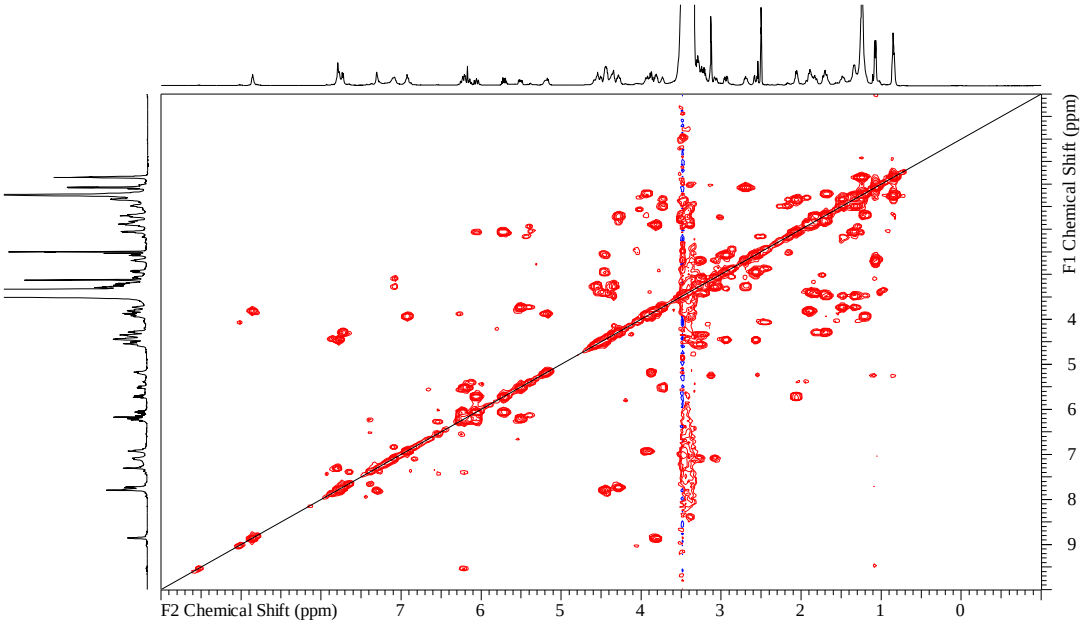

8.3.4. HSQC NMR spectrum of euglenatide A in DMSO-d_6

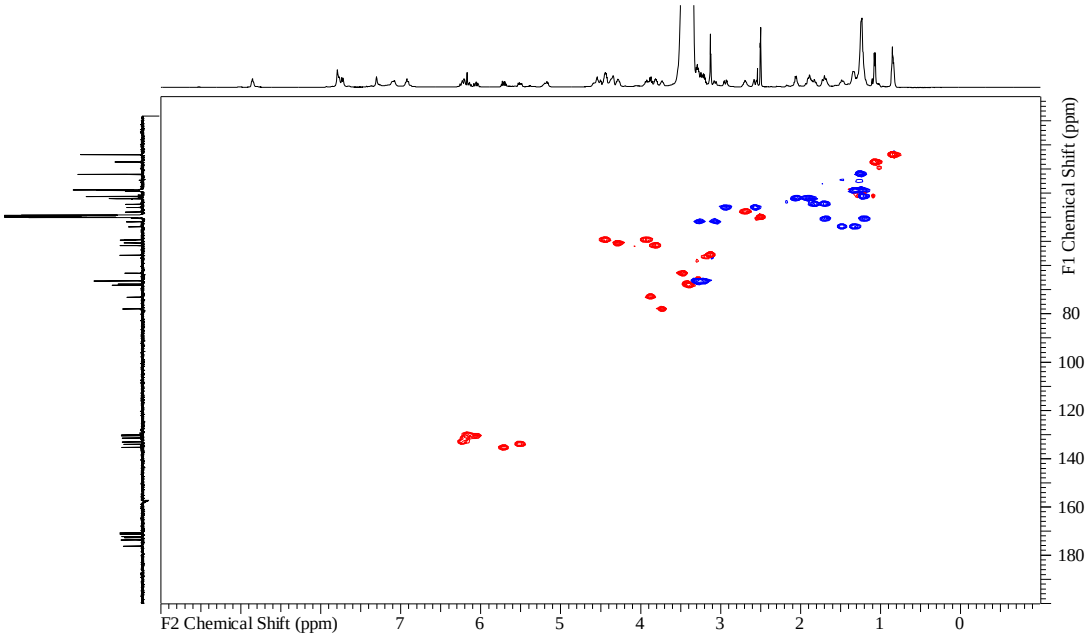

8.3.5. HMBC NMR spectrum of euglenatide A in DMSO-d_6

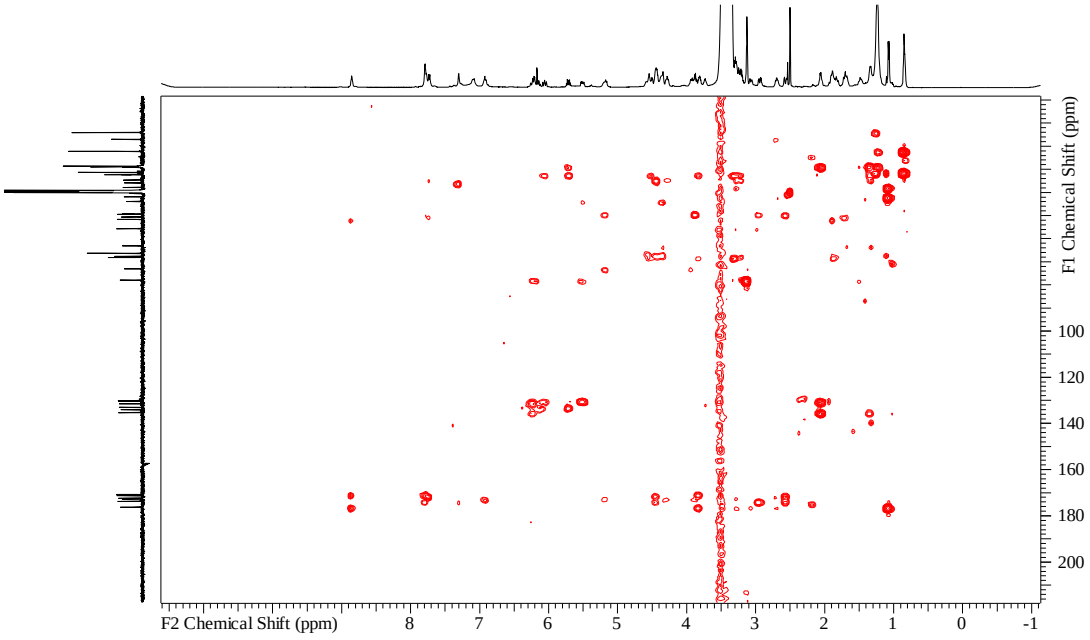

8.3.6. NOESY NMR spectrum of euglenatide A in DMSO-d_6

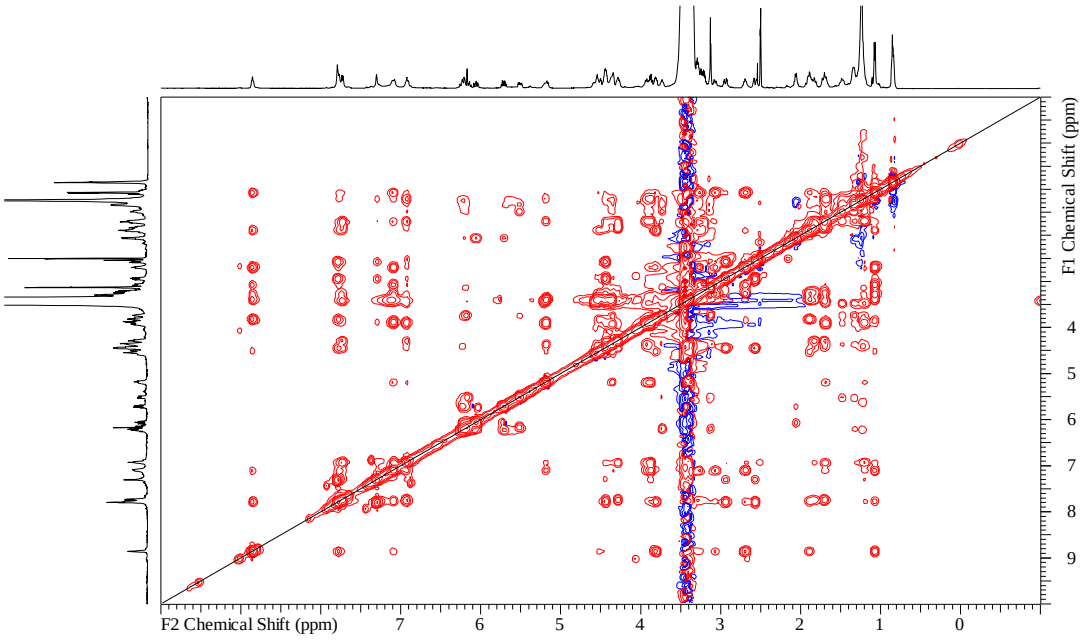

8.4. NMR spectra of euglenatide B in DMSO-d_6

8.4.1. ^{1}H NMR spectrum of euglenatide B in DMSO-d_6

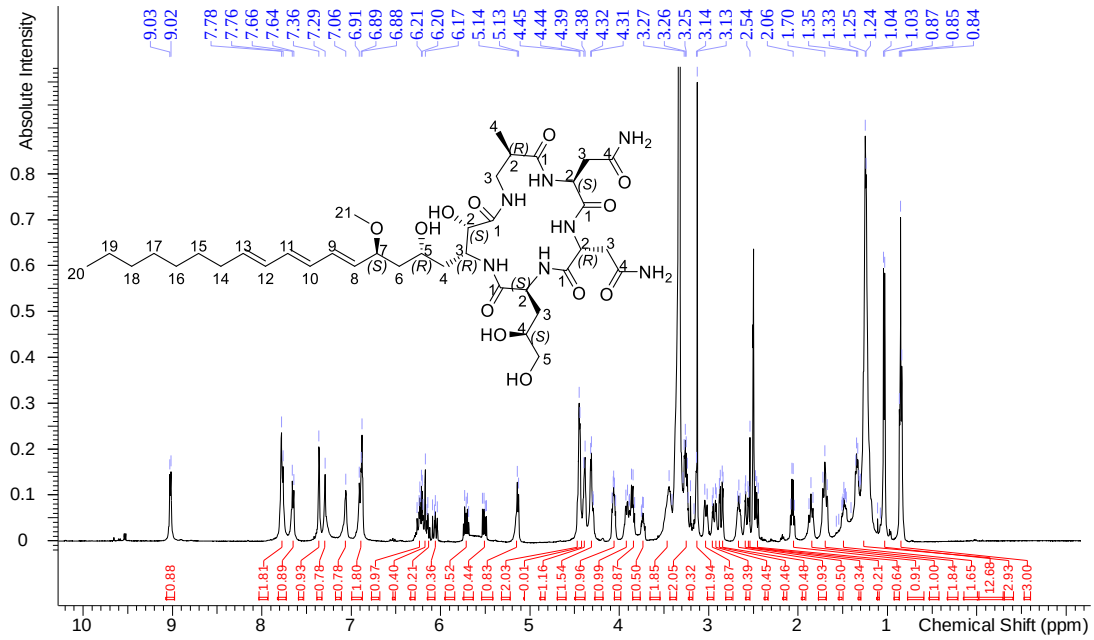

8.4.2. ^{13}C NMR spectrum of euglenatide B in DMSO-d_6

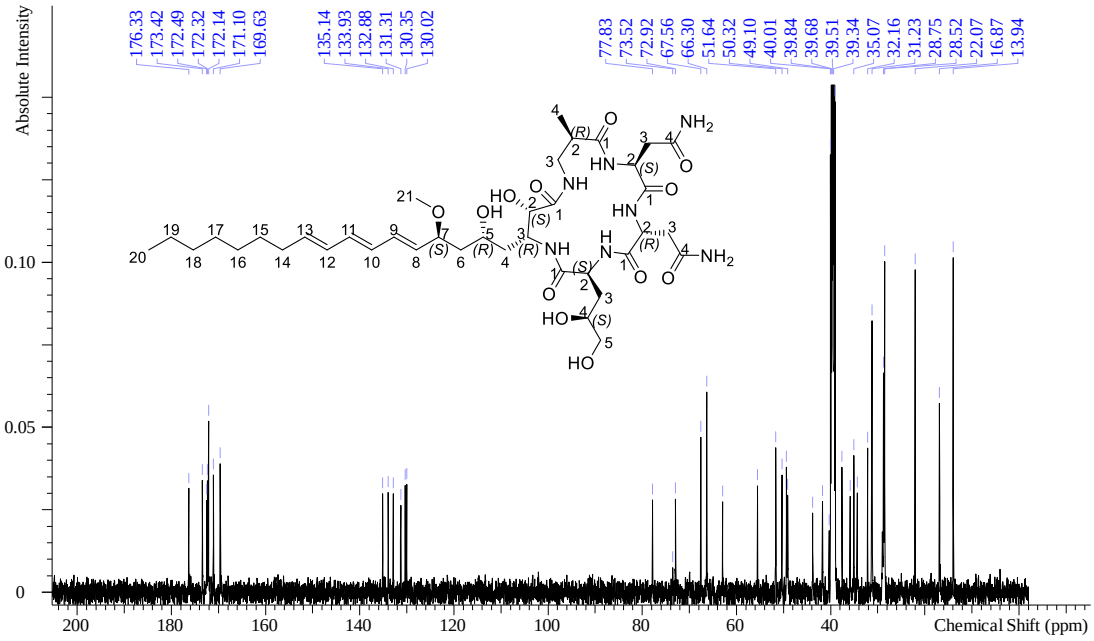

8.4.3. COSY NMR spectrum of euglenatide B in DMSO-d_6

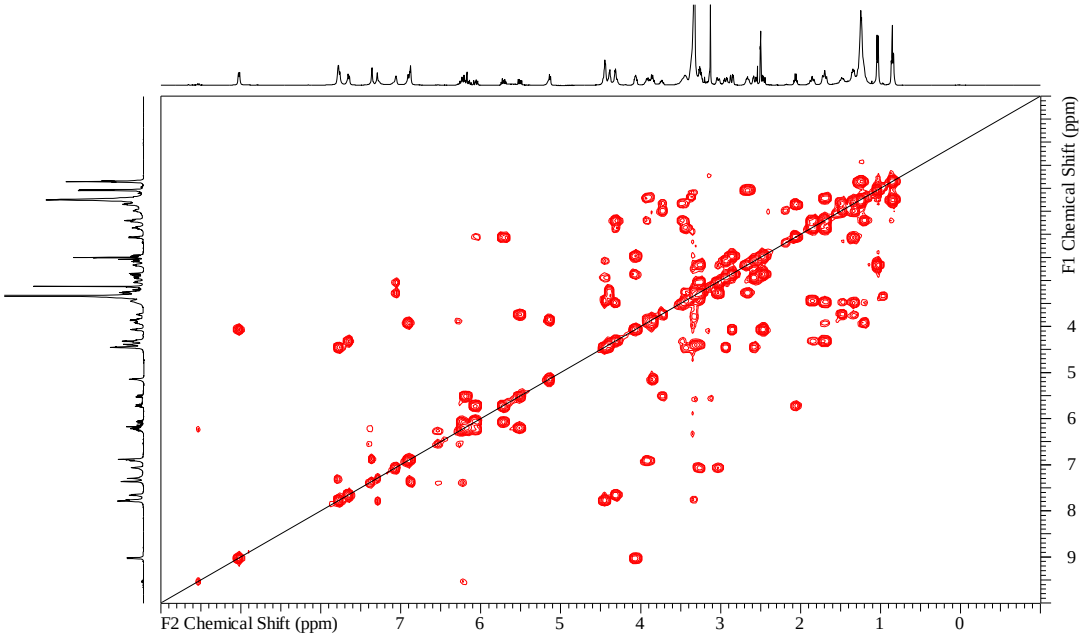

8.4.4. HSQC NMR spectrum of euglenatide B in DMSO-d_6

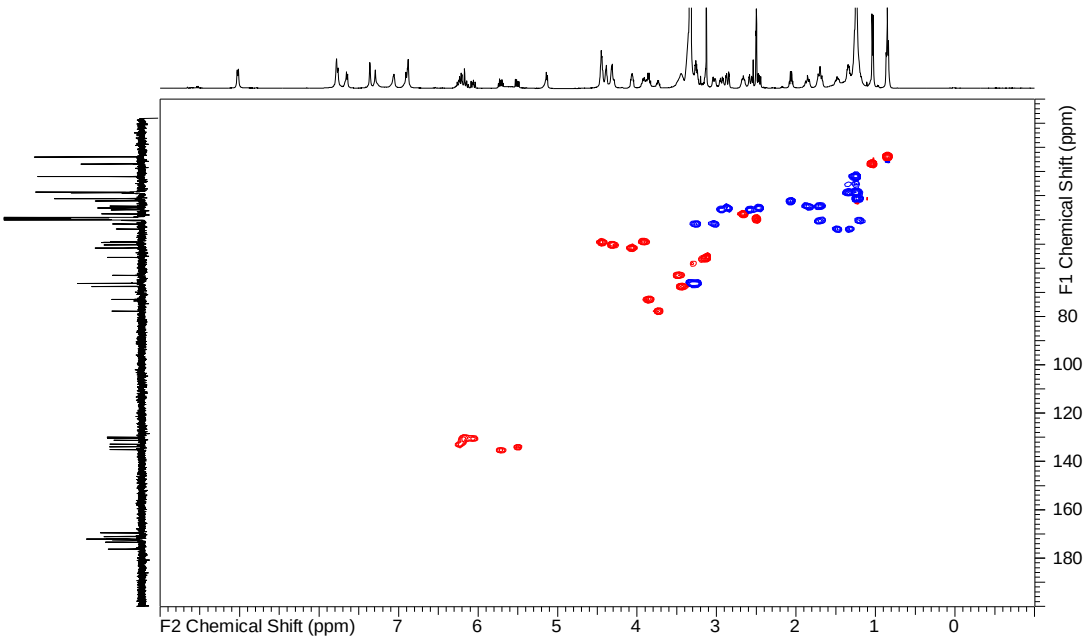

8.4.5. HMBC NMR spectrum of euglenatide B in DMSO-d_6

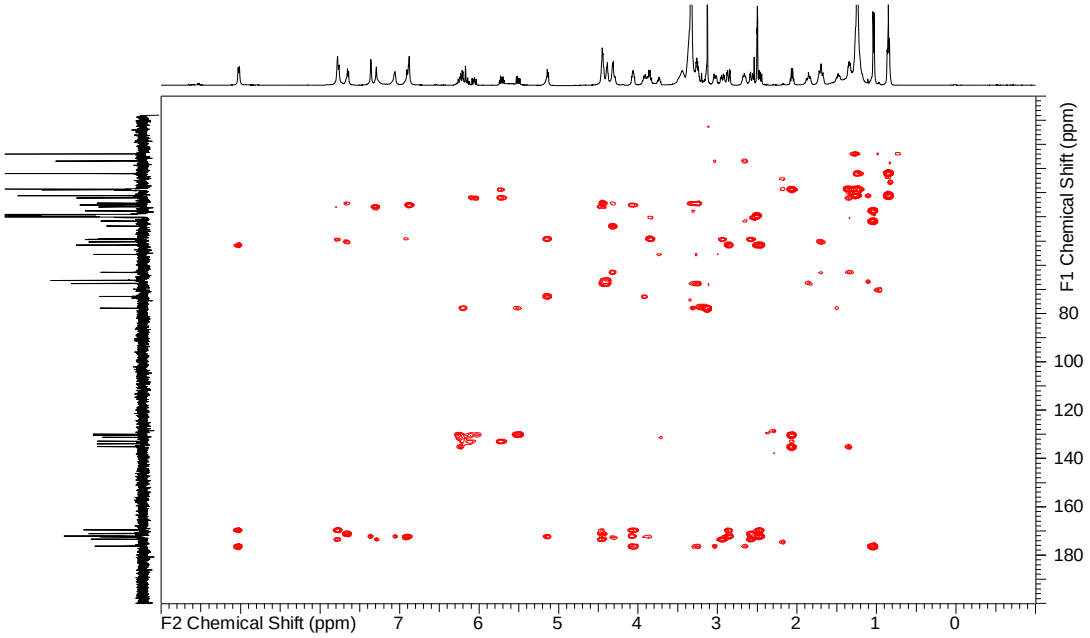

8.4.6. NOESY NMR spectrum of euglenatide B in DMSO-d_6

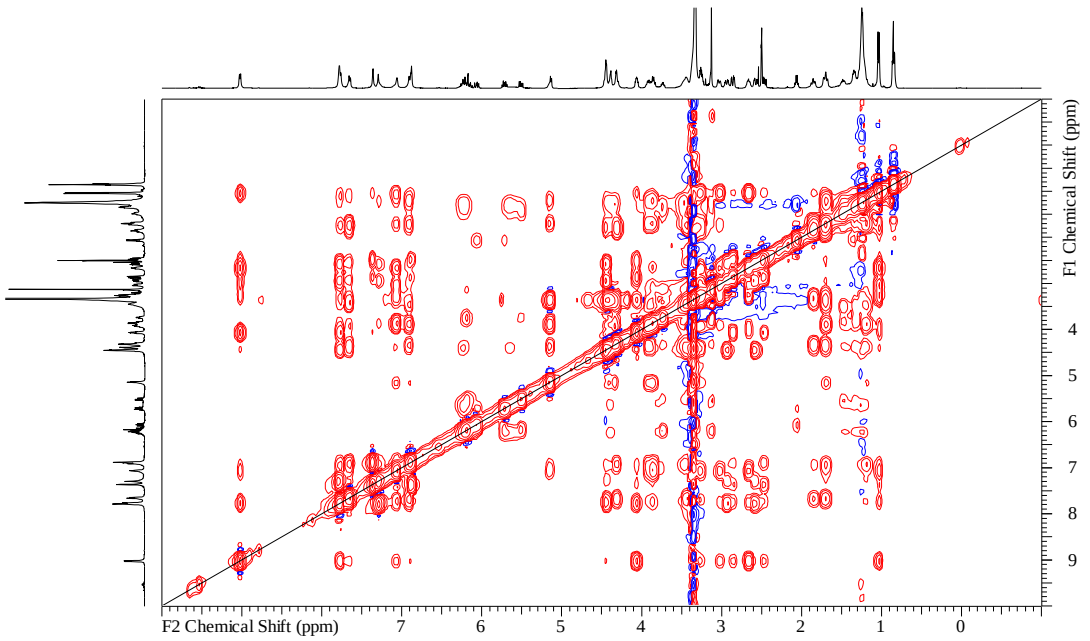

8.5. NMR spectra of euglenatide C in DMSO-d_6

8.5.1. ^{1}H NMR spectrum of euglenatide C in DMSO-d_6

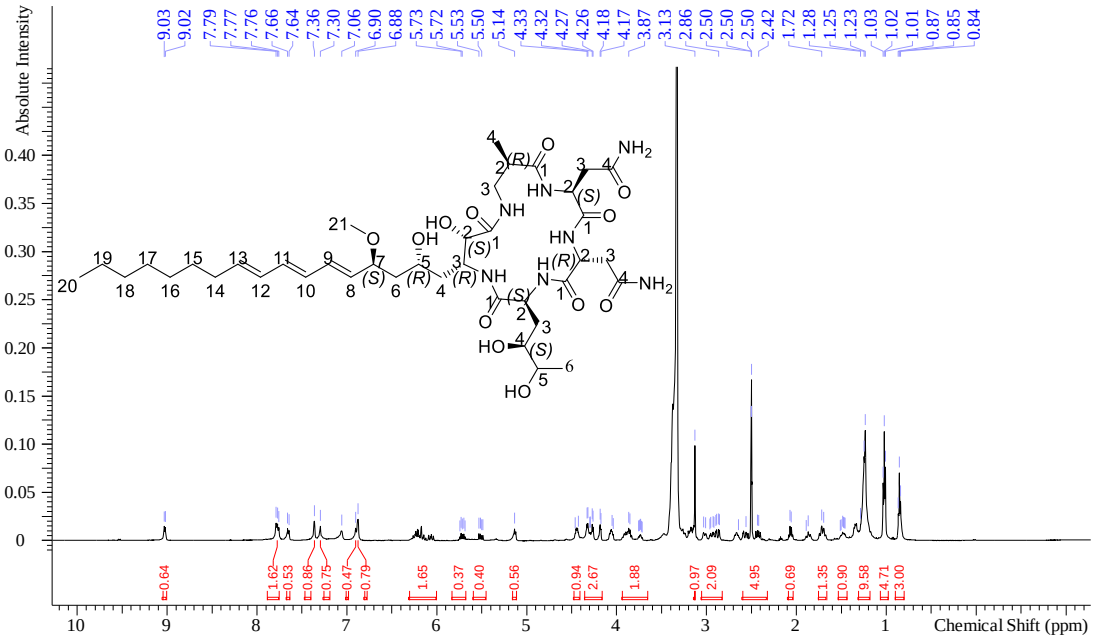

8.5.2. ^{13}C NMR spectrum of euglenatide C in DMSO-d_6

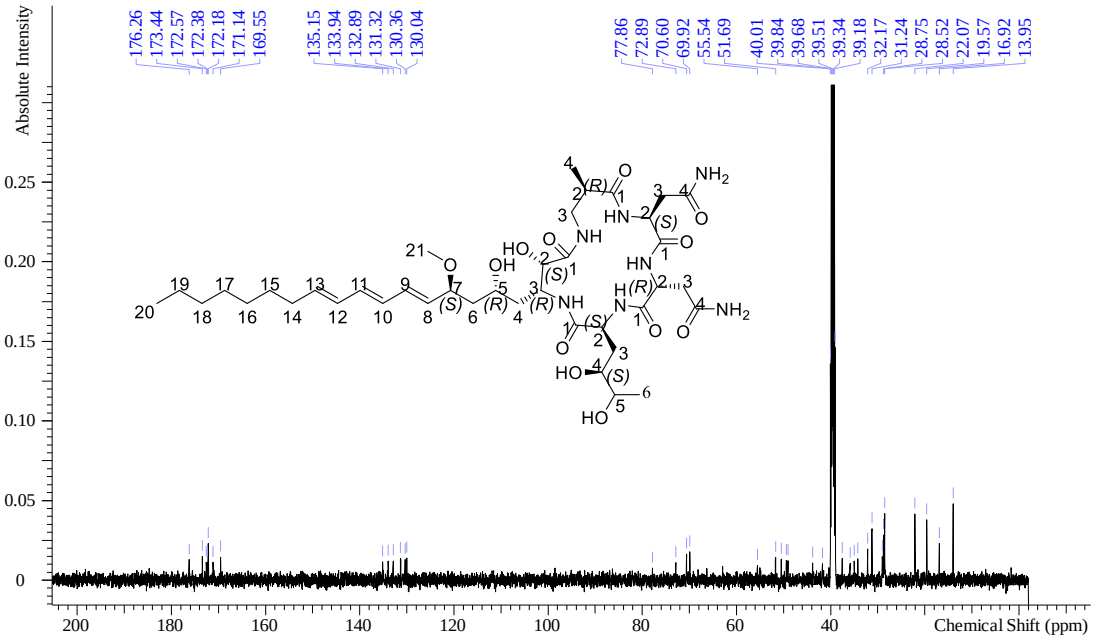

8.5.3. COSY NMR spectrum of euglenatide C in DMSO-d_6

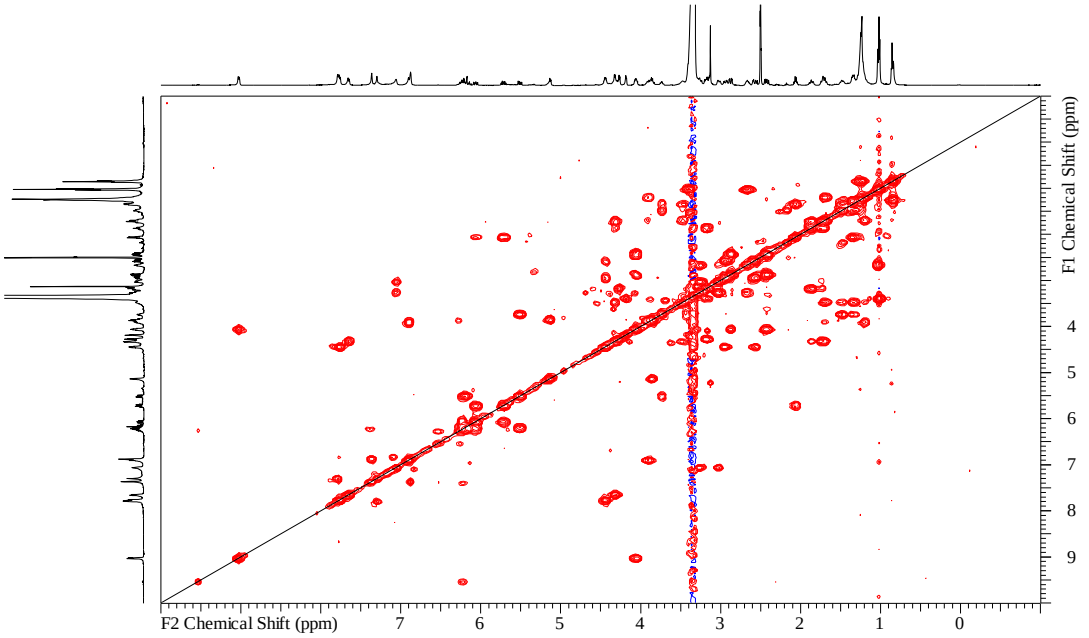

8.5.4. HSQC NMR spectrum of euglenatide C in DMSO-d_6

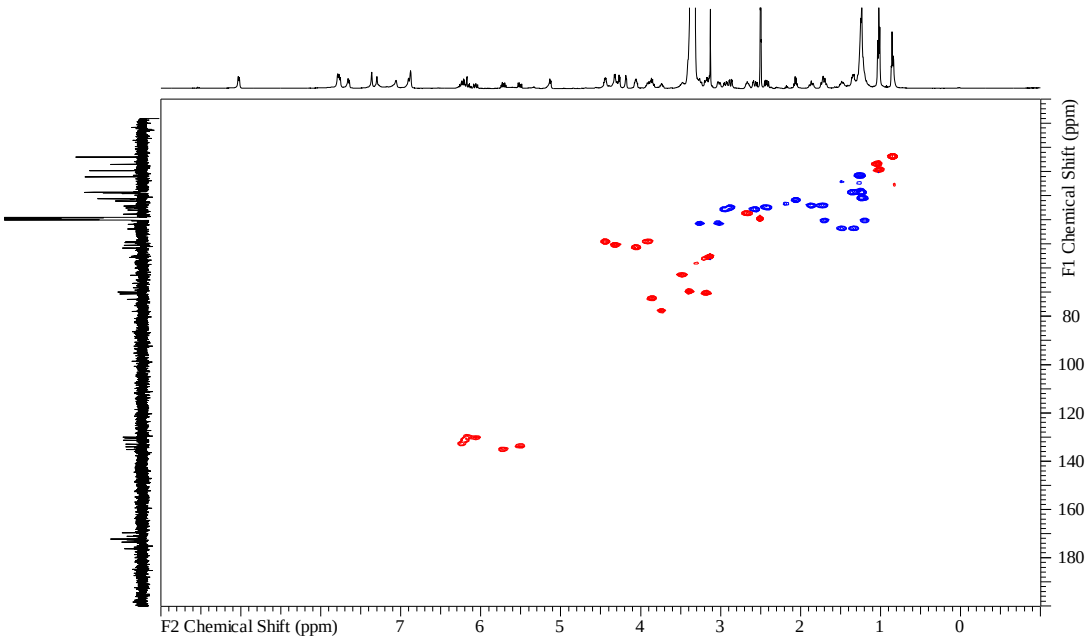

8.5.5. HMBC NMR spectrum of euglenatide C in DMSO-d_6

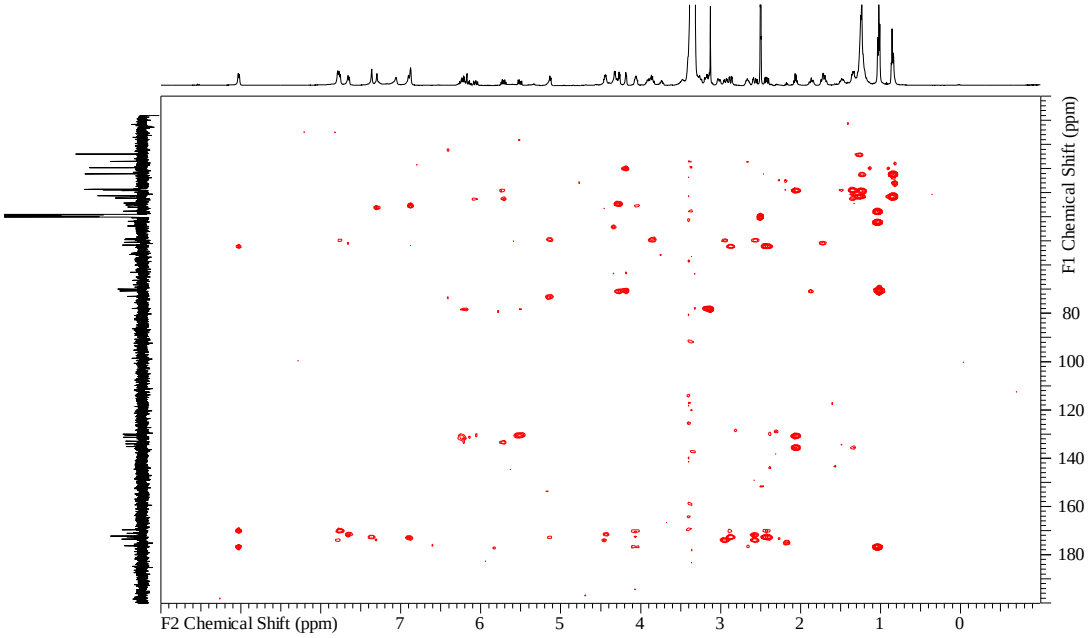

8.5.6. NOESY NMR spectrum of euglenatide C in DMSO-d_6

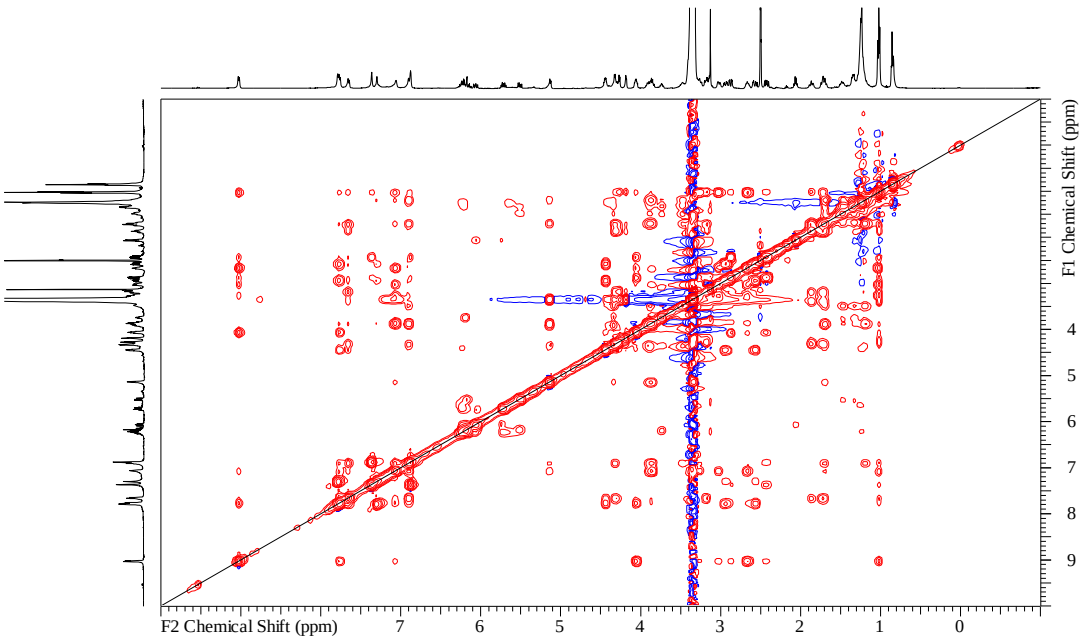

8.6. NMR spectra of euglenatide D in DMSO-d_6

8.6.1. ^{1}H NMR spectrum of euglenatide D in DMSO-d_6

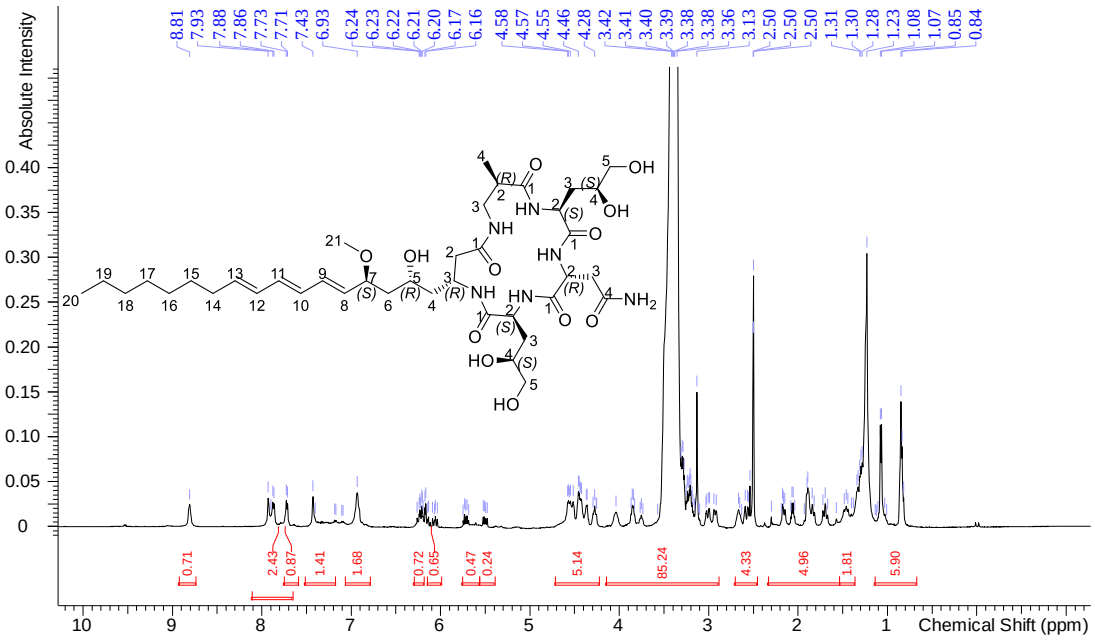

8.6.2. ^{13}C NMR spectrum of euglenatide D in DMSO-d_6

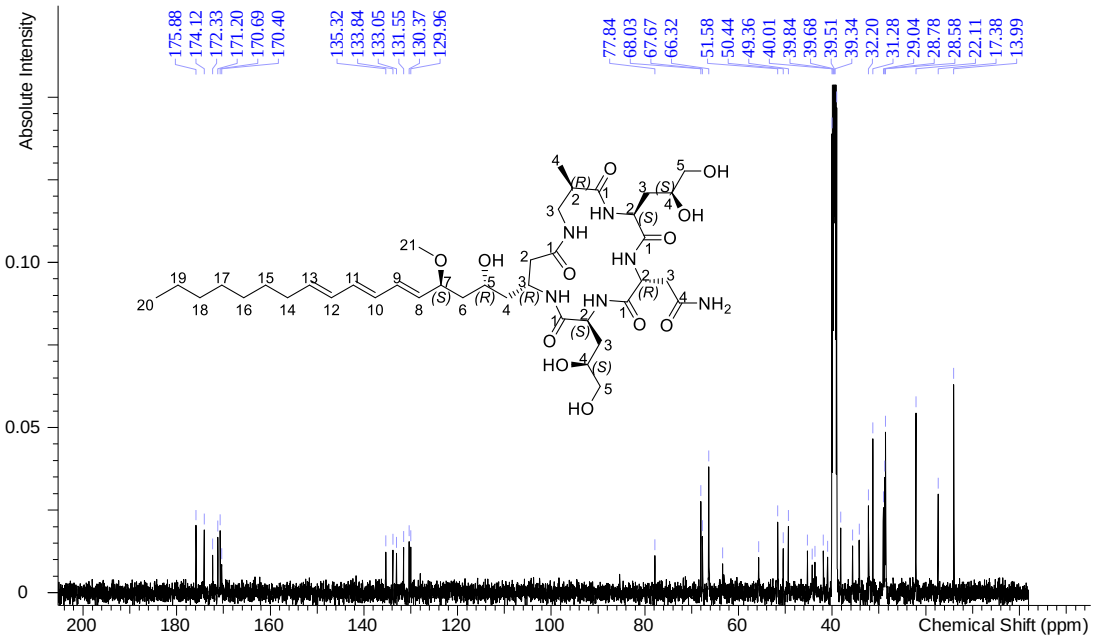

8.6.3. COSY NMR spectrum of euglenatide D in DMSO-d_6

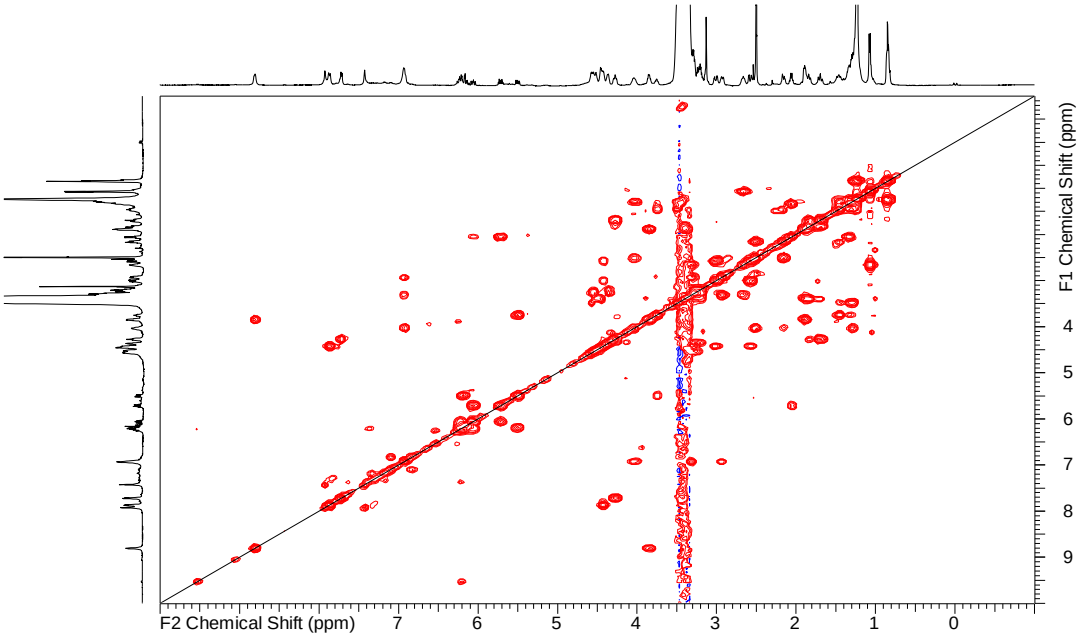

8.6.4. HSQC NMR spectrum of euglenatide D in DMSO-d_6

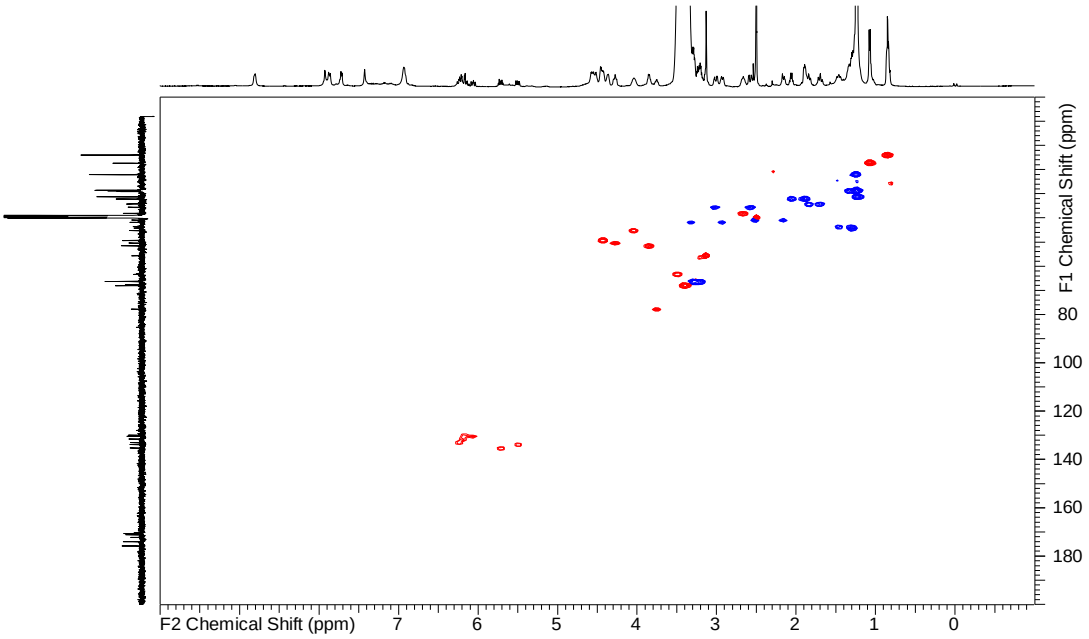

8.6.5. HMBC NMR spectrum of euglenatide D in DMSO-d_6

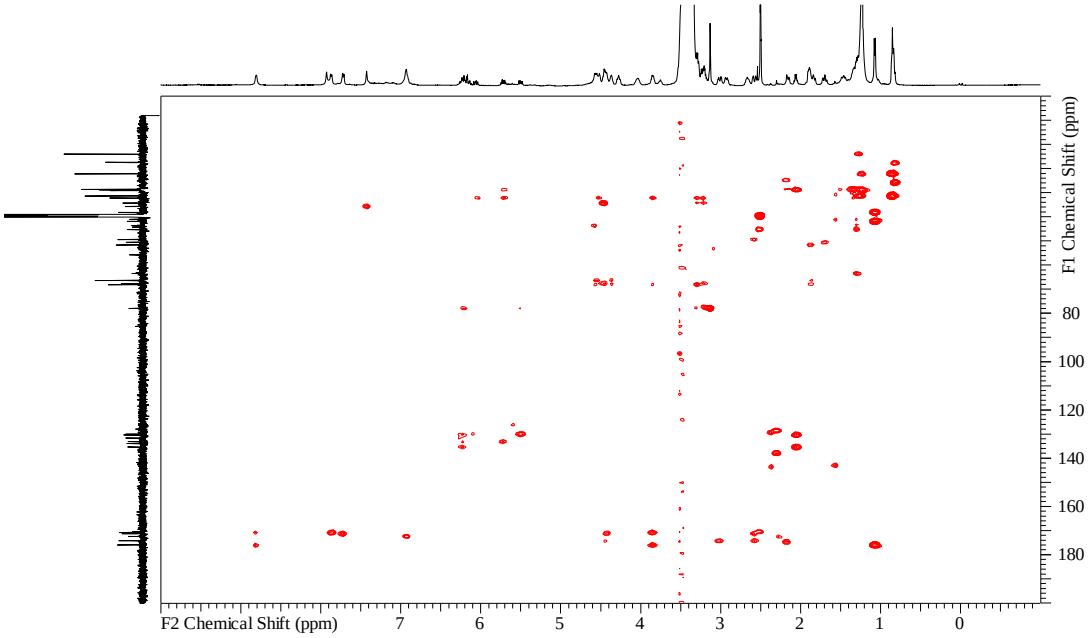

8.6.6. NOESY NMR spectrum of euglenatide D in DMSO-d_6

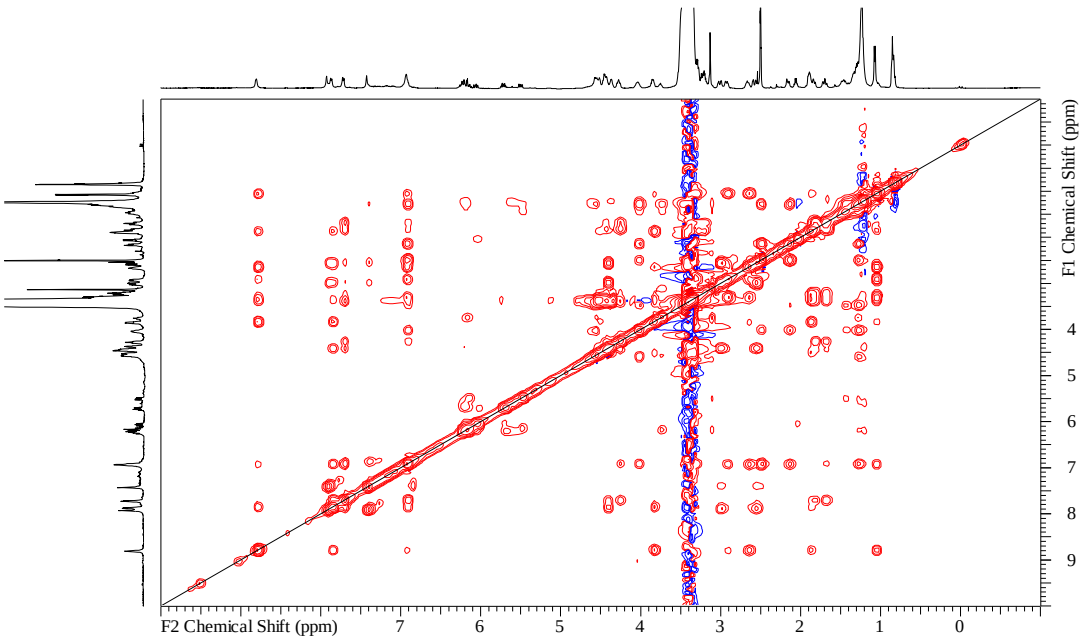

8.7. NMR spectra of euglenatide E in DMSO-d_6

8.7.1. ^{1}H NMR spectrum of euglenatide E in DMSO-d_6

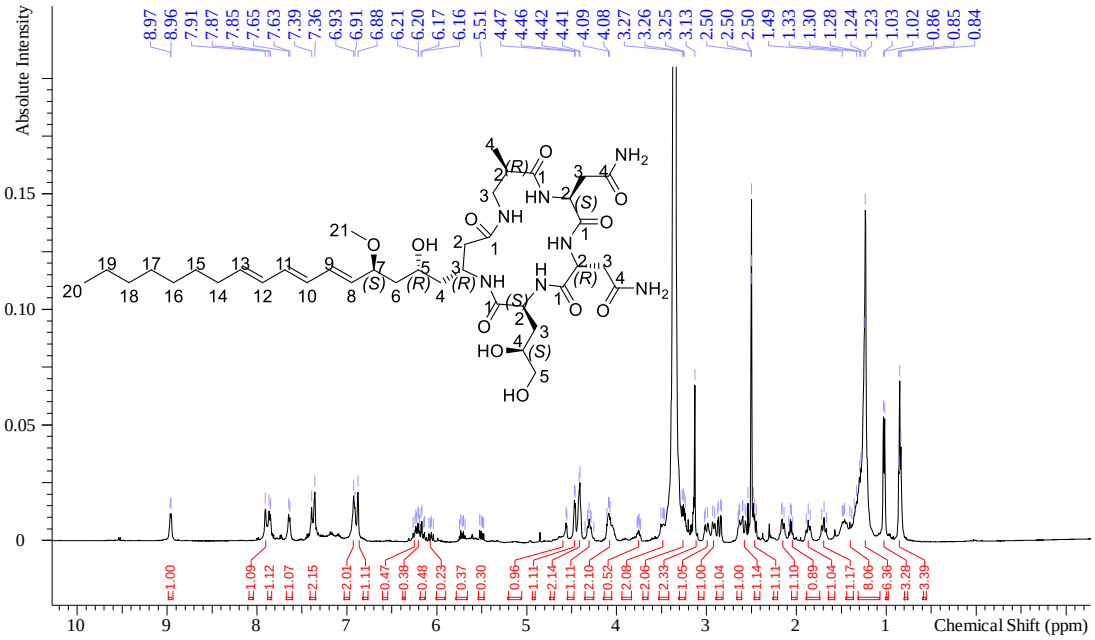

8.7.2. ^{13}C NMR spectrum of euglenatide E in DMSO-d_6

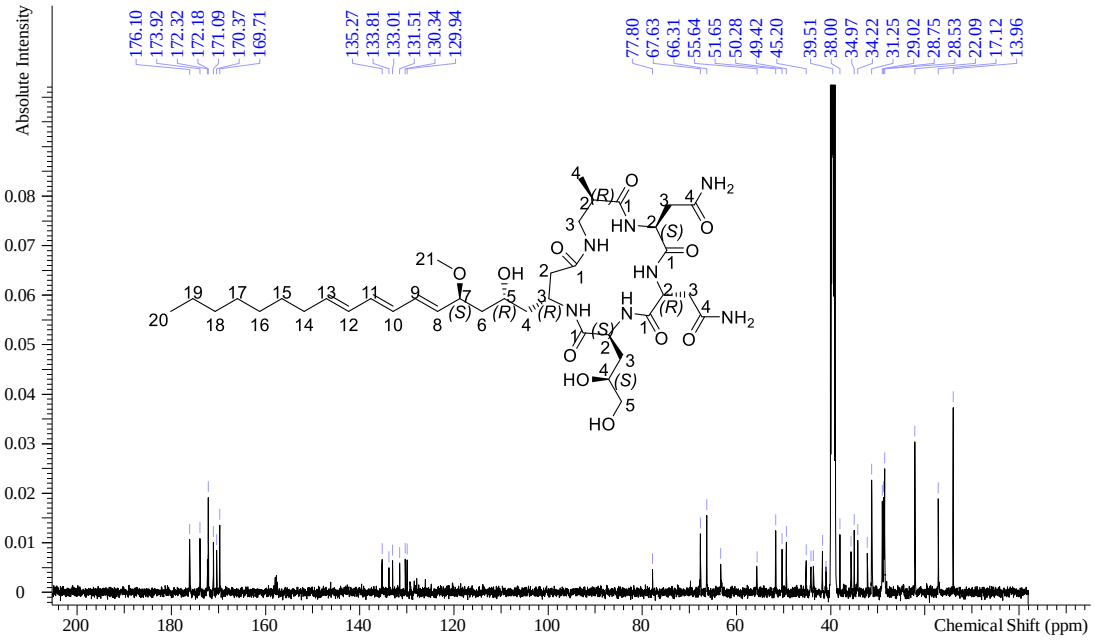

8.7.3. COSY NMR spectrum of euglenatide E in DMSO-d_6

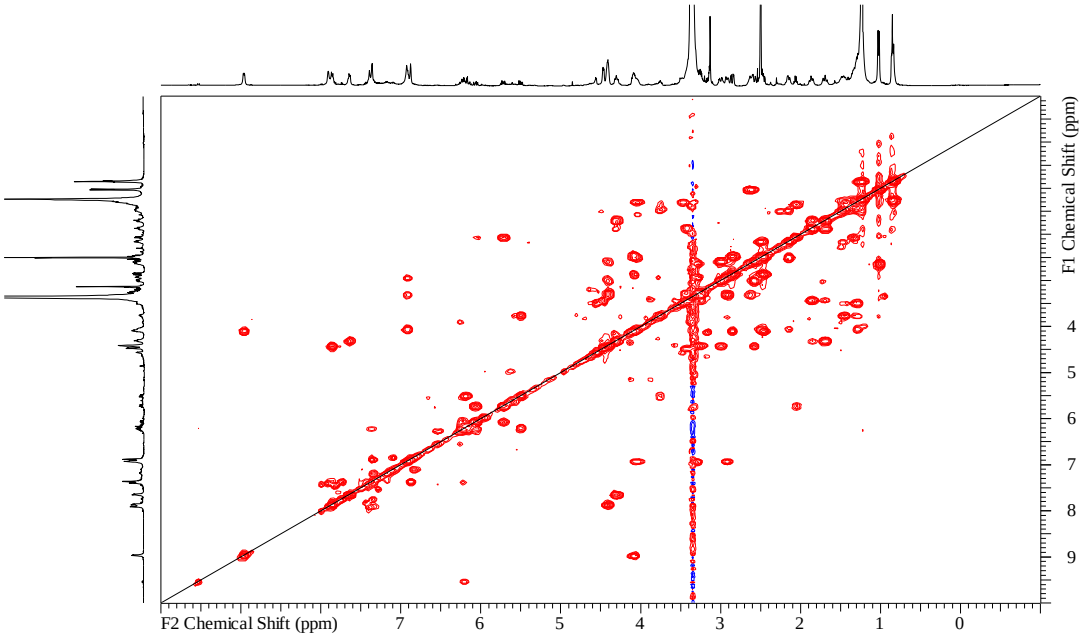

8.7.4. HSQC NMR spectrum of euglenatide E in DMSO-d_6

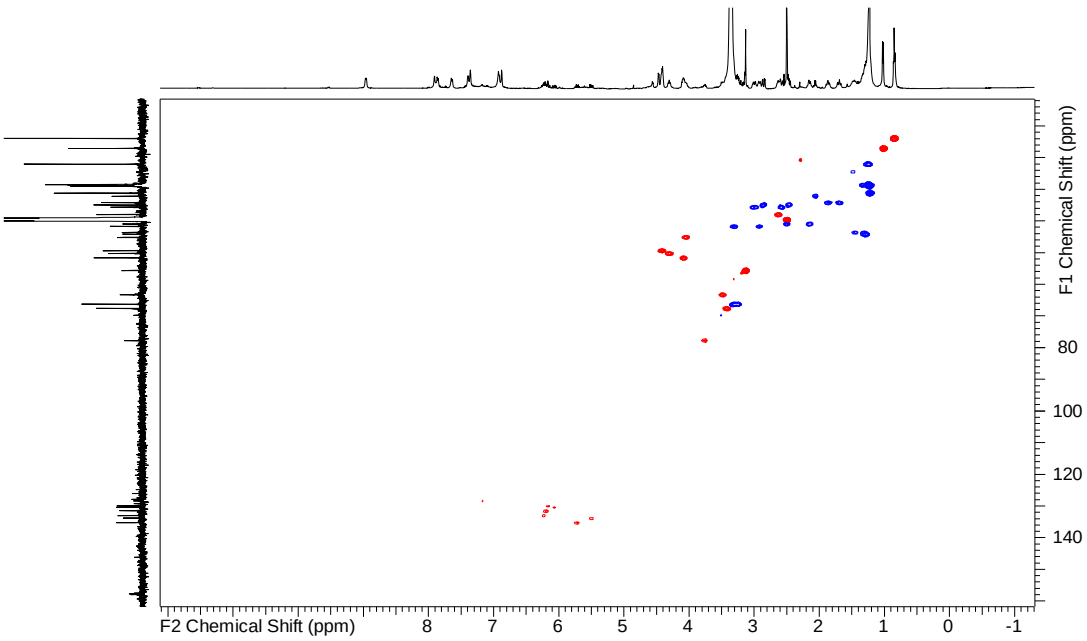

8.7.5. HMBC NMR spectrum of euglenatide E in DMSO-d_6

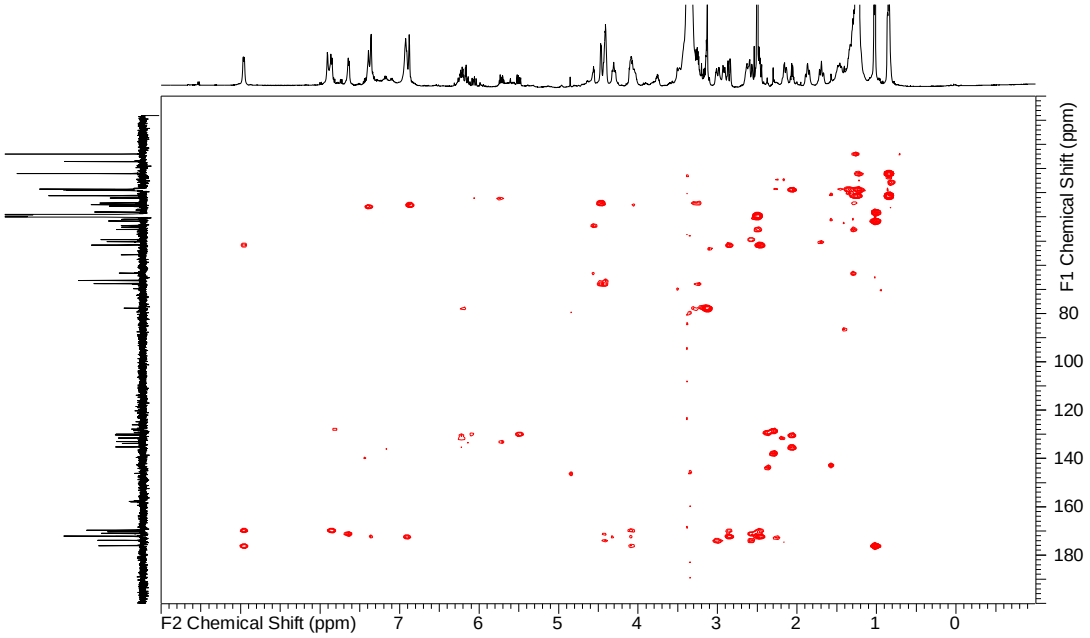

8.7.6. NOESY NMR spectrum of euglenatide E in DMSO-d_6

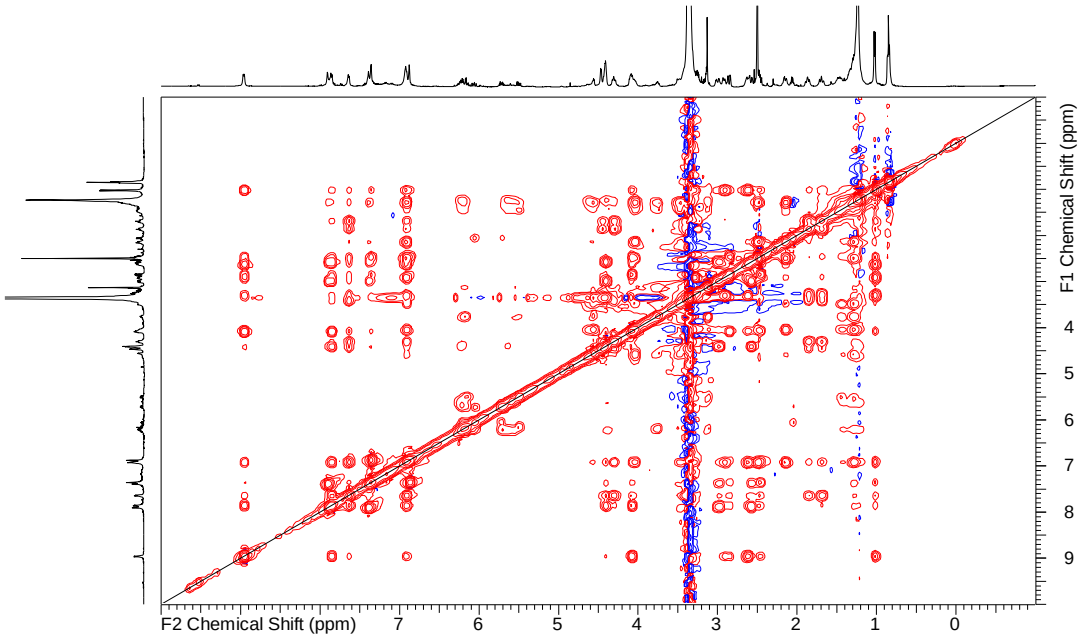

8.8. Comparison of ^{1}H and ^{13}C NMR chemical shifts in euglenatides with nemamide A triene sidechain

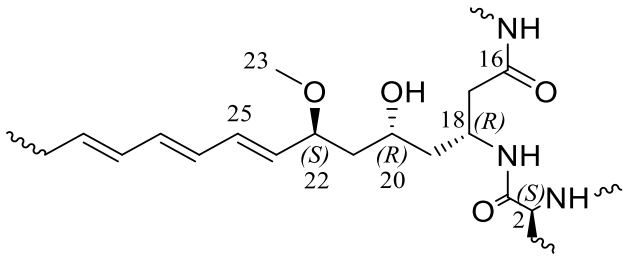

Proton position	nemamide A	euglenatide E	euglenatide B	Δδ
C17	2.18, brd (*J*17a,17b = 14.5) 2.47, overlap (*J*17b,18 = 9.8)	2.16, dd (13.8, 3.3), 2.47, overlap	3.86, dd (9.6, 7.7)	-0.02, 0
C18	4.08, m (*J*18,19 =6.7)	4.08, m	3.92, m	0
C19	1.32, m (*J*19,20 = 6.7)	1.31, m	1.20, m ,1.69 m	-0.01
C20	3.51, m (*J*20,21a = 8.2)	3.51, m	3.47, m	0
C21a	1.30, m (*J*21a,21b =14.5)	1.30, m	1.30, m	0
C21b	1.48, m (*J*21b,22 = 9.8)	1.48, m	1.49, m	0
C22	3.76, m (*J*22,24 = 7.5)	3.75, m	3.73, m	-0.01
C23	3.13, s	3.13, s	3.13, s	0
C24	5.51, dd (*J*24,25 = 15.4)	5.51, dd (*J* 14.6, 7.6)	5.51, dd (*J* 14.6, 7.6)	0
C25	6.19, dd (*J*25,26 = 11.2)	6.19, dd (*J* 14.6, 10.2)	6.20, dd (*J* 14.6, 10.3)	0

Carbon position	nemamide A	euglenatide E	euglenatide B	Δδ
C16	170.3	170.4	172.3	0.1
C17	40.6	40.9	72.9	0.3
C18	44.9	45.2	49.1	0.3
C19	43.7	44.2	40.3	0.5
C20	63.3	63.3	63.0	0
C21	43.5	43.6	43.8	0.1
C22	77.6	77.8	77.8	0.2
C23	55.5	55.6	55.5	0.1
C24	133.7	133.8	133.9	0.1
C25	131.3	131.5	131.3	0.2

8.9. Key NOESY and *J* coupling in euglenatide E

- Stereocenters at C-2 and C-18

  C2H (4.30 ppm) -N2H (7.64 ppm) (Observed in NOESY).
  C2H (4.30 ppm) -N18H (6.93 ppm) (Observed in NOESY).
  N2H (7.64 ppm) -N18H (6.93 ppm) (Observed in NOESY).
  H17b (2.47 ppm) -N18H (6.93 ppm) (Observed in NOESY).
  Strong *J* coupling H17b (2.47 ppm) -H18 (4.08 ppm) (*J*= 9.6).
  Weak *J* coupling H17a (2.16 ppm)-H18 (4.08 ppm) (*J*= 3.3).

- Stereocenters at C-18 and C-20

  H17a (2.16 ppm) -H20 (3.51 ppm) (Observed in NOESY).
  H18 (4.08 ppm)-H21b (1.48 ppm) (Observed in NOESY).
  H18(4.08 ppm)-H20 (3.51 ppm) (Observed in NOESY).
  H17a (2.16 ppm)-H21b (1.48 ppm) (Not observed in NOESY).
  Strong *J* coupling H20 (3.51 ppm)-H21a (1.30 ppm) (14.5).
  Weak *J* coupling H20 (3.51 ppm)-H21b (1.48 ppm) (5.1).

- Stereocenters at C-20 and C-22

  H20 (3.51 ppm)- H22 (3.75 ppm) (Observed in NOESY).
  H21a (1.30 ppm)- H24 (5.51 ppm) (Observed in NOESY).
  H21b (1.48 ppm)- H24 (5.51 ppm) (Observed in NOESY).
  Weak *J* coupling H22 (3.75 ppm)-H21a (1.30 ppm) (3.54).
  Strong *J* coupling H22 (3.75 ppm)-H21b (1.48 ppm) (8.9).

8.10. Key NOESY and *J* coupling in euglenatide B

- Stereocenters at C-2 and C-18

  C2H (4.32 ppm) -N2H (7.65 ppm) (Observed in NOESY).
  C2H (4.32 ppm) -N18H (6.90 ppm) (Observed in NOESY).
  N2H (7.65 ppm) -N18H (6.90 ppm) (Observed in NOESY).
  H17 (3.86 ppm) -N18H (6.90 ppm) (Observed in NOESY).
  Strong *J* coupling H17 (3.86 ppm) -H18 (3.92 ppm) (*J*= 9.6).
  J coupling OH17 (5.13 ppm)-H17 (3.86 ppm) (*J*= 7.7).

- Stereocenters at C-18 and C-20

  H17 (3.86 ppm) -H20 (3.47 ppm) (Observed in NOESY).
  H18 (3.92 ppm)-H21b (1.49 ppm) (Observed in NOESY).
  H18 (3.92 ppm)-H20 (3.47 ppm) (Observed in NOESY).
  H17 (3.86 ppm) - H21b (1.49 ppm) (Not observed in NOESY).
  Strong *J* coupling H20 (3.47 ppm)-H21a (1.30ppm) (14.5).
  Weak *J* coupling H20 (3.47 ppm)-H21b (1.49 ppm) (5.1).

- Stereocenters at C-20 and C-22

  H20 (3.47 ppm)- H22 (3.73 ppm) (Observed in NOESY).
  H21a (1.30 ppm)- H24 (5.51 ppm) (Observed in NOESY).
  H21b (1.48 ppm)- H24 (5.51 ppm) (Observed in NOESY).
  Weak *J* coupling H22 (3.73 ppm)-H21a (1.30 ppm) (3.54).
  Strong *J* coupling H22 (3.73 ppm)-H21b (1.49 ppm) (8.9).

8.11. Comparison of euglenatide E CD spectrum to nemamide A[186]

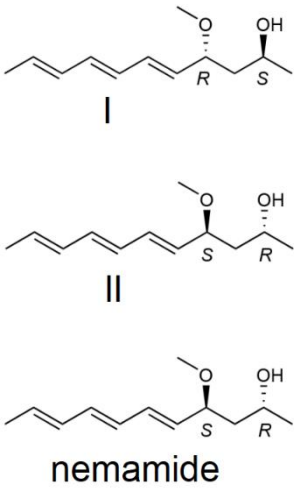

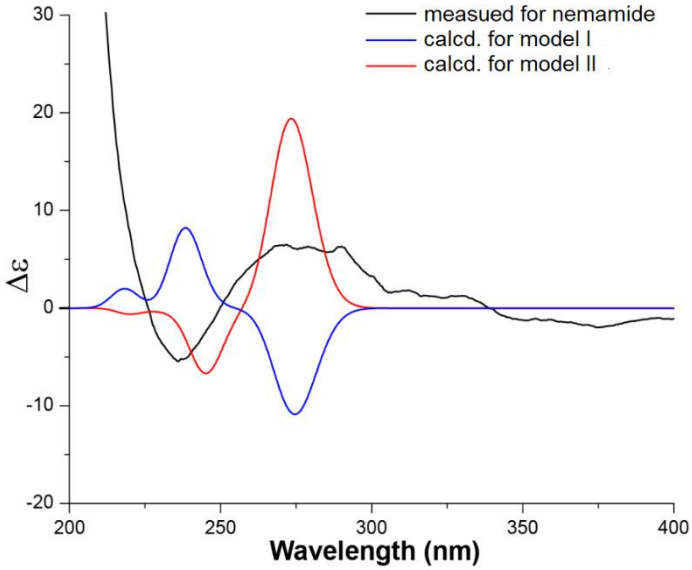

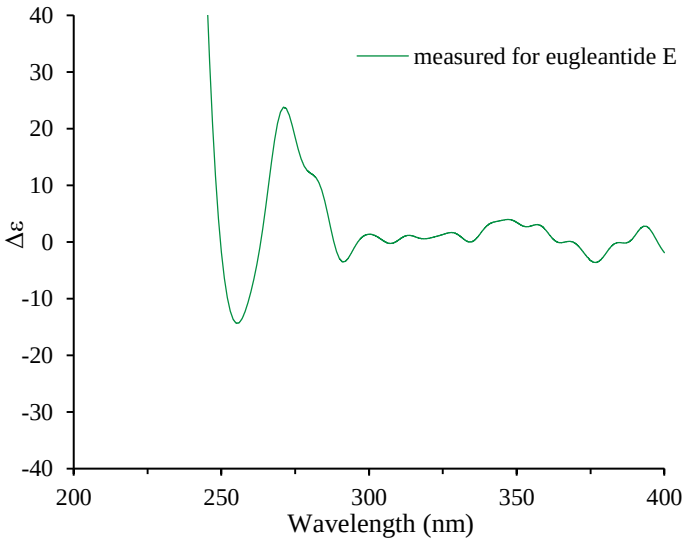

8.12. Antimicrobial activity of *E. gracilis* metabolites (A-E)

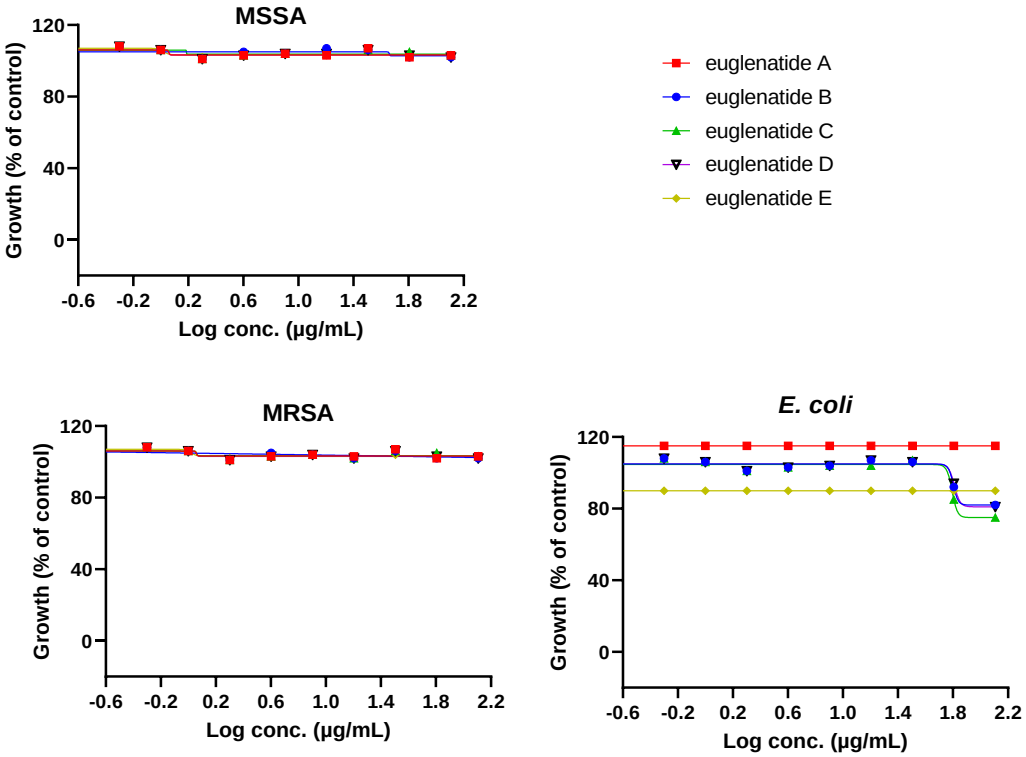

Figure 8.6 Dose–response curves of bacterial strains (MSSA, MRSA and E. coli) incubated with euglenatides A, B, C, D and E.

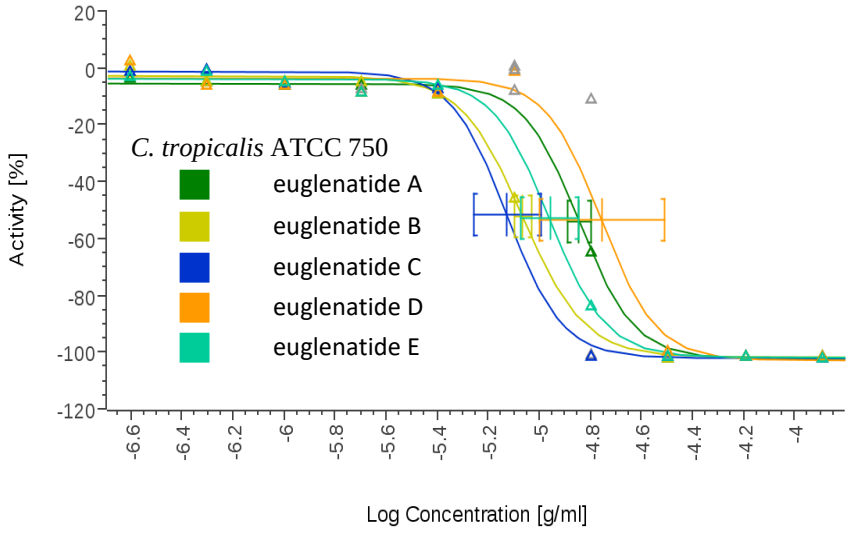

Figure 8.7 Euglenatides A-E dose-response curves tested against *C. tropicalis*. The growth inhibition with the compound is calculated relative to the growth inhibition in the negative controls that is equal to 0.

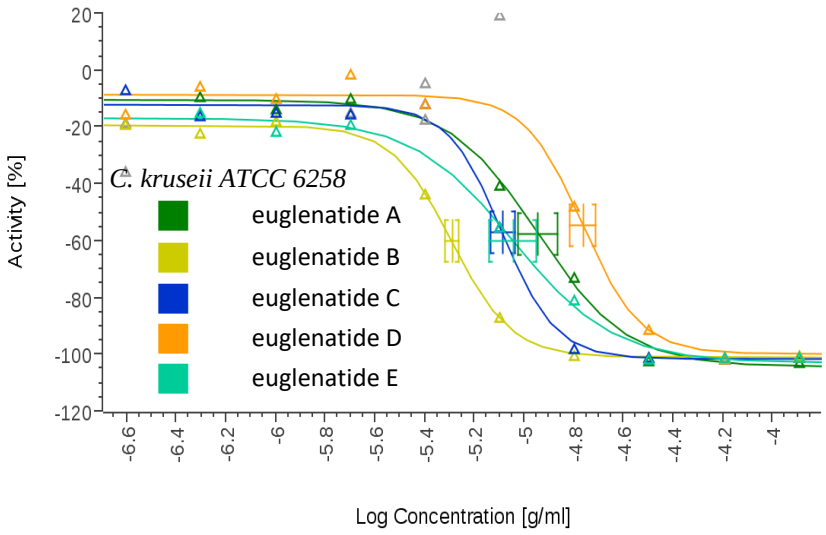

Figure 8.8 Euglenatides A-E dose-response curves tested against *C. krusei*. The growth inhibition with the compound is calculated relative to the growth inhibition in the negative controls that is equal to 0.

8.13. Lists of natural products known or predicted to be produced by *A. calidoustus*, *A. westerdijkiae* and their related species

Table 8.4 Known metabolites from *A. calidoustus* and *A. ustus*.

Chemical Name	Molecular Formula
11,12-Epoxy-7-drimene-6,9,11-triol; (6β,9α,11αOH)-form, 11-Ketone(lactone), 6-O-(2E,4E,6E-octatrienoyl)	C23H30O5
11,12-Epoxy-7-drimene-6,9,11-triol; (6β,9α,11αOH)-form, 11-Ketone(lactone), 6-O-(2E,4E-hexadienoyl)	C21H28O5
11,12-Epoxy-7-drimene-6,9,11-triol; (6β,9α,11αOH)-form, 11-Ketone(lactone), 6-O-(2Z,4E,6E-octatrienoyl)	C23H30O5
11,12-Epoxy-7-drimene-6,9,11-triol; (6β,9α,11αOH)-form, 11-Ketone(lactone), 6-O-(5-carboxy-2E,4E-pentadienoyl)	C21H26O7
11,12-Epoxy-7-drimene-6,9,11-triol; (6β,9α,11αOH)-form, 11-Ketone(lactone), 6-O-(6,6-dimethoxy-2E,4E-hexadienoyl)	C23H32O7
11,12-Epoxy-7-drimene-6,9,11-triol; (6β,9α,11αOH)-form, 11-Ketone(lactone), 6-O-(6-oxo-2E,4E-hexadienoyl)	C21H26O6
11,12-Epoxy-7-drimene-6,9,11-triol; (6β,9α,11αOH)-form, 11-Ketone(lactone), 6-O-(6R*,7R*-dihydroxy-2E,4E-octadienoyl)	C23H32O7

11,12-Epoxy-7-drimene-6,9,11-triol; (6β,9α,11αOH)-form, 11-Ketone(lactone), 6-O-(6R*,7S*-dihydroxy-2E,4E-octadienoyl)	C23H32O7
11,12-Epoxy-7-drimene-6,9,11-triol; (6β,9α,11αOH)-form, 11-Ketone(lactone), 6-O-(6R*,7S*-epoxy-2E,4E-octadienoyl)	C23H30O6
11,12-Epoxy-7-drimene-6,9,11-triol; (6β,9α,11αOH)-form, 11-Ketone(lactone), 6-O-(7-hydroxy-6-oxo-2E,4E-octadienoyl)	C23H30O7
11,12-Epoxy-7-drimene-6,9,11-triol; (6β,9α,11αOH)-form, 11-Ketone(lactone), 6-O-(7ξ-hydroxy-2E,4E-octadienoyl)	C23H32O6
11,12-Epoxy-7-drimene-6,9,11-triol; (6β,9α,11αOH)-form, 11-Ketone(lactone), 6-O-(9ξ-hydroxy-2E,4E,6E-decatrienoyl)	C25H34O6
11,12-Epoxy-7-drimene-6,9,11-triol; (6β,9α,11αOH)-form, 11-Me ether,6-O-(2E,4E,6E-octatrienoyl)	C24H34O5
11,12-Epoxy-7-drimene-6,9,11-triol; (6β,9α,11αOH)-form, 6-O-(2E,4E,6 E-Octatrienoyl)	C23H32O5
11,12-Epoxy-7-drimene-6,9-diol; (6β,9α)-form, 6-O-(2E,4E,6E -Octatrienoyl)	C23H32O4
2,11-Dihydroxy-7-drimen-6-one; 2α-form	C15H24O3
2,9,11-Trihydroxy-7-drimen-6-one; (2α,9α)-form	C15H24O4
2,9,11-Trihydroxy-7-drimen-6-one; (2β,9α)-form	C15H24O4
2-Hydroxy-1-(8-hydroxy-3-methyl-7-isoquinolinyl)-3-methyl-1-butanone	C15H17NO3
3,11-Dihydroxy-7-drimen-6-one; (3β,5α,9β,10β)-form	C15H24O3
3,7,16,18-Ophiobolatetraen-5-one; (16Z)-form	C25H36O
3,7,16,18-Ophiobolatetraen-5-one; (16Z)-form, 16,17-Dihydro	C25H38O
3,9,11-Trihydroxy-7-drimen-6-one; (3β,9α)-form	C15H24O4
5-Oxo-3,7,16,18-ophiobolatetraen-21-al	C25H34O2
5-Oxo-3,7,16,18-ophiobolatetraen-21-al; 2,6-Didehydro, 3β,4-dihydro, 21-alcohol	C25H36O2
5-Oxo-3,7,16,18-ophiobolatetraen-21-al; 21-Alcohol	C25H36O2
5-Oxo-3,7,16,18-ophiobolatetraen-21-al; 21-Alcohol, 18,19-dihydro, 18ξ,19-dihydroxy	C25H38O4
5-Oxo-3,7,16,18-ophiobolatetraen-21-al; Δ6-Isomer, 21-alcohol	C25H36O2
6-Ethyl-2,4-dihydroxy-3-methylbenzoic acid; Et ester	C12H16O4
6-Ethyl-2,4-dihydroxy-3-methylbenzoic acid; Me ester	C11H14O4

7(21),18-Ophioboladiene-3,8-diol; (3α,6β,8β)-form	C25H42O2
7,8-Dihydro-7,8-dihydroxy-3,5,7-trimethyl-6H-2-benzopyran-6-one	C12H14O4
7-Chloro-2-(3-furanyl)-1,3,8-trimethoxyxanthone	C20H15ClO6
7-Drimene-6,9,11-triol; (5α,6α,9α,10β)-form, 6-Ketone	C15H24O3
7-Drimene-6,9,11-triol; (5α,6α,9α,10β)-form, 6-Ketone, 11-aldehyde	C15H22O3
7-Drimene-6,9,11-triol; (5α,6α,9α,10β)-form, 6-Me ether	C16H28O3
7-Drimene-6,9,11-triol; (5α,6β,9α,10β)-form, 11-Aldehyde, 6-O-(2E,4E ,6E-octatrienoyl)	C23H32O4
7-Drimene-6,9,11-triol; (5α,6β,9α,10β)-form, 12-Hydroxy, 6-Me ether	C16H28O4
7-Drimene-6,9,11-triol; (5α,6β,9α,10β)-form, 12-Hydroxy, 6-O-(2E,4E,6 E-octatrienoyl)	C23H34O5
8-Drimene-6,7,11-triol; (6β,7α)-form	C15H26O3
8-Hydroxyergosta-4,6,22-trien-3-one; (8β,9α,14α,22E,24R)-form	C28H42O2
Aspergillamide A	C22H22N2O5
Aspergillamide A; 2-Epimer	C22H22N2O5
Austalide B	C26H34O8
Austalide B; 13-Ac	C28H36O9
Austalide B; 19α-Hydroxy	C26H34O9
Austalide B; 19α-Hydroxy, 13-Ac	C28H36O10
Austalide B; 19α-Hydroxy, 19-Ac	C28H36O10
Austalide B; 19α-Hydroxy, di-Ac	C30H38O11
Austalide H acid; 13-Ac, Me ester	C28H38O9
Austalide H acid; Me ester	C26H36O8
Austalide I	C27H34O8
Austalide J	C25H32O7
Austalide K	C25H32O5
Austalide K; 14β-Hydroxy	C25H32O6
Austamide	C21H21N3O3

Austamide; 12S,13-Dihydro	C21H23N3O3
Austamide; 12ξ-Hydroxy, 12,13-dihydro	C21H23N3O4
Austdiol	C12H12O5
Austin	C27H32O9
Austin; O-De-Ac	C25H30O8
Austocystin A	C19H13ClO6
Austocystin A; 2,3-Dihydro, O4-De-Me	C18H13ClO6
Austocystin A; 2,3-Dihydro, O6-de-Me	C18H13ClO6
Austocystin A; 4,6-Di-O-de-Me	C17H9ClO6
Austocystin A; O4-De-Me	C18H11ClO6
Austocystin F	C17H10O7
Austocystin F; 2,3-Dihydro	C17H12O7
Austocystin F; 4-Me ether	C18H12O7
Austocystin F; 8-Chloro, 4-Me ether	C18H11ClO7
Austocystin H	C22H18O7
Austocystin H; 2',3'-Dihydro, 3'-hydroxy	C22H20O8
Austocystin H; 2',3'-Dihydro, 3'-hydroxy, 4-Me ether	C23H22O8
Austocystin H; 3a-Deoxy, 2',3'-dihydro, 3'-hydroxy	C22H20O7
Austocystin H; 3a-Deoxy, 2',3'-dihydro, 3'-hydroxy, 4-Me ether	C23H22O7
Averufanin; (+)-form	C20H18O7
Brassicadiol; (ξ)-form, 2"ξ-Hydroxy	C15H22O4
Brassicadiol; (ξ)-form, 3"ξ-Hydroxy, 1",2"-didehydro(Z-)	C15H20O4
Cyclo[2-(1,1-dimethyl-2-propenyl) tryptophyl]prolyl	C21H25N3O2
Cyclo[2-(1,1-dimethyl-2-propenyl) tryptophyl] prolyl; 12,13-Didehydro	C21H23N3O2
Cyclopaldic acid	C11H10O6
Dehydroaustinol; Ac	C27H30O9

Deoxyisoaustamide	C21H21N3O2
Nidulin	C20H17Cl3O5
Nidulin; 4-Dechloro, O-de-Me	C19H16Cl2O5
Nidulin; O-De-Me	C19H15Cl3O5
Ophiobolin H	C25H38O3
Ophiobolin H; 5,6-Diepimer	C25H38O3
Ophiobolin H; 5,6-Diepimer, 5-Me ether	C26H40O3
Ophiobolin H; 5-Me ether	C26H40O3
Ophiobolin K	C25H36O3
Ophiobolin K; 6-Epimer	C25H36O3
Pergillin	C15H16O4
Pergillin; 2,10-Dihydro	C15H18O4
Phenylahistin	C20H22N4O2
Pseudodeflectusin; 1-Deoxy, 3,4-didehydro	C15H14O3
Pseudodeflectusin; Diepimer, 8S,10-dihydro, Me ether	C16H20O4
Pseudodeflectusin; Me ether	C16H18O4
Terretonin E; 1-Deoxy	C26H32O8
TMC 120A	C15H15NO2
TMC 120A; 2,11-Didehydro	C15H13NO2
TMC 120A; 2-Hydroxy	C15H15NO3
Ustic acid	C11H12O7
Ustusorane A	C15H18O4

Table 8.5 Known metabolites from *A. westerdijkiae* and *A. ochraceus*.

Chemical Name	**Molecular Formula**
2,3-Dihydro-1H-pyrrolo[2,1-c][1,4]benzodiazepine-5,11(10H,11aH)-dione; (S)-form, 7-Methoxy	C13H14N2O3
2-Benzyl-3-hydroxy-1-methyl-5-nonylpyrrolidine; (2S,3S,5R)-form	C21H35NO
3-(2-Chloro-3-hydroxybutenylidene)dihydro-4-hydroxy-5-methyl-2(3H)-furanone	C9H13ClO4
3,4-Dihydro-3,8-dihydroxy-3-methyl-1H-2-benzopyran-1-one; (±)-form, 3-Me ether	C11H12O4
3,4-Dihydro-4,8-dihydroxy-3-methyl-1H-2-benzopyran-1-one	C10H10O4
3,4-Dihydro-7,8-dihydroxy-3-methyl-1H-2-benzopyran-1-one	C10H10O4
3,4-Dihydro-8-hydroxy-3-methyl-1H-2-benzopyran-1-one; (R)-form, 5-Bromo	C10H9BrO3
3,6-Bis(2-methylpropyl)-2(1H)-pyrazinone	C12H20N2O
3,6-Bis(2-methylpropyl)-2(1H)-pyrazinone; 1-Oxide	C12H20N2O2
3,6-Bis(2-methylpropyl)-2(1H)-pyrazinone; 1-Oxide, Fe complex	C36H57FeN6O6
3,6-Bis(2-methylpropyl)-2(1H)-pyrazinone; 2''-Hydroxy	C12H20N2O2
3,6-Bis(2-methylpropyl)-2(1H)-pyrazinone; NH-form, 1,2''-Dihydroxy	C12H20N2O3
4-(Hydroxymethyl)-4,6-octadiene-2,3-diol; (E,E)-form	C9H16O3
4,6,8-Nonatriene-2,3-diol	C9H14O2
5-Hydroxy-6-decen-9-olide; (5R,9R)-form	C10H16O3
6,8-Dihydroxy-1-oxo-1H-2-benzopyran-3-carboxylic acid; 6-Me ether	C11H8O6
6,9,14-Trihydroxy-7-drimen-12,11-olide; (6β,9α)-form, 6-O-(4-Nitrobenzoyl)	C22H25NO8
Amauromine; 2,3-Diepimer	C32H36N4O2
Amauromine; 2,3-Diepimer, N1'-Me	C33H38N4O2
Asperchrome B1	C37H58FeN9O16
Asperchrome D	C33H52FeN9O15
Asperchrome E	C41H64FeN9O17
Aspergilliamide B	C11H20N2O4

Asperlactone	C9H12O4
Asperlactone; Deepoxy, 8ξ-chloro, 9ξ-hydroxy	C9H13ClO4
Asperlactone; Deepoxy, 9ξ-chloro, 8ξ-hydroxy	C9H13ClO4
Aspinolide B	C14H20O6
Aspinolide B; 5-Ketone	C14H18O6
Aspinonene	C9H16O4
Aspochracin	C23H36N4O4
Aspyrone	C9H12O4
Aspyrone; Deepoxy, 1'R-chloro, 2'S-hydroxy	C9H13ClO4
Aspyrone; Deepoxy, 1'S-methoxy, 2'R-hydroxy	C10H16O5
Aspyrone; Deepoxy, 2'S-chloro, 1'S-hydroxy	C9H13ClO4
Aspyrone; Deepoxy, 2'S-hydroxy	C9H14O4
Circumdatin A; (S)-form	C21H19N3O5
Circumdatin A; (S)-form, 5-Demethoxy	C20H17N3O4
Circumdatin C; (S)-form	C17H13N3O3
Circumdatin C; (S)-form, 6-Hydroxy	C17H13N3O4
Circumdatin C; (S)-form, Deoxy	C17H13N3O2
Circumdatin C; (S)-form, Deoxy, 15-hydroxy	C17H13N3O3
Circumdatin E; (S)-form	C20H17N3O4
Circumdatin E; (S)-form, 15-Deoxy	C20H17N3O3
Circumdatin E; (S)-form, 5-Methoxy	C21H19N3O5
Circumdatin L; (S)-form	C17H13N3O3
Cyclo(leucylprolyl); (3S,8aS)-form	C11H18N2O2
Cycloechinulin; (S)-form	C20H21N3O3
Des(diserylglycyl)ferrirhodin	C33H53FeN6O13
Destruxins; Destruxin B	C30H51N5O7

Diaporthin; (S)-form	C13H14O5
Diaporthin; (S)-form, O-De-Me	C12H12O5
Ergochromes; Ergochrome AA	C32H30O14
Ferrirubin; *-Deoxy	C41H64FeN9O16
Ferrirubin; 2,3 or 4-Ac	C43H66FeN9O18
Isoaspinonene	C9H16O4
Ochratoxin A	C20H18ClNO6
Ochratoxin A; 4R-Hydroxy-L-proline analogue	C16H16ClNO7
Ochratoxin A; 4S-Hydroxy	C20H18ClNO7
Ochratoxin A; Dechloro	C20H19NO6
Ochratoxin A; Et ester	C22H22ClNO6
Ochratoxin A; L-Lysine analogue	C17H21ClN2O6
Ochratoxin A; L-Serine analogue	C14H14ClNO7
Ochratoxin A; Me ester	C21H20ClNO6
Ochrindole A	C29H28N2O3
Ochrindole A; 10-Hydroxy	C29H28N2O4
Ochrindole A; O1-De-Me	C28H26N2O3
Ochrindole D	C27H22N2O3
Penicillic acid	C8H10O4
Sclerotiamide; (-)-form	C26H29N3O5
Sclerotiamide; (-)-form, 5-Chloro	C26H28ClN3O5
Sclerotigenin; 15-Hydroxy	C16H11N3O3
Stephacidin A; (+)-form	C26H29N3O3
Stephacidin A; (+)-form, 8,20-Dihydro, 8,9-didehydro, 20β-hydroxy, N9 -oxide	C26H29N3O5
Stephacidin A; (+)-form, 9,21-Didehydro	C26H27N3O3
Stephacidin A; (+)-form, 9,21-Didehydro, N9-oxide	C26H27N3O4

Stephacidin B	C52H54N6O8
Viomellein	C30H24O11
Xanthomegnin	C30H22O12

Table 8.6 Natural product BGCs predicted by antiSMASH from *A. calidoustus*.

Region	Type	Most similar known cluster		Similarity
1.4	T1PKS	asperthecin	Terpene	85%
2.2	T1PKS,NRPS-like	cichorine	Polyketide	100%
2.3	terpene	clavaric acid	Terpene	100%
2.4	T1PKS	naphthopyrone	Polyketide	100%
2.7	T1PKS,indole	neurosporin A	Polyketide	26%
2.9	T1PKS	epipyriculol	Polyketide	29%
3.2	NRPS	N-Acetyltryptophan	NRP	66%
3.3	T1PKS	trypacidin	Polyketide	28%
4.4	T1PKS	aflavarin	Polyketide	60%
4.5	T1PKS	pyranonigrin E	Polyketide	100%
4.9	T1PKS,NRPS-like	cichorine	Polyketide	100%
5.2	terpene	shearinine D	Terpene	9%
6.6	T1PKS	aspernidine A	Polyketide	100%
6.7	NRPS	cyclo-(D-Phe-L-Phe-D-Val-L-Val) / cyclo-(D-Tyr-L-Phe-D-Val-L-Val) / cyclo-(D-Tyr-L-Trp-D-Val-L-Val) / cyclo-(D-Phe-L-Trp-D-Val-L-Val) / cyclo-(D-Phe-L-Phe-D-Val-L-Ile) / cyclo-(D-Phe-L-Phe-D-Ile-L-Val) / cyclo-(D-Tyr-L-Trp-D-Val-L-Ile) / cyclo-(D-Tyr-L-Trp-D-Ile-L-Val) / cyclo-(D-Tyr-L-Phe-D-Val-L-Ile) / cyclo-(D-Tyr-L-Phe-D-Ile-L-Val)	NRP: Cyclic depsipeptide	100%
7.2	NRPS	nidulanin A	Polyketide	75%
8.2	T1PKS	ankaflavin / monascin / rubropunctatine / monascorubrin	Polyketide: Iterative type I	8%
8.3	terpene	squalestatin S1	Terpene	60%

Region	Type	Most similar known cluster		Similarity
8.4	T1PKS,terpene	shearinine D	Terpene	9%
10.1	NRPS,T1PKS	emericellamide A / emericellamide B	NRP	80%
14.1	NRPS-like,terpene	clavaric acid	Terpene	100%
21.1	indole,NRPS	notoamide A	NRP	16%
24.1	T1PKS	paraherquonin	Polyketide + Terpene	62%

Table 8.7 Natural product BGCs predicted by antiSMASH from *A. westerdijkiae*.

Region	Type	Most similar known cluster		Similarity
89.1	indole	notoamide A	NRP	11%
136.1	T1PKS	viriditoxin	Polyketide	22%
161.2	NRPS,T1PKS	pyranonigrin E	Polyketide	100%
161.4	NRPS	ochratoxin A	NRP + Polyketide	80%
181.2	NRPS-like	aspergillic acid	NRP	57%
181.5	T1PKS,NRPS-like	equisetin	NRP + Polyketide	18%
183.5	T1PKS	neurosporin A	Polyketide	20%
183.7	NRPS,indole	notoamide A	NRP + Terpene + Alkaloid	38%
184.1	NRPS	asperphenamate	NRP	75%
187.1	NRPS	serinocyclin A / serinocyclin B	NRP	100%
188.4	T1PKS	asperlactone	Polyketide	100%
191.1	terpene	botrydial	Terpene	13%
195.2	NRPS,indole	hexadehydroastechrome / terezine-D / astechrome	NRP	75%
195.3	NRPS,T1PKS	UNII-YC2Q1O94PT	Polyketide	100%
197.1	NRPS	serinocyclin A / serinocyclin B	NRP	100%
198.2	terpene	squalestatin S1	Terpene	40%
217.2	NRPS-like	ochrindole A	Other	29%
221.1	NRPS,NRPS-like	patulin	Polyketide: Iterative type I	20%

8.14. Spectra of *A. calidoustus* and A. *westerdijkiae metabolites*

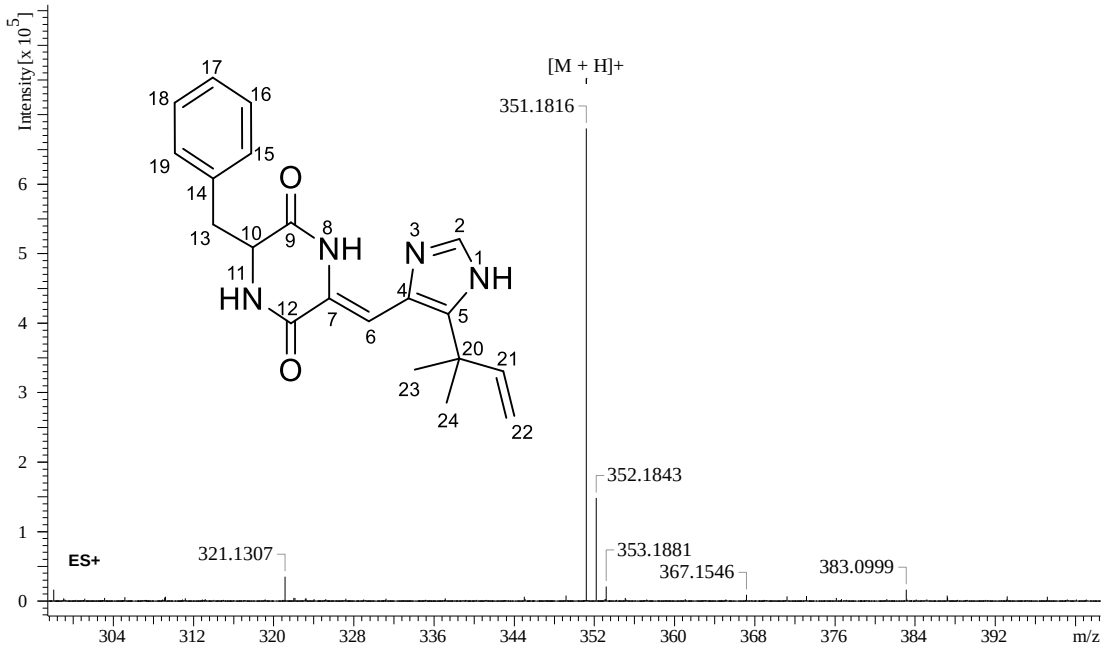

Figure 8.9 HRMS spectrum of phenylahistin.

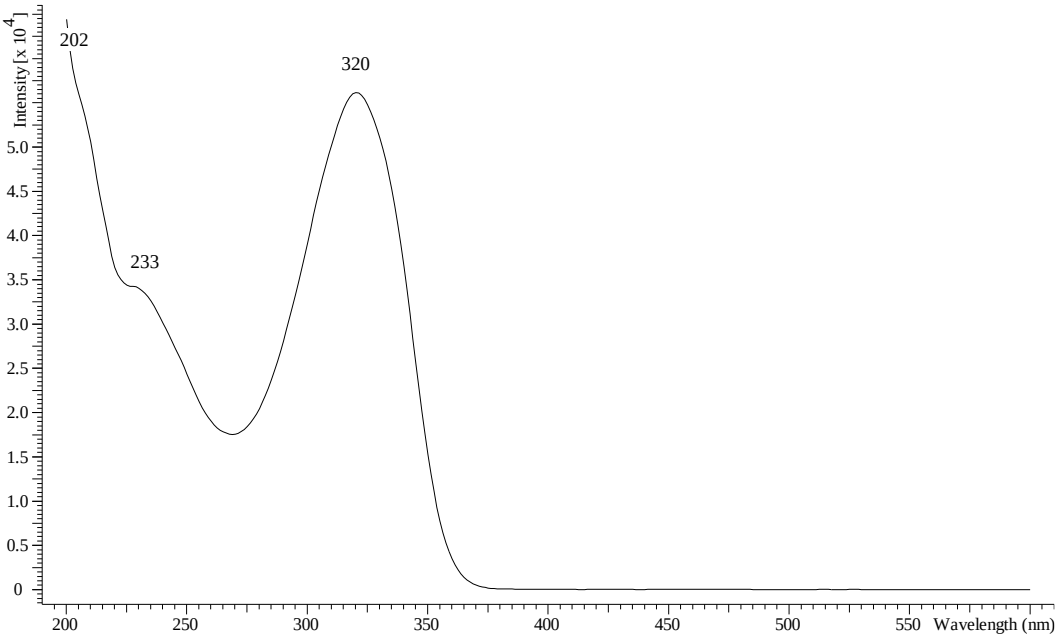

Figure 8.10 UV spectrum of phenylahistin.

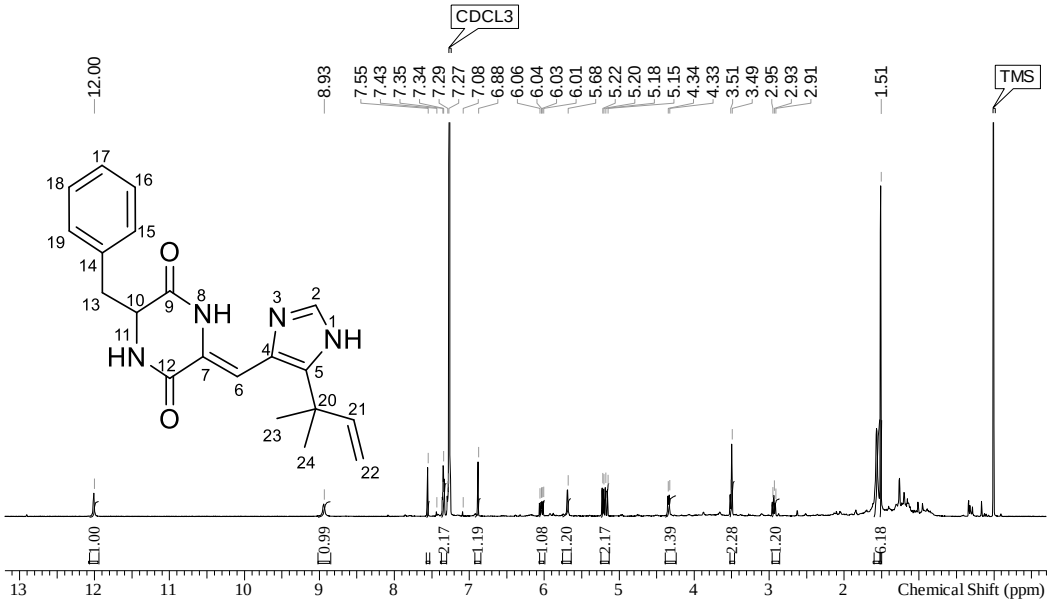

Figure 8.11 ^{1}H NMR spectrum of phenylahistin in $CDCl_3$.

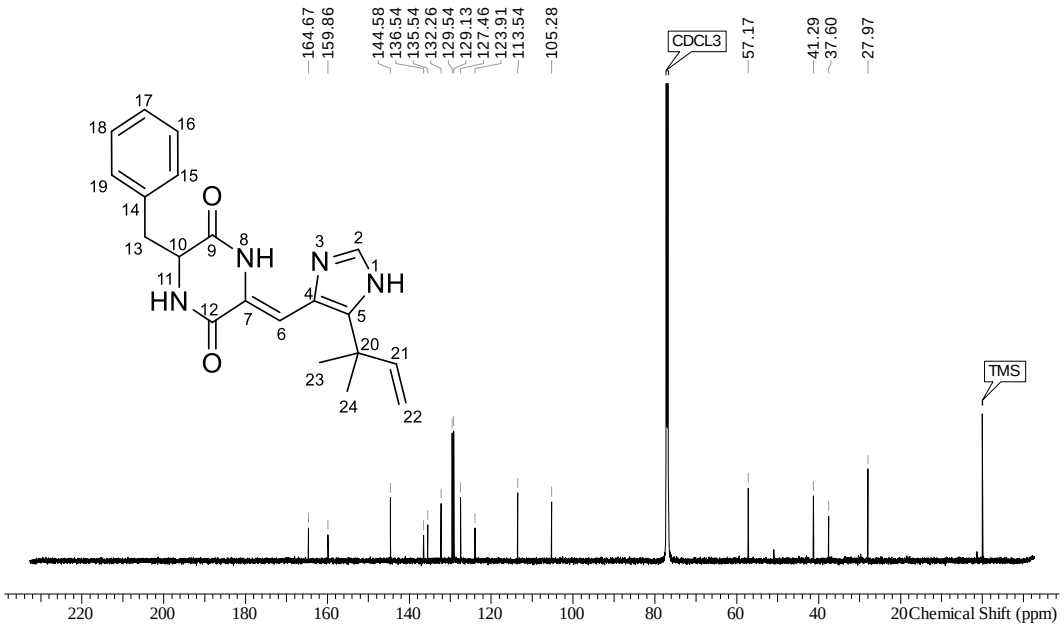

Figure 8.12 ^{13}C NMR spectrum of phenylahistin in $CDCl_3$.

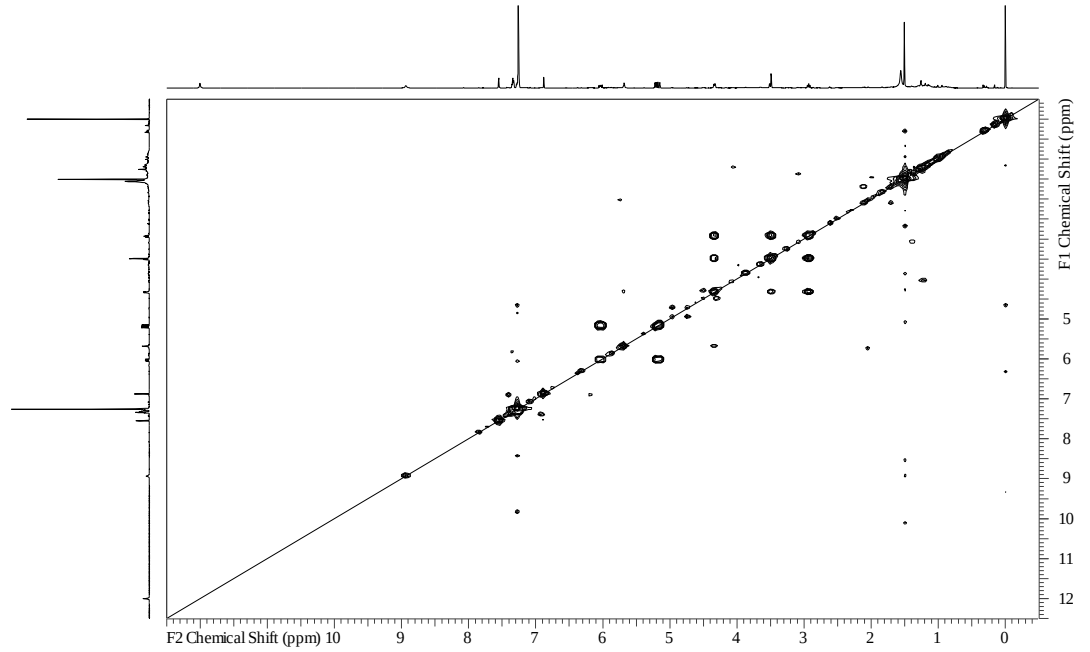

Figure 8.13 COSY NMR spectrum of phenylahistin in $CDCl_3$.

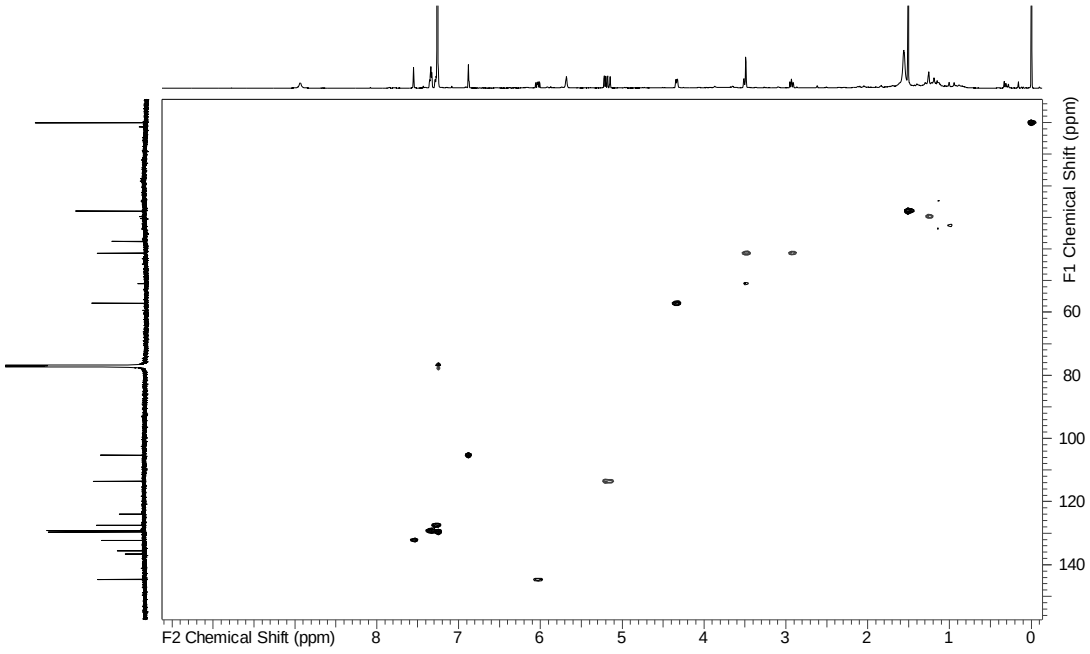

Figure 8.14 HSQC NMR spectrum of phenylahistin in $CDCl_3$.

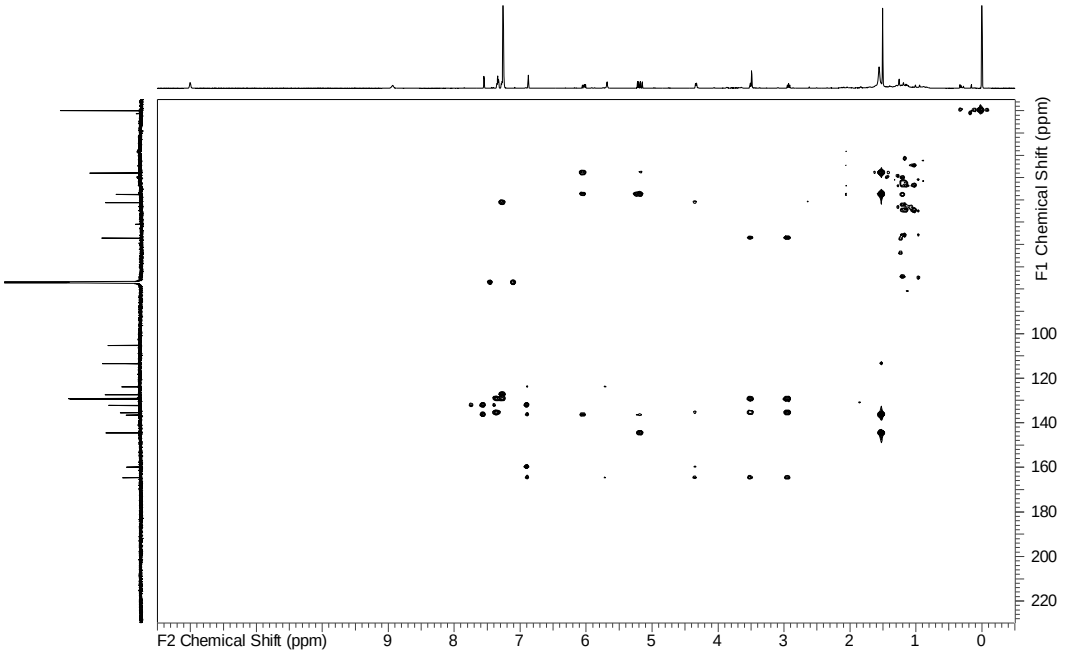

Figure 8.15 HMBC NMR spectrum of phenylahistin in $CDCl_3$.

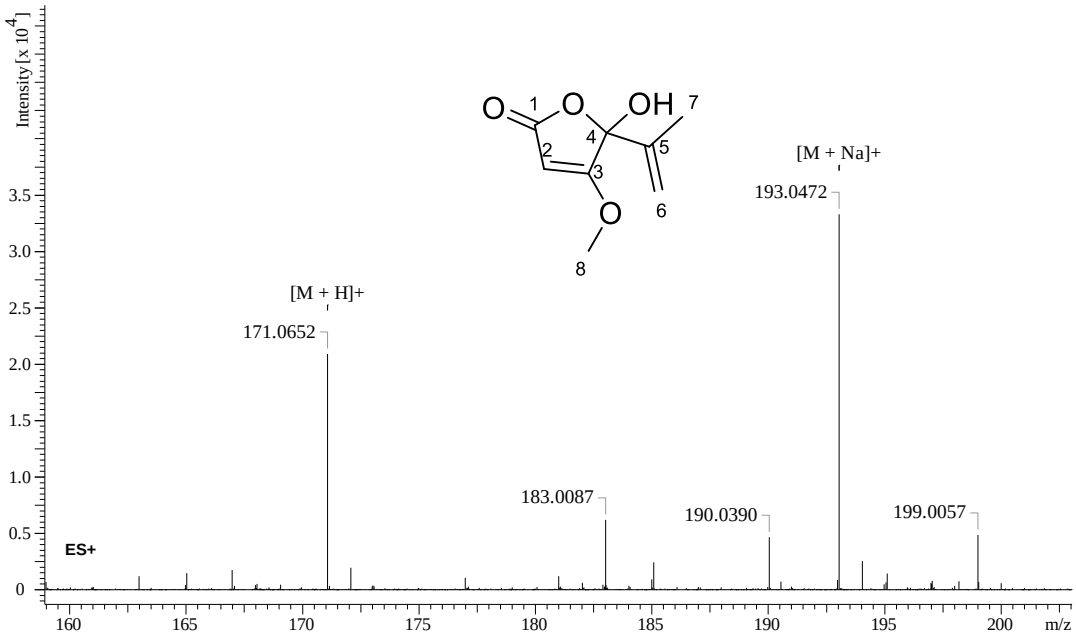

Figure 8.16 HRMS spectrum of penicillic acid.

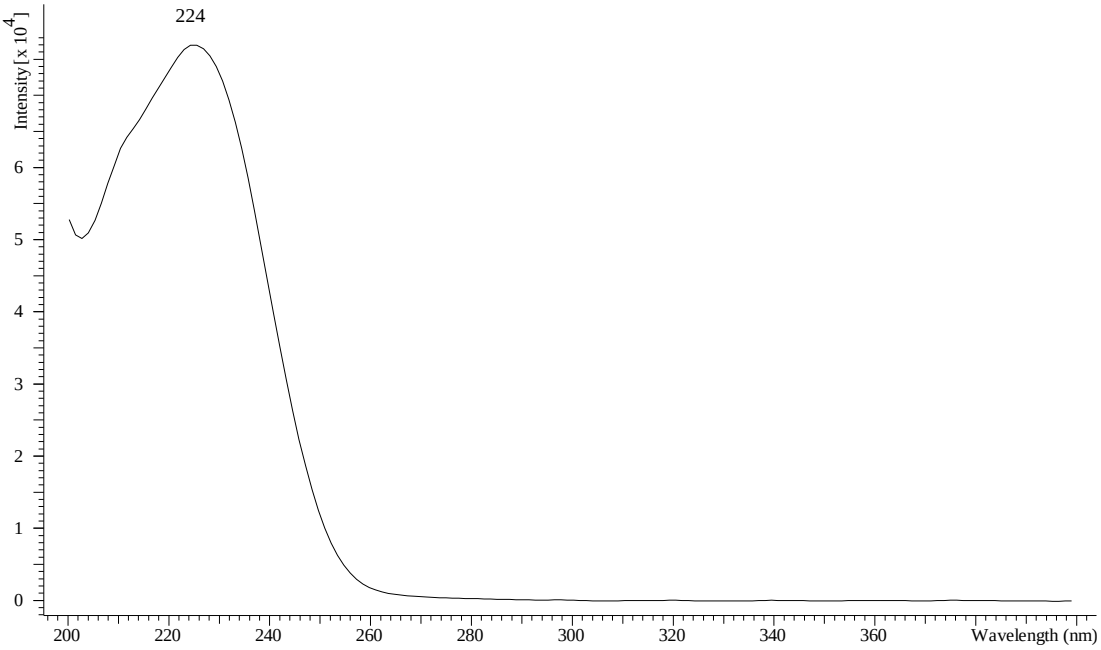

Figure 8.17 UV spectrum of penicillic acid.

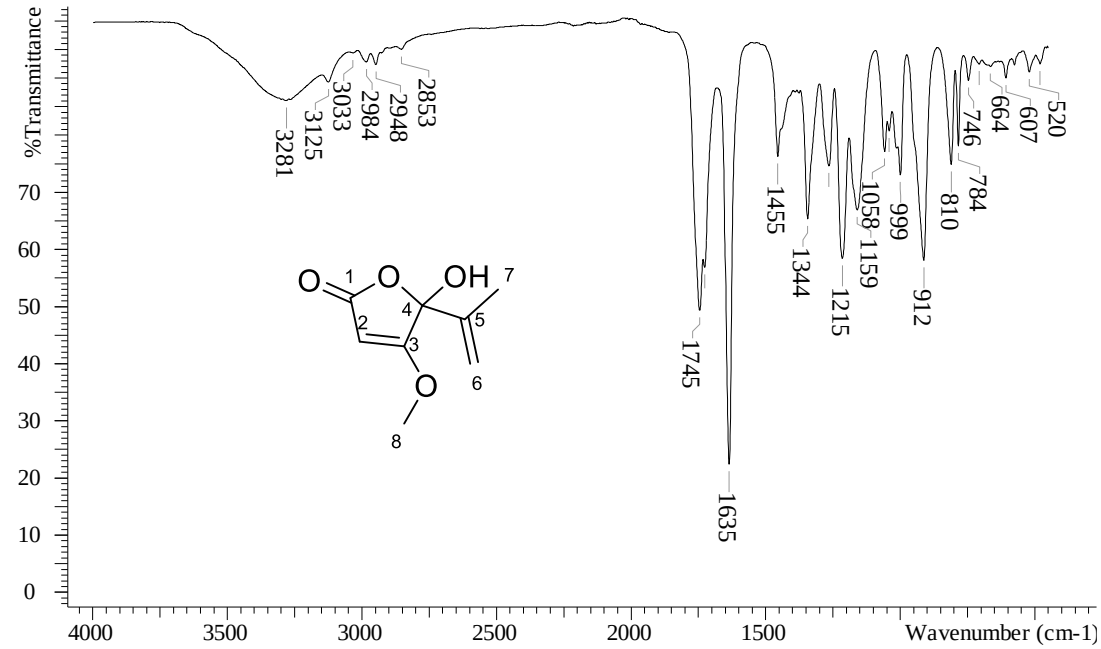

Figure 8.18 IR spectrum of penicillic acid.

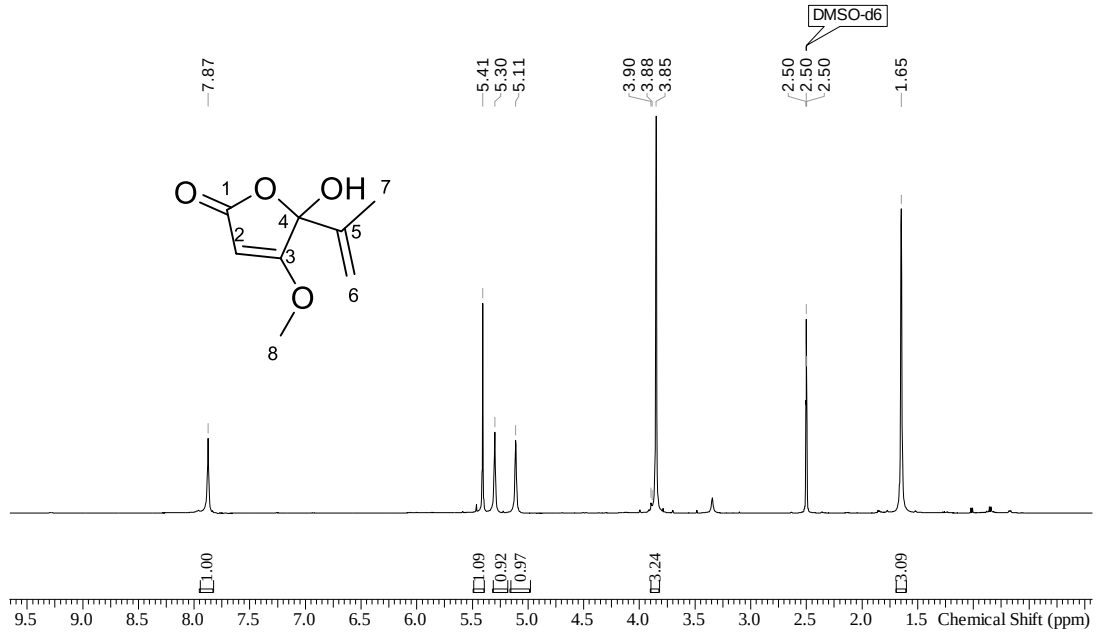

Figure 8.19 ^{1}H NMR spectrum of penicillic acid in DMSO-*d6*.

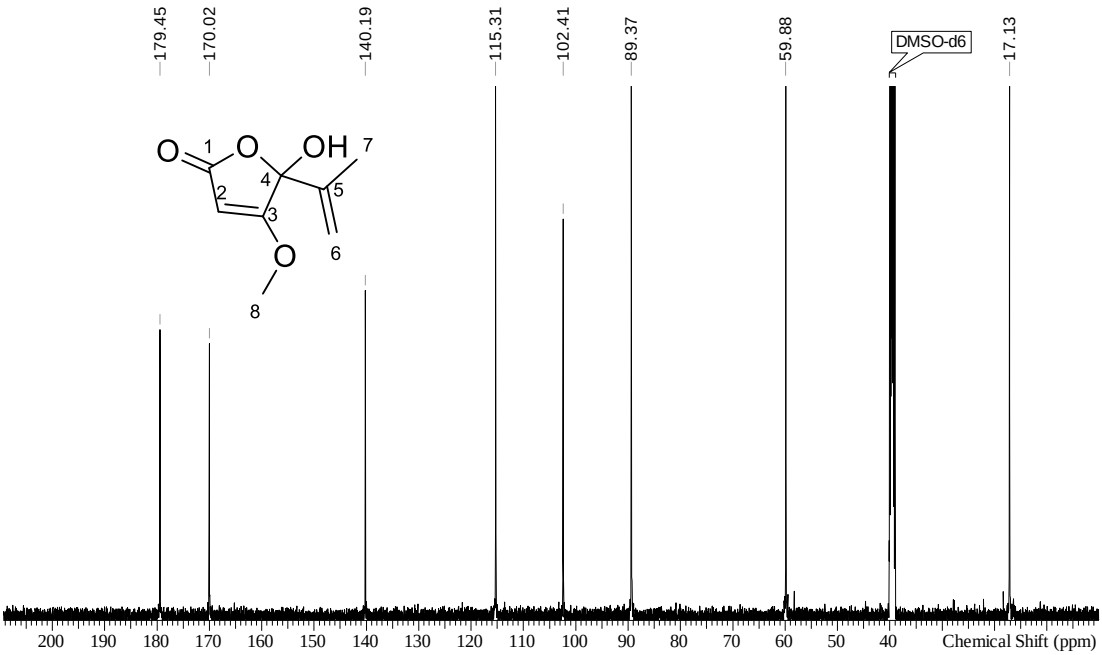

Figure 8.20 ^{13}C NMR spectrum of penicillic acid in DMSO-*d6*.

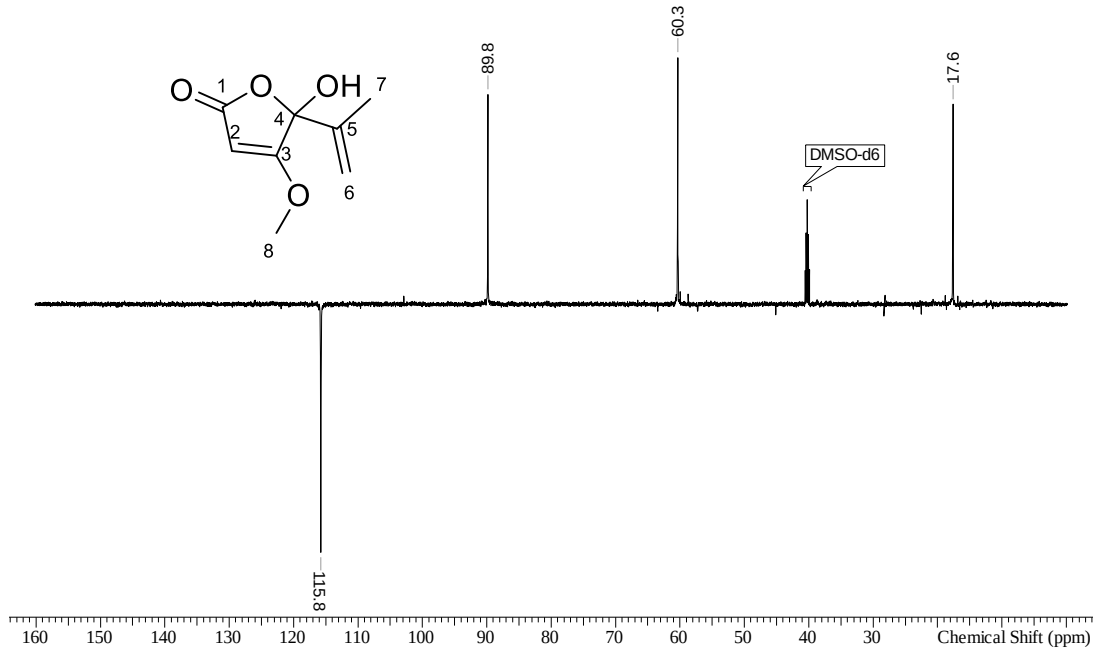

Figure 8.21 DEPT 135 NMR spectrum of penicillic acid in DMSO-*d6*.

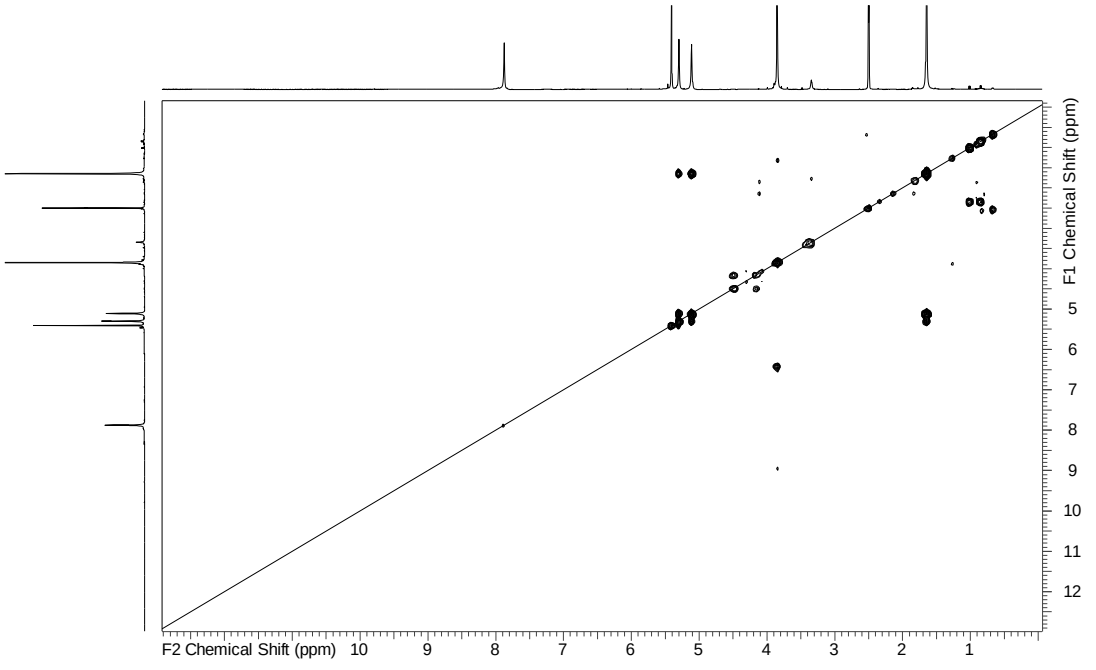

Figure 8.22 COSY NMR spectrum of penicillic acid in DMSO-*d6*.

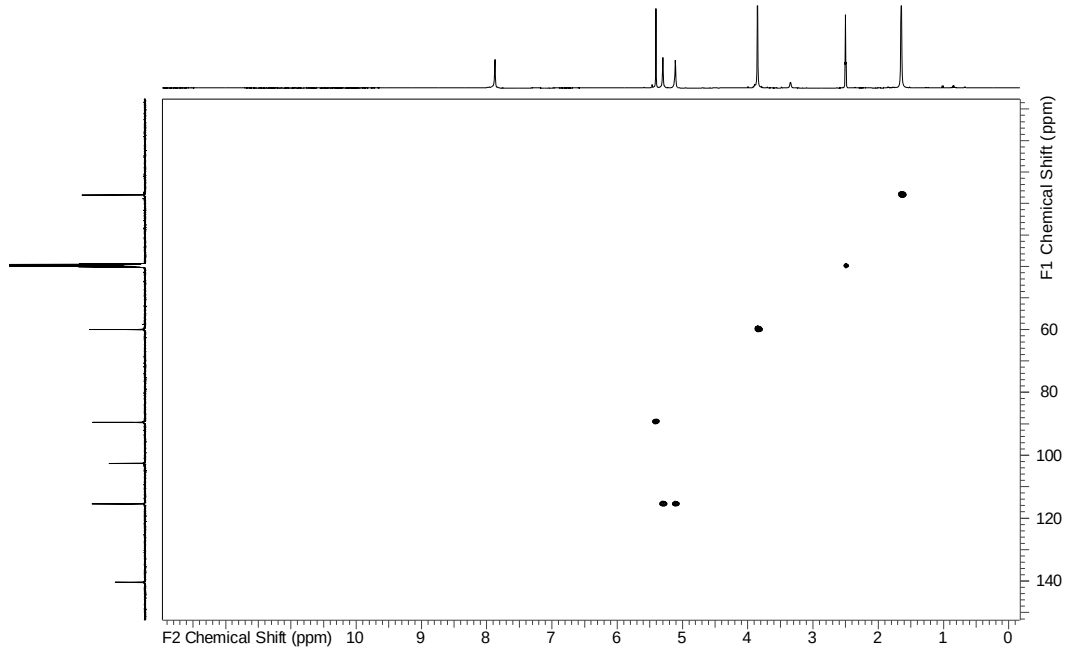

Figure 8.23 HSQC NMR spectrum of penicillic acid in DMSO-*d6*.

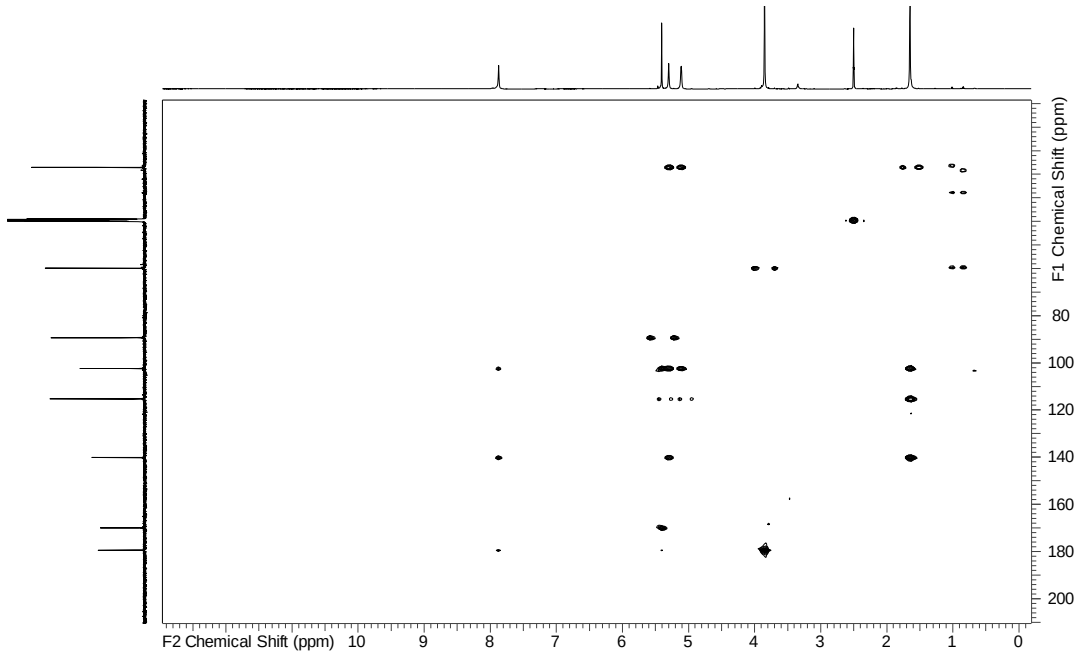

Figure 8.24 HMBC NMR spectrum of penicillic acid in DMSO-*d6*.

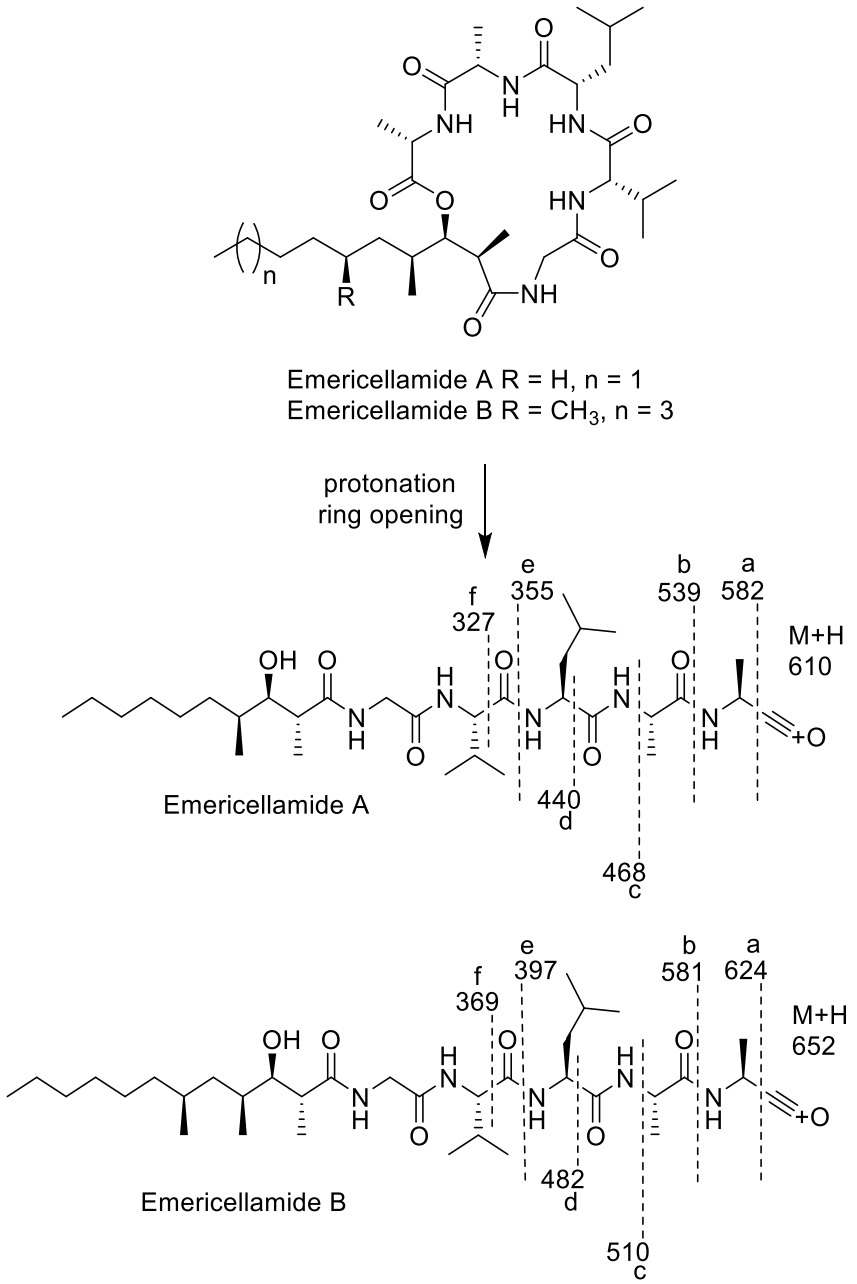

Figure 8.25 Fragmentation patterns of emericellamides A and B.

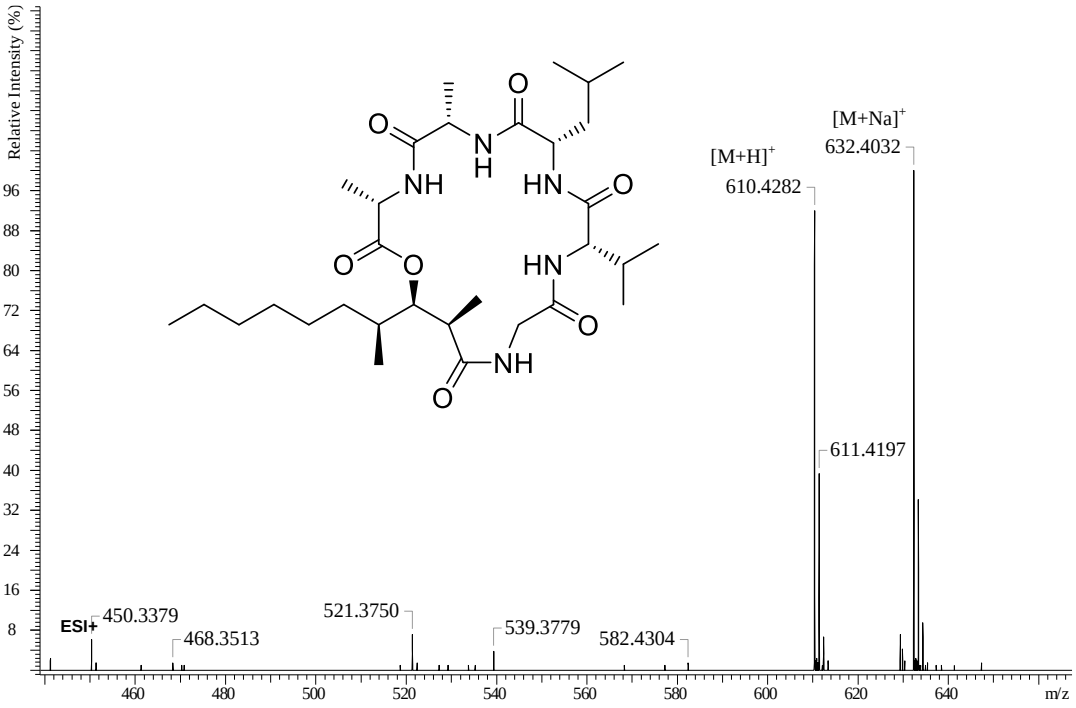

Figure 8.26 MS spectrum of emericellamide A.

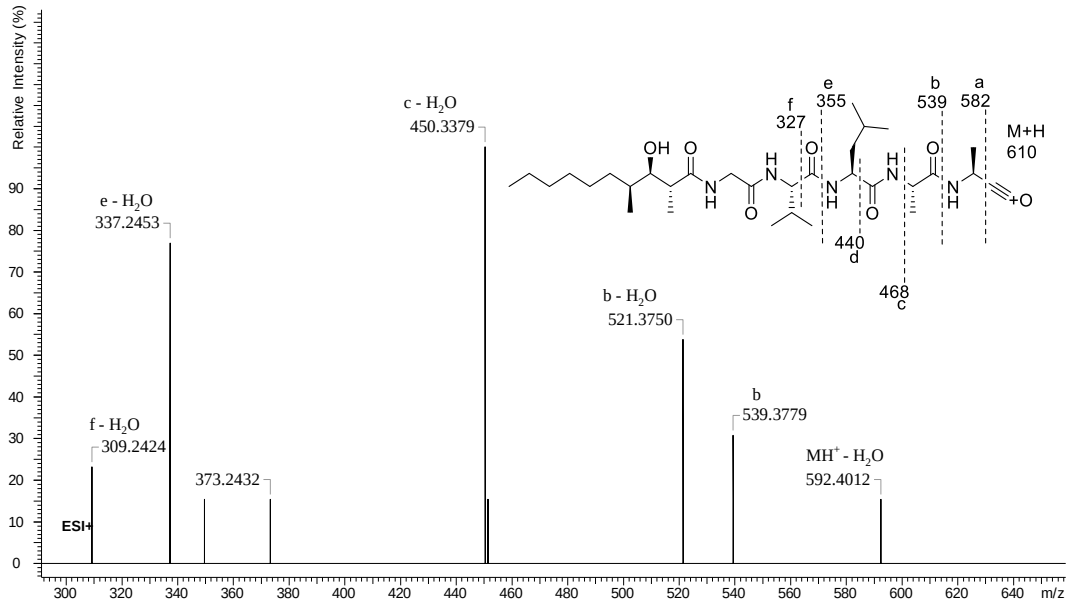

Figure 8.27 MS/MS spectrum of emericellamide A.

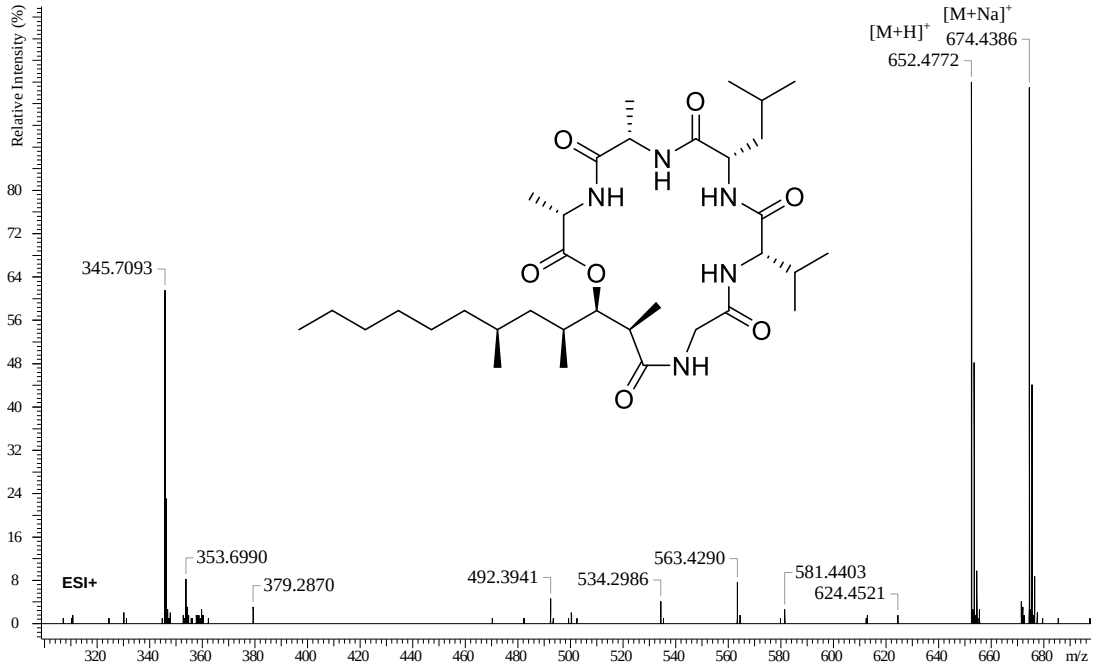

Figure 8.28 MS spectrum of emericellamide B.

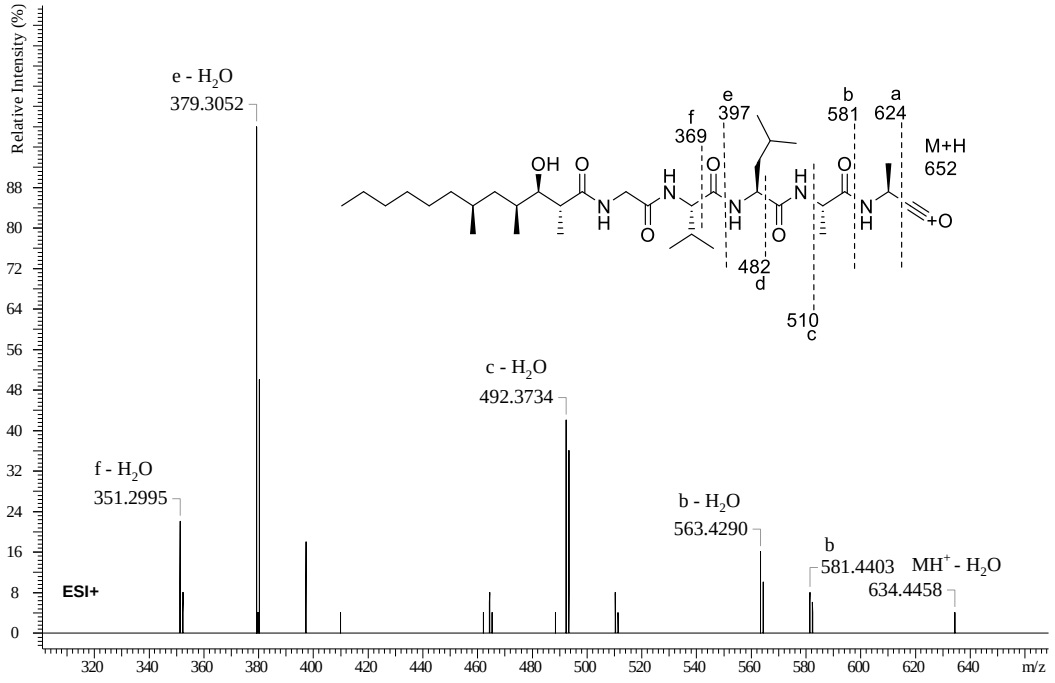

Figure 8.29 MS/MS spectrum of emericellamide B.

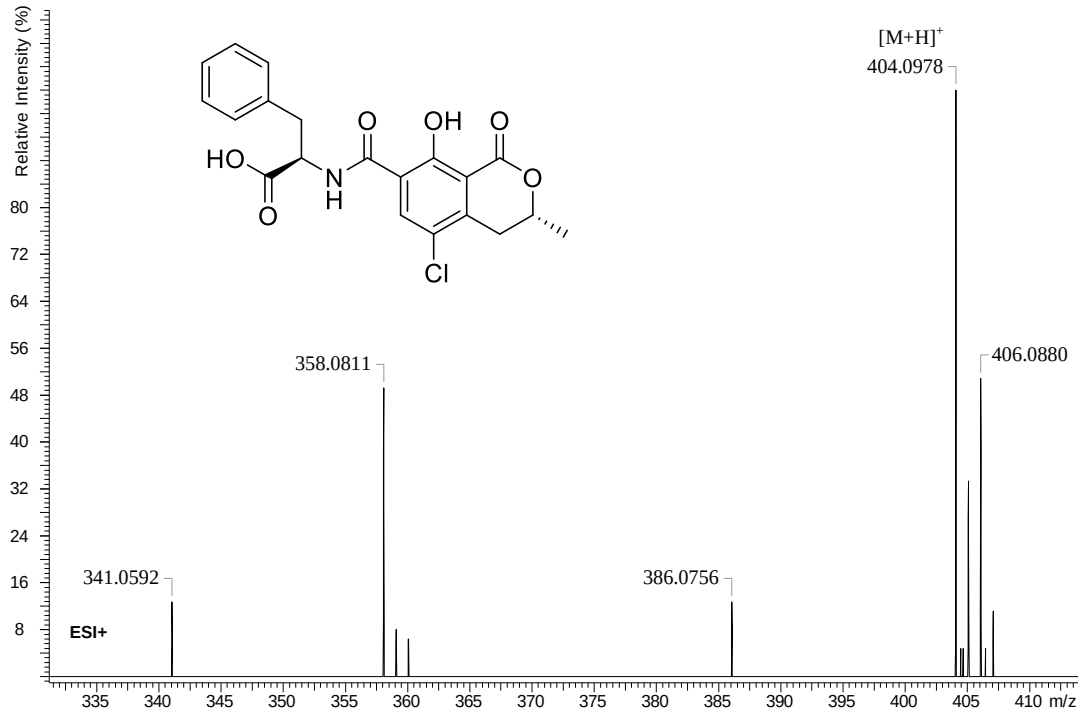

Figure 8.30 MS spectrum of ochratoxin A.

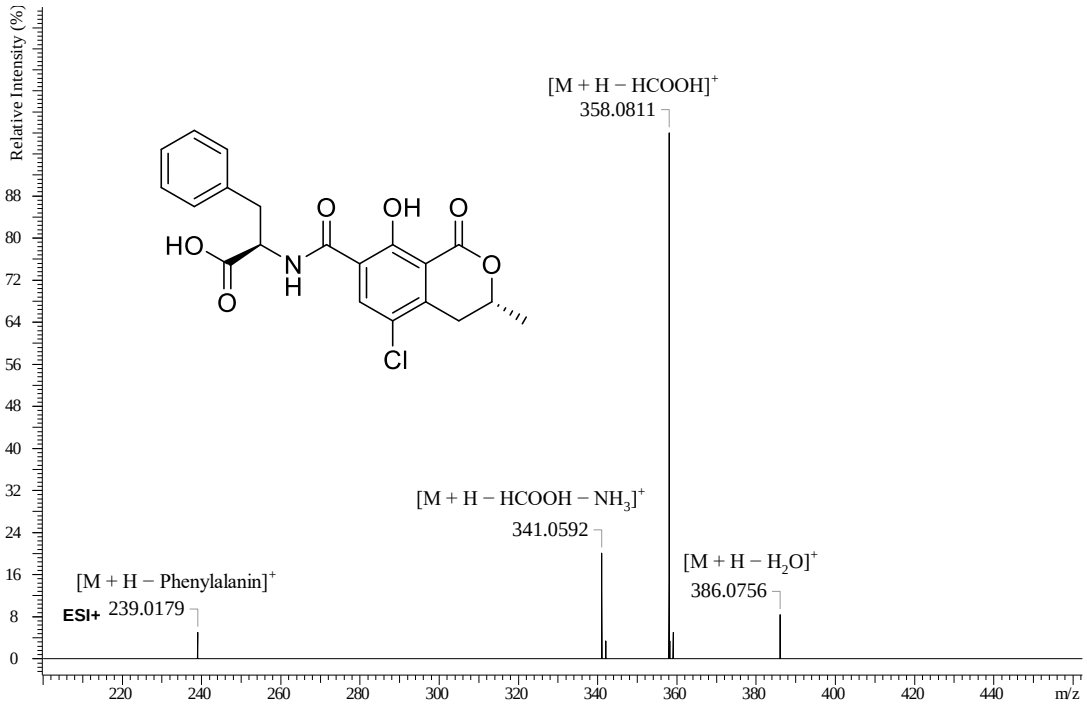

Figure 8.31 MS/MS spectrum of ochratoxin A.

8.15. Predicted gene clusters for emericellamides and ochratoxin A

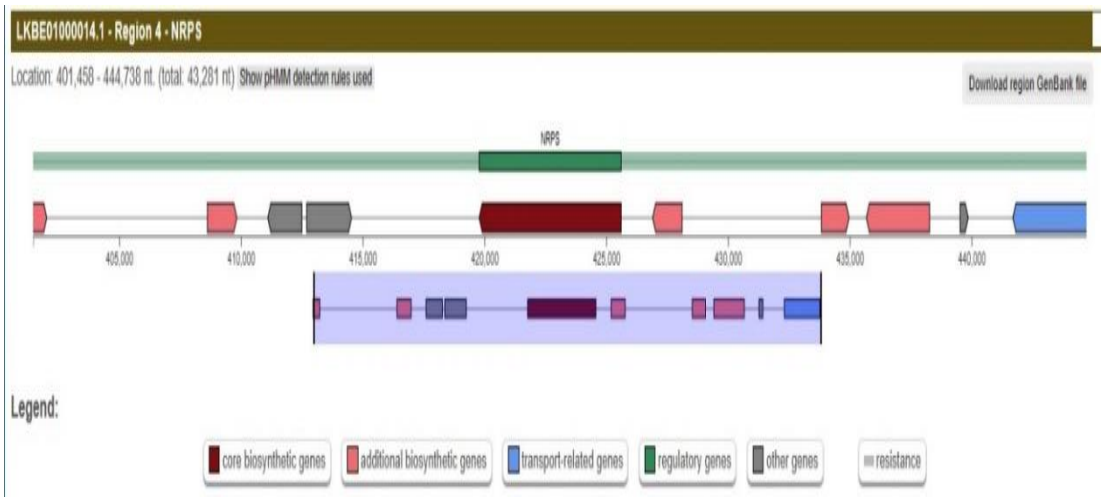

Figure 8.32 Ochratoxin A predicted gene cluster.

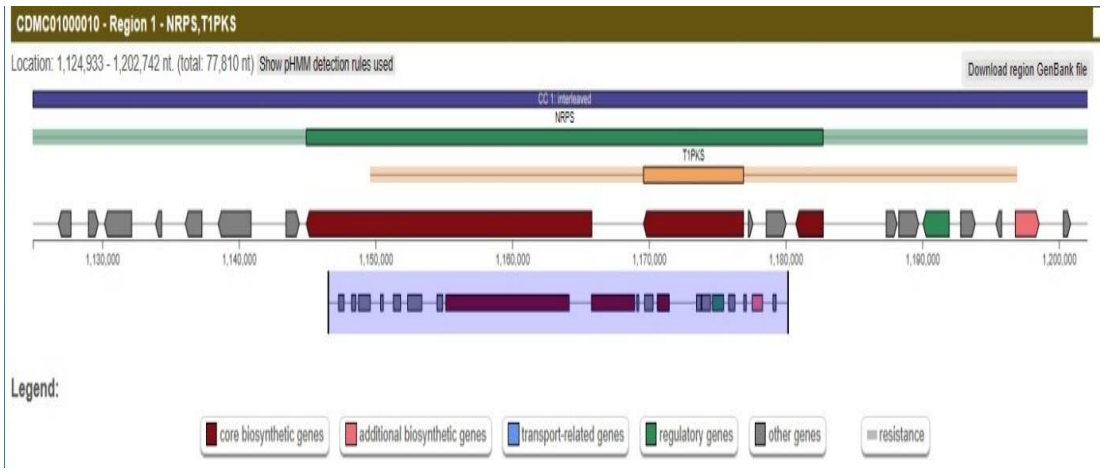

Figure 8.33 Emericellamides A and B predicted gene cluster.

8.16. The complete chromatograms for chapter 2

8.16.1. The complete chromatograms for Figure 2.2

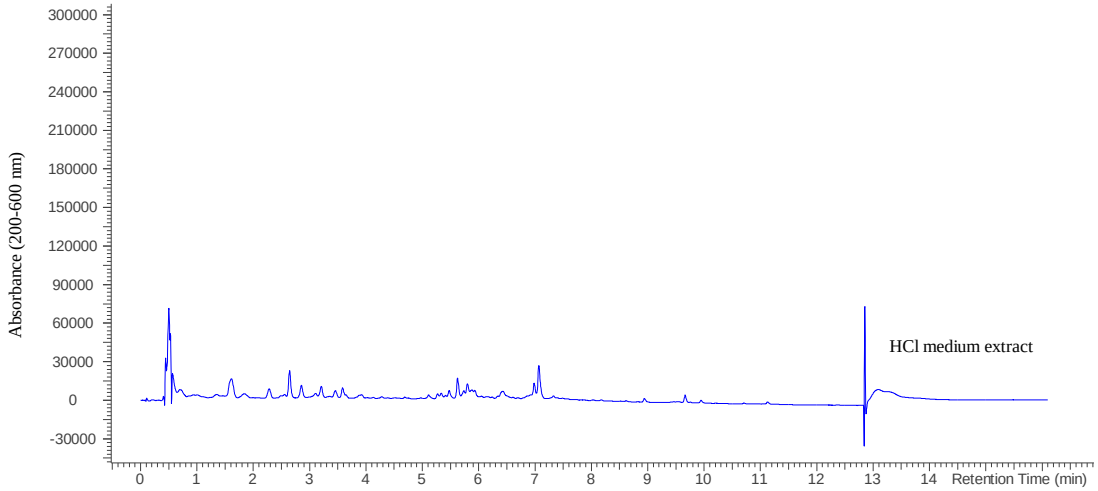

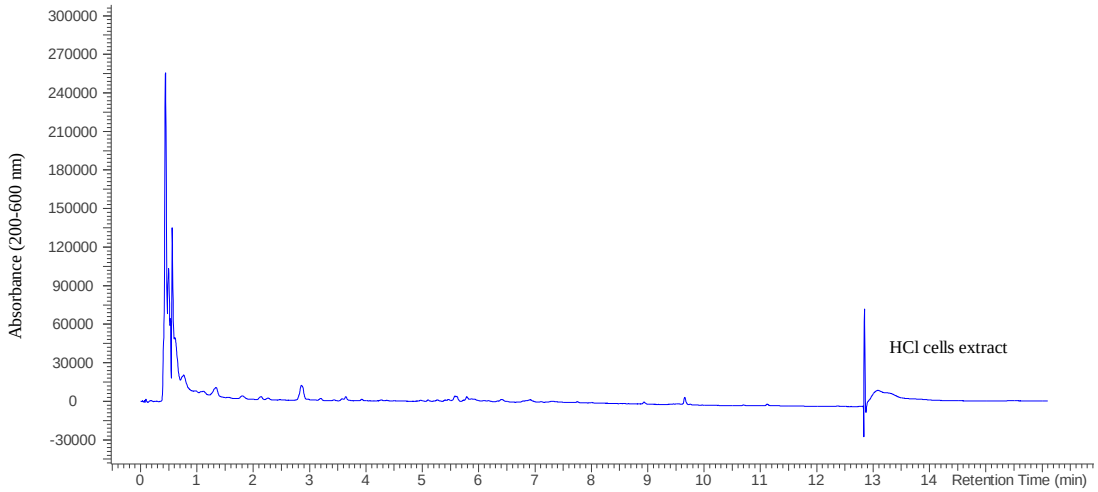

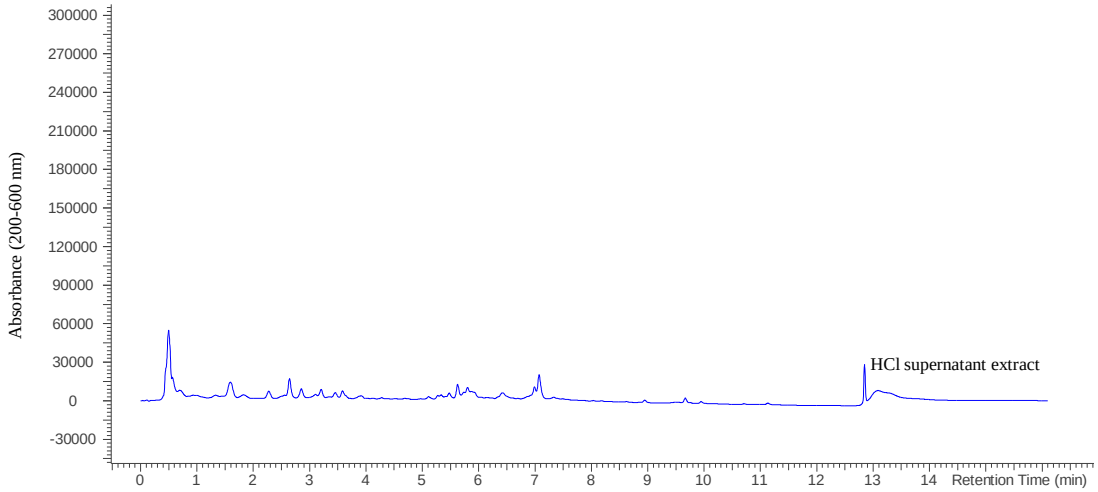

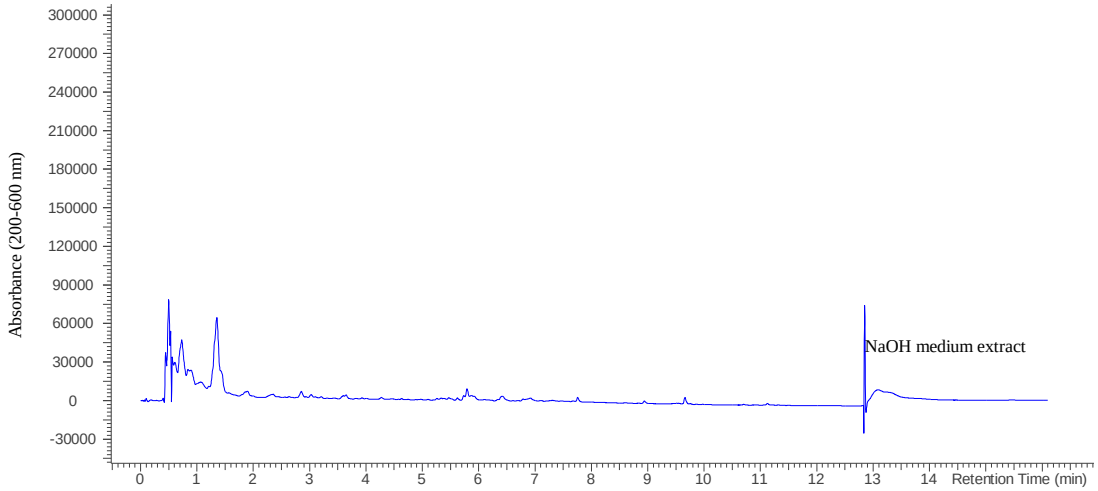
Absorbance (200-600 nm)
300000
270000
240000
210000
180000
150000
120000
90000
60000
30000
0
-30000
0 1 2 3 4 5 6 7 8 9 10 11 12 13 14 Retention Time (min)
NaOH medium extract

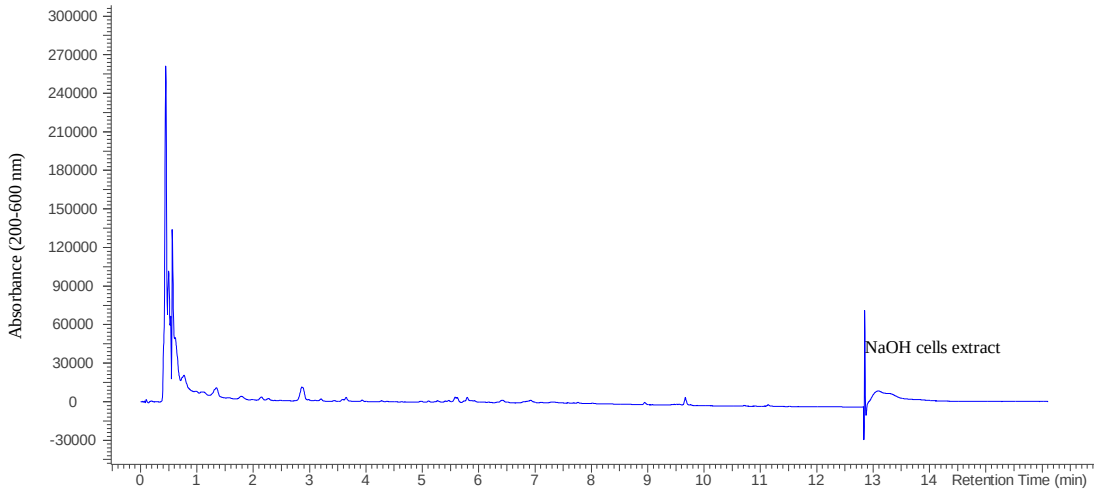
Absorbance (200-600 nm)
300000
270000
240000
210000
180000
150000
120000
90000
60000
30000
0
-30000
0 1 2 3 4 5 6 7 8 9 10 11 12 13 14 Retention Time (min)
NaOH cells extract

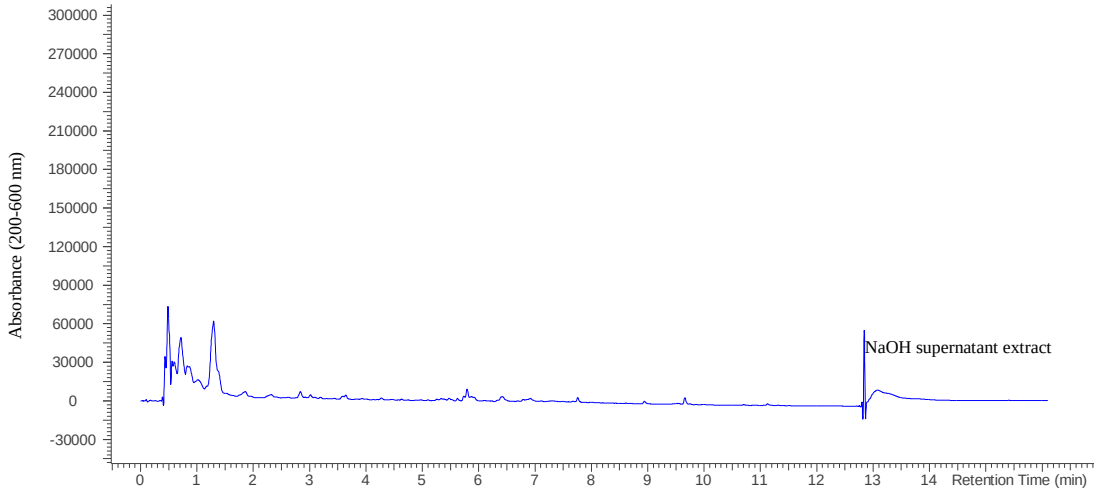
Absorbance (200-600 nm)
300000
270000
240000
210000
180000
150000
120000
90000
60000
30000
0
-30000
0 1 2 3 4 5 6 7 8 9 10 11 12 13 14 Retention Time (min)
NaOH supernatant extract

8.16.2. The complete chromatograms for Figure 2.4

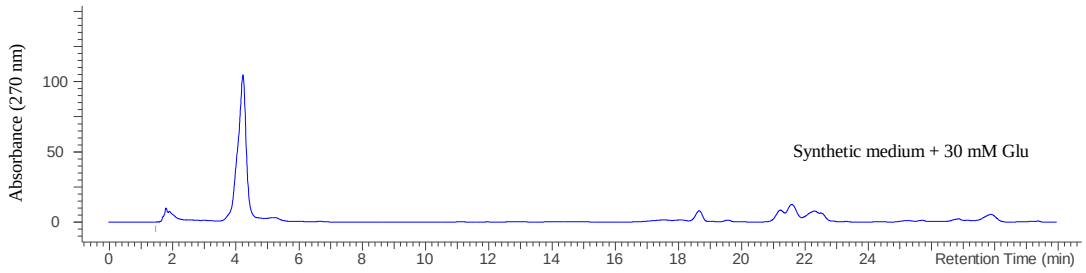

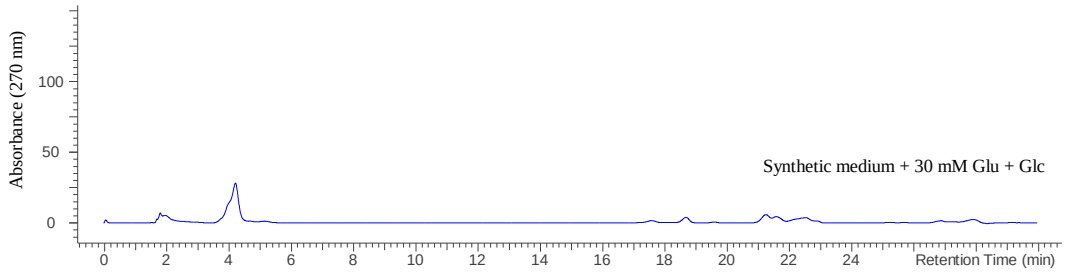

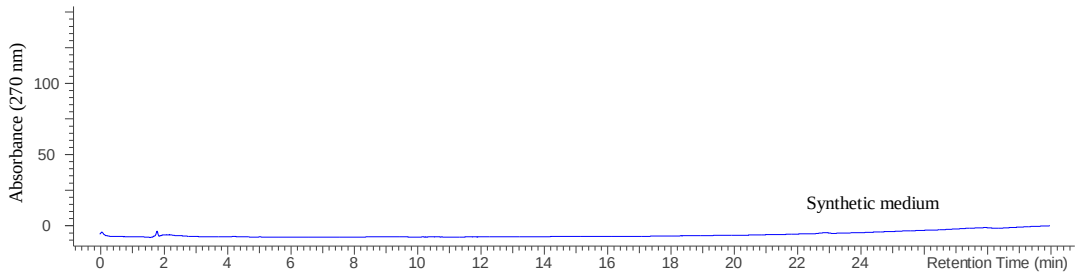

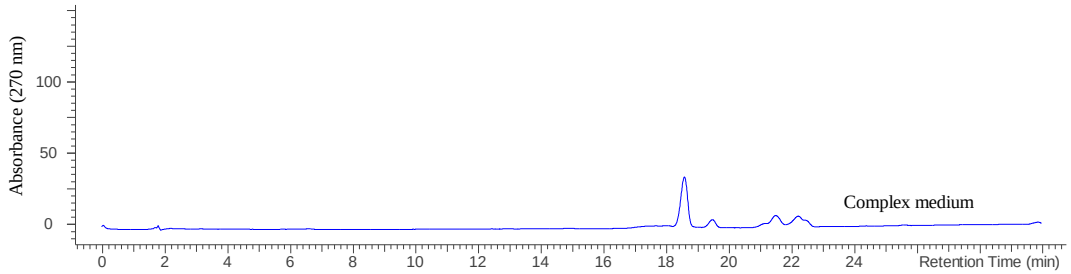

8.16.3. The complete chromatograms for Figure 2.10

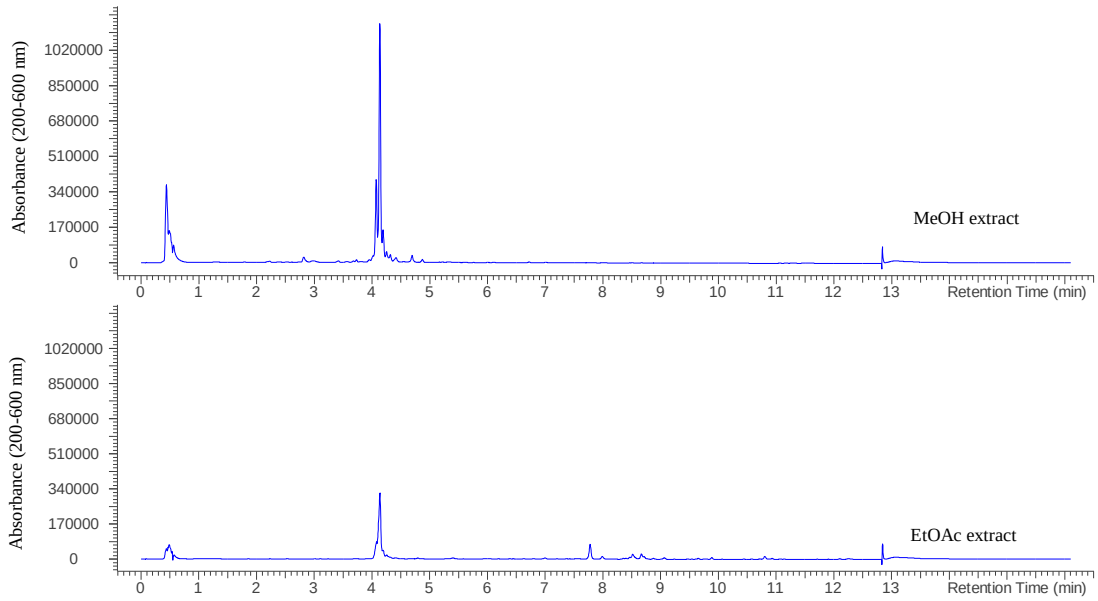

8.16.4. The complete chromatograms for Figure 2.12

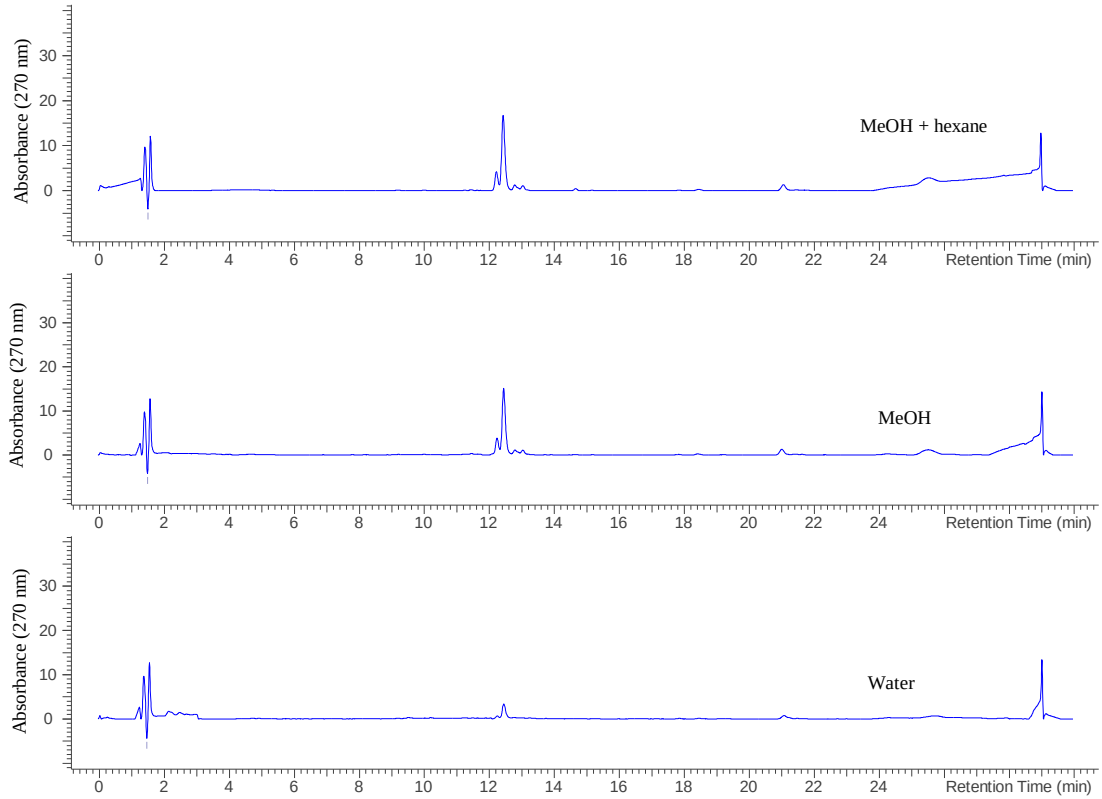

8.16.5. The complete chromatograms for Figure 2.13

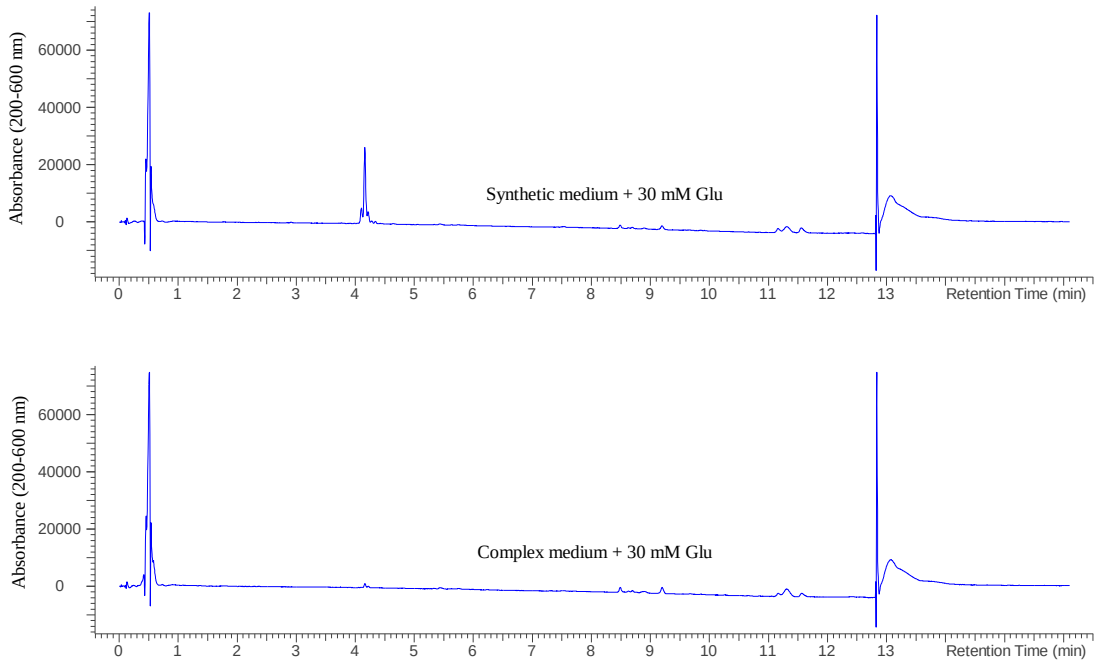

8.16.6. The complete chromatograms for Figure 2.14

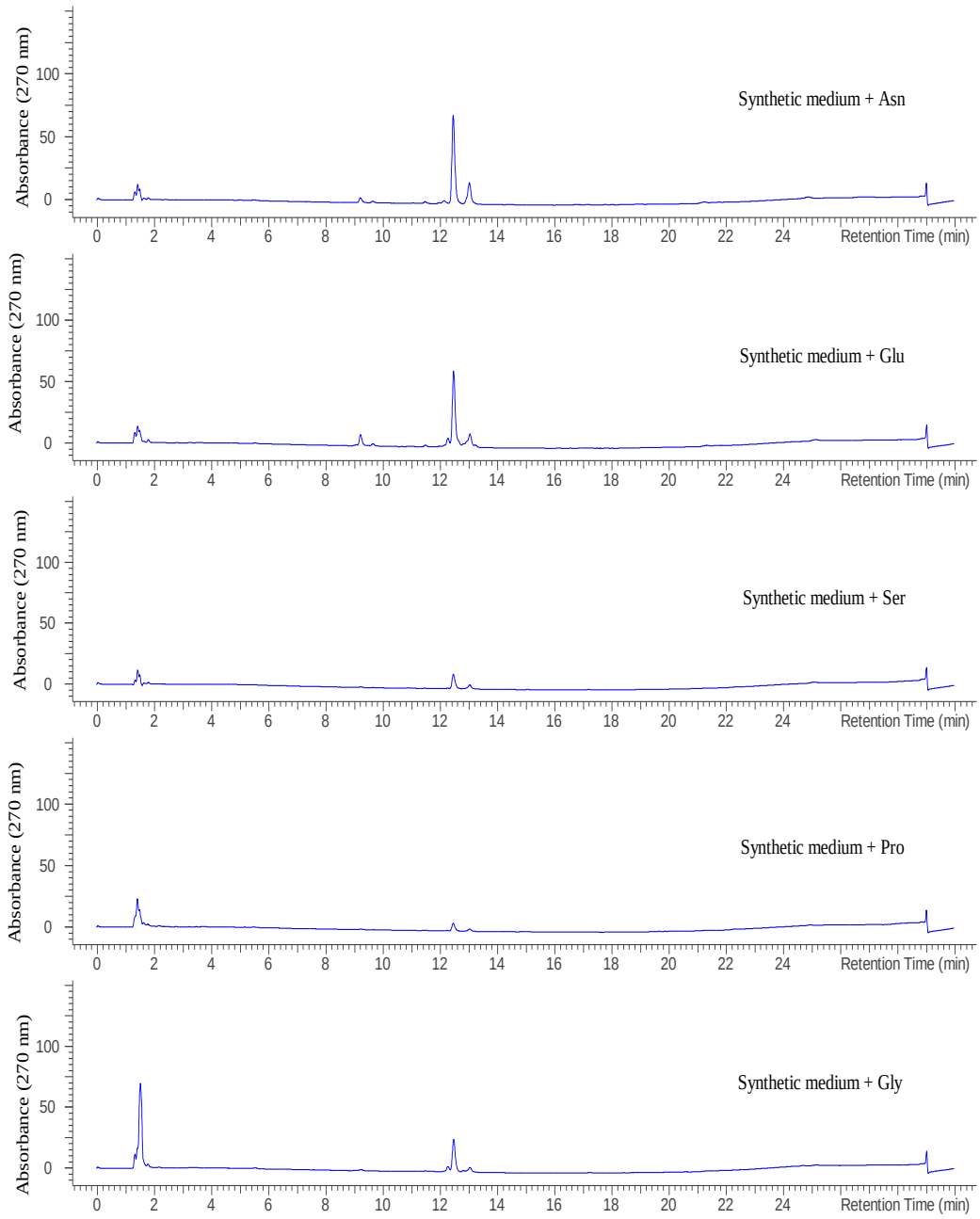

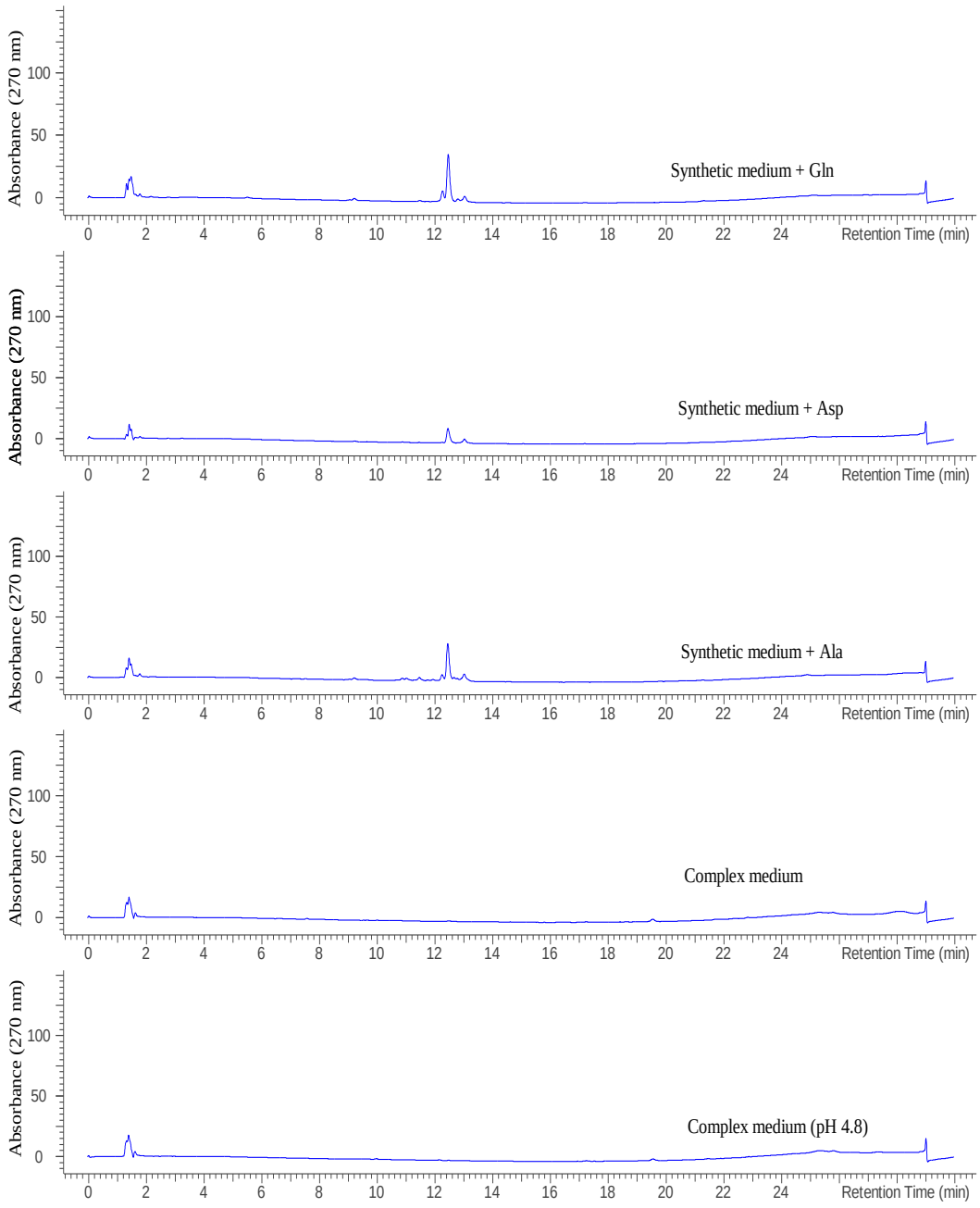
Absorbance (270 nm)
100
50
0
Synthetic medium + Gln
0 2 4 6 8 10 12 14 16 18 20 22 24
Retention Time (min)
Absorbance (270 nm)
100
50
0
Synthetic medium + Asp
0 2 4 6 8 10 12 14 16 18 20 22 24
Retention Time (min)
Absorbance (270 nm)
100
50
0
Synthetic medium + Ala
0 2 4 6 8 10 12 14 16 18 20 22 24
Retention Time (min)
Absorbance (270 nm)
100
50
0
Complex medium
0 2 4 6 8 10 12 14 16 18 20 22 24
Retention Time (min)
Absorbance (270 nm)
100
50
0
Complex medium (pH 4.8)
0 2 4 6 8 10 12 14 16 18 20 22 24
Retention Time (min)

8.16.7. The complete chromatograms for Figure 2.15

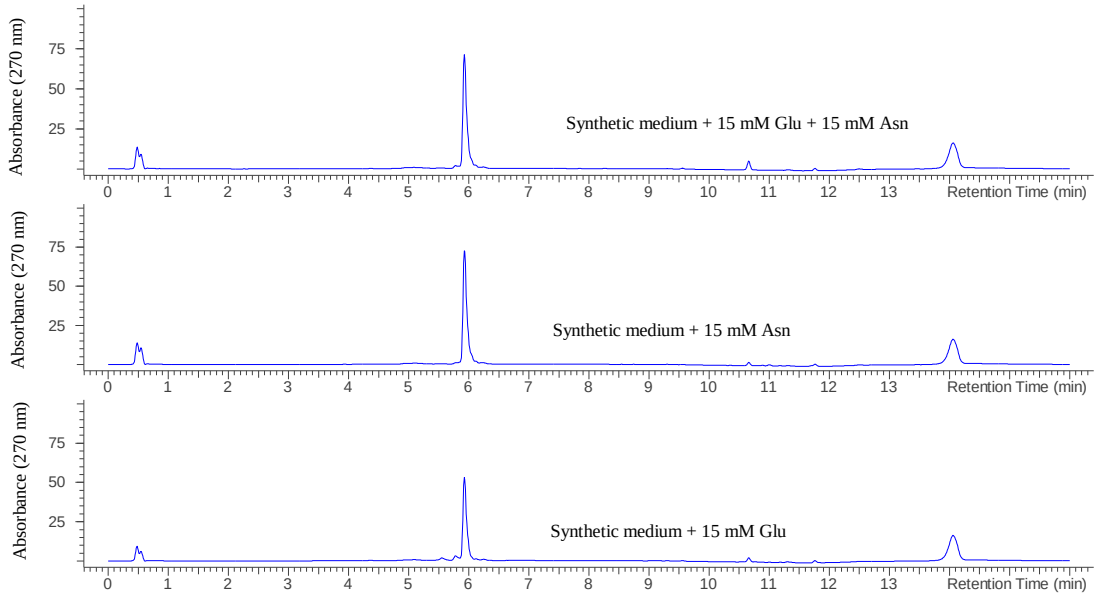

8.16.8. The complete chromatograms for Figure 2.16

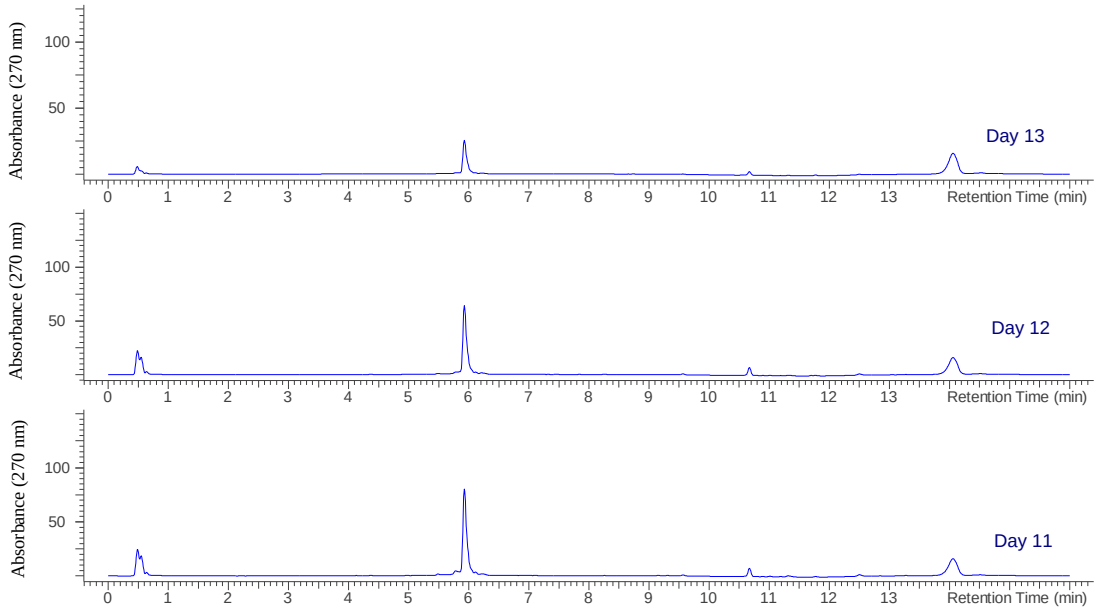

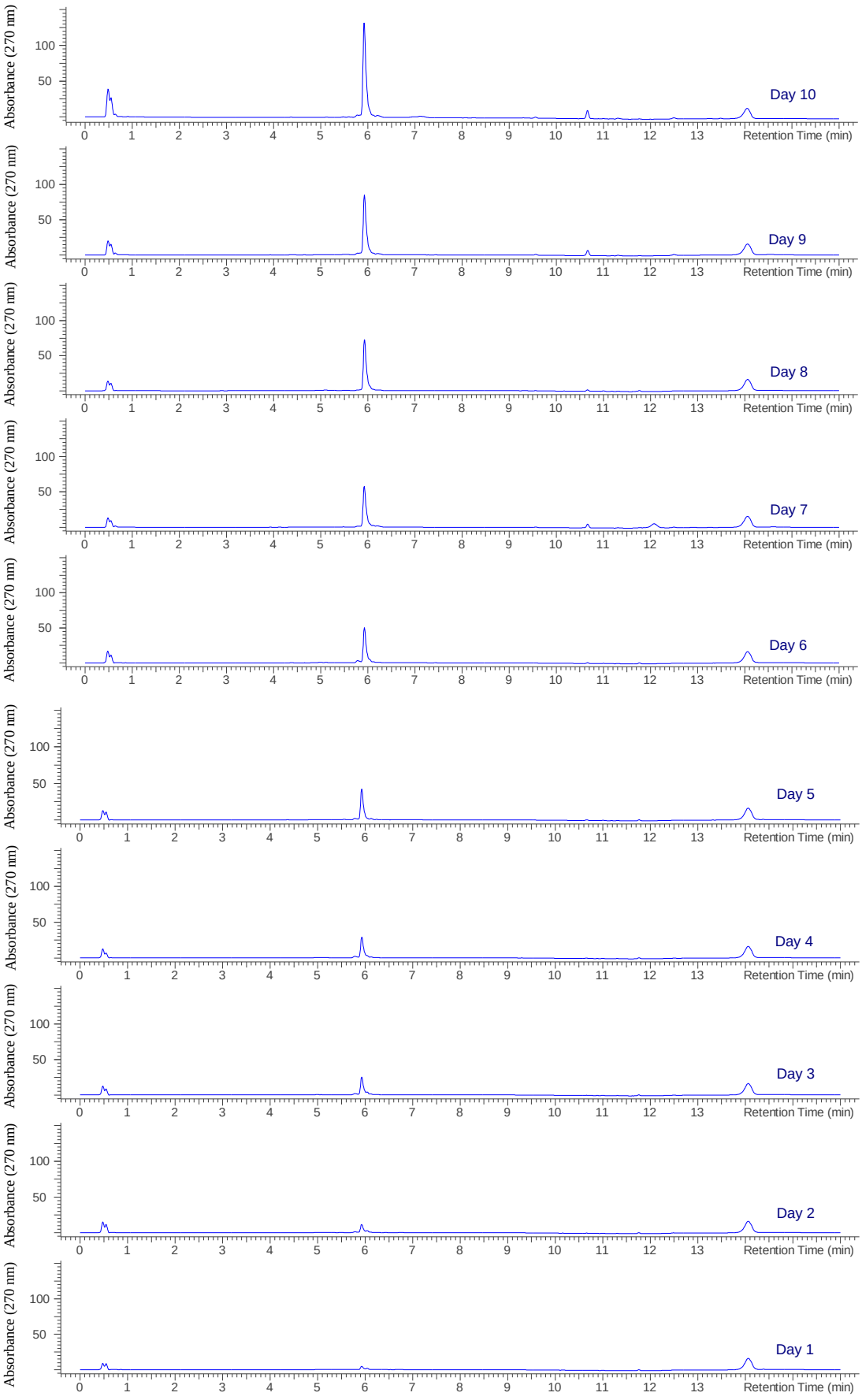
Absorbance (270 nm)
100
50
0 1 2 3 4 5 6 7 8 9 10 11 12 13
Retention Time (min)
Day 10
Day 9
Day 8
Day 7
Day 6
Day 5
Day 4
Day 3
Day 2
Day 1

8.17. The complete chromatograms for chapter 3

8.17.1. The complete chromatograms for Figure 3.4

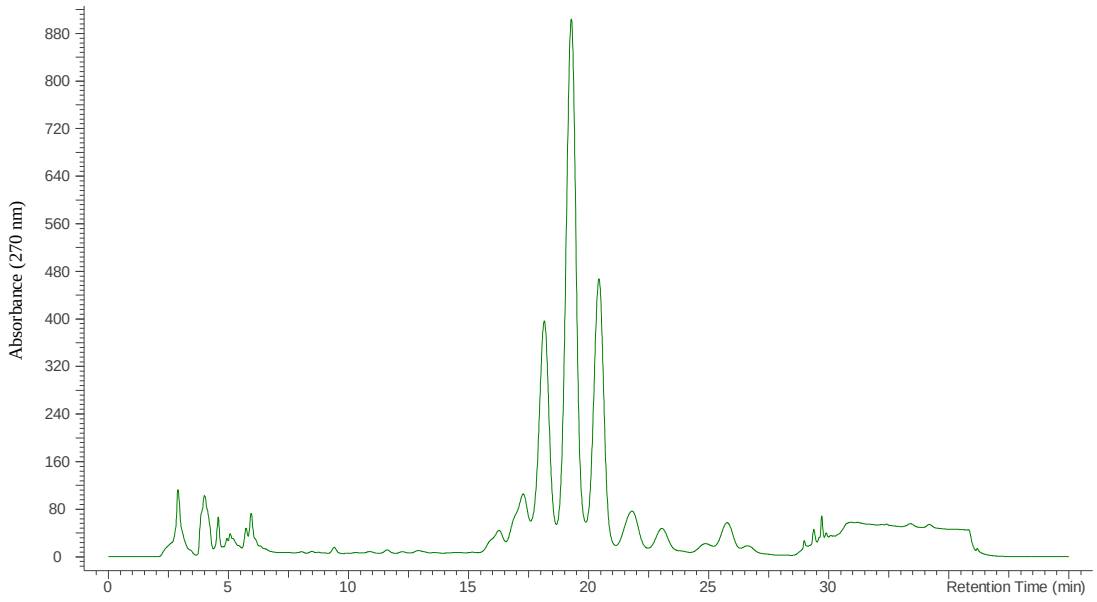

8.17.2. The complete chromatograms for Figure 3.30

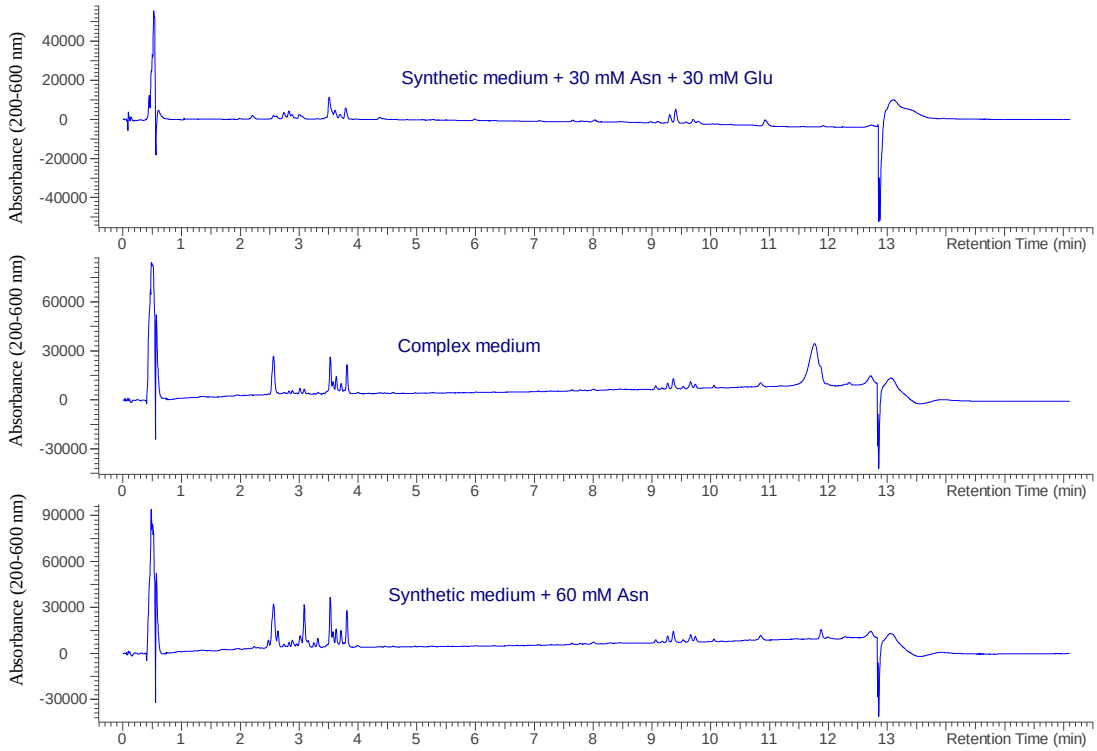

8.17.3. The complete chromatograms for Figure 3.31

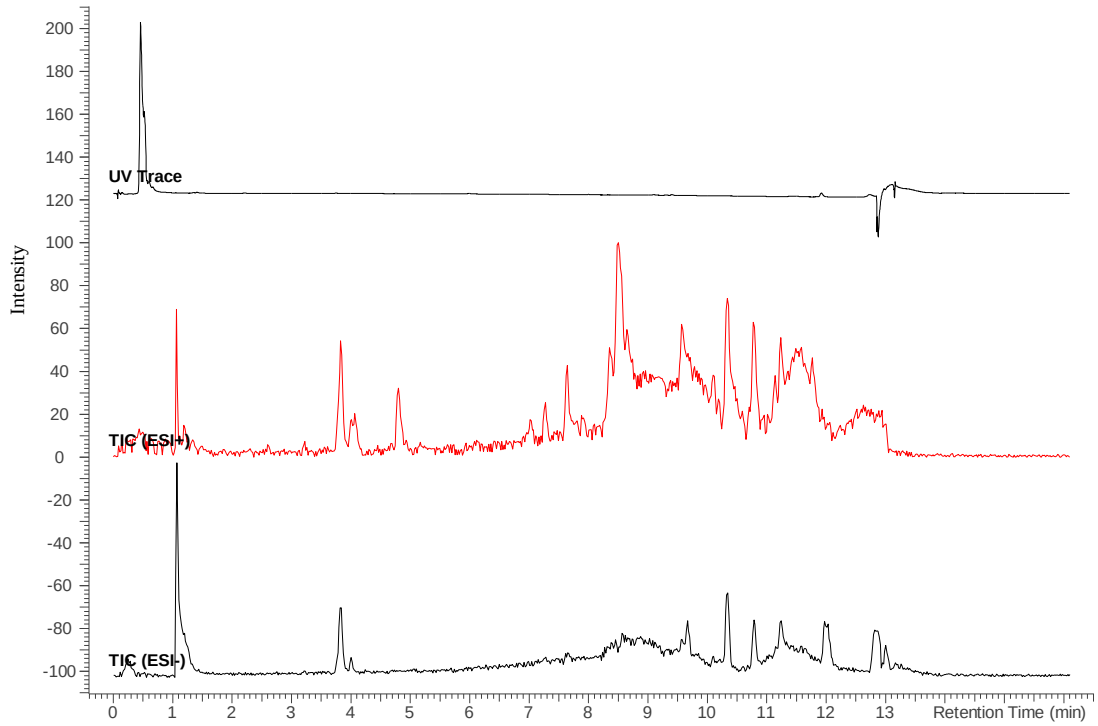

8.17.4. The complete chromatogram for Figure 3.33

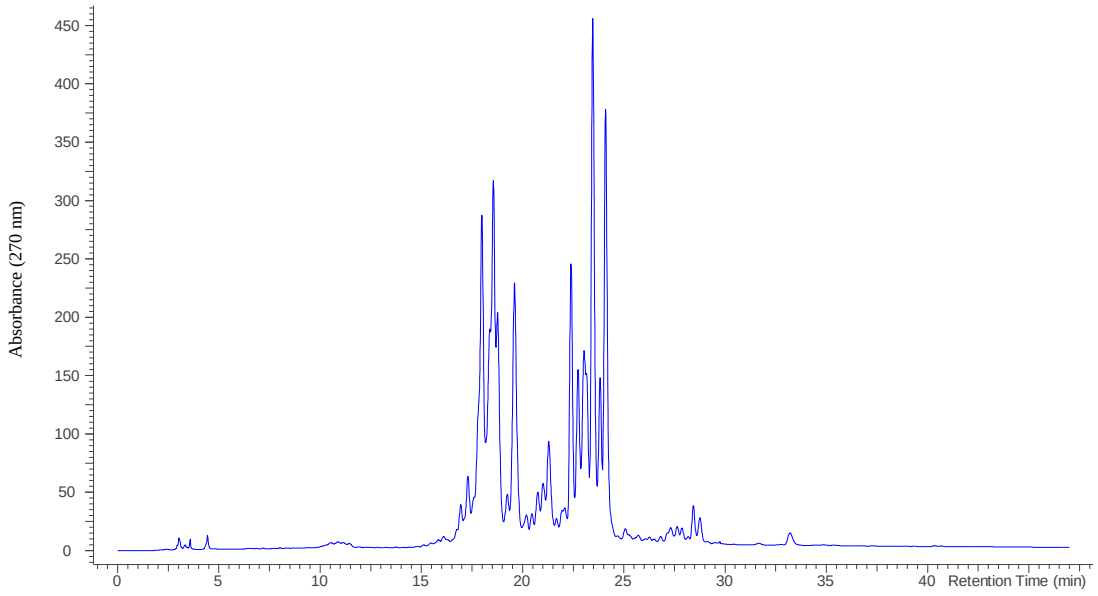

8.18. The complete chromatograms for chapter 4

8.18.1. The complete chromatograms for Figure 4.3

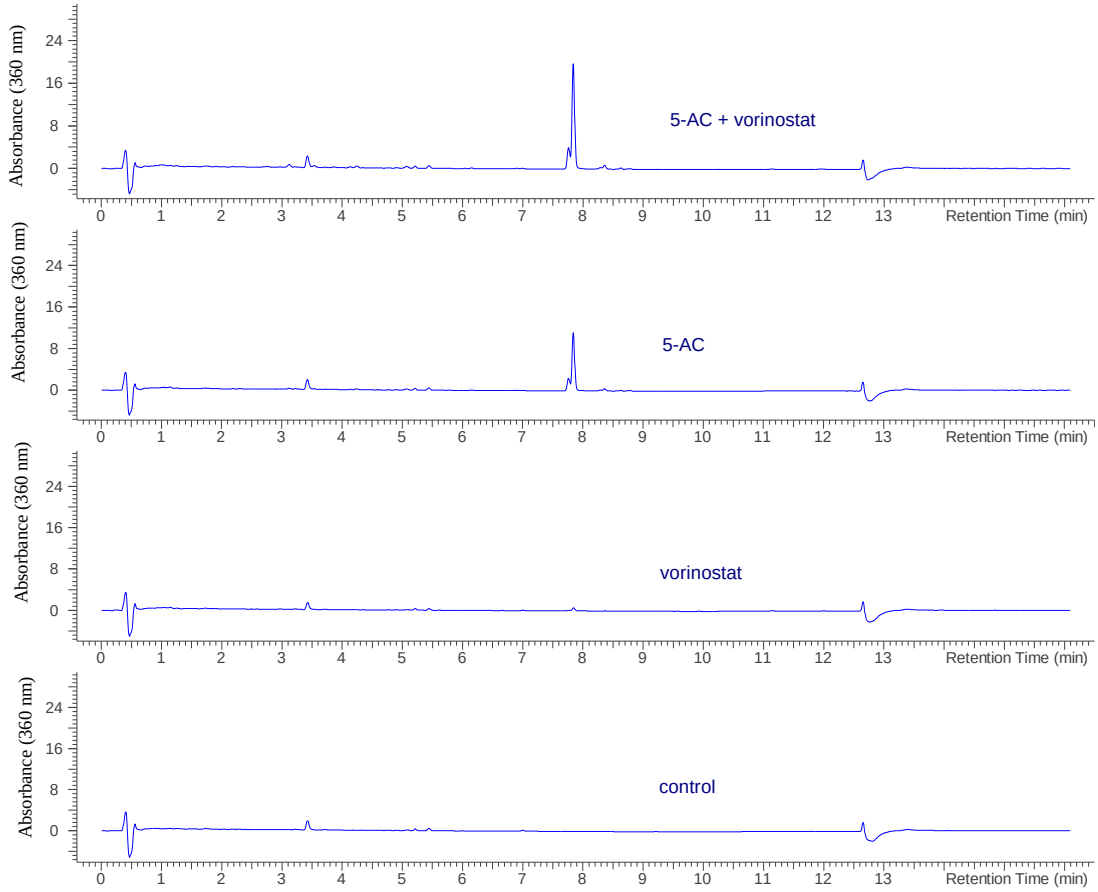

8.18.2. The complete chromatograms for Figure 4.4

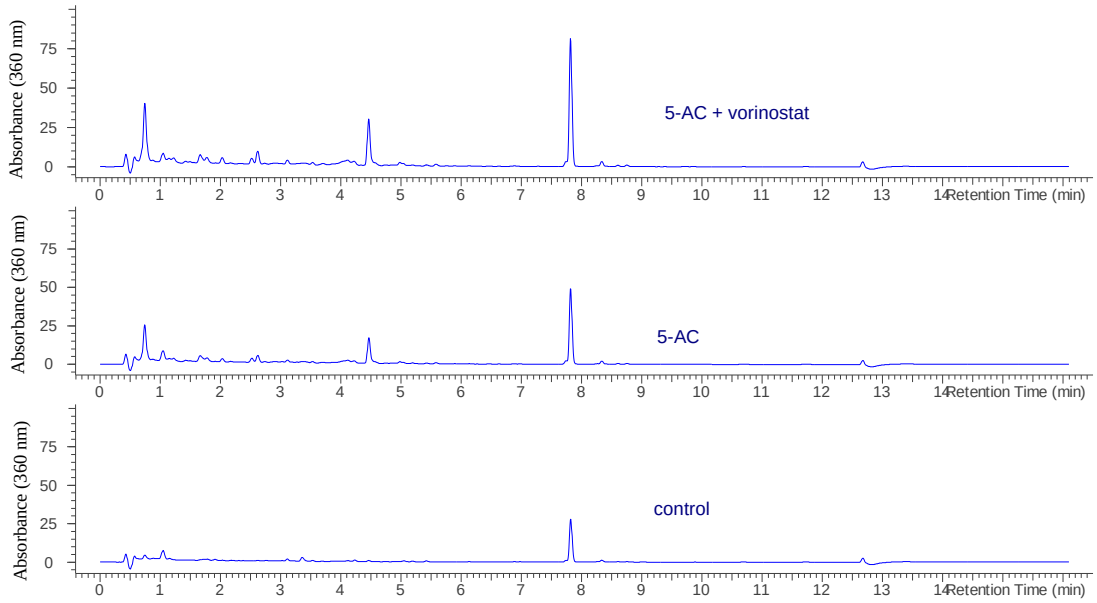

8.18.3. The complete chromatograms for Figure 4.5

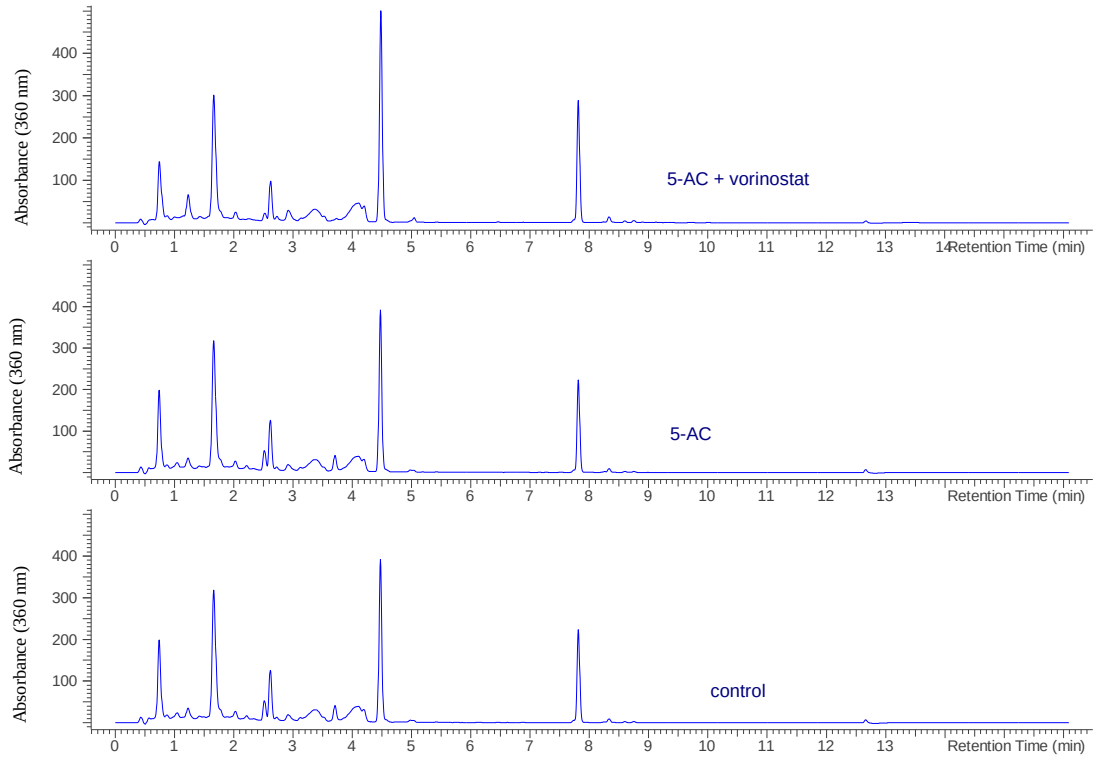

8.18.4. The complete chromatograms for Figure 4.12 (A)

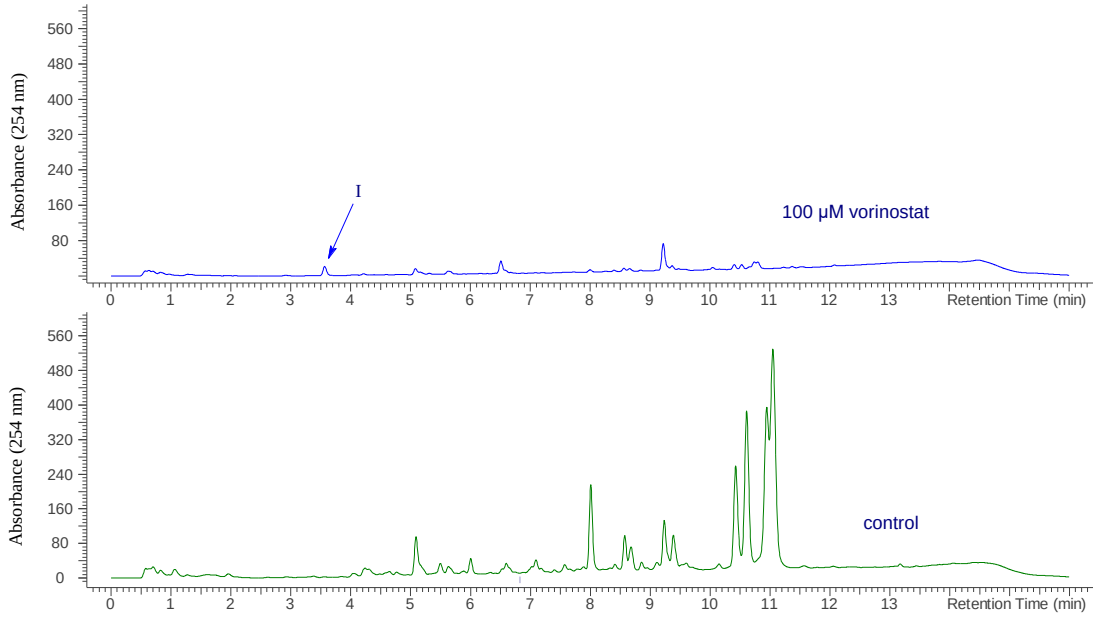

8.18.5. The complete chromatograms for Figure 4.12 (B)

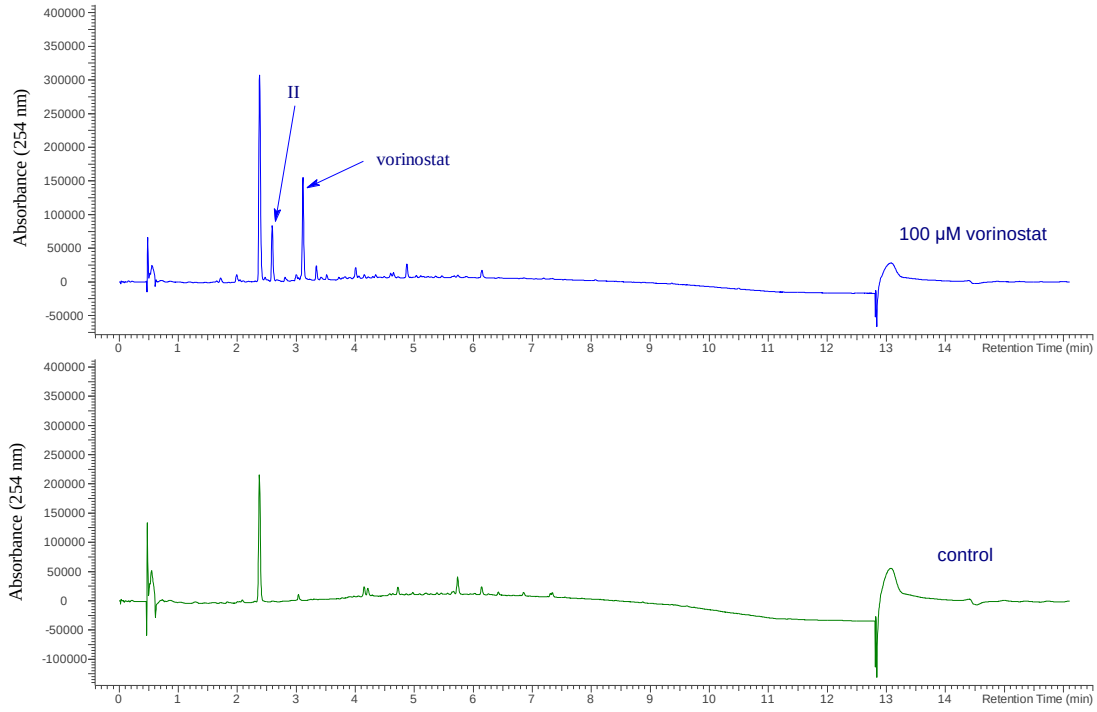

8.19. The complete chromatograms for chapter 5

8.19.1. The complete chromatograms for Figure 5.2

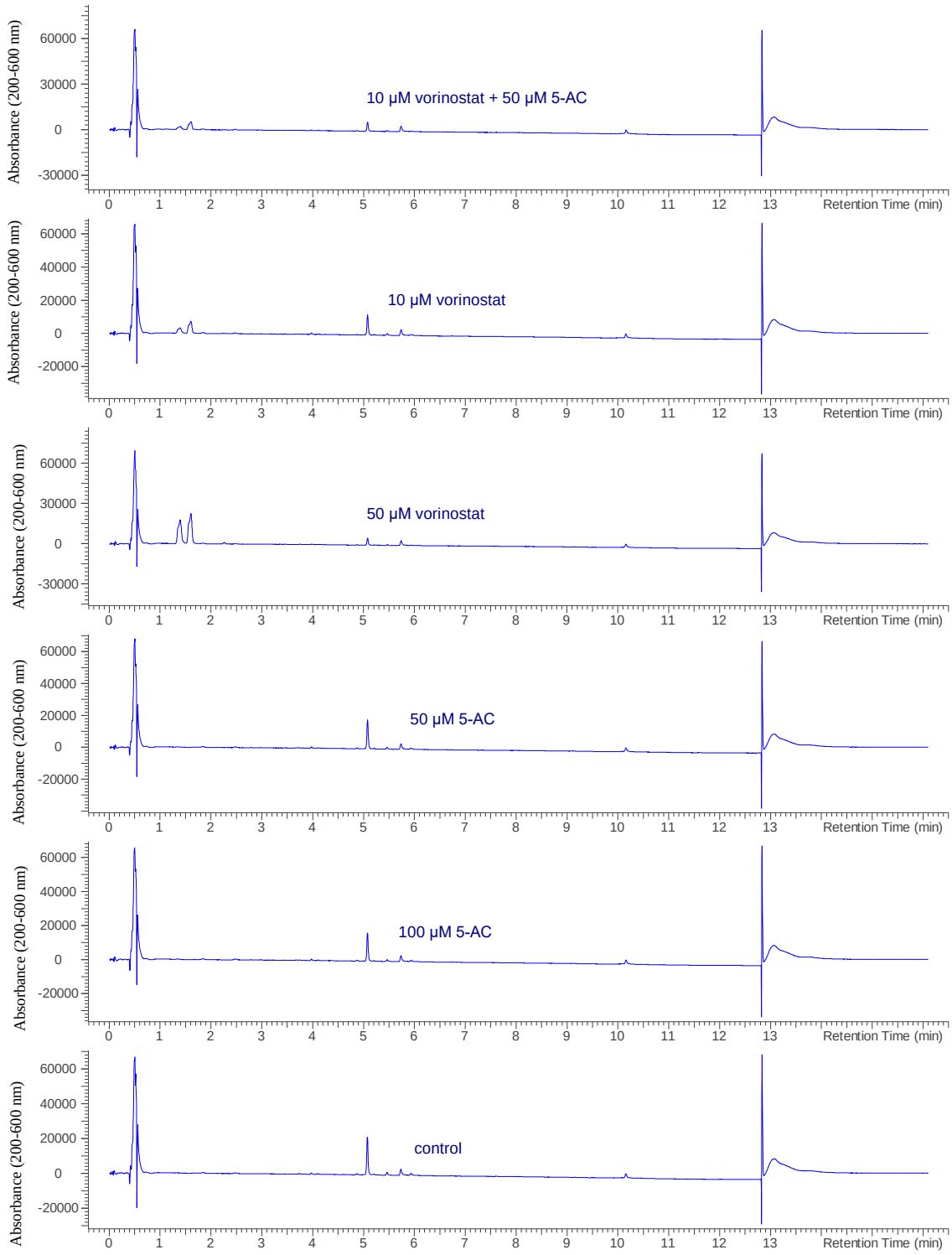

8.20. The complete chromatograms for chapter 5

8.20.1. The complete chromatograms for Figure 5.3

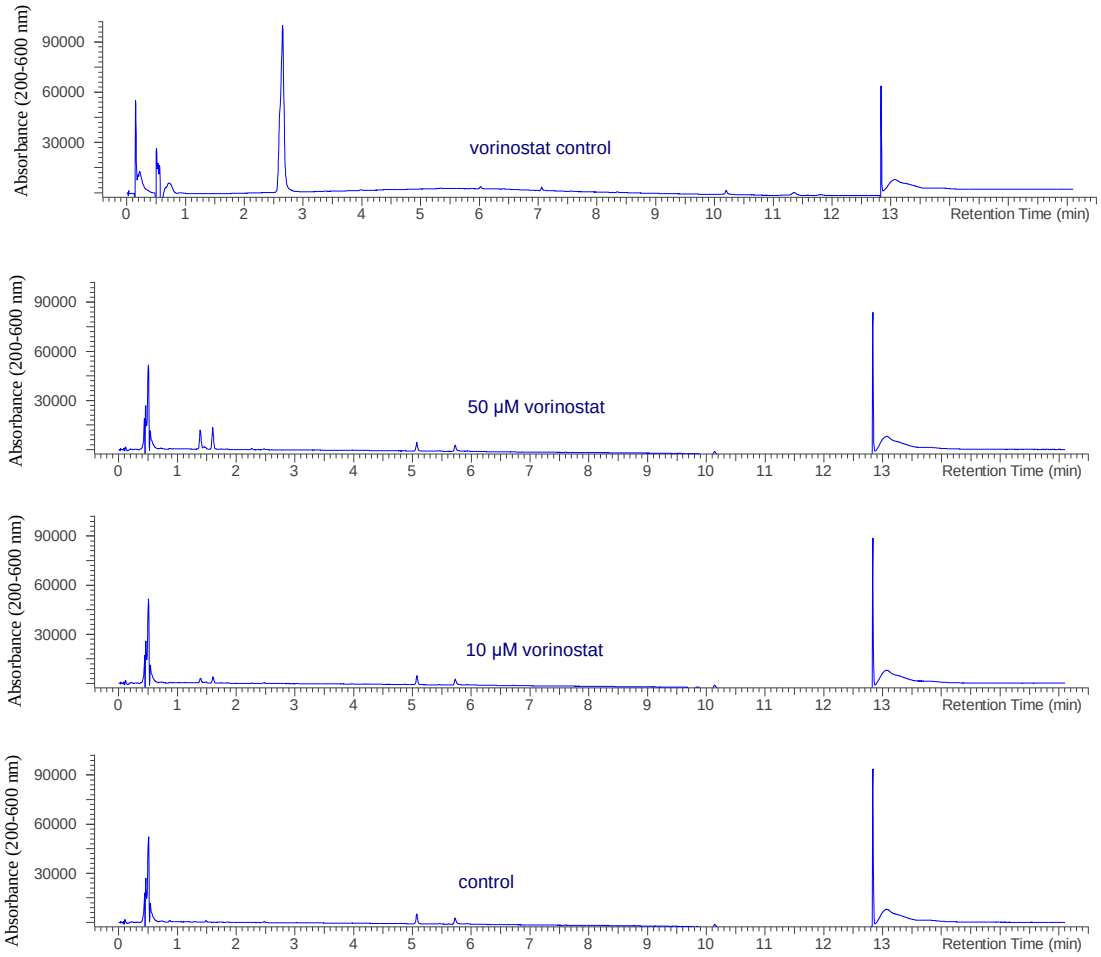

8.20.2. The complete chromatograms for Figure 5.6

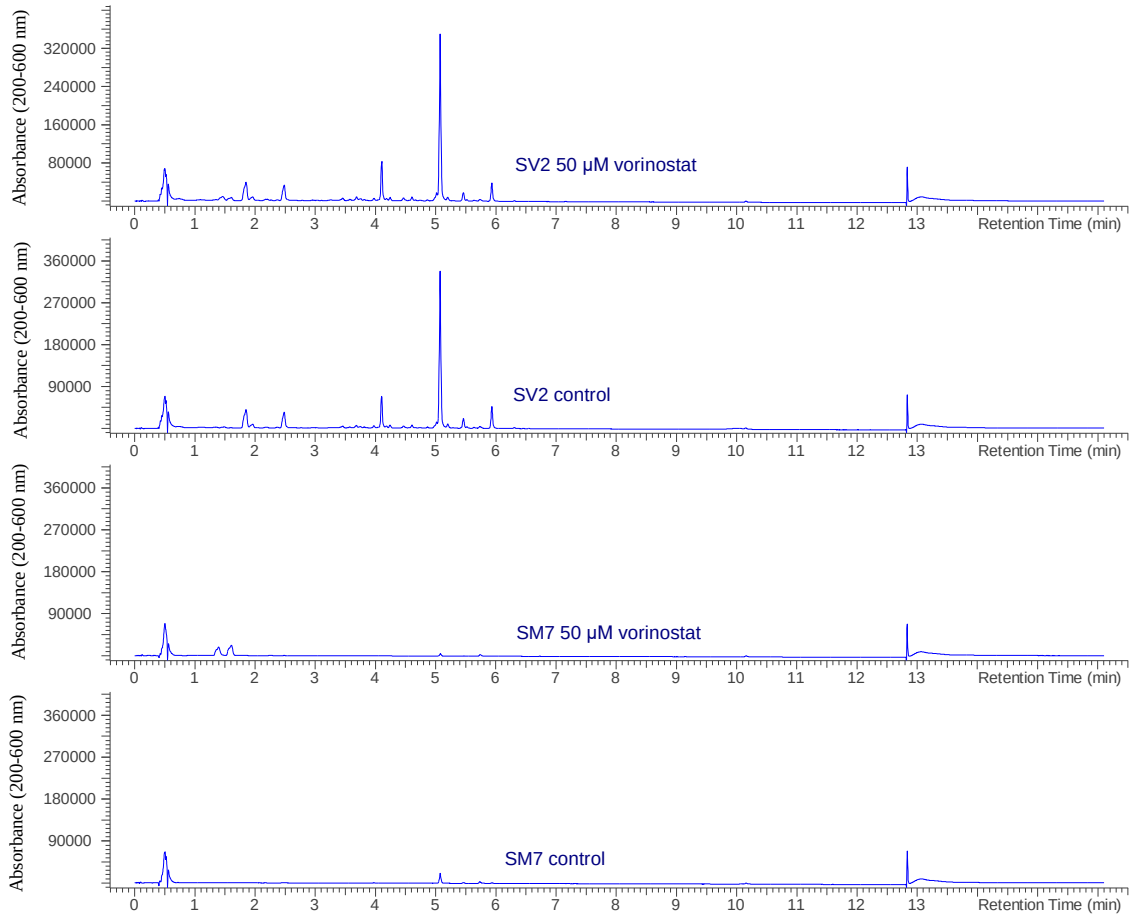

8.20.3. The complete chromatograms for Figure 5.7